OPTICAL STUDIES OF THE UPPER ATMOSPHERE

by

K. Bartusek, B.Sc. (Hons)

A Thesis

presented for the degree of

DOCTOR OF PHILOSOPHY

at the

UNIVERSITY OF ADELAIDE

(Physics Department)

May, 1970.

Frontispiece. The author (left) and colleague Mr. D.J.Gambling with the instrumentation van housing the laser radar system.

CONTENTS

SUMMARY

Various methods that have been used to study the aerosol concentration and composition in the upper atmosphere are reviewed, and the advantages and limitations of optical methods are discussed. It is shown that the laser radar technique has significant advantages over other ground-based methods, and the effect of various equipment parameters on the performance of a complete system is considered.

The thesis describes in detail the design, construction and operation of the laser radar system situated at Adelaide, South Australia (35°S, 139°E), together with the method of analysis of the resulting records. The results of observations carried out during the period April 1969 to January 1970 are presented. The equipment is currently capable of producing continuous scattering profiles over an altitude range extending from 3 to 60 km.

The variation in atmospheric scattering for altitudes above 40 km is found to be essentially the same as that predicted for a molecular atmosphere. Enhanced scattering is observed in the 10 to 30 km altitude region, and this is attributed to the well-known stratospheric aerosol layer. It is shown that similar measurements carried out by other workers in the northern hemisphere are essentially in agreement with the results obtained in the present study.

A marked seasonal variation is found in the peak aerosol concentration in the stratosphere. Such a variation has been inferred

from the results of other measurements carried out earlier at nearly the same latitude by other workers.

Aerosol concentrations deduced from the laser radar data are compared with the results obtained by direct particle sampling measurements, and it is concluded that a significant proportion of the stratospheric aerosol is of volatile form.

The technique of measuring atmospheric turbidity by observing the rate of change of sky brightness during twilight is described. Measurements using the twilight technique are compared with near-simultaneous measurements using the laser radar, and the significance of the twilight observations is discussed.

PREFACE

To the best of the author's knowledge this thesis contains no material previously published or written by another person, except where due reference is made in the text. It contains no material which has been submitted or accepted for the award of any other degree or diploma in any University.

K. Bartusek.

University of Adelaide
May, 1970.

ACKNOWLEDGMENTS

The work described in this thesis was carried out in the Physics Department of the University of Adelaide under the supervision of Dr. F. G. Elford. The author is grateful to Dr. Elford for help and encouragement throughout the course of the work.

The author is indebted to Mr. D. J. Gambling, who assisted with the final installation and operation of the equipment, and who provided the computer programmes required for analysis of the data. The author is grateful to Mr. C. F. Vaskess and the late Mr. E. J. Connock for much of the detailed mechanical design of the equipment. Most of the mechanical construction and assembly were carried out by Mr. N. Manuel. Thanks are also due to Mr. L. Thomas, who constructed much of the electronic and ancillary equipment.

Acknowledgement is due to Dr. F. Jacka, who, as Director of the Mawson Institute for Antarctic Research, made available the Mt. Torrens field station during the early stages of the observational programme, and to Mr. B. Rofe of the Weapons Research Establishment for arranging the loan to the University of the instrumentation van used in the later stages of the study.

Finance for the laser project was provided by the Commonwealth Department of Supply, and the University of Adelaide. The author is grateful to the University for award of a Research Grant.

CHAPTER 1

SURVEY OF AEROSOL MEASUREMENTS

1.1 Introduction

The distribution of particulate matter in the atmosphere is of interest in many branches of physics and meteorology. In the low levels of the troposphere, the presence of dust, or haze, affects visibility, and is of importance in air pollution studies. In the higher regions of the atmosphere, the aerosol becomes important as a nucleating and catalytic agent, and possibly in determining the radiation balance of the atmosphere. For these reasons, a description of the particulate content of the upper atmosphere, and its variation with altitude, location and season, is often required. However, because of the difficulties inherent in the measurement of high altitude particle concentrations, present knowledge of all these parameters is very limited.

The techniques which have been used to measure atmospheric aerosol concentrations may be divided into two main classes. The first class consists of those measurements in which a vehicle, such as an aircraft, balloon or rocket, is used to carry equipment into the region to be studied. "In situ" sampling is carried out, either optically, by light scattering measurements, or by direct collection of particles on specially prepared surfaces for later analysis. The second class consists of those techniques in which observations are carried out remotely, usually from the ground. These experiments are almost invariably optical in nature.

1.2 Vehicle-Borne Measurements

The first comprehensive study of high-altitude aerosols was carried out by Junge and his co-workers. Using particle sampling equipment carried aloft by balloons (Junge, Chagnon and Manson, 1961; Junge, 1961; Chagnon and Junge, 1961) and by aircraft (Junge and Manson, 1961) they obtained information about the distribution and nature of aerosols up to an altitude of 30 km. On the basis of the observed vertical concentration profiles, they classified the particles into three size ranges, each originating from an apparently different source.

The concentration of particles in the size range 0.01 - 0.1 μ (the Aitken nuclei) was found to decrease slowly and irregularly with altitude, reaching a value of about 100 cm^{-3} at the tropopause. The decrease in concentration thereafter became more rapid, falling to a few particles per cm^3 at about 5 km above the tropopause (Fig. 1.1(a)). The vertical profile suggested that the stratospheric nuclei were of tropospheric origin, and were transported upwards into the stratosphere by vertical mixing, or horizontal transport through the tropopause gap.

Fig. 1.1(b) illustrates the observed vertical concentration profile of the second class of particles, those in the size range 0.1 - 1 μ. The main feature of all the observed profiles for the particles in this class was a broad maximum between 15 and 25 km altitude. The maximum concentration was found to be approximately 0.1 cm^{-3} at an altitude of 20 km. Aircraft sampling over the latitude range 40°S to 70°N showed

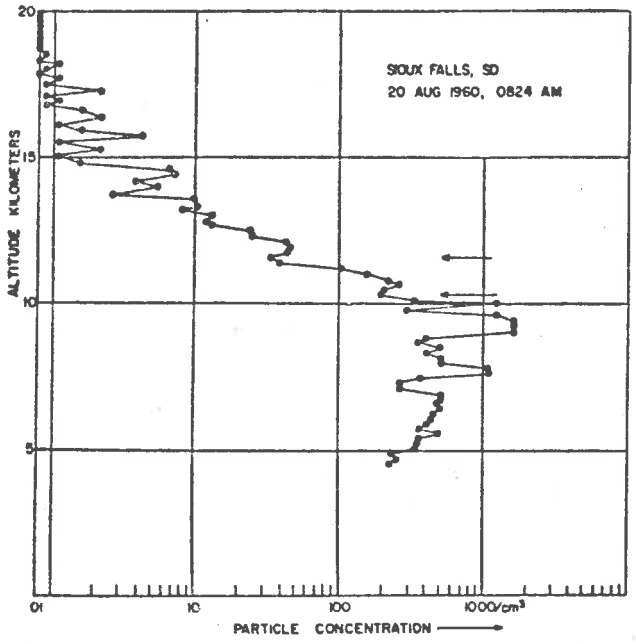

(a) Vertical profile of condensation nuclei.

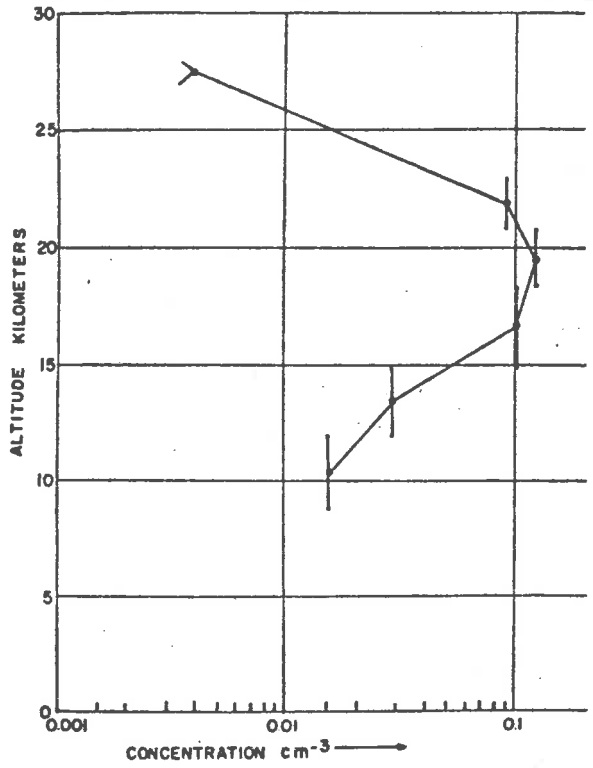

(b) Vertical profile of particles in 0.1 - 1 u range.

Figure 1.1 Vertical profiles of particles found by Junge et al.(1961).

that this feature was remarkably constant with location and time, indicating the existence of a broad, world-wide stratospheric aerosol layer. The existence of such a layer had been proposed earlier by Gruner (1958) to explain the formation of the "purple light" during sunset.

The particles collected from the stratosphere were found to contain a high proportion of sulphur, and were later found by Friend et al. (1961) to consist chiefly of ammonium sulphate and possibly persulphate. Junge et al. considered that the particles had been formed within the stratosphere by oxidation of sulphur-bearing gases originating at the earth's surface.

Junge, Chagnon and Manson (1961) found that the size distribution of particles in the range $0.1 - 1\mu$ could be described by a power law of the form

$$dn/d(\log r) \propto 1/r^{a} \qquad \ldots 1.1$$

or, equivalently,

$$dn/dr \propto 1/r^{a+1} \qquad \ldots 1.2$$

The value of the exponent a was found to be about 2. The power law size distribution was found to apply for particle sizes down to 0.15μ, at which point the decrease in collection efficiency of the impactors used in the study caused a rapid cut-off. Junge et al. concluded that the true lower size limit of particles in this class was below $0.1\ \mu$.

The third class of particles found by Junge et al. consisted of

particles with radii greater than 1 μ. The concentration of these particles was found to be very low, and to decrease with increasing size much more rapidly than those in the 0.1 - 1 μ size range. These particles were considered to be of extra-terrestrial origin.

Although Junge et al. found the concentration and size distribution of stratospheric aerosols to be remarkably constant in location and time, their results have not been confirmed by later measurements. Rosen (1964), using a balloon-borne photoelectric particle counter, found a peak concentration of 3 cm^{-3} of particles larger than 0.28μ radius, at an altitude of 16 km. A possible explanation for the order of magnitude higher concentration found by Rosen may lie in the fact that the photoelectric particle counter measures volatile as well as non-volatile aerosols, and this could indicate the presence of considerable condensation.

Mossop (1965), using aircraft to collect stratospheric particles on specimen grids for later analysis, found sulphate particle concentrations somewhat lower than those reported by Junge et al. In direct contrast with the results of Junge et al., Mossop found a definite peak in the particle size distribution, at a radius of about 0.4 μ, and a decreasing concentration with increasing particle size which was proportional to the fourth power of the radius (a = 3 in Equation 1.2). Mossop concluded that his collections of the stratospheric aerosol were not typical, but his results were later confirmed by the work of Friend (1966), who also found a peak in the size distribution, at

about 0.3 μ radius. Friend showed that the size distribution could be described as log-normal, with geometric mean radius 0.305μ , and a geometric standard deviation of 1.30.

One of the important consequences resulting from the assumption of a simple power law size distribution (with exponent a = 3) for the atmospheric aerosol is the λ^{-1} wavelength dependence of the aerosol extinction coefficient (Ullrich, 1964). This dependence has been found empirically in the low troposphere, under conditions when the visual range exceeded 1 km. These results would indicate therefore that there is a transition in the aerosol size distribution, from a simple power law in the low troposphere, to the lognormal distribution proposed by Friend for the stratosphere. This conclusion is supported by the measurements of Clifford and Ringer (1969), who found that an approximately power law size distribution satisfied low in the troposphere was "compressed" at higher altitudes, by reduction of both the largest and smallest sizes. In the low stratosphere, the distribution was found to peak in the vicinity of 0.5 μ particle radius.

The lack of latitude dependence found by Junge et al. for the concentration and size distribution of the stratospheric aerosol layer has not been confirmed by later measurements carried out by Rosen (1968). Using a photoelectric counter, Rosen found 5 to 10 times more dust in the equatorial stratosphere than at higher latitudes. At low latitudes the dust was contained within a well-defined layer between 16 and 23 km altitude, while the dust at high latitudes was found to have almost the

same concentration between 5 and 15 km, falling off with constant mixing ratio thereafter. The size distribution, described by the ratio of the concentration of particles with diameter greater than 0.2μ to those with diameter greater than 0.8μ, was also found to be variable with both latitude and altitude, and indicated a steeper size distribution at low latitudes.

From the above discussion, it is clear that the results obtained by vehicle-borne measurements of the properties and distribution of atmospheric aerosols are not in good agreement. The lack of a consistent description of the atmospheric aerosol is unfortunate, since it makes difficult the interpretation of results obtained by the ground based class of experiments, as will be shown later.

1.3 Ground-Based Measurements

The ground based measurements to be considered have all utilized optical techniques, and may be sub-divided into two classes, depending on whether a natural or artificial source of illumination was used. The first recorded case of the use of natural illumination would appear to be the measurement of the extent of the earth's atmosphere by Alhazen, an 11th-century pioneer in experimental physics. By measuring the duration of twilight in terms of the depression of the sun below the horizon, he was able to estimate the height of the atmosphere as 52,000 canes. It is now known that this height contains more than 99.9% of the entire air mass.

In more recent years, Fesenkov (1923) proposed the use of the twilight phenomenon to study atmospheric structure. This type of measurement has been carried out by a large number of workers, many of whom specifically sought to deduce the aerosol component from the overall scattering profile (for example, Volz and Goody, 1962; Bigg, 1956). The results of all the twilight investigations have been discussed in detail by Rozenberg (1966). However, the work of Bigg (1956, 1964) is of particular interest. By a series of extremely simple measurements of the rate of change of sky brightness during twilight he obtained profiles to an altitude of 90 km which have a remarkable similarity to atmospheric turbidity profiles obtained by other experiments. However, details of Bigg's analysis have been criticized by a number of other workers. Megrelishvili (1958) pointed out that Bigg had made no allowance in his analysis for attenuation of the solar radiation grazing the earth, while Volz and Goody (1962) claimed that relative intensity measurements, such as Bigg's, were inadequate for determining quantitative data on atmospheric dust, and that absolute measurements were required. A further complication in the analysis of twilight data is due to the uncertain contribution that multiple scattering makes to the total sky brightness. Although Fesenkov (1934) has proposed a method for measuring the brightness contribution due to multiple scattering in regions of the sky close to the horizon, it is clear that the simple analysis adopted by Bigg will not be adequate for solar depressions greater than a few degrees, when the proportion of secondary to primary scattered intensities becomes significant Divari

and Plotnikova, 1966). In view of these criticisms, it clearly would be desirable to compare the results obtained from a twilight scattering experiment with those obtained simultaneously by some other measurement, whose interpretation is less subject to uncertainty, and hence to determine the reliability of the twilight method.

The use of artificial light sources was first suggested by Synge (1930), who proposed that the beams of several powerful searchlights should be concentrated at a high region of the atmosphere, and the scattered radiation measured photoelectrically. The experiment involving multiple searchlights was never carried out, but in 1937, Hulburt photographed the beam of a single high power searchlight to an altitude of 28 km. The beam was inclined at an angle of 30° to the horizontal, and photographed from a site 18.4 km away. By densitometric analysis of the resulting plates, Hulburt compared the amount of scattering observed with that expected from Rayleigh scattering by a molecular atmosphere. He found good agreement between measured and predicted scattering for heights above 10 km, while below 10 km, he observed considerably enhanced scattering which he attributed to the presence of haze and dust in the lower regions of the atmosphere.

Johnson, Meyer, Hopkins and Hook (1939) refined the method by using a more powerful searchlight, and a photoelectric detection system. The searchlight beam was modulated at 10 c.p.s. and a tuned amplifier was used at the receiver in order to help discriminate against sky background radiation. Scattering profiles were obtained in good agree-

ment with those predicted for a purely molecular atmosphere for altitudes between 8 and 34 km.

Using the same basic technique, Elterman (1951) obtained atmospheric density measurements to an altitude of 67 km and later used these to deduce corresponding temperature profiles over the 10-60 km altitude range (Elterman, 1954). From a later series of measurements, Elterman obtained a large number of profiles of aerosol attenuation coefficient over the 2-35 km height range. (Elterman, 1966 and 1967).

All the searchlight systems described so far suffered a common disadvantage, through their use of a continuous transmitted beam. In order to obtain adequate height resolution in the measurements, it was necessary for the receiver to scan the transmitted beam, step by step. This necessitated a considerable separation between the receiver and transmitter sites, with attendant problems of communication. Considerable time was taken to obtain a single profile, during which time the profile itself may have changed. Analysis of the data was further complicated by the changing geometry of the scattering situation.

These disadvantages may be overcome by the use of a pulsed transmission technique, in which a single short pulse of light is transmitted, and the scattering is recorded as the pulse propagates upwards. The transmitter and receiver may then be placed at a common site, with their beams permanently aligned. The terms "bistatic" and "monostatic" have been used by some authors to distinguish the two techniques, and

the methods are illustrated in Fig. 1.2.

Friedland, Katzenstein and Patrick (1956) first utilized the monostatic technique, by making use of one of the high power flash tubes which were then becoming available. The pulse emitted by the flashtube was of 50 Klumen intensity, and 20 μsec duration, and enabled them to obtain instantaneous scattering profiles to an altitude of 40 km. The flashtube light source however still suffered two disadvantages in common with the continuous light sources. The first of these was the broadband nature of the emitted radiation, which offered no possibility of discriminating against the sky background intensity, which was also broadband in character. The second disadvantage was caused by the fact that the sources were extended, essentially isotropic radiators, making it difficult to produce a collimated beam without loss of a large proportion of the light.

These disadvantages have been overcome by the development of the pulsed laser light source. First described by Maiman in 1960, the ruby laser is capable of producing short pulses of intense, highly collimated and nearly monochromatic radiation at a wavelength of 6943$\mathring{A}$. By means of the Q-switching technique described by McClung and Hellwarth (1963), it is possible to generate pulses having a total duration considerably less than one microsecond, and with peak powers of many megawatts.

1.4 Measurements Using a Laser Source

It is of interest to compare the performance to be expected from a

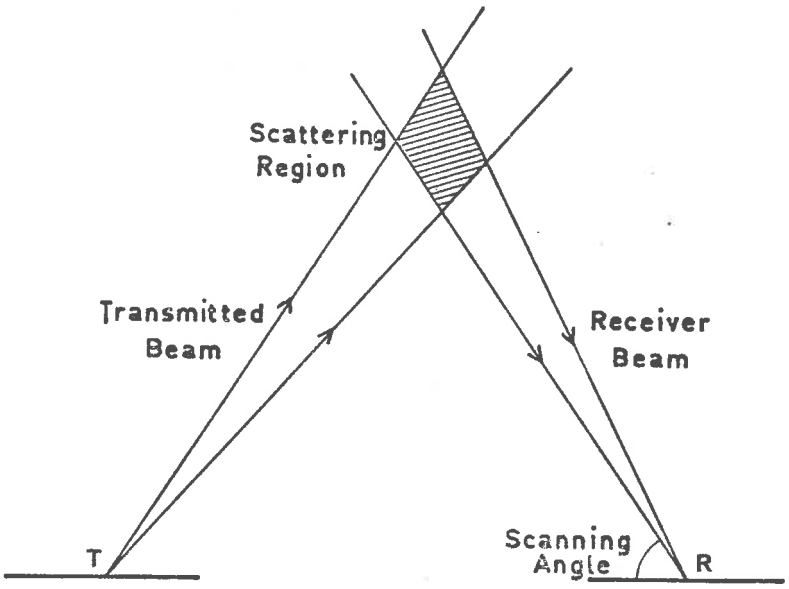

(a) Bistatic arrangement

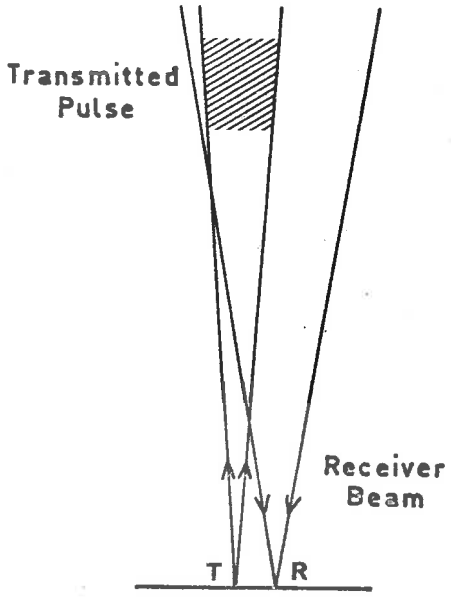

(b) Monostatic arrangement

Figure 1.2 Possible arrangements of transmitter T and receiver R for atmospheric optical sounding.

laser with that obtained by Friedland et al. (1956) using a flash tube as the light source. The spectral emission of the light source used by Friedland et al. reached its peak value at 4400Å. Assuming a black body spectral distribution, this would correspond to a colour temperature of about 6000°K, and by means of the usual photometric conversion, it is found that 500lumens is equivalent to approximately 1.4×10^5 watts in the visible region of the spectrum. Since the detector response would extend somewhat outside this region, the effective emitted power will be taken as 2×10^5 watts. The intensity of light scattered from a pulse by an extended medium is proportional to the total energy in the pulse, and for a pulse length of 20 μ sec, the total effective energy emitted by the flash tube would be 4 joules. However, not all of this energy appeared in the transmitted beam, due to the finite aperture of the collimating system. The effective transmitted energy will therefore be taken as approximately 1 joule per pulse.

This energy is of the same order of magnitude as that which may be obtained from a typical laser. The important advantage of the laser source is that the emission is contained in a total bandwidth of less than 1Å, while that from the flashtube is spread more or less evenly over more than 3000Å. In the case of the laser system, it is relatively easy to limit the receiver bandwidth to less than 10Å, thus improving the signal to noise ratio by more than 300 times compared to the flash tube system. Further improvements are possible because of the improved collimation achievable with a laser transmitter, and to the reduced losses due to scattering of light in the low regions of the atmosphere

at the longer wavelength laser radiation. Some of these improvements will, however, be offset by the lower efficiencies achievable by presently available detectors at the longer wavelength.

Fiocco and Smullin (1963) were the first to report the use of a laser radar for upper atmosphere research. Using equipment which they had earlier used to detect laser echoes from the moon, (Smullin and Fiocco, 1962) they observed Rayleigh molecular scattering at heights up to 50-60 km. At greater heights, up to 140 km, they observed very weak echoes, which they ascribed to dust layers. Similar experiments were described by Collis and Ligda (1966), McCormick et al. (1966 and 1967), Bain and Sandford (1966(a)) and Clemesha, Kent and Wright (1966, 1967(a), 1967(b)). The results of all these workers were in quite good agreement over the height range 10 - 50 km. The observed variation in atmospheric scattering followed that predicted for a purely molecular atmosphere, with the exception of a region extending from approximately 12 to 30 km. In this region, all workers observed an enhancement in scattering, which was attributed to the well-known stratospheric aerosol layer (Junge, Chagnon, Manson, 1961).

Results obtained for altitudes above 50 km have been inconclusive, and to some extent contradictory. While some groups (for example, Fiocco and Smullin, 1963; McCormick et al. 1966) observed regions of enhanced scattering at altitudes up to 140 km, the existence of these was challenged by Bain and Sandford (1966(b)) and by Clemesha, Kent and Wright (1967(a)). These workers pointed out that the occurrence of

peaks in the scattering profiles obtained at high altitudes was highly dependent on the care with which sources of noise had been eliminated from the laser system. It was apparent that many of the early experimental results had been affected by such factors as unsuppressed laser fluorescence, and momentary photomultiplier overload. More recent results, obtained with equipment in which care had been taken to eliminate spurious signals, showed much smaller deviation from the expected scattering profile at high altitudes (for example, Kent, Clemesha and Wright, 1967).

In spite of the experimental difficulties, the laser radar technique has been shown to be capable of producing profiles of atmospheric scattering coefficient over an altitude range extending from low in the troposphere up into the mesosphere. It is clear that the interpretation of laser radar results is considerably more straightforward than that of data obtained from experiments using natural light sources. The laser radar technique thus offers, for the first time, a possibility for the world-wide observation and comparison of atmospheric scattering profiles, obtained on a routine basis by a number of ground-based observing stations. By this means, world-wide profiles of atmospheric turbidity could be obtained, and large scale atmospheric circulation studied by observing the movement and dispersion of dust injected into the stratosphere by phenomena such as volcanic action, and nuclear explosions.

A map showing the distribution of existing and planned laser radar

facilities (to mid-1963) has been published by Geyer (1963). It is noteworthy that all the facilities shown were located in the northern hemisphere. In order to provide complementary data from the southern hemisphere, a laser radar has been constructed at Adelaide, South Australia (lat. 35°S). Although construction of the system began in 1964, completion of the work was seriously delayed by difficulties experienced with the laser generator, with the result that observations did not commence until April, 1968. In the following chapters, the detailed design and construction of the complete system will be described. The primary aim throughout has been the construction of a laser radar system which would be reliable, and as free as possible from any sources of noise which could affect the accuracy of the measurements.

CHAPTER 2

SYSTEM PERFORMANCE CALCULATIONS

2.1 Introduction

In order to proceed with the design of a practical laser radar system, it is necessary to consider the effect of various equipment parameters on the performance of a complete system. In this section the formulae describing the performance of a laser radar will be developed. Actual equipment parameters will be assumed, and the formulae evaluated in order to predict the signal strengths and signal to noise ratios for the case of scattering by a purely molecular atmosphere over the 10 - 90 km altitude region. In this way a basis against which actual results may be compared will be established.

2.2 Laser Radar Geometry

The optical radar geometry is illustrated in Fig. 2.1. A transmitter T emits a short pulse of light which travels upwards in a narrow beam with divergence θ_t. The light scattered from the pulse into a small solid angle $d\omega$ is collected by an optical receiver R. The field of view θ_r of the receiver is somewhat larger than the transmitter beam divergence θ_t, so that the transmitted pulse lies entirely within the receiver's field of view above some minimum height h_o.

The minimum height h_o which can be observed depends on the beam

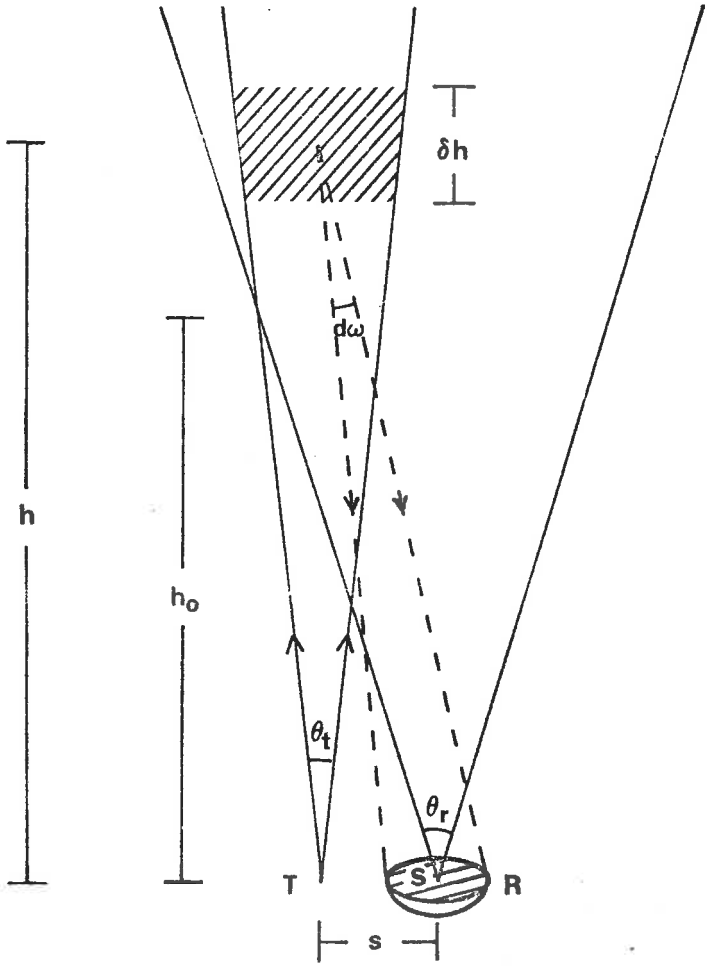

Figure 2.1 Optical radar geometry.

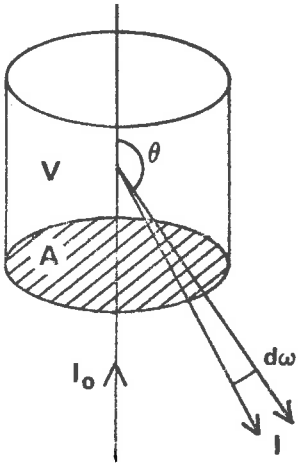

Figure 2.2 Scattering geometry.

divergences θ_r and θ_t, and on the center-to-center separation s between the transmitter and receiver. From the geometry of the situation, it can be shown that

$$h_o = s/(\tan\theta_r - \tan\theta_t)$$

$$\simeq 2s/(\theta_r - \theta_t) \qquad \ldots 2.1$$

if both θ_r and θ_t are small.

It is desirable to make θ_r as small as possible, in order to minimize the contribution of the sky illumination to the total signal level. The lower limit to θ_r will be set both by the minimum achievable transmitted beam divergence θ_t, and by the lowest required observable height h_o. As h_o is directly proportional to the receiver-transmitter separation s, it is desirable also to make s as small as possible.

2.3 Scattering from Air Molecules

The theory of scattering by particles much smaller than the wavelength of light was first developed by Lord Rayleigh (1871), and the scattering of light by gas molecules is therefore commonly referred to by the term Rayleigh scattering. In this section the formulas describing the signal obtained from scattering by air molecules will be developed.

Since the transmitted beam divergence is small, the laser pulse

may be considered to illuminate a cylindrical volume element V of the atmosphere at height h, where the molecular density is n(h). If I_o is the irradiance (energy flux/unit area) incident on the scattering volume, then, under steady state conditions, the flux F scattered through angle θ into a small solid angle $d\omega$ (Fig. 2.2) is given by Van de Hulst (1957) as

$$F = I_o V B(\theta,\phi) d\omega$$

where $B(\theta,\phi)$ is the scattering function, for plane polarised light, of the molecules contained in the volume V, which appears as a point source to the receiver. The angle ϕ is the angle between the direction of electric polarisation of the incident light and the plane containing the incident and scattered waves.

Now consider the case of a laser source emitting a short light pulse of duration τ, which propagates upwards with the velocity of light, c. The instantaneous value of the flux at the receiver R at any time t is due to the photons contained within a thin imaginary shell, defined at a time t' earlier than t by $r(t') = c(t-t')$, as shown in Fig. 2.3(a). At this time, the laser pulse is at the point h(t'). As t' varies, the shell contracts towards R with velocity c, and at the same time the pulse moves outwards, also with velocity c. Let t'_o and $t'_o + dt'$ be the times when the shell just makes and breaks contact with the illuminated volume V, of length dh (Fig. 2.3(b)). Then at any time t' between t'_o and $t'_o + dt'$ the contribution to the

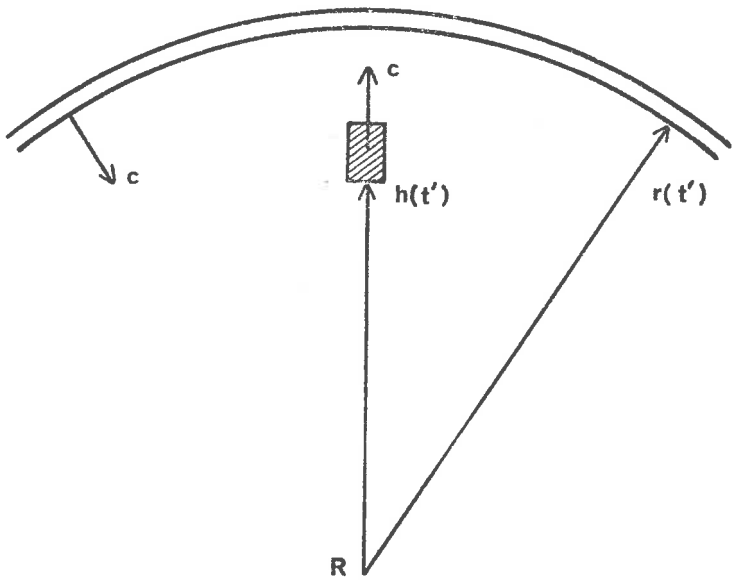

Figure 2.3(a) Relative positions of the laser pulse and imaginary shell at the time t'.

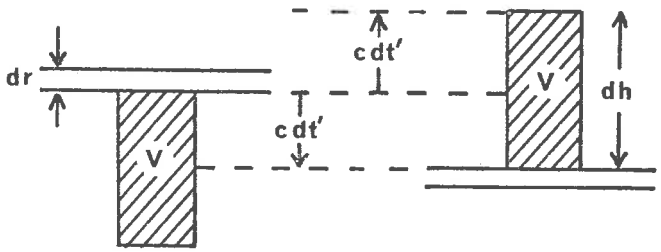

(i) time t'_o (ii) time $t'_o + dt'$

Figure 2.3(b) Elementary shell dr just making (i) and breaking (ii) contact with laser pulse.

total flux from a layer of thickness dr is $I_o V\beta(\theta,\phi) d\omega\, dr/dh$. The number of layers that contribute to the flux during the time dt' is cdt'/dr. But from Fig. 2.3(b),

$$2cdt' = dh$$

where $dh = c\tau$

thus $$dt' = \tau/2.$$

The total flux is therefore given by

$$F = \int I_o V\beta(\theta,\phi) d\omega \qquad \ldots 2.2$$

If the total energy in the pulse is E, and the transmission of the atmosphere to height h is denoted by T, then

$$I_o = TE/A\tau$$

where A is the base area of the illuminated volume V at height h. Thus

$$V = \theta\, \tau A$$

and the signal flux F_s at the receiver is given by

$$F_s = \int \pi r^2 \alpha\beta(\theta,\phi) d\omega$$

If the collecting surface of the receiver has area S, then

$d\omega = S/h^2$

and $$F_s = \pi r^2 \alpha\beta(\theta,\phi) S/2h^2 \qquad \ldots 2.3$$

The scattering function $\beta(\theta,\phi)$ is the product of the volume

scattering coefficient per unit length β and the phase function $P(\theta,\phi)$.

$$B(\theta,\phi) = \beta P(\theta,\phi)$$

The volume scattering coefficient is the product of the scattering cross-section per molecule σ and the molecular number density $n(h)$, so that

$$B(\theta,\phi) = \sigma n(h) P(\theta,\phi)$$

For plane polarised light, the phase function is

$$P(\theta,\phi) = \frac{3}{8\pi}(\cos^2\phi \cos^2\theta + \sin^2\phi)$$

and for natural unpolarised light,

$$P(\theta) = \frac{3}{16\pi}(1 + \cos^2\theta)$$

In the case of a typical optical radar, with close spacing between transmitter and receiver, the scattering angle θ is very nearly equal to 180° throughout the height range, and both phase functions reduce to

$$P(\pi) = 3/8\pi$$

The backscattering coefficient thus becomes

$$B(\pi) = 3\sigma n(h)/8\pi$$

and the signal flux F_s at the receiver is

$$F_s = 3cTr^2 s\, \sigma n(h)/16\pi h^2 \qquad \ldots 2.4$$

2.4 Signal Recording

The light flux gathered by the collecting surface of the receiver is directed on to a photomultiplier detector. Photons incident on the photoemissive surface of the detector give rise to free electrons. After amplification by the dynode system of the photomultiplier, these photoelectrons are counted, either individually as discrete pulses, or in integrated form as an electric current. The number of photoelectrons produced by each incident photon is defined as the quantum efficiency q of the photodetector, and is always less than one.

Not all the light flux gathered by the collecting surface of the receiver reaches the photodetector, since light is lost at each optical surface in the receiver, and in any narrowband optical filters used to discriminate against the broad-band sky background radiation. To take these losses into account, the overall optical efficiency of the receiver will be designated by η, defined as the ratio of light flux at the photoemissive surface to the light flux incident on the receiver.

If a total of P photons is emitted in one laser pulse, then $P = E\lambda/hc$, where h is Planck's constant, and equation 2.4 can be used to calculate the received photoelectron count rate $N_s(h)$:

$$N_s(h) = 3\pi\lambda T^2 S \eta q \sigma n(h)/16\pi kh^2 \qquad \ldots 2.5$$

In practice, recording of weak signals is preferably carried out by counting the pulses corresponding to individual photoelectrons, since

in this way the noise associated with the multiplication process in the photomultiplier is of no consequence. The pulses are counted over a series of small time intervals Δt, corresponding to some definite height interval

Assuming that the time intervals are so small that $N_s(h)$ is essentially constant during Δt, the total signal count recorded in one time interval (channel) is $C_s(h) = N_s(h)\Delta t$ and, from equation 2.5,

$$C_s(h) = 3E\lambda T^2 S\eta Q\sigma n(h)\Delta h/8\pi ckh^2 \qquad ...2.6$$

In order to evaluate equations 2.5 and 2.6 for different values of the height h, it is necessary to assign numerical values to the parameters in the two equations. The values used have been listed in Table 2.1. The pulse energy E is determined by the characteristics of the laser used as the basis of the optical radar. A value of 1 joule has been chosen as being typical for commercially available units. The channel width Δh is determined by the resolution required from the system and has been chosen to be 1 km. The operating wavelength λ is fixed for a laser using ruby as the active element, although some "tuning" of the wavelength is possible by varying the temperature of the ruby rod. Abella and Cummins (1961) estimated the temperature dependence to be 0.065Å/deg. Long (1963) has indicated that the facility of tuning the laser wavelength may be needed in order to avoid the strong water vapour absorption lines between 6942Å and 6944Å (Fig. 2.4(a)). Since water vapour is always present in the atmosphere, operation at any of the absorption line wavelengths would seriously

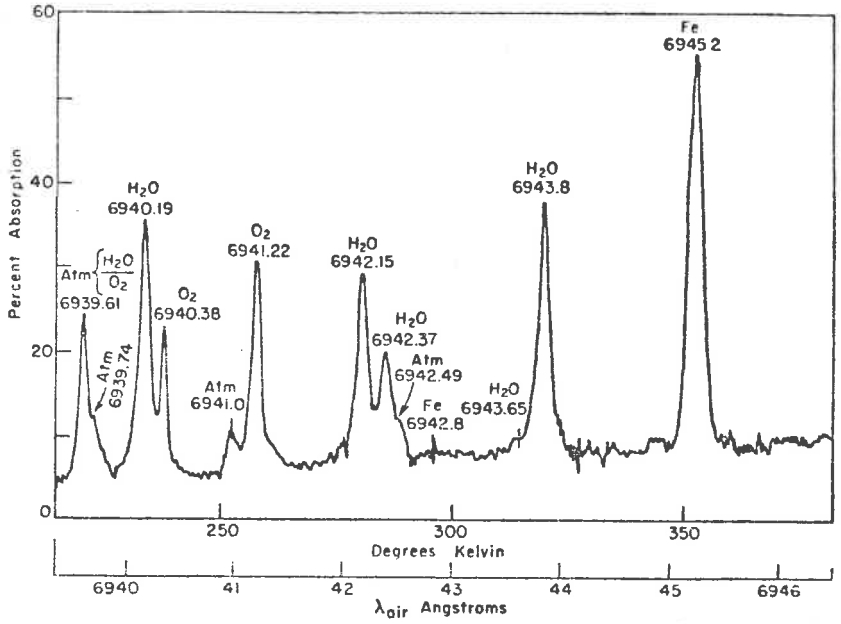

Figure 2.4(a) Atmospheric absorption spectrum between 6940 and 6946 Å (Long,1963).

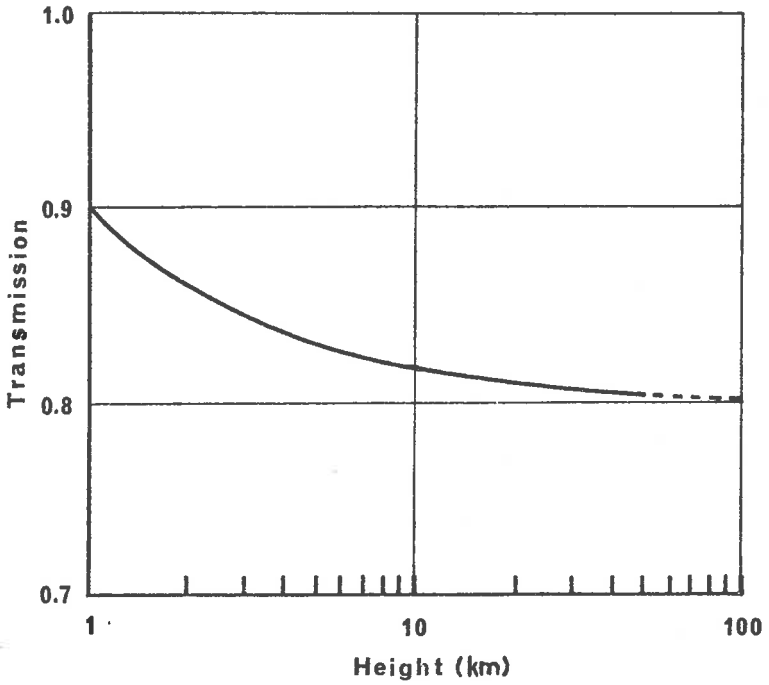

Figure 2.4(b) Atmospheric transmission at 0.7u (Elterman,1964).

decrease the atmospheric transmission T.

The value of T is one of the most difficult parameters to estimate reliably, since its value will vary considerably with local atmospheric conditions. It is clear, however, that most of the attenuation takes place in the first few kilometres above the earth's surface, as shown in Fig. 2.4(b). This curve has been calculated from Elterman's (1964) tabulations of absorption coefficient vs. height for 0.70 microns. Although these tabulations have been based on a model atmosphere containing only molecular, aerosol, and ozone components, results are substantially in agreement with those obtained from airborne nephelometer measurements over Woomera, South Australia (Koerber and Crosby, 1960). The value of T will therefore be taken as constant for heights above 10 km, and equal to 0.8.

The collecting surface area S corresponds to that of a 12" diameter mirror. The receiver efficiency η has been chosen equal to 0.25, and assumes the use of a narrow-band interference filter having approximately 50% transmission. The remaining losses are due to reflections at air-glass surfaces. The quantum efficiency ζ is 3%, and represents that of a photomultiplier with R.C.A. type S-20 photocathode.

The molecular scattering cross-section σ has been tabulated for different wavelengths by Penndorf (1957), and corresponding to a wavelength of 0.7 microns, $\sigma = 1.7 \times 10^{-31}$ m^2 .

TABLE 2.1

E	laser pulse energy	1.0 joule
λ	operating wavelength	6943Å
T	atmospheric transmission	0.8
S	collecting surface area	0.07 m^2
η	receiver efficiency	0.25
Q	p.m. quantum efficiency	0.03
Δh	recording channel width	1 Km
c	velocity of light	3×10^8 m.sec^{-1}
k	Planck's constant	6.63×10^{-34} joule.secs
σ	scattering cross-section/molecule	1.7×10^{-31} m^2

Using the values in Table 2.1, equations 2.5 and 2.6 have been evaluated at 10 km height intervals between 10 and 90 km, and the results are shown in Table 2.2. At each height, column (3) shows the signal pulse count rate $N_s(h)$, and column (4) shows the total signal count recorded from a 1 km height interval centred at that height for each laser firing.

2.5 Signal to Noise Ratios

A number of factors will influence the accuracy of the results obtained from an optical radar. These may be grouped into 3 main categories:

1. Sources of optical noise

TABLE 2.2

(1) Height h(km)	(2) Density $n(h)m^{-3}$	(3) Signal Count Rate $N_s(h)sec^{-1}$	(4) Signal Count Per 1km.channel $C_s(h)$	(5) Signal/Noise Ratio N_s/N_n	(6) Total Count Rate $N(h)$	(7) Total Count per channel $C(h)$	(8) Integrations for >5% accuracy
10	8.6×10^{24}	3.1×10^{8}	2.0×10^{3}	3.1×10^{6}	3.1×10^{8}	2.0×10^{3}	1
20	1.8×10^{24}	1.6×10^{7}	1.1×10^{2}	1.6×10^{5}	1.6×10^{7}	1.1×10^{2}	4
30	3.8×10^{23}	1.5×10^{6}	1.0×10^{1}	1.5×10^{4}	1.5×10^{6}	1.0×10^{1}	40
40	8.3×10^{22}	1.9×10^{5}	1.3×10^{0}	1.9×10^{3}	1.9×10^{5}	1.3×10^{0}	310
50	2.1×10^{22}	3.0×10^{4}	2.0×10^{-1}	3.0×10^{2}	3.0×10^{4}	2.0×10^{-1}	2×10^{3}
60	6.4×10^{21}	6.4×10^{3}	4.3×10^{-2}	6.4×10^{1}	6.5×10^{3}	4.4×10^{-2}	9.3×10^{3}
70	1.8×10^{21}	1.3×10^{3}	8.9×10^{-3}	1.3×10^{1}	1.4×10^{3}	9.6×10^{-3}	4.9×10^{4}
80	4.2×10^{20}	2.4×10^{2}	1.6×10^{-3}	2.4×10^{0}	3.4×10^{2}	2.3×10^{-3}	3.5×10^{5}
90	6.6×10^{19}	2.9×10^{1}	2.0×10^{-4}	2.9×10^{-1}	1.3×10^{2}	8.7×10^{-4}	9.2×10^{6}

2. Sources of electrical noise

3. Statistical errors

These categories will now be discussed individually.

2.5.1 Sources of optical noise

Assuming operation at a suitable site, where illumination of the night sky by artificial light sources is negligible, there will be three sources of optical noise:

(a) Laser fluorescence

(b) Higher order scattering

(c) Night sky radiation

Fluorescent radiation is emitted by a laser following emission of the main laser pulse, when the population inversion, and hence gain, of the laser material has fallen to a level below that necessary to sustain laser action. Although the intensity of the fluorescent radiation is many orders of magnitude lower than that of the laser pulse, it persists for several milliseconds following the main pulse. Scattering of the fluorescent radiation from the first few kilometers of the atmosphere could thus mask scattering from the main laser pulse at greater heights. Fortunately, the fluorescent "tail" may be removed from the transmitter output by means of an optical shutter, and the design of a suitable shutter will be described in a later section.

Contamination of the signal by higher order scattering is caused

by light scattered from the transmitted pulse at low altitudes travelling a distance outside the field of view of the receiver, being scattered back into the receiver beam, and then being scattered a third time to reach the receiving mirror. Calculations of this effect are difficult and unreliable due to the strong dependence on scattering conditions very near the earth's surface. The pulsed searchlight experiments of Friedland et al. (1956) indicate that the effect of multiple scattering is small, being typically less than one percent of the normal signal.

The effect of multiple scattering may be checked experimentally by deliberate misalignment of the transmitter and receiver, so that the transmitted beam and receiver field of view just fail to overlap. Under these conditions, any signal received as a result of laser firing must be due to multiple scattering.

The night sky radiation at medium latitudes, under moonless conditions, comes mainly from three sources; the airglow, the integrated starlight, and the zodiacal light. The background intensity will thus vary not only with time, but also with the region of sky being observed. The starlight contribution is concentrated towards the galactic plane, while the zodiacal light is concentrated towards the plane of the ecliptic and the longitude of the sun.

Direct measurements of night sky emission do not separate the contributions from the airglow and zodiacal light. In the region 6900-7000$\mathring{A}$, Broadfoot and Kendall (1968) quote a mean intensity of

approximately 2 Rayleighs/Å (1 Rayleigh is equivalent to 10^{10} photons m^{-2} sec^{-1}) after taking steps to minimize the stellar background contribution in their measurements. Since in the red and far red region of the spectrum the starlight contribution varies between 10% and 50% (Chamberlain, 1961), the total night sky radiation in this wavelength range will lie between 2 and 4 R/Å, with the maximum value occurring when the region of sky being observed includes the milky way.

Although the background radiation is by no means uniform over the wavelength spectrum, it is essentially wideband in comparison with the laser output bandwidth of 0.1Å or less. It is therefore possible to reduce the background contribution by the use in the receiver of a narrow-band optical interference filter with bandpass centred on the laser wavelength.

The photon rate collected by the receiving mirror is $RB(\omega_r/4\pi)S$ where R is the background intensity in Rayleighs/Å, B is the filter bandwidth, ω_r is the receiver solid angle field of view, and S is the receiver collecting area. The received photoelectron count rate N_b due to sky radiation is therefore given by

$$N_b = RB\theta_r^2 S\eta Q/16 \text{ sec}^{-1} \qquad \ldots 2.7$$

where θ_r is the receiver beamwidth, η is the receiver efficiency, and Q the photomultiplier quantum efficiency.

From equation 2.7 it can be seen that the noise count rate is reduced as the filter bandwidth is decreased. Unfortunately the peak

transmission of an interference filter also decreases as the bandwidth is reduced, typical values quoted by manufacturers being 50-60% transmission at 20Å bandwidth, and 40-50% at 10Å, with a rapid decrease as the bandwidth is reduced below 10Å. In order to be consistent with the 50% filter transmission assumed in Section 2.4, a bandwidth of 10Å will be assumed in the evaluation of equation 2.7.

The receiver field of view θ_r should also be made as small as practicable to reduce the sky noise contribution. The minimum value of θ_r will be determined by the transmitted beam divergence θ_t, and by the increasing difficulty of maintaining receiver-transmitter collimation for very small fields of view. A value of 0.001 radian should be relatively easy to achieve for θ_t, making a value of 0.002 radian for θ_r reasonable.

On substituting these values into equation 2.7, together with a value for N of 4 Rayleighs/Å, we obtain $N_b = 52\ sec^{-1}$. By comparison with the figures for signal count rate N_s in Table 2.2, it can be seen that the count rate due to sky radiation becomes equal to the signal count rate at an altitude between 80 and 90 km.

2.5.2 Sources of Electrical Noise

The predominant source of electrical noise will be photomultiplier dark current. Even when operated in complete darkness, electrons are emitted by a photocathode and amplified by the multiplier system, to appear at the anode as pulses indistinguishable from those due to

signal photons. Thermionic emission appears to be responsible for the largest component of the dark current, which is therefore strongly temperature dependent. The dark current depends, in addition, on the type of photocathode material, and varies widely between individual tubes of the same type.

At the laser wavelength, the most suitable photocathode material is the tri-alkali type (E.M.I. S-20). Experiments carried out on several examples of this type of tube by Gadsden (1965) indicate dark current count rates of 2×10^2 to 2×10^3 sec^{-1} at room temperature, falling to 10-30 sec^{-1} when the tubes were cooled to $-10^{\circ}C$. It is evident that even a low noise tube, if operated at room temperature, would seriously increase the total noise count rate. Cooling of a selected low-noise tube should reduce the electrical noise contribution to a value small compared with that due to sky radiation.

2.5.3 Statistical Errors

From Table 2.2 it can be seen that the signal return per laser firing from heights above 40 km consists of less than one count per kilometer channel width. It is evident therefore that in order to obtain a statistically significant result from the upper regions of the atmosphere, some form of integration of the signal over a large number of laser firings will be necessary.

Suppose that after a number of such integrations a total count of C pulses has been received from a given height interval. This count

number contains both the signal pulses C_s and the noise pulses C_n, such that $C = C_s + C_n$. The average number of noise pulses $\overline{C}_n$ expected during the total integration period can be determined quite accurately by an extended measurement of the background count rate. The difference between the total count and the expected background is the desired signal count C_s. The fractional error e in a measurement of C_s is defined by $e = \Delta C_s / C_s$, where ΔC_s is the standard deviation. Then, after Morton (1968),

$$e = C^{\frac{1}{2}} / (C - \overline{C}_n) \qquad \ldots 2.8$$

2.5.4 Discussion

The total noise count rate N_n is the sum of the contributions due to sky radiation and photomultiplier dark current, and on the basis of the estimates in Sections 2.5.1 and 2.5.2 could range upwards from 50 pulses per sec. depending on the quality of the photomultiplier detector. A value for N_n of 100 sec^{-1} should thus be fairly representative, and will be used in the following discussion.

Values of the signal to noise ratio $N_s(h)/N_n$ have been tabulated in column (5) of Table 2.2. The total count rate $N(h) = N_s(h) + N_n$ is tabulated in column (6), and the total count $C(h)$ recorded in each 1 km wide channel per laser firing is shown in column (7). It can be seen that the signal to noise ratio becomes unity at an altitude between 80 and 90 km, suggesting that altitudes of this order could be reached if sufficient accuracy could be achieved in the measurements

of C(h) and $\overline{C}_n$. Because of the small values of the total count recorded in each channel per firing at heights above 20 km, it is evident that this accuracy will only be achieved by repeated laser firings, and integration of the count from each height range.

Using equation 2.8, the number of such integrations necessary to achieve an accuracy of 5% at each height has been calculated, and tabulated in column (5) of Table 2.2. It is evident that the maximum height of any region which can be studied by a laser radar having the parameters assumed in this chapter will be set not by noise limitations, but by the time available for one complete observation, and on the repetition rate of the laser. Even at a repetition rate of one firing per second, a time of 100 hours would be required to achieve 5% accuracy at 80 km altitude.

The count recorded in each channel for each laser firing may be increased by increasing the width of each channel. However, if the channel width is such that the count rate N(h) changes significantly during the time that a channel is open, then corrections may be necessary to the total count recorded in each channel in order to deduce the actual count rate corresponding to a given height.

The number of firings necessary to obtain a measurement at a given height to a given degree of accuracy can be reduced by an increase in the laser energy output per pulse, or by increasing the receiver collecting surface area. An increase in laser output energy would

have the further advantage of improved signal to noise ratio throughout the height range, and would be necessary for observations above 70-80 km. For observations below 70 km, the signal to noise ratio is adequate with 1 joule output energy, and an increase in collecting surface area would produce a corresponding decrease in the number of laser firings needed to reach a given height.

At low altitudes, where count rates are high, the rate at which data can be acquired is most likely to be set by the resolving time of the recording system. Owing to the random rate of arrival of signal photons, there is a certain possibility that more than one pulse will arrive during the resolving time of the pulse counter. Thus the observed count rate n will be smaller than the true rate N. If the resolving time of the counter is t, then the total "dead time" of the counter per second is nt, and

$$\frac{N}{n} = \frac{1}{1-nt} \qquad \ldots 2.9$$

Suppose that the observed count rate is to be within 5% of the true count rate, and the resolving time of the recording system is 10^{-7} sec. Then the maximum rate at which random pulses can be recorded is 5×10^{5} sec^{-1}. In practice, corrections could be calculated from equation 2.9 and applied to the observed count rate in order to maintain 5% accuracy for observed count rates up to 2 or 3 times higher than 5×10^{5} sec^{-1}. At still higher count rates, however, the corrections would become excessive, requiring the resolving time to be known very

accurately.

If the count rate from a given height exceeds the maximum rate which can be accepted by the recording system, optical filters or some other means may be used to attenuate the received light flux in order to reduce the count rate to the required amount. This has the undesirable effect of reducing the count rate from greater heights, where the count rate may already be very low. It is clear therefore that the resolving time of the counting system will determine not only the rate at which data can be acquired from low altitudes, but also the dynamic range of the laser radar, and hence the height range which may be covered in one sequence of firings.

CHAPTER 3

THE LASER

3.1 Introduction

Early in 1964 a number of American and British manufacturers was approached regarding the supply of a suitable laser. In June 1964, a unit was ordered from RCA of Burlington, Mass., U.S.A., to the following specifications:

Energy Output	-	1 Joule
Pulse Length	-	< 1 μsec.
Repetition rate	-	1 pulse/sec.

The laser, with spare ruby rod and flash tube, was received in May 1965. No power supplies or cooling systems were supplied by the manufacturer.

The following sections of this chapter describe in detail the characteristics of the laser, and the design and construction of the necessary power supplies and cooling system. A number of modifications made to the laser in order to ensure adequate reliability and life will also be described, since the need for these modifications considerably delayed completion of the laser radar system.

3.2 Description of Laser

The laser element is a ruby rod (6" long by 5/16" diameter) having

a brewster face at one end and a total internally reflecting end or wedge cut at the other. The optical cavity is formed between the wedge cut on the ruby, and a sapphire optical flat having 16% reflectivity. Q-switching and a 90° change in direction of the beam are accomplished by a rotating prism within the optical cavity.

The ruby rod is at one focus of an elliptical cavity, and is optically pumped by an E.G. and G. type FX-55 Xenon flash tube at the other focus of the cavity. Both the ruby rod and flash tube are enclosed in glass water-jackets. The complete laser is enclosed in a gas-tight cover, and operates in an atmosphere of dry nitrogen. The nitrogen atmosphere is necessary to prevent rapid deterioration of the aluminised reflecting surfaces of the elliptical cavity, and to prevent condensation of moisture on the cooling jackets.

The Q-switch prism is driven by a small synchronous motor. A transistorised inverter to supply the 400Hz driving voltage for the motor, and the electronics needed to provide the high-voltage trigger for the flash tube, are mounted on the laser base plate. A magnetic pick-up coupled to the rotating prism assembly provides synchronisation between triggering of the flash tube and prism rotation. A contact closure external to the laser ensures flash-tube triggering during the following Q-switch cycle. As originally supplied by the manufacturer, the Q-switch prism was driven at 48,000 r.p.m.

3.3 Cooling System

The ruby rod and flash tube are mounted in separate water jackets, each requiring a pumping and cooling system. The water used to cool the flash tube is at ambient temperature, and must be de-ionized, since the water flows over the high-voltage terminals of the tube. The water supplied to the ruby rod is maintained at a temperature of 40°F.

No specification for flow rate or cooling capacity were supplied by the manufacturer, and the required quantities had to be estimated. It was reasoned that adequate circulation would be achieved if the water in each water jacket were changed completely at least once for each laser firing. At a repetition rate of 1 firing per second, this requires a flow rate of approximately 1 gal/minute.

At the maximum repetition rate, the power input to the flash tube is 2000 joules/sec, which is equivalent to 7200 BTU/hour. Approximately 35% of this power is absorbed as heat in the water jacket surrounding the flash tube, the remainder reaching the ruby as radiation in the 0.35 - 1.1μ range. (Gones and Newell, 1966). The required cooling capacities of the two systems are therefore 2500 BTU/hour for the flash tube, and 4700 BTU/hour for the ruby.

A closed circuit cooling system was constructed to meet these specifications. A pair of "Gono" pumps of approximately 1 gal/min capacity were used to circulate water around the ruby and flash tube

from separate storage tanks. Flow gauges and by-pass valves were incorporated in each cooling system so that the flow rates could be individually controlled. A stainless steel storage tank of approximately 1 gallon capacity was used to supply water to the flash tube through a combination of nylon and natural rubber tubing. The use of metal fittings other than stainless steel was avoided to minimise ionic contamination of the water. A 4-gallon storage tank coupled to a sealed-unit refrigeration plant of 6000 BTU/hour capacity was used to supply water at 40°F to the ruby rod. Two separate thermostats controlled the refrigerator, and a temperature stability of ± 1°F could be maintained.

During tests of the cooling system, a brown deposit gradually formed on the inside surface of the glass water jackets surrounding both the ruby rod and flash tube. The deposit seriously decreased the amount of excitation energy reaching the ruby after approximately 100 flashes. Cleaning of the water jackets involved a considerable amount of dismantling and rebuilding, followed by the need for optical realignment of the laser. The cause of the contamination was eventually traced to the neoprene stators used in the "Mono" pumps. Small particles of neoprene suspended in the water deposited on the glass surfaces under the conditions of extreme irradiation during firing of the flash tube.

The "Mono" pumps were therefore replaced by a pair of "Charles Austen" centrifugal pumps. In these pumps there is no contact between

the rotor and stator, thus minimising the possibility of abrasion which could cause small particles of solid material to enter the water. At the same time, the flexible nylon tubing originally used in the cooling system was replaced with rigid nylon tubing, to eliminate any plasticisers which may also have contaminated the water.

The modified system has proved quite satisfactory in service. As a precautionary measure, the water in each system is changed approximately once a month, and no further problem with water jacket deposition has been encountered.

3.4 Nitrogen System

The nitrogen supply to the laser consists of a standard 220 c.ft. cylinder of industrial dry nitrogen. Pressure reduction is achieved by a medical oxygen regulator assembly, since it was found that industrial units would not provide satisfactory regulation at the very small rates of flow required. A flow gauge and pressure safety valve have been incorporated in the system.

3.5 Main Power Supply

The electrical energy required by the Xenon flash tube is stored in a capacitor bank, and discharged through the flash tube when this is triggered by a high-voltage pulse. The function of the power supply is to re-charge the capacitor bank between flash-tube firings. The current capability of the power supply determines the maximum

achievable repetition rate. In order to limit the peak current density in the flash tube, the current pulse is shaped to be approximately rectangular. This is achieved by arranging the storage capacitors and a suitable inductance into a lumped-constant delay line, referred to as the pulse forming network (P.F.N.). The characteristic impedance Z_o of the delay line must be matched to the load resistance of the flash tube when ionized (0.6 ohms).

The total capacitance C and inductance L of the P.F.N. are determined by the required values of pulse length τ and characteristic impedance Z_o. From Craydon (1956)

$$\tau = 2\sqrt{LC} \qquad Z_o = \sqrt{L/C}$$

The energy E stored in the P.F.N. is determined by the voltage V to which the capacitors are charged:

$$E = \tfrac{1}{2} CV^2$$

Specifications supplied with the laser called for a pulse length of 0.5 msec, and an energy of 2000 joules. A suitable P.F.N. would thus consist of 400 μF capacitance and 144 μH inductance and would be charged to 3 KV. In order to approximate a delay line as closely as possible, the total inductance and capacitance must be divided into a number of equal sections. As the number of sections is increased, the rise and fall times of the resultant current pulse are reduced. Since in the present application short rise and fall times are not

required, a 4-section P.F.N. was designed, each section containing two 54 μ F pulse discharge capacitors. These capacitors are specifically designed for use in a P.F.N., having low self-inductance and high discharge-current capability.

During discharge of the P.F.N. a current of 2500 amps will flow. The inductance used in the P.F.N. must therefore have a low resistance if ohmic losses are not to be excessive. The actual coil consists of 114 turns of 9 S.W.G. enamelled copper wire on a former of 3.5" diameter and 21" length. The resistance of the coil is 0.05 Ω. The output of the P.F.N. is connected to the laser head by a pair of heavy duty welding cables, rated for 300 amps continuous current. It is estimated that under these conditions ohmic losses are less than 10%.

The current pulse produced by the P.F.N. was checked by charging the network to a few volts, and switching the output across a 0.6 Ω resistance. The resultant voltage pulse produced across the resistance was recorded on a storage oscilloscope. The pulse was found to have rise and fall times of 0.1 and 0.2 msec respectively, and to be 0.5 msec wide at the 50% points.

To charge the P.F.N. to 3 kV in a time of 1 second requires a steady current of 1.2 amps. It is evident that because of the large current and long charging period involved, the resonant charging technique usually used in R.F. radar transmitters cannot be used to control the charging current.

In order to allow testing of the laser head to proceed, a simple low current power supply (Mk.1) was initially constructed using a power transformer which was already available. The power transformer, rated at 0.35 amps output current, was used in conjunction with a full-wave rectifier to produce an output voltage of 3 kV. The maximum output current of the rectifier was limited to 0.3 amps by a series resistance, and fed to the P.F.N. The P.F.N. voltage thus rose exponentially towards 3 kV, and the recycling time of the Mk.1 power supply was approximately 15 secs.

This power supply was later rebuilt in an attempt to increase the firing rate, while still using the same transformer-rectifier system. By reconnecting the transformer voltage tappings to produce the highest voltage possible, and reducing the series resistance, the peak charging current was increased to 0.7 amps, while the average current was still within the transformer rating of 0.35 amp. In this way a recycling time to 2000 joules of 6-7 secs was achieved. The charging resistors were forced-air cooled by a small fan.

The circuit of the Mk.2 power supply is shown in Fig. 3.1. In this circuit, the voltage across the P.F.N. is monitored by a Schmitt trigger circuit, and the charging current is interrupted when a preset voltage has been reached. The P.F.N. may be charged, and the laser triggered, by manual operation of the "CHARGE" and "FLASH" buttons, or automatically by switching to the "AUTO" mode of operation. In this mode, the P.F.N. is recharged and the laser fired automatically, at the highest repetition rate allowed by the charging circuit. The

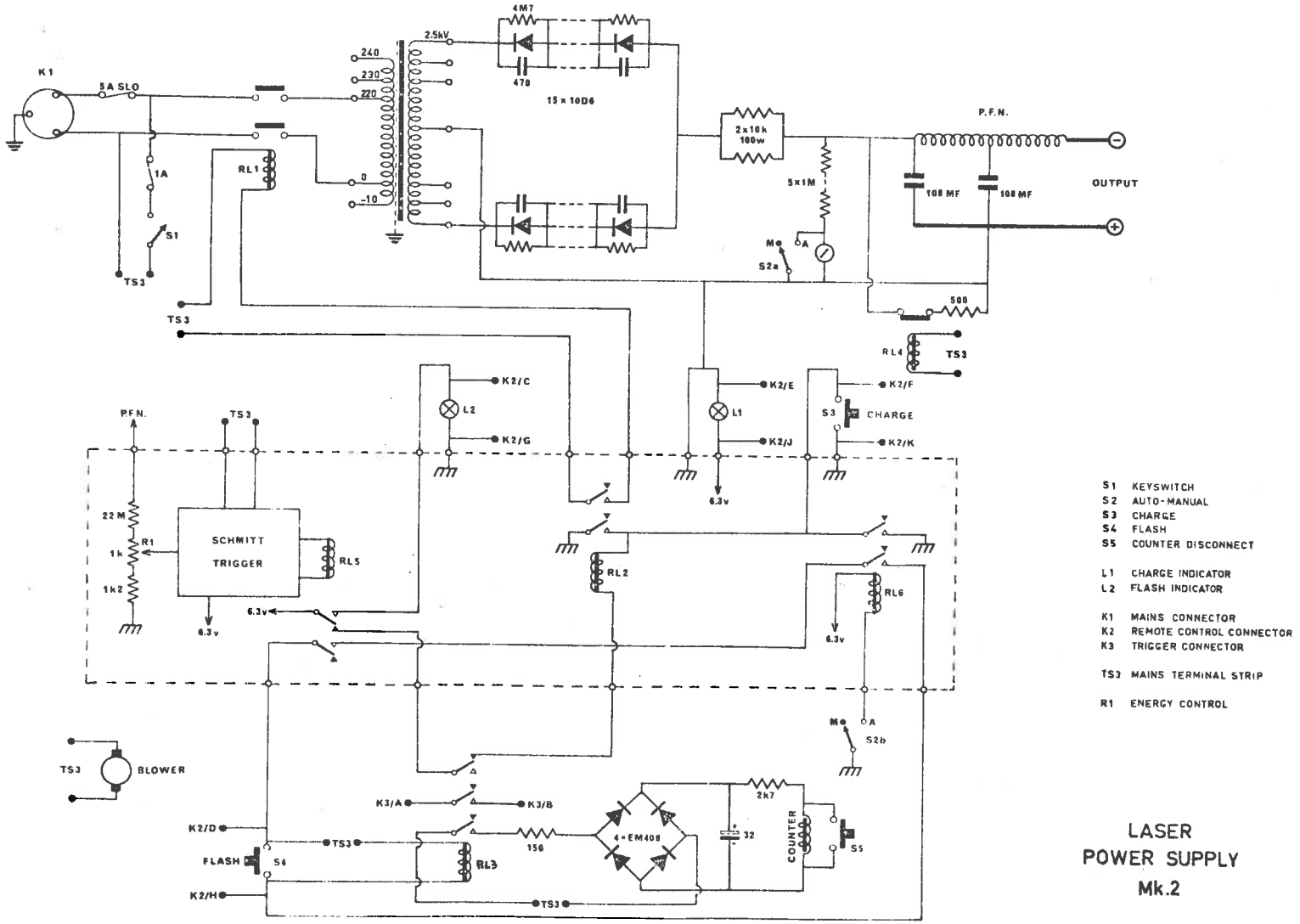

Figure 3.1 Circuit diagram of main laser power supply.

number of times that the laser has been fired is counted and displayed by a mechanical register, and a front panel meter calibrated in Joules measures the energy stored in the P.F.N.

Refer to Fig. 3.4 and consider the Manual mode of operation (Switch S2 in M position). When the "CHARGE" button S3 is pressed, relay RL2 closes, and is held closed after S3 is released by the latching action of one of its contacts. The closure of RL2 causes contactor RL1 to close, applying power to the transformer and rectifier, and causing the charging cycle to begin. The P.F.N. voltage is monitored by the Schmitt trigger, and when a value preset by means of potentiometer R1 has been reached, relay RL5 closes. The closure of RL5 causes the "FLASH" indicator lamp L2 to light, and relay RL2 and hence contactor RL1 to open, thus interrupting the charging current. Closure of RL5 causes RL2 to open, thus ensuring that RL1 will not close again when the P.F.N. is discharged until S3 is pressed. Pressing the "FLASH" button S4 will now cause relay RL3 to close, thus triggering the laser via trigger connector K3. Closure of RL3 will also cause a voltage pulse to operate the mechanical register, indicating a laser firing.

In the Automatic mode of operation (Switch S2 is in the A position) relay RL6 is closed, causing RL2 and hence RL1 to be held closed at all times except when RL5 is closed, i.e. when the P.F.N. is fully charged. Closure of RL5 now also causes RL3 to close, thus triggering the laser and activating the counter. The cycle is repeated auto-

matically as RL5 opens, causing RL2 to close. In the Automatic mode, the front panel meter is shorted out by switch S2a to avoid continuous pointer movement.

As a safety precaution, a discharging resistance is connected across the capacitor bank at all times when the power supply is not in operation. The resistance is disconnected by contactor RL4 when mains power is applied.

For reasons explained in later sections, most of the work carried out with the laser has been at input energies of 600-700 joules. In order to maintain the flash-tube operating voltage above the 1100 volts minimum quoted by the manufacturer, it is necessary to charge the P.F.N. to at least 2200v, since during discharge only one half of the P.F.N. voltage appears across a matched load. The P.F.N. has therefore been shortened to two sections of total capacitance 216 μF, requiring 2300v for 600 joules. The discharge pulse is approximately 0.3 msec long, with rise and fall times of 0.1 msec and 0.15 msec respectively. The recycling time to 600 joules is 2 seconds.

3.6 Low Voltage Power Supplies

The triggering and motor driving circuits incorporated in the laser require the following D.C. supplies:

50v at 0.4 amps
25v at 0.25 amps
12v at 0.05 amps

Three mains operated regulated power supplies were constructed to these specifications, and enclosed in a single cabinet.

3.7 Laser Tests and Modifications

Following completion of the power supplies and cooling unit, the laser was set up in the laboratory with its output aperture directed towards a diffusing screen, and a photocell placed close to and facing the screen was connected to an oscilloscope in order to monitor the laser light output. Initial attempts to trigger the laser produced no light output at all, and it was found that the flash tube was not firing. Investigation revealed that the tube triggering voltage was of opposite polarity to the voltage supplied by the P.F.N., due to an incorrect polarity indication on a drawing supplied with the laser.

Reversal of the P.F.N. connections enabled the flash-tube to be fired. The flash-tube light output waveform was monitored by means of the photocell, and found to consist of a pulse with shape approximately equal to that predicted for the P.F.N. current pulse. However, there was no sign of a much shorter, high intensity pulse which would correspond to laser action. It was therefore decided to check the optical alignment of the laser, since this could have been disturbed during shipment.

No alignment instructions had been supplied with the laser, and a technique had to be evolved which would allow all surfaces to be made optically parallel. Attempts to align the surfaces with the aid

of a standard 2" aperture auto-collimator failed because of the small aperture of the laser optics, and the strong absorption inside the ruby. Eventually the beam from a small He-Ne gas laser was found to be sufficiently intense to produce quite strong reflections from all surfaces, and alignment was carried out with the aid of a small telescope, as described in detail in Section 3.8.

Following completion of the alignment, the laser was again set up in front of a screen and photocell, and tested. This time, laser action was observed, as evidenced by a short, very high intensity pulse superimposed on the flash tube light output waveform. A piece of black P.V.C. tape placed across the laser output window showed a blister mark after a single laser firing, and this has since been used whenever an immediate check for laser action is required.

In order to examine the true shape of the laser output pulse with greater detail, the photocell was replaced with an E.G. & G. type SD100 high speed photodiode. When connected to a Tektronix 517A oscilloscope, the rise time of the complete system is 7 nsec. The pulse shape observed has been reproduced in Fig. 3.2(a), and it can be seen that the laser output pulse consisted of 6 spikes in a total interval of 2 μ sec. It was also observed that the number and total duration of the spikes varied from shot to shot in a random fashion.

Since uncertainty in the pulse shape and duration could lead to errors in timing, and hence in the estimation of the range of an echo,

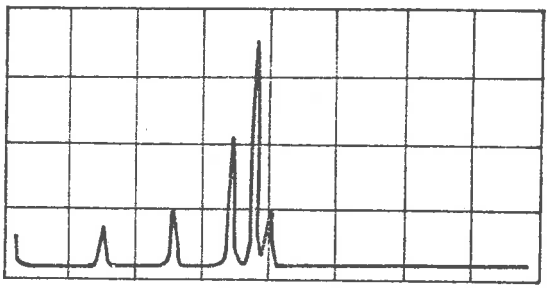

0.5 usec/div.

(a) Pulse shape originally observed

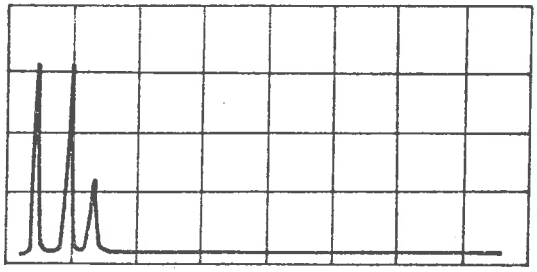

0.5 usec/div.

(b) Normal laser output pulse shape

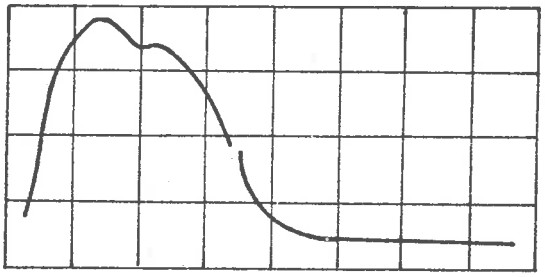

0.1 msec/div.

(c) Flash tube light output

Figure 3.2 Laser light output waveforms.

the reason for the unsatisfactory pulse shape was investigated. The Q-switch housing was disassembled, and it was found that the Q-switch prism was badly pitted on its hypotenuse face, from which the laser beam is totally internally reflected. It was clear that the scattering occurring at the damaged surface was the cause of the unsatisfactory pulse shape.

No apparent reason for the damage could be found, and a new prism was therefore ordered from an optical manufacturer and installed. The prism was made from fused quartz ("spectrosil"), with surfaces flat to 0.1 of a wavelength of sodium light, and angles accurate to $\pm$ 2 seconds of arc. At the same time, the rotating Q-switch assembly was dynamically balanced, in order to eliminate some vibration which had been apparent in the system.

Following optical alignment, tests with the new prism installed showed that at 2000 joules input to the laser, the output consisted of 5 spikes in approximately 0.5 μsec. However, after 30 or 40 flashes, pitting again became obvious on the prism. The output energy declined, and the number of output spikes increased to about 10 in 4 or 5 μsec. It was thus apparent that the prism could not withstand the radiation intensity inside the optical cavity. Since this can be caused by "hot spots" in the radiation pattern of an individual ruby rod, it was decided to try the spare rod which had been supplied with the laser.

However, attempts to align the laser using the spare rod and a new prism proved unsuccessful, due to the fact that the ruby rod was

found to split an incident gas laser beam into two distinct reflected beams. No laser action could be obtained when the alignment was completed using only one or other of the reflected beams. The ruby rod was removed from its water jacket, and the angle of the wedge was measured. The angle was found to differ from 90 deg. by 1 min 36 sec, and the rod was therefore returned to the manufacturer as faulty.

While awaiting the arrival from the manufacturer of a specially selected, superior internal quality (S.I.Q.) Czochralski-grown ruby rod, a number of other modifications were tried using the original ruby rod. The Q-switch speed was reduced from 45,000 r.p.m. to 24,000 and eventually to 12,000 r.p.m. in an attempt to lower the lasing threshold, and hence the input energy necessary to achieve a given output. However, no increase in Q-switch life was observed, confirming the fact that the power density in the optical cavity, and not the degree of excitation of the ruby, was responsible for the damage.

Following installation of the new S.I.Q. ruby rod, experiments showed that the lasing energy threshold was lower, and the far-field radiation pattern of the output was more uniform. Unfortunately the life of the Q-switch was not increased significantly. After further discussion with the manufacturers of the laser, the quartz Q-switch prism was replaced by one made of a borosilicate crown glass, of refractive index 1.56. The refractive index of quartz (1.41) is such that the critical angle for total internal reflection is very nearly 45°, and it was reasoned that a higher refractive index would prevent

the possibility of light "leakage" through the T.I.R. face under high radiant intensities, and consequent damage to the face. This modification did improve the Q-switch life to some extent, particularly for output energies of around 0.5 joules.

The result of these experiments indicated that it would not be possible to obtain anywhere near 1 joule of output energy from the laser, and at the same time to achieve a reasonable life for the Q-switch prism. It is now believed that the reason for this lies in the relatively small diameter of the ruby rod (5/16"), since it has been noted that laser systems supplied by other manufacturers to approximately the same performance specifications generally make use of considerably larger rods, a typical diameter being 0.5". Since it would not be possible to fit a larger rod to the present laser without completely rebuilding the system, experiments were carried out in order to see if the life could be improved to a useful extent by reducing the output energy requirement. A new prism was installed, and it was found that a life of 10,000 shots was obtained when output energy was maintained between 0.2 and 0.3 joules. It was subsequently found that if the output energy were more carefully controlled to a maximum of 0.2 joules, a life in excess of 20,000 shots could be obtained with no sign of damage apparent on the prism surface. It would therefore appear that the threshold for prism damage lies between 0.2 and 0.3 joules. The laser is now considered to have an output capability of 0.2 joules, and most of the results presented in later sections have been obtained using this value of energy.

During the course of these experiments, a number of other modifications had to be carried out to the laser. Both the water-jacketed flash tubes supplied with the laser failed after less than 100 shots at 2000 joules input, due to fracture of the glass water jackets. Close examination of the water jackets and flash tubes revealed fine flaking of the glass on the outer surface of the water jacket, indicating the use of an unsuitable type of glass. Considerable pitting had also taken place on both the flash tube terminals and the aluminium end caps of the water jacket, obviously due to inadequate contact, and consequent arcing. It was further obvious that no allowance had been made for differential expansion between flash tube and water jacket during operation. A new water jacket was therefore constructed from quartz tubing and having stainless steel end caps. Contact to the flash tube terminals is by 8 slightly flexible "fingers" which allow the contact to slide should the flash tube expand during operation. Measurements have shown a contact resistance of 0.002 ohms. The end-caps are held to the outer tube by rubber O-ring seals, allowing a flash-tube to be withdrawn and replaced without the need to remove the water jacket from the laser.

The original Q-switch housing as supplied with the laser had to be dismantled completely each time a prism was changed. Because of the large number of prisms which had been fitted to the housing, it was found that the bearing journals and also the locating pins between sections of the housing were becoming seriously worn. A new Q-switch housing was therefore constructed, which incorporates several improve-

nents. Prisms may now be changed without dismantling of the housing, and the timing of the flash tube trigger pulse may be varied simply by loosening a locking collar over the upper part of the Q-switch housing.

It was found that the laser was prone to trigger randomly from noise pulses picked up by the external trigger lead. This problem has been overcome by fitting a small relay inside the laser housing.

The laser head in its current state of development is shown in Fig. 3.3. An input energy of approximately 600 joules produces an output energy of 0.2 joules, consisting of 3 spikes in 0.5 μsecs. The output waveform is shown in Fig. 3.2(b). The input energy must be gradually increased to compensate for flash-tube ageing, to approximately 700 joules after 10,000 shots. Flash tubes are replaced when triggering becomes unreliable. The flash tube light output pulse shape is shown in Fig. 3.2(c), and consists of a pulse about 0.3 msec wide. The short break in the pulse trailing edge corresponds to laser action. For a given input energy, maximum output energy is obtained when the flash tube is triggered 0.3 - 0.4 msec before the prism Q-switch reaches the position which allows laser action.

3.3 Optical Alignment of the Laser

The experimental arrangement used for optical alignment of the laser is illustrated in Fig. 3.4, and the essential components are shown in simplified form in Fig. 3.5. The sapphire flat which forms

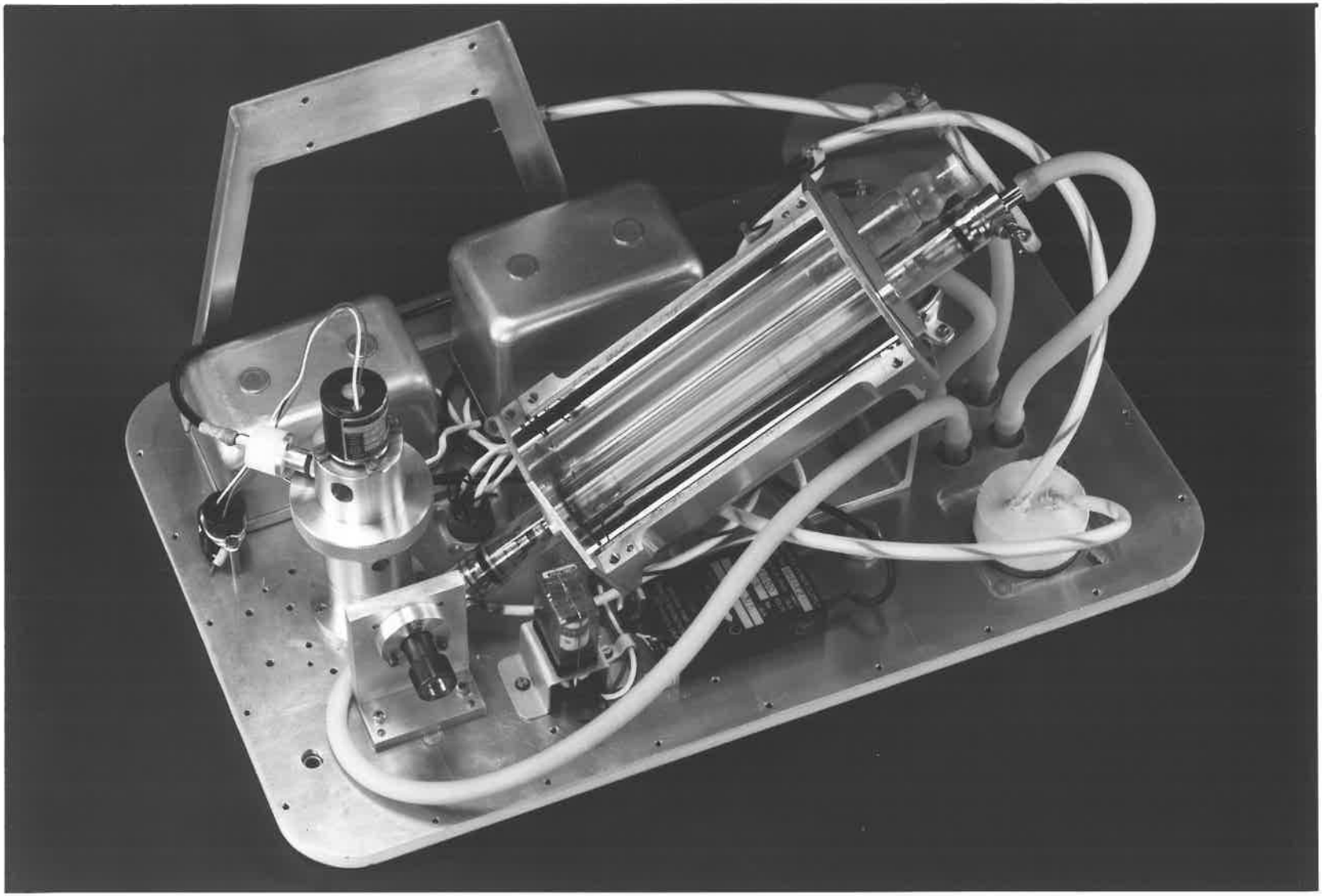

Figure 3.3 The laser, with cover removed.

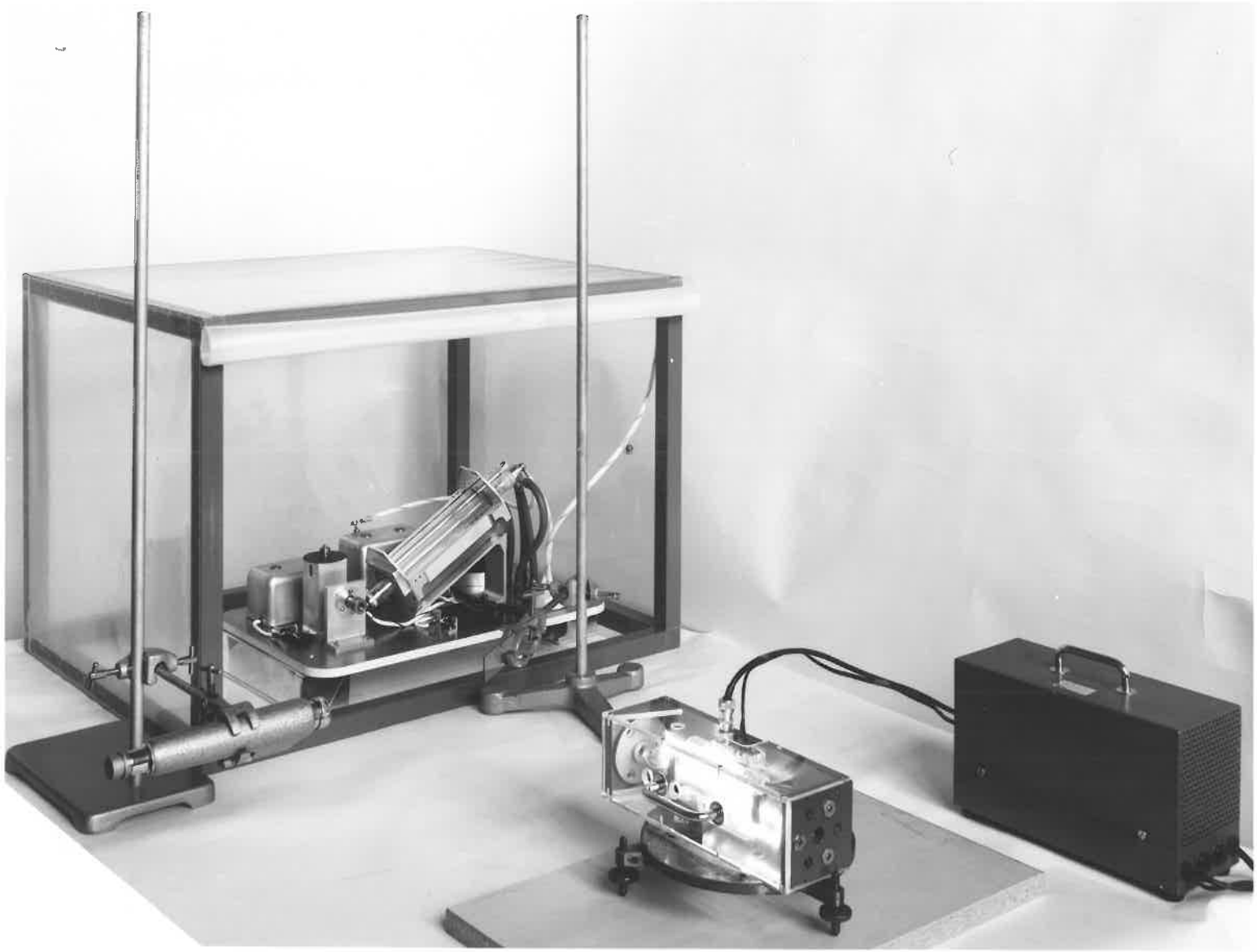

Figure 3.4 The arrangement used for optical alignment of the laser.

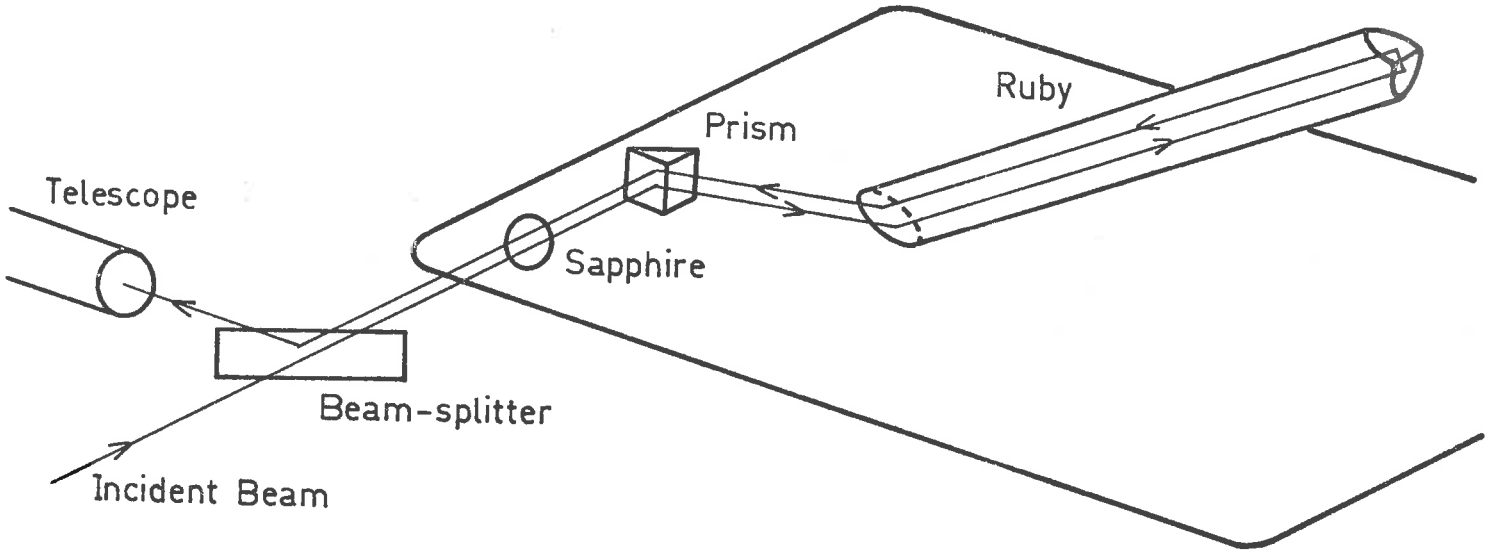

Figure 3.5 The optical components involved in alignment of the laser.

the front reflecting surface of the laser optical cavity is removed, and the narrow well-defined beam of a low-power He-Ne gas laser is directed at the Q-switch housing aperture. The positions of both the gas laser and Q-switch prism are adjusted so that the gas laser beam is central to both the Q-switch entrance and exit apertures, and also to the Brewster face of the ruby. The incident gas laser beam thus defines the physical axis of the laser optical cavity.

Because of the wedge cut at the far end of the ruby rod, the reflected gas laser beam will always be parallel to the incident beam in the vertical plane. The two beams will however be vertically displaced if the incident beam does not lie along the physical axis of the ruby. The ruby is therefore moved back and forth along its axis until the returning gas laser beam enters the Q-switch housing at the same height as the incident beam. The two beams are then brought into coincidence by a slight rotation of the ruby around its axis, since this has the effect of rotating the reflected beam around a cone having the incident beam as its axis.

At this stage, a semi-silvered beam splitting plate is placed between the ruby and gas lasers, at 45° to the gas laser beam axis, so that the reflected beams from the Q-switch and ruby surfaces can be observed in an alignment telescope pointed at the beam splitting plate. Two spots are seen in the alignment telescope, one corresponding to reflections from the Q-switch prism faces, and one due to reflection from the ruby wedge cut. Although the spots will not in general be

coincident, no attempt is made to align the surfaces, since during normal operation the rotation of the prism brings the surfaces into alignment in the horisontal direction, while the wedge cut on the ruby makes the system self-aligning in the vertical direction. The sapphire flat is now replaced and the reflection from this is aligned to be in the same vertical plane as that from the ruby, and in the same horizontal plane as that from the prism.

The alignment procedure so far described is sufficient to ensure laser action. At input energies near threshold, it will also produce near-optimum output beam divergence. The output beam shape may be checked by photographing the spot produced by the laser beam on a screen placed approximately 15 feet from the laser. A Polaroid camera with a red filter placed over the lens is set up in front of the screen. The camera shutter is opened, the laser is fired, and the shutter is closed.

The far-field patterns recorded by this technique at several values of input energy have been reproduced in Fig. 3.6. The increase in output beam divergence, particularly in the plane of rotation of the Q-switch, can be seen, and is due to the excitation of more off-axis modes as input energy is increased. At high input energies, it has been found that laser action can take place between the ruby rod and the face of the Q-switch prism, independently of the sapphire flat. This effect can lead to two distinct output beams if the optical cavity formed between the ruby and the prism face is completed earlier in the Q-switch cycle than that formed between the ruby and sapphire flat.

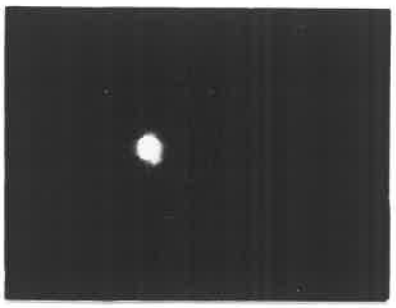

600 Joules

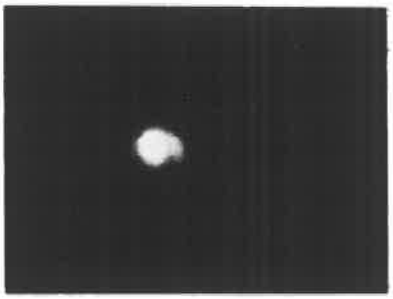

670 Joules

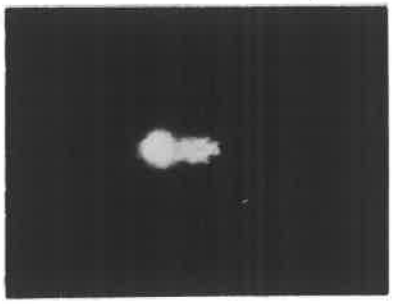

733 Joules

Figure 3.6 Laser far-field output patterns at various values of the input energy.

The excitation remaining in the ruby following oscillation between ruby and prism is sufficient to allow oscillation between ruby and sapphire flat, due to the higher reflectivity of the sapphire.

It has been found possible to reduce the output beam divergence at high input energies by tilting the sapphire flat about an axis parallel to that of the Q-switch. By this means, the sapphire flat can be made to complete the optical cavity before the Q-switch face, thus preventing the possibility of laser action between the ruby and prism face. In this way the total duration of lasing, and hence the output beam divergence, will be reduced. When the laser has been carefully adjusted, the output beam divergence is approximately 10 mrad near threshold, and increases to approximately 12 mrad for output energies near 1 joule.

CHAPTER 4

LASER RADAR DESIGN AND CONSTRUCTION

4.1 Introduction

The laser radar system which has been evolved is a compromise between several conflicting requirements. It had originally been hoped that a system could be constructed which would enable the 80 km altitude region to be studied, since other workers (for example, Bigg, 1956) had claimed to have observed dust layers, of possibly extra-terrestrial origin, in this region. However, initial calculations, the results of which have been summarized in Table 2.2, showed that this could not be achieved with a system using a laser output energy of one joule, and a receiving mirror having a diameter of approximately 12 ins. A higher laser output energy was ruled out by the high cost and lower achievable repetition rates of high energy lasers. On the other hand, calculations showed that an increase in receiver collecting surface area of 100 times would be necessary to achieve an accuracy of 10% at 80 km after 200 firings using a 5 km range gate. Such an increase in collecting surface area was also ruled out by considerations of cost, and by the desirability of making the equipment transportable, so that it could be moved should the first choice of operating site prove unsatisfactory.

An examination of Table 2.2 shows that a laser radar based on a one joule laser and 12 in. receiving mirror should allow scattering

profiles to an altitude of 40 km to be obtained readily, while profiles to 60 km should be obtainable by combining the results of several nights of observations. A limited increase in receiver surface area, such as could be obtained by using several 12in. mirrors aligned to a common focus, would not increase the maximum observable height significantly, while adding considerably to the complexity of the system. The laser radar to be described therefore uses a single parabolic mirror of 12 ins. diameter and 6 ft. focal length.

A simplified diagram of the complete laser radar is shown in Fig. 4.1. In the following sections the design and construction of the various components will be described.

4.2 Optical Design of Receiver

A ray diagram of the optical receiver is shown in Fig. 4.2. In this diagram the receiver mirror has for simplicity been replaced by an objective lens of diameter d_o and focal length f_o. The receiver field of view ϕ is defined by an aperture of diameter a at the focus of the objective lens. Light passing through the aperture is collimated by a field lens of focal length f_f and passed through the interference filter to the surface of the photoelectric detector. The distance x between the field lens and detector surface is such that an image of the objective lens is formed on the detector surface by the field lens. This is normal photometer practice and desirable in this case since it is intended that final alignment between transmitter and receiver beams will be carried out by movement of the

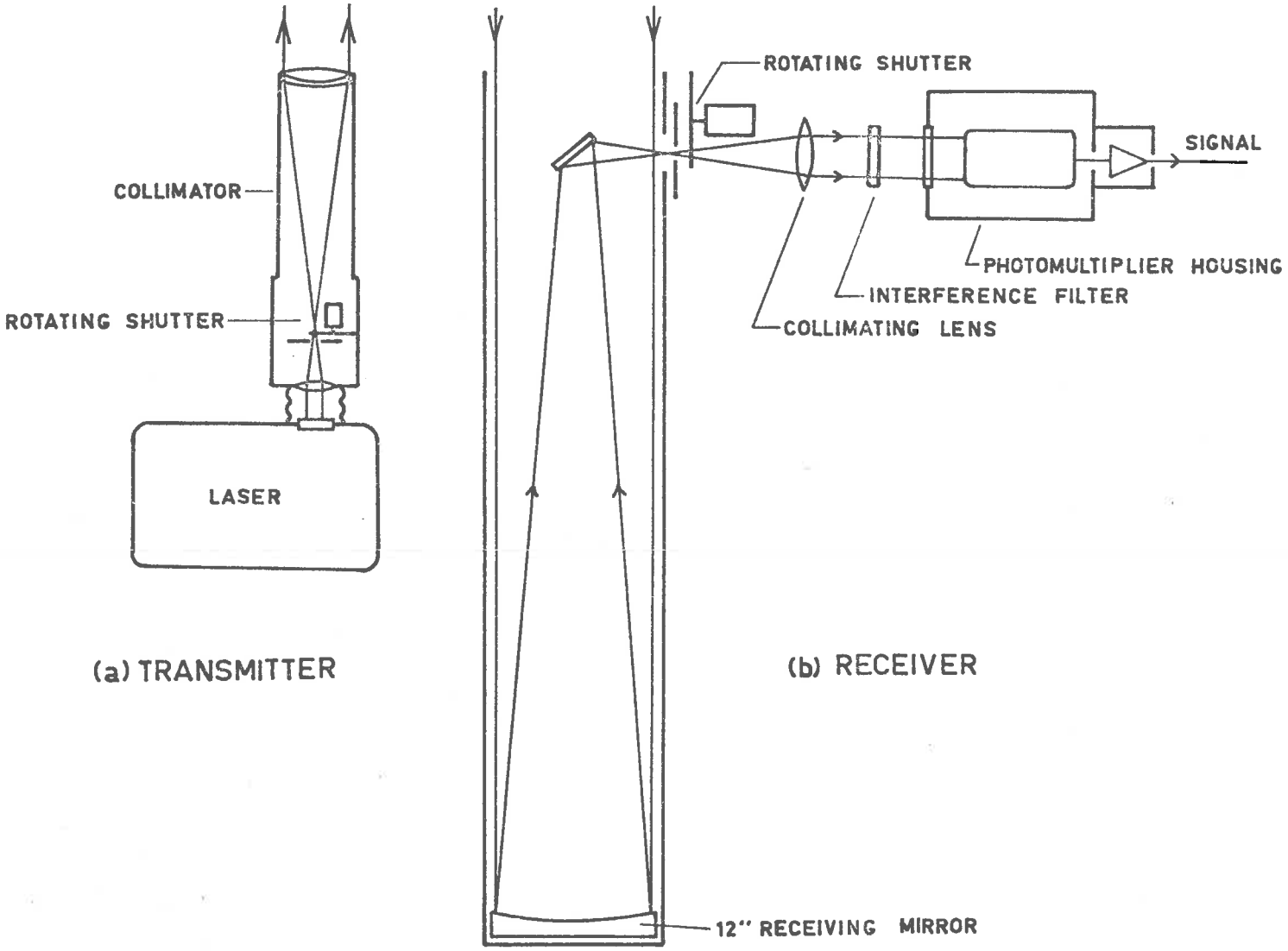

Figure 4.1 Essential components of the laser radar.

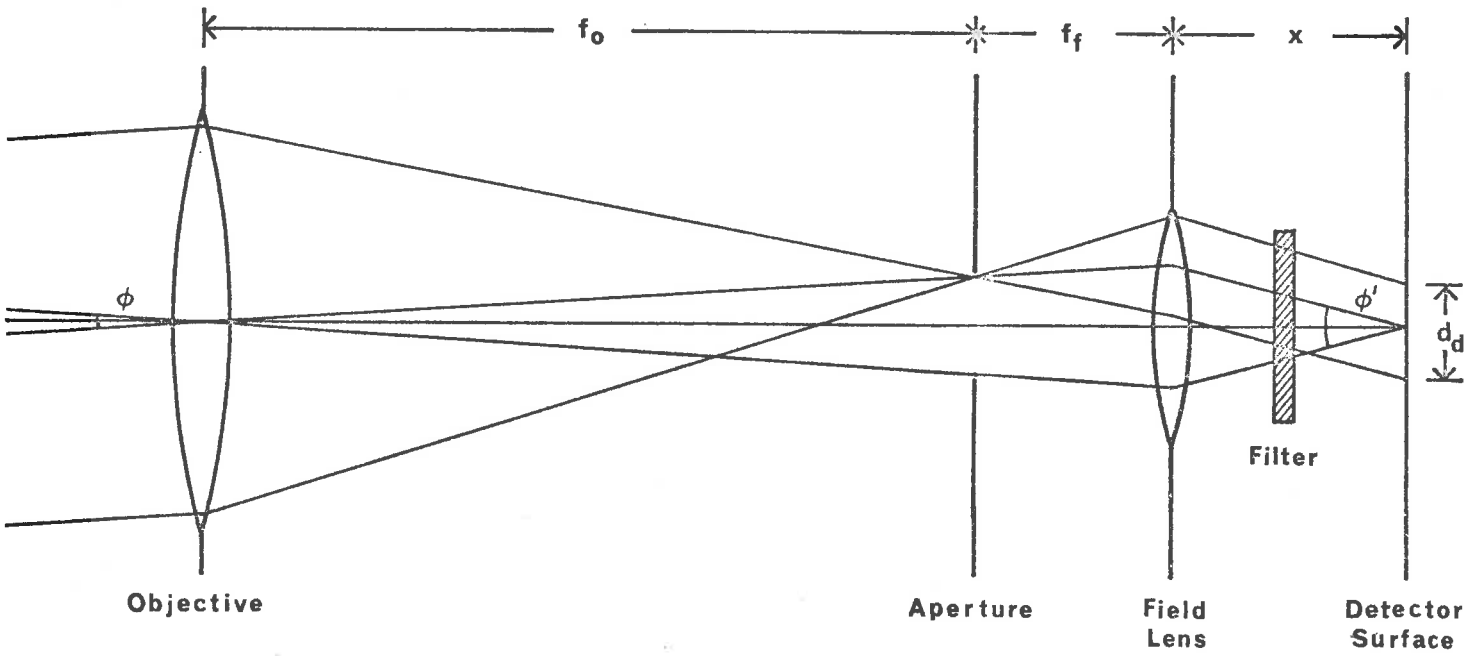

Figure 4.2 Equivalent ray diagram of the optical receiver.

receiver aperture. The above condition ensures that the spot of light does not move across the detector surface. The distance x between the field lens and detector surface is given by

$$x = f_f(1 + f_f/f_o)$$

For a given aperture diameter a, the divergence angle ϕ' of the beam of light passing through the interference filter is determined by the focal length f_f of the field lens. For a narrow band interference filter, ϕ' should be no greater than a few degrees, to avoid widening of the filter bandwidth. However, as f_f is increased, the necessary detector surface diameter d_d increases, and the field lens and filter diameters also increase. From the geometry of the system, it can be shown that

$$d_d = f_f\, d_o/f_o$$

and

$$d_f = \phi' x + d_d$$

In the present system, the focal length of the objective is 71 ins. and an aperture of diameter 0.142 ins. defines a field of view of 2 mrad. The field lens has a focal length of 6 ins. and the value of ϕ' is thus 1.4^o. The values of d_d and d_f are 1.02 ins. and 1.17 ins. respectively. These values allow a standard 2 in. diameter interference filter to be used in conjunction with a 2 in. diameter photomultiplier tube.

4.3 Receiver Construction

4.3.1 The Telescope

A general view of the optical receiver is shown in Fig. 4.3. The main telescope tube is 6 ft. long and 15 ins. square, and consists of a frame made from 1 in. square section mild steel tubing, covered over most of its surface by 16 gauge mild steel sheets riveted to the frame. Removable aluminium panels provide access to the mirror cell at the base of the tube, and to a spider support for an elliptical optical flat near the top of the tube.

The mirror which forms the receiver collecting surface has a diameter of 12 ins, and a thickness of 1.5 ins. The mirror is mounted in a cell, which is in turn supported on an aluminium casting bolted to the base of the telescope tube (Fig. 4.4). Three adjustment screws threaded through the aluminium casting support the mirror cell in such a way that the cell may be tilted during optical alignment. Three bolts fixed to the mirror cellare used to tighten the cell against the adjustment screws when alignment is completed.

In order to minimise distortion of the relatively thin mirror, the cell incorporates a self-balancing 9-point flotation system, which has been described by Hindle (1957). The mirror is supported on 9 slightly flattened ball bearings carried by 3 pivoted triangular steel plates, and arranged in such a way that each of the 9 bearings supports an equal portion of the weight of the mirror. The pivots of the triangular plates are directly in line with the screws which support the mirror cell, so that any distortion of the cell resulting from

Figure 4.3 Optical receiver with covers removed.

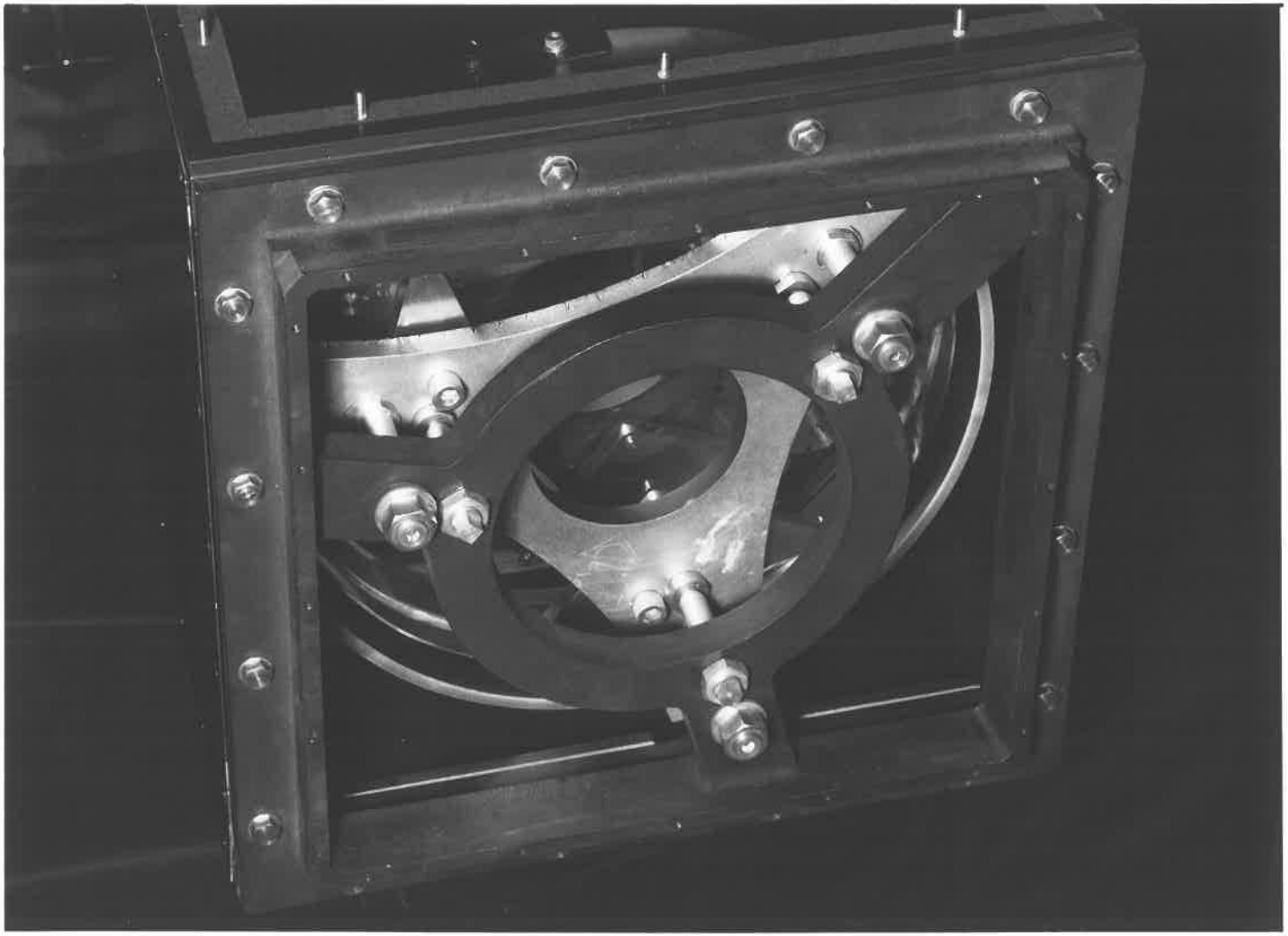

Figure 4.4 Mirror cell and mounting detail.

tightening of the locking bolts does not affect the mirror alignment. It has been found that the mirror cell may be removed from the telescope tube, and replaced, without the need for subsequent realignment of the system.

Light gathered by the main mirror is directed to the subsidiary optics by a small elliptical mirror mounted at 45° to the tube axis near the top of the telescope tube. The mirror is held centrally in the tube by a 4-section spider support fixed to the tube frame. The mirror mounting incorporates adjustments that allow the mirror to be moved along the tube axis, and the angular setting of the mirror to be varied.

4.3.2 The Subsidiary Optics

The subsidiary optics are mounted on an aluminium casting bolted to the side of the telescope tube frame. The casting and subsidiary optics are shown in Fig. 4.5. The small aperture which defines the field of view of the telescope is mounted on a carriage which may be moved in two mutually perpendicular directions by means of micrometer screws. By this means the field of view of the receiver may be aligned with the transmitted beam. The aperture carriage is in turn mounted on an L-shaped bracket which may be moved parallel to the optical axis of the receiving system, thus allowing the aperture to be placed in the focal plane of the telescope mirror.

Light passing through the aperture is recollimated by the field

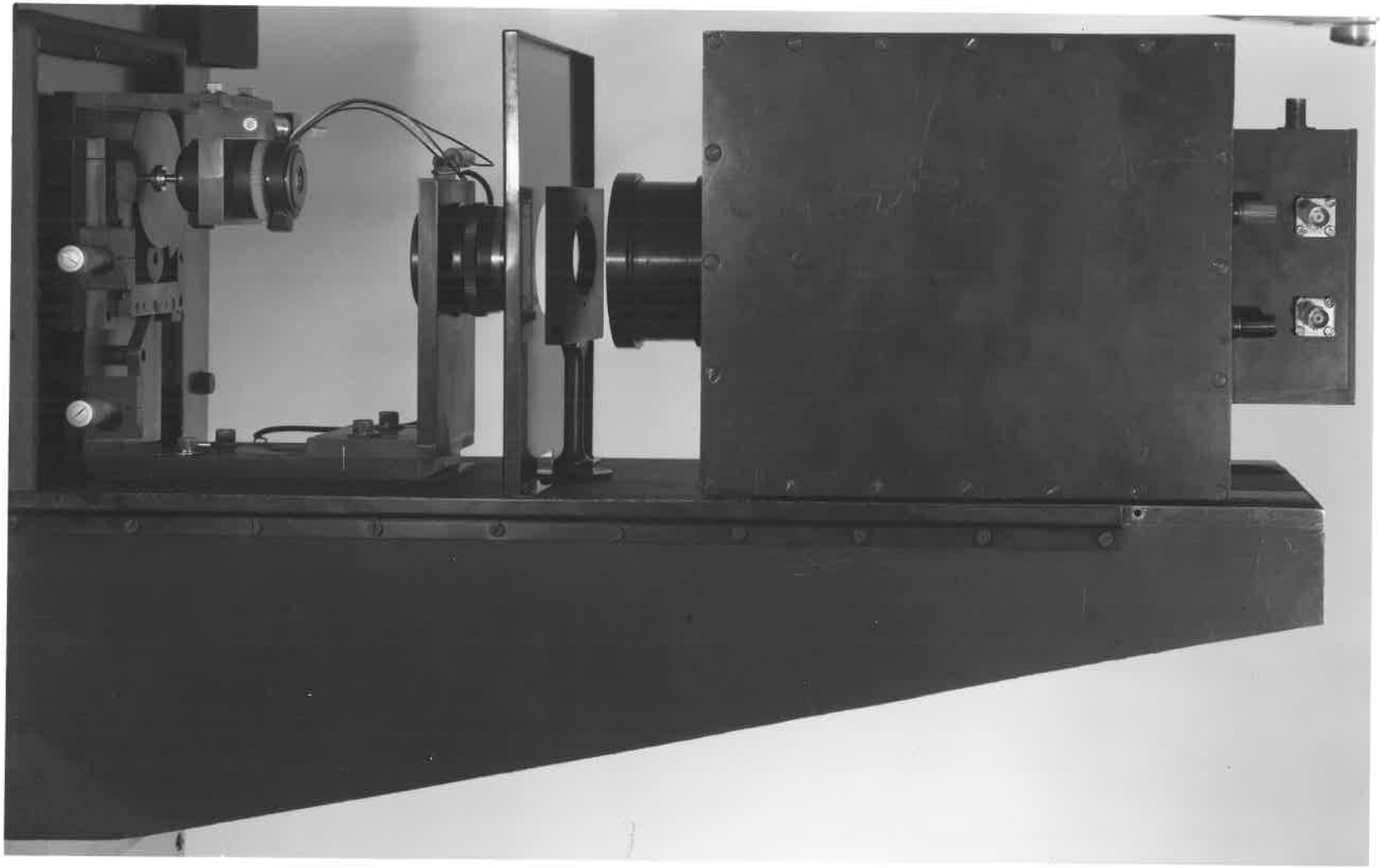

Figure 4.5 Receiver subsidiary optics, and support casting.

lens, which is a standard photographic objective, of focal length 6 ins., and numerical aperture f/4. The lens is threaded into an L-shaped bracket which is fixed to the bracket carrying the aperture. The distance between the aperture and the field lens is adjustable, in order to allow the aperture to be positioned at the focus of the field lens during alignment.

The bandwidth of the receiver is determined by a narrow-band interference filter. The filter is 2 ins. square, and has a bandwidth of 8.5Å with a peak transmission of 45%. The peak wavelength at normal incidence is 6946.5Å, and the filter is "tuned" to the laser wavelength of 6943Å by tilting it with respect to the beam axis. This is achieved by rotating the filter mount about a vertical axis by means of a cam fixed to the mount underneath the main casting, and operated by a knob on a shaft passing out through the side of the casting. A baffle plate mounted close to the filter prevents light reflected from the surface of the interference filter from reaching the photo-multiplier detector.

During operation, the subsidiary optics are covered by an inverted "U"-shaped aluminium cover. The casting and all aluminium components have been blackened by anodising, and all brass and steel metalwork has been chemically blackened in order to reduce as much as possible the scattering of stray light within the optical system.

4.3.3 The Detector Housing

The photomultiplier is housed in a refrigerated box, which is bolted to the end of the casting through slotted holes, so that it may be moved along the optical axis during focussing. Lateral location is provided by guide rails on the casting locating in grooves machined into the base of the housing.

A cross-sectional drawing of the photomultiplier housing is shown in Fig. 4.6. The photomultiplier tube socket is fixed to an ebonite base, which is in turn mounted to the preamplifier housing. The complete photomultiplier tube sub-assembly is held in the housing by 4 screws which pass through the preamplifier box. The photomultiplier dynode resistor chain is mounted in a cavity machined into the ebonite base, and the dynode voltages are fed to the tube socket by nylon feed through insulators mounted through the ebonite base. The photomultiplier is enclosed by a full-length magnetic shield of "Conetic" material, connected to cathode potential.

The photomultiplier tube is cooled by means of a Peltier battery, which is attached to a copper tube surrounding the photomultiplier. When cooled with water at 5°C, obtained from the laser cooling system, the Peltier battery is capable of lowering the temperature of the photomultiplier tube to -10°C in 40 minutes. Cooling water is circulated to the Peltier battery through nylon connections in the base of the housing. Expanded polystyrene is used to provide thermal insulation between the copper tube and the walls of the photomultiplier housing.

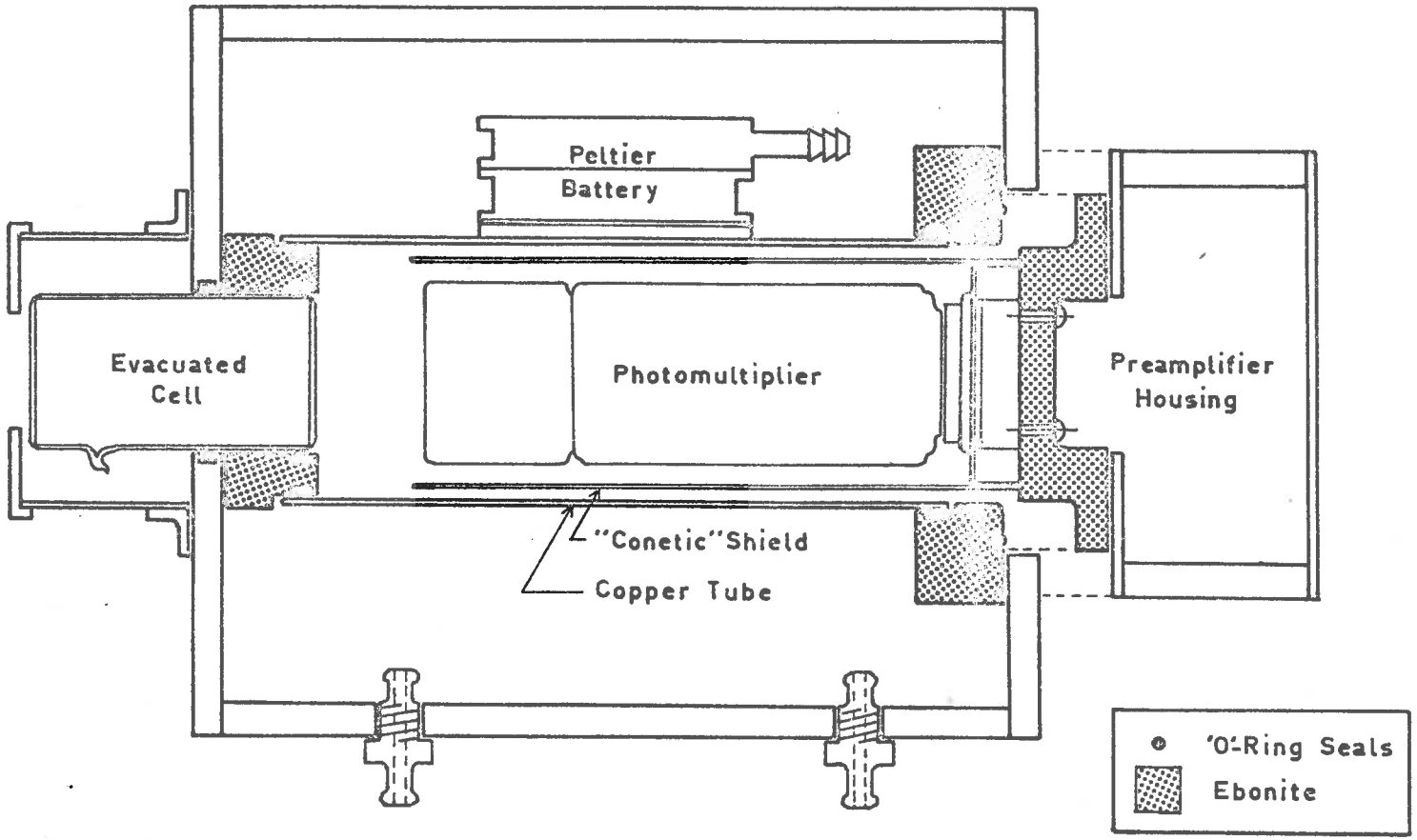

Figure 4.6 Sectional view of refrigerated housing, with photomultiplier sub-assembly partially withdrawn.

The front window of the photomultiplier housing consists of an evacuated glass cell, constructed by fusing a glass disc to each end of a length of thin-walled glass tube. Because of the length of the cell, the front glass surface remains at approximately ambient temperature, thus preventing the condensation of moisture on this surface. The partial vacuum inside the cell reduces heat transfer between the inner and outer glass plates. A cylindrical aluminium shield fixed to the front of the housing protects the protruding section of the glass cell from damage.

4.3.4 The Rotating Shutter

A rotating shutter is located immediately behind the aperture which defines the field of view of the receiver. The function of the shutter is to block the receiver aperture for a short time following laser firing. If this were not done, strong scattering from the first few kilometers of the earth's atmosphere would seriously overload the photomultiplier.

The shutter is rotated at 24,000 r.p.m. by a hysteresis synchronous motor, which is supplied with 115v. R.M.S., 400 Hz power from the same inverter that supplies the laser Q-switch motor. The speed of rotation of the receiver shutter is thus synchronised with that of the laser Q-switch. However, a means of adjusting the phase between the motors is necessary in order to allow signal recording to be carried out over different height regions, and because it has been found that the position of the motor shafts in relation to the peak of the driving

voltage is different each time that the motors reach synchronism after being switched on. The phase variation is achieved by rotation of the receiver motor about its axis. A nylon ring gear clamped to the motor housing is rotated by a worm gear fixed to a shaft perpendicular to the motor axis, passing out through the cover over the subsidiary optics.

The shutter phase variation could have been achieved electrically instead of mechanically, by varying the phase of the driving voltage supplied to the motor. However, this would have required the use of a phase shifting circuit capable of handling high power with low losses, or alternatively, the use of a separate power amplifier for each motor. It was considered that the mechanical system described above would be simpler and more stable. The two-bladed receiver shutter rotates at twice the speed of the laser Q-switch, so that it is never necessary to rotate the motor through more than 90° during the phasing operation.

The delay between laser firing and receiver shutter opening is adjusted so that the receiver aperture is completely uncovered by the time that the scattered light has returned from the lowest level of the height range to be studied. The minimum delay which may be used is determined by the shutter opening time, and by the jitter between the rotation of the shutter and the laser Q-switch. The shutter opening time is approximately 30 μsec. The jitter is presumably caused by momentary drag in the motor and Q-switch bearings. Measurements have

shown that it is quite random, and has a peak value of approximately 20 μsec. It is clear therefore that the minimum delay which can be used is approximately 50 μsec, corresponding to an altitude of 8 km.

4.4 Receiver Optical Alignment

To align the receiver, all optical components are removed from the telescope tube and casting, and the tube is placed horizontally on a long bench. In order to determine the physical axis of the telescope tube, a square metal plate with a small hole drilled at its exact centre is fixed to each end of the tube. By placing the eye close to one of these small holes, and sighting through the other, it is possible to position a point source of light exactly on the tube axis, but outside the tube itself. One of these point sources is placed at each end of the tube, so that the distance between each source and the nearer end of the telescope tube is approximately equal to the focal length of the receiver mirror (6 ft.). The point sources each consist of a low-voltage lamp positioned behind a small hole drilled in an aluminium plate. The metal plates are now removed from the ends of the telescope tube, and the diagonal mirror is placed approximately in position.

By means of an autocollimation technique, the aperture which defines the field of view of the receiver is adjusted to lie at the focus of the field lens. The aperture-field lens assembly is now placed in position on the receiver casting, and the field lens is replaced by a metal plate having a pinhole at its exact centre. By

sighting through the pinhole and the centre of the field-defining aperture, the centre of the diagonal mirror may be set on the optical axis defined by the field lens. For purposes of this adjustment, the centre of the diagonal mirror is defined by the intersection of two threads stretched across the mirror surface. The angle of the diagonal mirror is next adjusted until the image of the illuminated pinhole placed near the far end of the telescope tube falls centrally in the aperture. Under these conditions, a beam travelling along the optical axis defined by the field lens will be reflected by the diagonal on to the physical axis of the telescope tube.

At this stage, the main mirror is placed in position in the receiver, and tilted by means of the mirror cell adjusting screws until the image formed by the mirror of the illuminated pinhole in front of the telescope tube lies over the pinhole itself. The mirror optical axis now lies on the telescope tube axis, and hence on the optical axis of the receiver. Both illuminated pinholes, and the pinhole placed in the field lens mount, may now be removed.

An autocollimation technique is again used to position the receiver aperture at the focus of the main mirror. The aperture is illuminated by a small torch, and observed through a low-power microscope. A flat mirror is placed at the entrance of the telescope tube, and tilted until the reflected image of the aperture falls over the aperture itself, so that both may be seen in the microscope. The receiver aperture is moved along the receiver axis until both the aperture and its image simultaneously appear in focus in the microscope.

The field lens is now replaced, and the detector housing is placed in position on the casting. The housing must be adjusted so that an image of the main mirror is formed on the photomultiplier surface by the field lens. To carry out this adjustment, the photomultiplier tube is removed from the housing and a translucent screen is placed inside the housing, in the same plane as that occupied by the photomultiplier surface. A small globe is held near the front surface of the main mirror and the detector housing is moved along the optical axis until the image of the lamp observed on the translucent screen appears in good focus. The lamp and translucent screen may now be removed.

4.5 Transmitter Collimator Design

The laser output beam with a divergence of 12 mrad must be reduced to a beam with a divergence of 1 mrad or less. This may be achieved by passing the beam through a collimator consisting of a short focal length primary lens and a longer focal length collimating lens. The diameter of the output beam is increased by a factor equal to the ratio of the focal lengths of the two lenses, while the beam divergence is reduced by the same ratio. Since the laser output beam has a diameter of approximately 0.25 ins., and a de-magnification ratio of 12 is required, the collimating lens will need to have a diameter of at least 3 ins. if vignetting of the output beam is not to occur.

Two possible optical arrangements of the collimator are shown in Fig. 4.7(a). It can be seen that the same results would be achieved

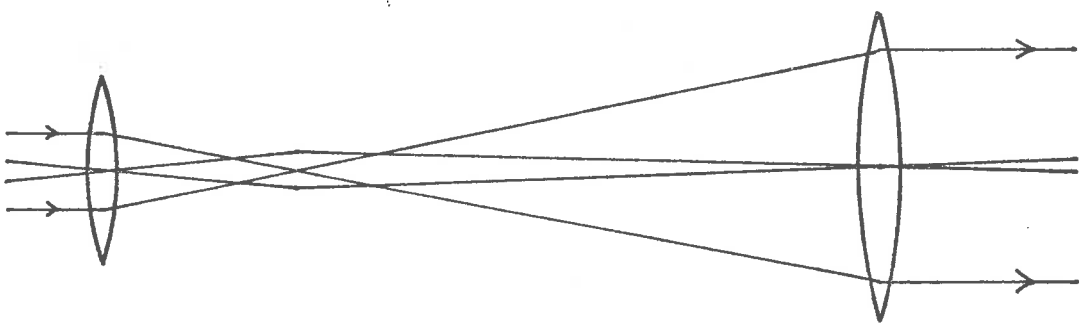

Astronomical telescope system

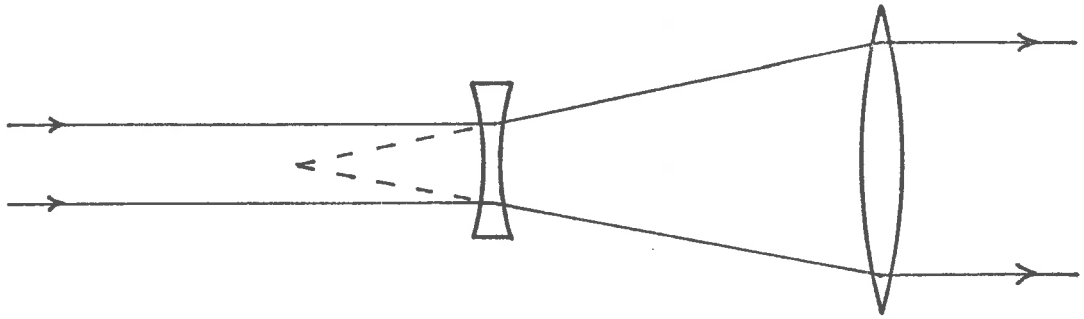

Galilean telescope system

Figure 4.7(a) Possible collimator optical systems.

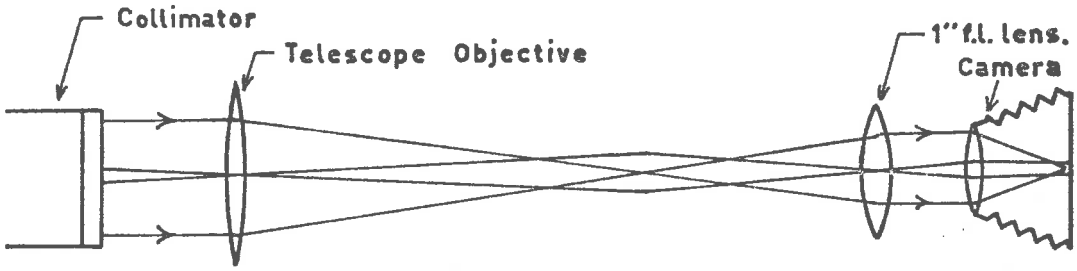

Figure 4.7(b) Collimator test system (not to scale).

by using either a converging or diverging lens for the primary element, the resulting systems being similar to an astronomical and a Galilean telescope respectively. The advantages of the Galilean system are its shorter overall length, and the fact that the laser beam does not pass through a real focus. The high electric field intensities produced at the focus can lead to dielectric break-down of the air, and consequent energy loss from the beam. However, for reasons discussed in Chapter 2, it is necessary to incorporate a mechanical shutter in the transmitter, and since this is most easily done at a point where the beam has very small cross-section, the astronomical telescope system was used. Subsequent testing with laser output energies up to approximately 0.5 joules showed that there was no significant energy loss from the beam in passing through the focus.

A coated, cemented doublet lens of focal length 24 ins. and diameter 3.5 ins. which was already available was used for the collimating lens. However, it was considered desirable to avoid the use of cemented construction in the case of the primary lens, since the small cross-section of the beam at this point, and consequent high power density, could lead to deterioration of the lens cement. Because the laser output beam is monochromatic, it is not necessary that the lenses used in the collimator should be colour-corrected and a simple plano-convex lens of focal length 2.2 ins. and diameter 1 in. was used as the primary lens. The plano-convex form of the lens ensures near minimum spherical aberration for a given focal length (Jenkins and White, 1957). Because of the small angular field required, this is

the only aberration of importance in the present application.

The transmitter shutter is required to close as quickly as possible following emission of the main laser pulse in order to cut off the subsequent low intensity, long duration fluorescent radiation from the ruby. For a transmitter output beam divergence of 1 mrad, the size of the spot of light produced at the focus of the collimator lens will be 0.02½ ins., and a disc of diameter 2 ins. rotating at 12,000 r.p.m. is capable of closing an aperture of this size in 20 μsec. However, the minimum possible closing time will be longer than this, because of jitter between rotation of the shutter and the laser Q-switch, which has been found to have a peak value of 20 μ sec. (Section 4.3.4).

To calculate the required shutter closing time, the relative intensities of the laser pulse and the fluorescent radiation must be known. Attempts to measure this relation failed because of the large dynamic range required for the measurement. However, the attempted measurements did show that the intensity of the fluorescent radiation is at least six orders of magnitude lower than the laser pulse intensity.

The maximum rate of change of signal strength with pulse altitude occurs near the ground. Hence the greatest contribution to the total signal by scattering from the fluorescent tail will occur when the end of the tail is just at the region of total beam overlap (height h_o in Chapter 2). For the equipment described in this chapter,

the value of h_o is approximately 1 km, and if we assume that the total backscattering coefficient of the atmosphere is proportional to the sum of the Rayleigh and aerosol attenuation coefficients tabulated by Elterman (1964), then it is possible to calculate the contribution to the total signal from a fluorescent tail of a given length, and having a given intensity. Calculations based on a fluorescent tail having an intensity six orders of magnitude lower than that of a 0.5 μsec long pulse showed that the contribution from the tail to the total scattering will not exceed 5% provided that the tail length is less than 15 km, or 50 μsec. The relative contribution from the tail will decrease as the pulse and fluorescent tail propagate upwards. It is clear therefore that a shutter closing time of 50 μsec or less is desirable.

4.6 Transmitter Collimator Construction

A view of the laser generator, the collimator, and the mounting arrangement for both is shown in Fig. 4.8, while a simplified diagram of the complete transmitter system is shown in Fig. 4.1(a). The collimating lens is mounted in a cell which is threaded into the end of an aluminium tube, which is in turn rigidly fixed to a steel base plate. The base plate also carries the rotating shutter assembly, and the primary lens mount. The primary lens is mounted in a bracket which may be moved along the collimator axis in order to allow accurate focussing of the collimator.

The rotating shutter consists of a disc of diameter 2.5 ins.,

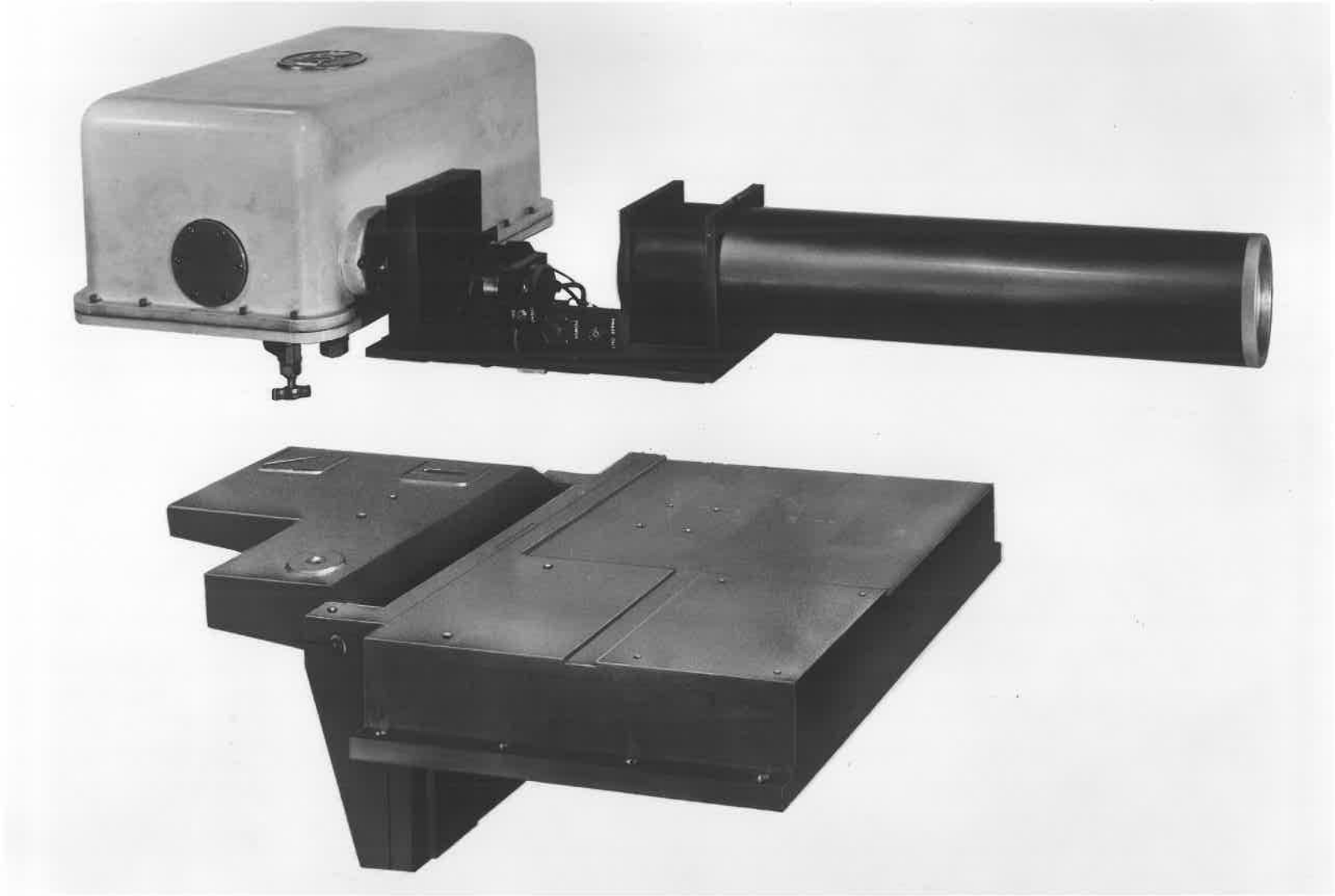

Figure 4.8 Mounting arrangement for the laser and collimator.

having four slots 0.2 in. wide cut in its periphery, and driven at 12,000 r.p.s. by a synchronous motor. As in the case of the receiver shutter, the speed of rotation of the motor is synchronised with that of the motor driving the laser Q-switch, and the relative phase of the two motors is varied by rotation of the shutter motor about its axis. A baffle plate is placed close to the rotating disc, in order to prevent leakage of fluorescent radiation around the edges of the disc.

In order to facilitate phasing of the transmitter shutter, an optical pick-up has been incorporated in the shutter assembly. A pre-focussed subminiature "endoscope" lamp is used to illuminate a pin-hole, an image of which is formed on the shutter disc by a microscope objective. Light passing through the shutter falls on a small photo-diode, the output of which is brought out through a coaxial connector at the side of the collimator housing. An alkaline battery mounted on the base-plate provides power for the lamp. The optical pick-up is positioned so that the time interval between a pick-up output pulse and the shutter opening is the same as the interval between a Q-switch pulse and laser emission. Phasing is carried out by displaying on a dual-beam oscilloscope both the optical pick-up pulse and the laser Q-switch pulse, and then phasing the transmitter shutter so that the Q-switch pulse occurs approximately 50 μsec before the shutter closing phase.

In designing the mount for the laser and collimator, provision had to be made for adjustments which would allow the laser output beam

to be aligned with the collimator axis, and to be centred with respect to the collimator lens apertures. It was also desirable that all rotational adjustments should be made to the laser, and not to the collimator, so that the collimator axis, and hence the transmitted beam, should remain parallel to the datum line of the whole equipment, to which the receiver axis is also made parallel.

These requirements have been met by the mount shown in Fig. 4.8. Cast from aluminium alloy, the mount consists of 3 sections. These are the hinged platform, which supports the laser; the mounting bracket; and the main box, which supports the collimator. A steel pin fixed to the laser base plate directly beneath the sapphire flat and passing through the hinged platform allows the laser to be rotated about one axis. Two bolts fixed to the laser base plate and passing through slotted holes in the hinged platform allow the laser to be locked in position. Rotation of the laser about a second axis at right angles to the first is achieved by tilting of the hinged platform, which is finally locked in position by a clamp beneath the platform.

Slotted mounting holes in the collimator base plate and in the mounting bracket allow transverse movement between the laser and collimator and permit both to be moved with respect to the main box. In each case, a tongue and groove between the sliding components maintains angular alignment between the laser and collimator.

An energy monitor is permanently mounted on the main box casting at the side of the collimator. The energy monitor is a T.S.C. Model

100 ballistic thermopile. The laser output beam is directed into the energy monitor by means of two prealigned right-angled glass prisms, mounted on the main box. One of these prisms is removable, to allow the laser beam to enter the collimator for normal operation. The energy monitor may be seen in Fig. 4.10.

4.7 Optical Alignment of the Transmitter

To align the transmitter, the laser and collimator are mounted on the casting, which is supported on a bench so that the collimator tube is horizontal. The lenses, the rotating shutter and the baffle are removed from the collimator. A flat mirror is held across the end of the collimator tube, and an auto-collimator is set up in front of the mirror and normal to it. The beam of the auto-collimator is thus parallel to the physical axis of the collimator. The flat mirror is removed, and the laser tilted by means of both angular adjustments on its mounting platform until the reflection from the sapphire flat, as seen in the auto-collimator, indicates that the flat is also normal to the auto-collimator beam. Under these conditions, the emitted laser beam will be parallel to the collimator axis.

The auto-collimator is removed, and the collimator primary lens is placed in position. A translucent diffusing screen is taped across the exit end of the collimator tube, and a Polaroid camera with a red filter placed over its lens is set up to photograph the diffusing screen. The purpose of the filter is to discriminate against ambient illumination, allowing the camera shutter to be held open while the

laser is fired. The resultant photograph shows the relation between the laser beam and the collimator exit aperture. If the laser beam is not centred within the aperture, an appropriate transverse adjustment is made to either the laser or the collimator, depending on the direction of movement required. The amount of movement may be monitored by means of a dial gauge fixed to a suitable part of the assembly.

When the laser beam has been centred with respect to the exit aperture, the collimating lens is inserted and the collimator focussed to produce the smallest possible output beam divergence. This is achieved with the aid of an auxiliary optical system, illustrated in fig. 4.7(b), which is set up on the bench in front of the collimator. A telescope objective lens, of focal length 7 ft. is set up in front of the collimator lens, and its focus located by means of an auto-collimation technique using a small illuminated pinhole. A lens of focal length 1 in. is set up on the far side of this focus, using an auto-collimation technique on the same pinhole, which is then removed. The two lenses form a telescope, with a magnification factor of 84, focussed to infinity. A Polaroid camera with its lens focussed to infinity and covered with a red filter is set up close to the 1 in. focal length lens to complete the testing system. A divergent beam incident on the telescope objective lens produces a spot in the plane of the film whose diameter is proportional to the beam divergence. With a camera lens of focal length 5 ins., the sensitivity of the system is 0.5 mins.arc/in. at the film plane. The output beam from the collimator must be attenuated by means of neutral density filters in order

to avoid over-exposure of the film. The required filter factor is approximately 2×10^3.

To carry out the collimator focussing, the collimator primary lens is moved in increments of 0.050 ins., monitored by a dial gauge, the laser is fired each time, and the size of the spot produced on the film is recorded. In this way, a graph of beam divergence vs lens position may be drawn, and the best focus found.

The final result of these adjustments indicated a beam divergence of 0.001 radian, at the point where the intensity was 3 orders of magnitude lower than at the center of the beam. At the position of best focus, the spot was very nearly circular. The best focus occurred when the primary lens was 0.080 ins. away from the focal position for parallel light. However, focussing was not critical, a deviation of $\pm$ 0.050 ins. increasing the beam divergence by less than 10%. This is due to the small numerical aperture (f/8) and hence large depth of focus of the collimator optical system.

4.8 Complete Radar Mounting Arrangements

The mounting frame which supports the complete laser radar system is shown in Fig. 4.9. The receiver and transmitter are each bolted to one side of a rectangular frame, which is in turn supported by 4 inverted-V tubular struts, bolted at their base to a floor-frame. The whole assembly is quite rigid, and no trouble has been experienced with vibration or long-term mis-alignment.

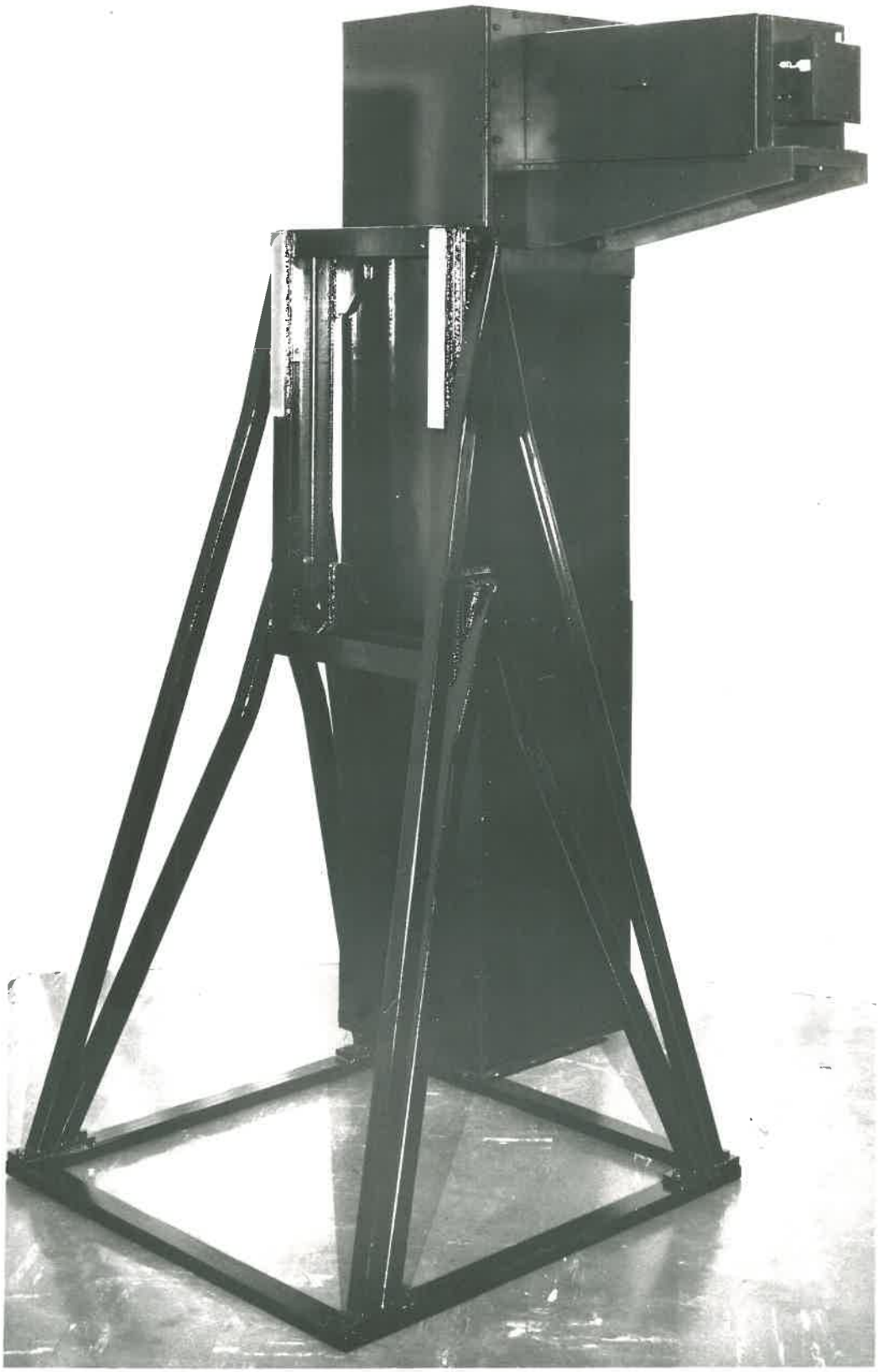

Figure 4.9 Laser radar supporting frame.

The mounting frame was made from welded 4 ins. x 2 ins. U-section mild steel. Mounting pads for the transmitter and receiver, and for the support struts, were welded to the frame. After heat treatment to normalise stresses, the mounting pads were machined flat. The support struts were made from 1.25 ins. square section tube, with mounting pads welded to each end. These are bolted to the frame at the top, and to the floor-frame at the bottom. The whole assembly may be dismantled for transport.

4.9 Installation and Final Alignment

Initially, the laser radar was installed at the Mawson Institute for Antarctic Research field station at Mt. Torrens (elevation 1913 ft.), approximately 30 miles from the city of Adelaide. The field station has been constructed so that instruments inside the building can observe the sky through a row of hinged panels in the center of the roof. The complete radar installation inside the building is shown in Fig. 4.10.

For reasons discussed in Chapter 6, the laser radar was later removed from Mt. Torrens, and installed in a mobile instrumentation van, which is shown in the Frontispiece. A hinged hatch was constructed in the roof of the van to allow the equipment to observe the sky. The radar receiver and transmitter are supported on a pair of steel beams welded directly to the chassis, thus helping to isolate the equipment from any vibrations set up in the floor of the van. The complete installation is shown in Fig. 4.11.

Figure 4.10 Laser radar installed at the field station.

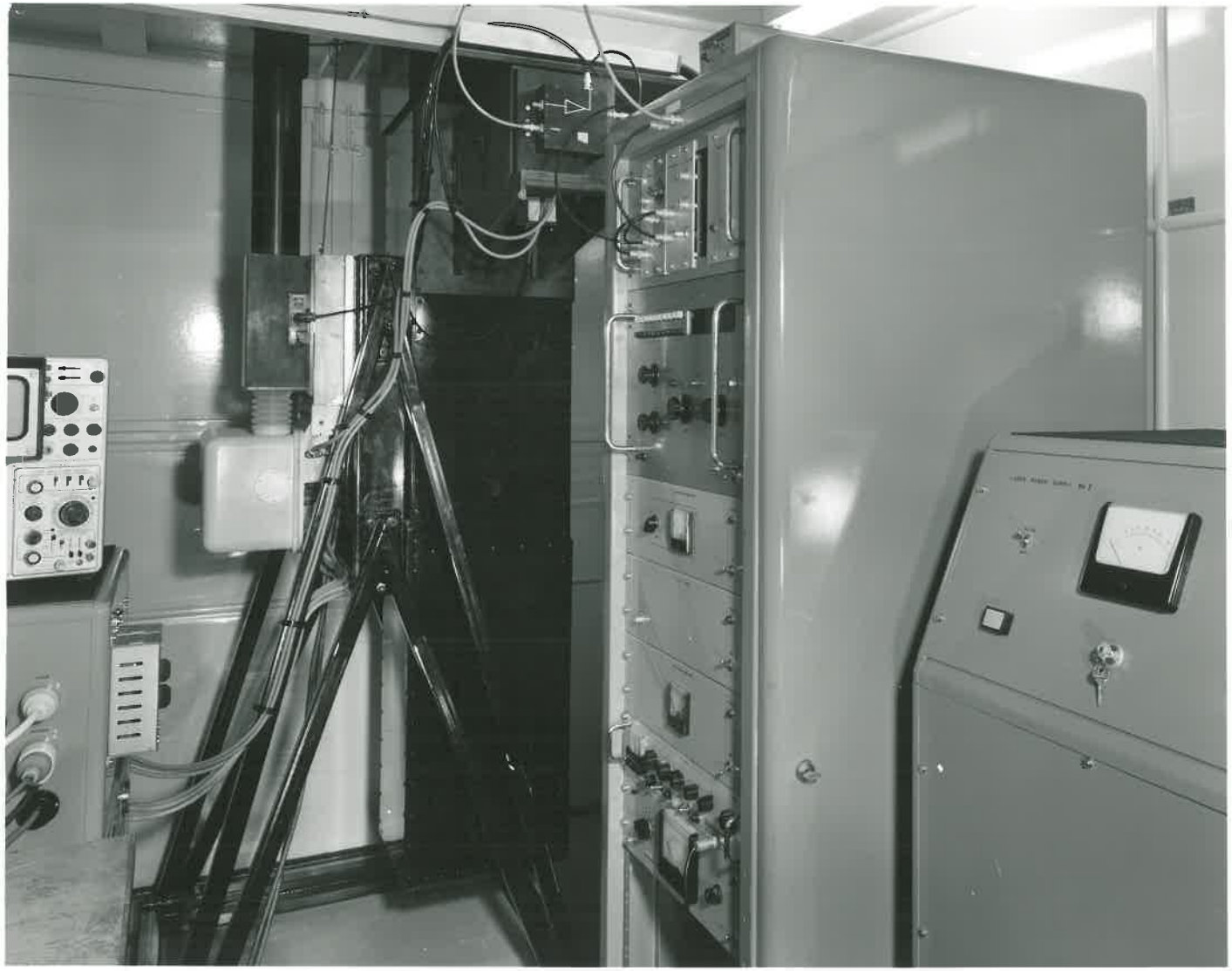

Figure 4.11 The laser radar installed inside the instrumentation van.

Alignment of the receiver's field of view with the transmitted beam was in each case carried out after the equipment had been installed. The procedure made use of an auxiliary optical system placed above the roof over both the receiver and transmitter apertures. The system is shown in Fig. 4.12, and consists of a frame carrying a pair of accurately machined guide rails which carry a sliding lens platform. The lens, of focal length 26 ins., has a piece of thin aluminium foil mounted in its focal plane.

To carry out the alignment, the sliding lens is positioned over the exit aperture of the transmitter, and the laser is fired, producing a small hole in the aluminium foil. The lens assembly is moved along the guide rails over the receiver aperture, without disturbing its angular orientation with respect to the optical axis of the system. The angular orientation may be checked by means of two sensitive spirit levels mounted on the lens platform. The small hole in the aluminium foil is illuminated from above, and the field of view of the receiver is adjusted until the image of the hole is central in the receiver aperture. Coarse adjustments of the receiver are made by tilting the main mirror on its 3 mounting screws, and fine adjustment is by means of the micrometer screws on the aperture mount. A low power microscope is used to view the aperture and the image of the small hole.

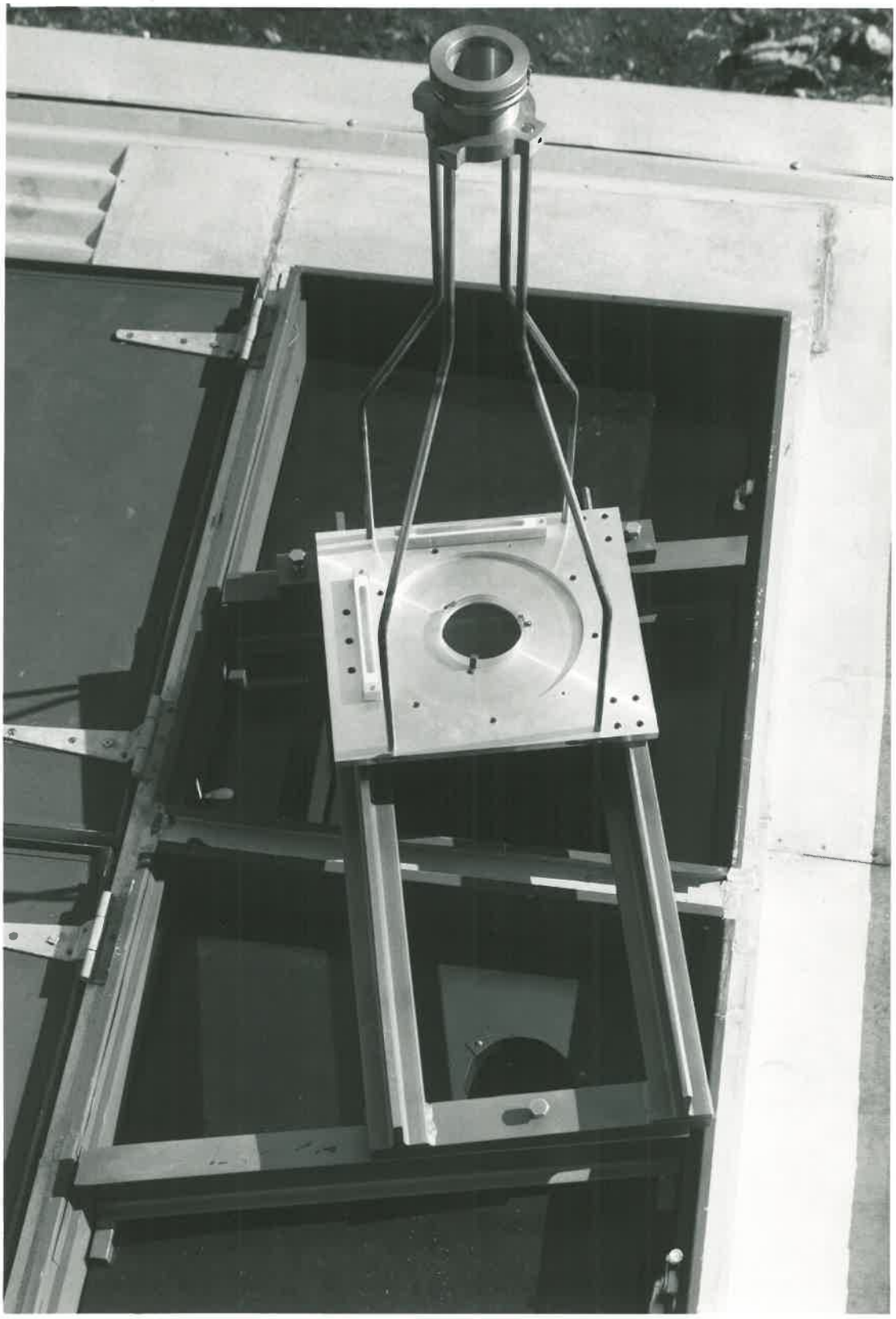

Figure 4.12 Receiver and transmitter collimation procedure.

CHAPTER 5

RADAR ELECTRONICS AND RECORDING SYSTEM

5.1 Introduction

Fig. 5.1 is a block diagram of the complete laser radar electronics. The main and auxiliary power supplies provide the D.C. potentials required by the laser, and were described in Chapter 3. The 400 Hz inverter consists of a commercial DC-AC converter unit, and provides 115 r.m.s. volts of 400 Hz square wave to the receiver shutter motor. A transformer connected to the converter supplies 50 r.m.s. volts to the transmitter shutter motor, and 6 volts to the laser. A separate power amplifier mounted inside the laser provides power for the Q-switch motor.

A thin wire stretched across the transmitter output aperture directs a small fraction of the transmitted light to an E.G. and G. type SD100 high-speed photo-diode, the output of which is displayed on a Tektronix 517A oscilloscope. The oscilloscope allows a constant visual check to be maintained on the laser output pulse shape, while the voltage pulse available at the "+ Gate" connector each time that the oscilloscope's timebase is triggered is used to trigger the radar recording system.

Depending on the height range to be studied, one of two alternative signal recording techniques is used. The signal strength from altitudes below approximately 10 km is sufficiently high to allow an

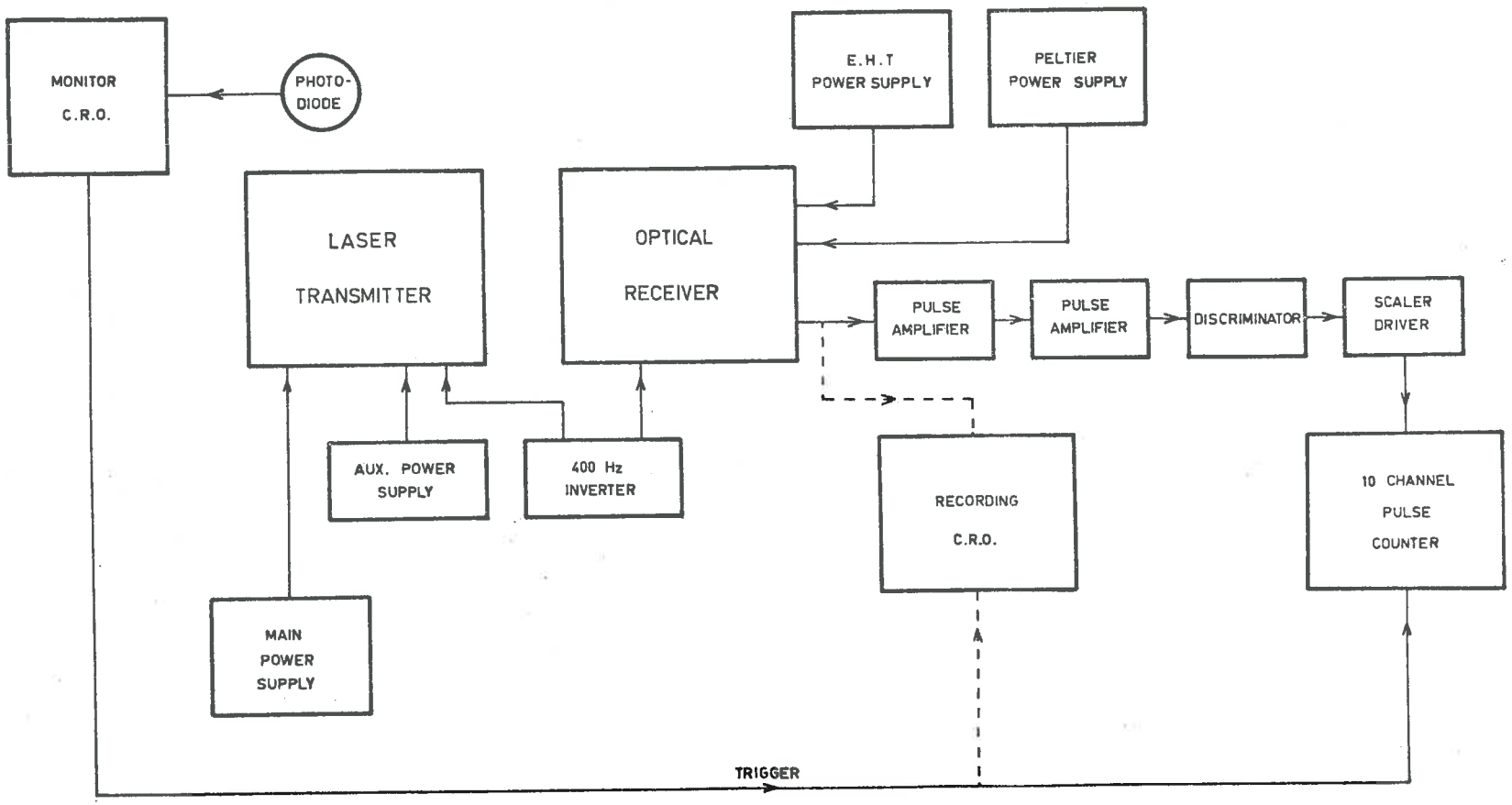

Figure 5.1 Block diagram of laser radar electronics.

analogue recording technique to be used. From altitudes above 10 km, the signal strength is such that the photomultiplier output current may be resolved into pulses corresponding to the arrival of individual photons, and a digital signal recording technique is used. In the following sections, the recording systems and circuitry will be described.

5.2 Digital Recording System

The electrical pulses which appear at the photomultiplier anode corresponding to individual photons incident at the photocathode have a continuous size distribution, extending from zero amplitude to 3 or 4 times the most probable amplitude (Morton, 1968). For greatest counting efficiency, therefore, the counting system should accept pulses having very small amplitudes. Such a system however would be unduly sensitive to noise picked up by connecting leads, or introduced through power supplies, and in practice the counting system is designed to have a definite threshold of sensitivity. In the present system, the sensitivity threshold is determined by a "Nanosecond Systems" Model 105F high-speed discriminator. This unit has an input impedance of 50 ohms, and the threshold may be varied by means of a front-panel control between limits of 50 mV and 700 mV.

Fig. 5.2(a) shows the integral pulse height distribution at the anode of an E.M.I. type 9558B photomultiplier, measured with an anode load resistance of 50 ohms. The measurements were carried out at the highest tube gain recommended by the manufacturers (2000 Amp/lumen) and

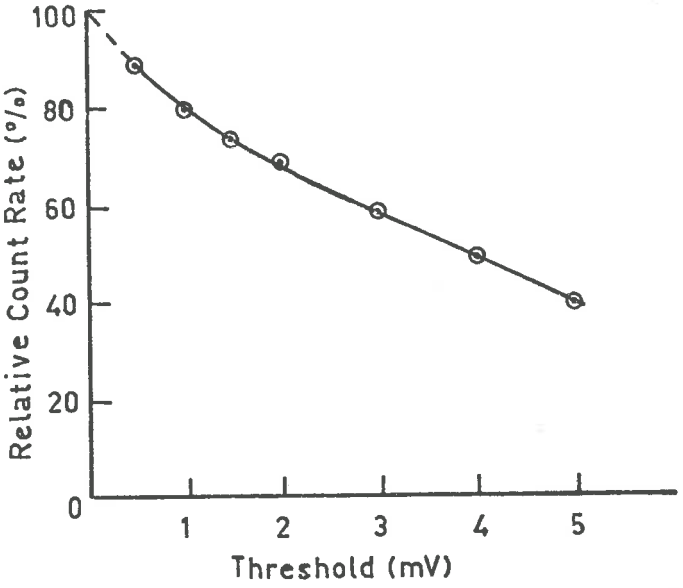

Figure 5.2(a) Photomultiplier integral pulse height distribution.

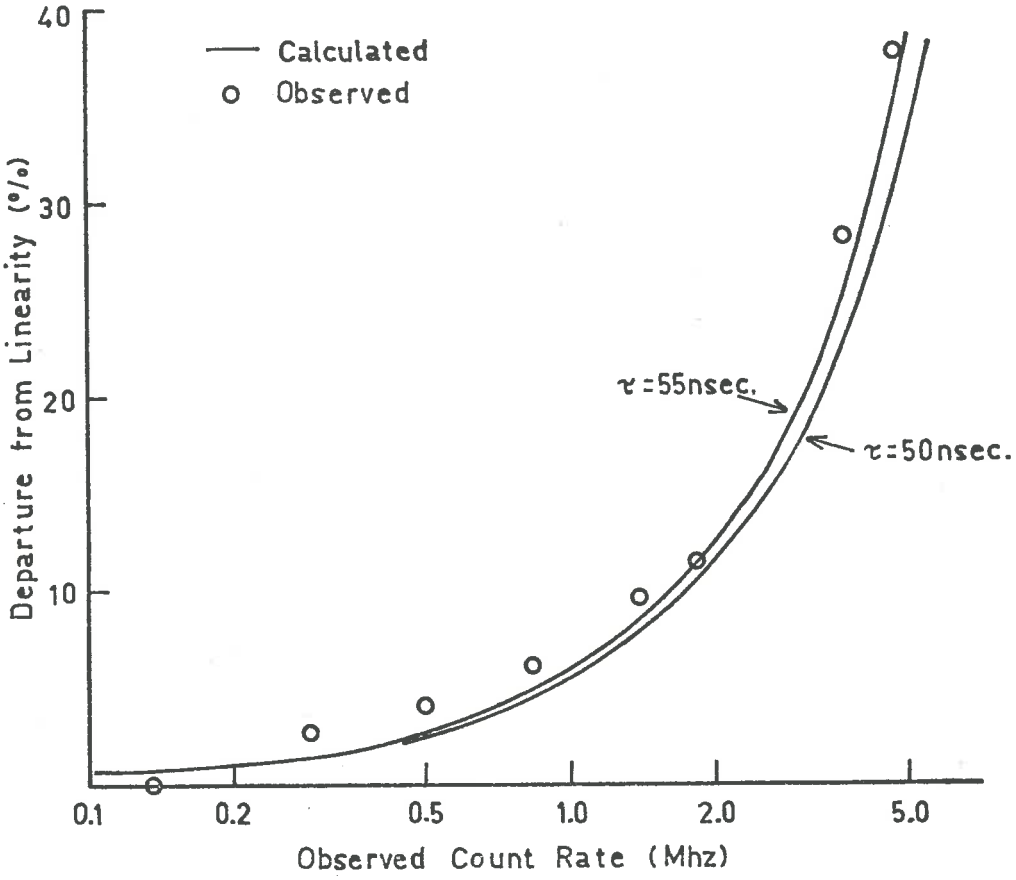

Figure 5.2(b) Departure from linearity of counting system.

it may be seen that approximately half of the output pulses have amplitudes smaller than 4 mV. For this reason, considerable amplification is required between the photomultiplier anode and the discriminator input, and this is achieved by two similar pulse amplifiers in cascade, each with a gain of 10. The first of these amplifiers (the preamplifier) is mounted on the photomultiplier housing, and its output is passed through 50 ohm coaxial cable to the second amplifier, in the recording electronics rack.

The circuit of the preamplifier, shown in Fig. 5.3(a), is similar to that described by Jackson (1965) with the exception that the peaking chokes and feedback capacitor have been eliminated in order to improve the stability of the amplifier, by reducing its bandwidth. The risetime of the amplifier is 3 nsec, which is sufficient to pass the 6 nsec risetime photomultiplier pulses. Both amplifiers are D.C. coupled, thus eliminating the possibility of baseline shifts at high count rates. This is important in the present application, since the recording system must be able to handle a very wide dynamic range.

The output of the discriminator consists of negative pulses, approximately 12 nsec wide and 350 mV in amplitude. These pulses must be converted to positive pulses of at least 3V amplitude and 25 nsec width, before being passed to the counter which forms the recording system. This is achieved by the scaler driver, the circuit of which is shown in Fig. 5.4. The operation of this unit is as follows. The transistors T1 and T2 form a fast monostable circuit, in which both transistors are normally conducting, and are cut off by a negative pulse

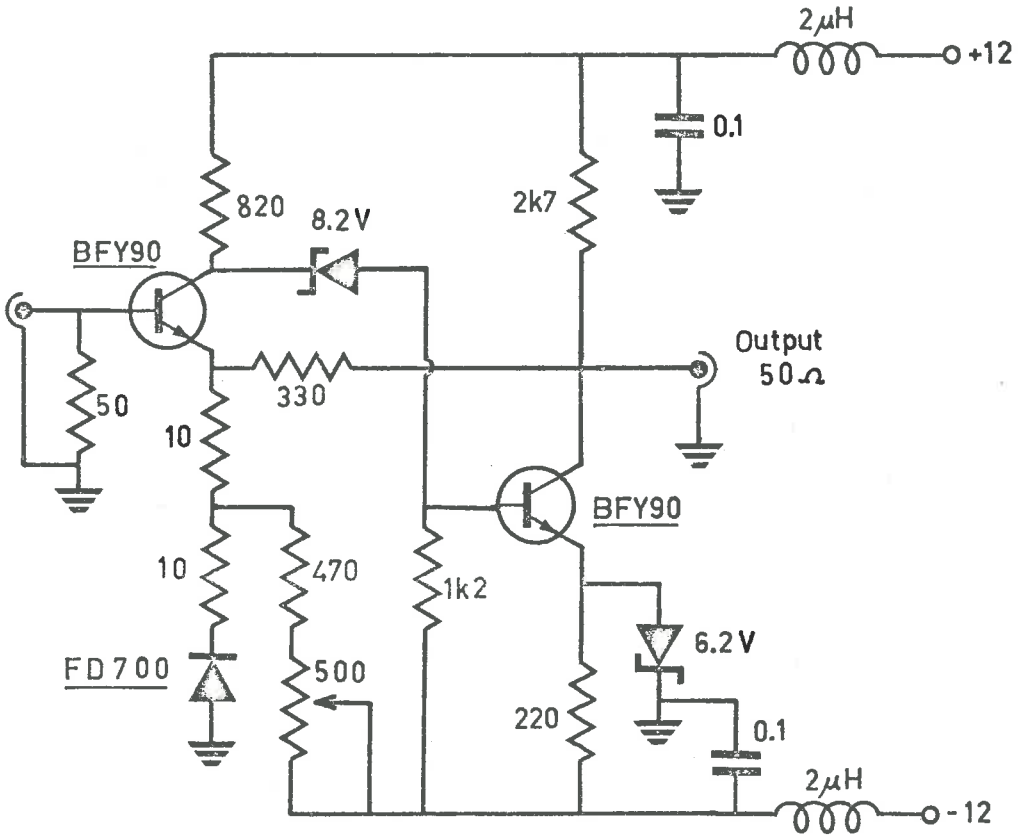

Figure 5.3(a) Circuit of pulse preamplifier.

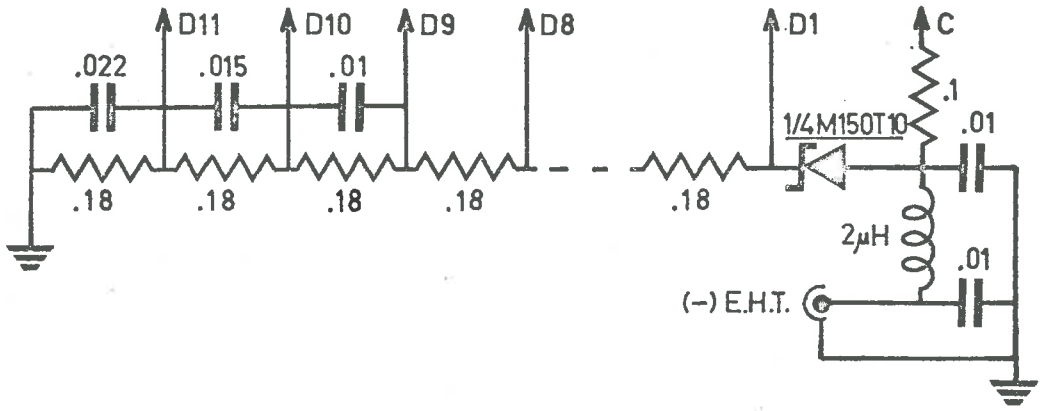

Figure 5.3(b) Photomultiplier dynode voltage divider.

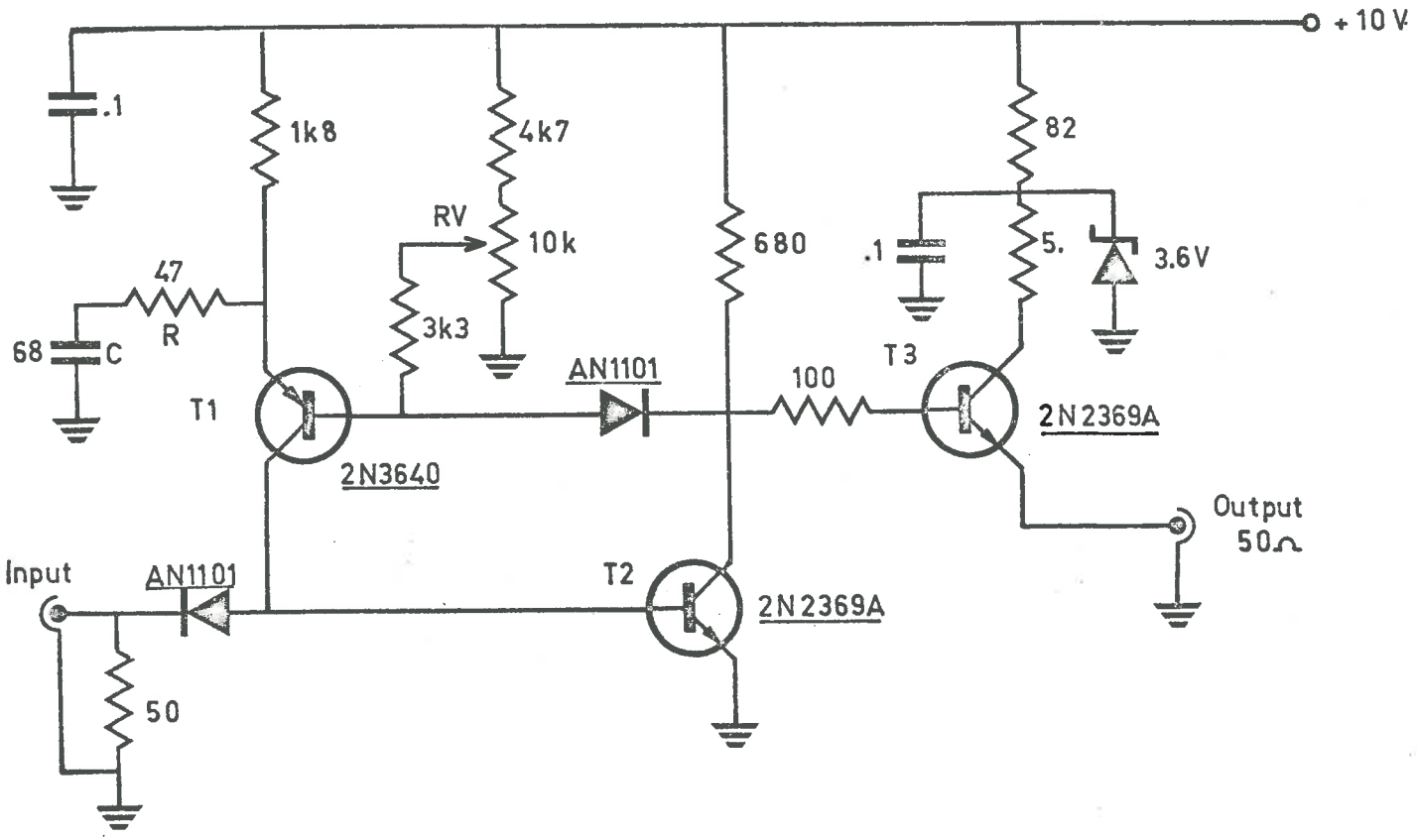

Figure 5.4 Circuit diagram of scaler driver unit.

applied to the input. The transistors remain in this condition until capacitor C charges through resistance R to restore both transistors to their stable conducting state. The multivibrator pulse width is thus determined by the time constant of R and C, but may be varied over a small range by the width control RV, since this varies the potential to which C must charge to restore conduction in T1. Transistor T3 provides a low output impedance suitable to drive a 50 ohm coaxial cable.

Signal recording is carried out in a 10-channel counter, which has been specifically designed and constructed for the laser radar. The requirements of high counting rate and small dead time between channels could not be met by any readily available commercial unit. The circuits and construction of the 10-channel counter are described in detail in the Appendix. The counter channels form 10 successive range recording intervals and may be set at 1,2,4 or 8 km width by means of a front panel control. The height at which recording begins may be set to 10, 20, 40 or 80 km by a time delay between the arrival of a trigger pulse and the opening of the first channel. In a later modification, the 10 km delay setting was replaced by one of 12 km, in order to facilitate the overlapping of data obtained from different height ranges.

The maximum counting rate is not the same for each of the 10 channels, being dependent on the characteristics of the individual microcircuits used for the input stage of each channel. However, the counting rate is in no case less than 20 MHz for regularly spaced pulses (50 nsec resolving time) and is typically 25 MHz. The resolving time of the discriminator, which has been set at approximately 50 nsec, thus determines the

resolving time of the complete recording system.

The linearity of the pulse counting system has been checked in the laboratory. A small incandescent lamp connected to a stabilised, variable power supply was used to illuminate the detector photocathode. The photomultiplier anode current, and the corresponding pulse count rate recorded by the counting system, were measured at a number of different lamp intensities. If it is assumed that the anode current is proportional to the illumination incident on the detector photocathode, then the result shows the linearity between light intensity and the resultant count rate. The departure from linearity was found to be essentially in agreement with that predicted by equation 2.9, as shown in Fig. 5.2(b). It can be seen from this graph that corrections must be applied to the recorded pulse counts for average count rates higher than 0.2 - 0.3 MHz.

5.3 Analogue Recording System

In the analogue recording technique, the photomultiplier output current waveform is displayed directly on the screen of a Tektronix 564 storage oscilloscope. The oscilloscope's timebase speed and delay settings are adjusted to display the signal from the height region of interest.

In order to cover the altitude region between 1 and 10 km, a dynamic range in the recording system of approximately 3½ orders of magnitude is required. Attempts were made to compress this signal amplitude range into a voltage range which could be stored in one

sweep on the oscilloscope screen by passing the signal through a logarithmic amplifier. A commercial logarithmic amplifier was tried, and found not to be sufficiently accurate in its transfer characteristic. A logarithmic amplifier which had been constructed was found to be accurate within 5% in its transfer characteristic over 4 orders of magnitude, but could not be made sufficiently rapid in its speed of response.

These experiments were therefore abandoned, and signal recording is at present carried out by storing the results of several firings successively on the oscilloscope screen, at progressively higher sensitivity settings of the vertical amplifier. In this way, a number of traces are obtained, each allowing the signal from a different region of the height range to be measured. The traces are photographed, manually digitised, and plotted as a composite curve.

For reasons discussed in Section 4.3.4, it is not possible to use the rotating shutter in the receiver for observations below approximately 10 km. During the recording sequence, therefore, as the oscilloscope sensitivity is increased, severe overloading of the oscilloscope amplifier takes place due to the strong scattering from the low regions of the atmosphere. It has been found, however, that recovery of the amplifier from overload is sufficiently rapid to allow the technique described above to be used. A neutral filter placed over the receiver aperture is used to limit the maximum light intensity incident on the photomultiplier to prevent overloading of the photocathode.

5.4 The Photomultiplier

The detector is required to have the highest possible quantum efficiency at the operating wavelength, in order to convert the greatest possible fraction of the received photon flux into electrical signal. Of the currently available photocathode materials, the "trialkali" type (E.M.I. S-20) offers the highest quantum efficiency at 0.7 μ, a value of 0.03 being typical. The actual value of quantum efficiency varies significantly between individual examples of the same type of tube, and selection of a tube for the highest possible quantum efficiency would therefore appear to be desirable.

All recordings carried out with the present system have utilized an E.M.I. type 9558B photomultiplier, with only an average value of quantum efficiency. A specially selected type 9558A tube has been obtained, which has a quantum efficiency at 0.7 μ approximately 2 times higher than that of the 9558B tube. Unfortunately, the tube was found to suffer from instability at operating voltages approaching those necessary to achieve sufficient electron multiplication, or gain. A high value of gain is necessary to ensure that the greatest possible fraction of the output pulses have amplitudes greater than the counting system threshold, and an average gain of 10^7 is desirable. The selected tube has therefore not been used.

A high value of tube gain is not necessary for the analogue recording technique, and could, in fact, lead to overloading of the tube anode. In order to allow the tube gain to be varied by changes in the overall operating voltage while maintaining the quantum efficiency

of the tube at a constant value, it is necessary to stabilise the voltage between the cathode and first dynode. This has been achieved by means of a zener diode. The resistor chain used to provide the required dynode potentials for the tube is shown in Fig. 5.3(b).

A Peltier battery is used to cool the photomultiplier in order to reduce the dark count rate. The cooling system is capable of lowering the temperature of the tube to -15°C, and at this temperature the dark count is 120 pulses/sec, compared to 1900 pulses/sec at room temperature (21°C). The Peltier battery is a small water-cooled unit, requiring a D.C. supply of 5 amps at 5 volts. The circuit of a constant current power supply to meet this requirement is shown in Fig. 5.5. The two transistors form a Darlington amplifier, with its input maintained at a constant voltage by zener diode Z_2. The second transistor therefore maintains a constant current flow through its emitter resistance, R1. The current through the Peltier battery may thus be preset by adjustment of R1, and becomes independent of the length or resistance of connecting leads. The purpose of zener diode Z_1 is to absorb the voltage spike generated by the filter choke when the output load is disconnected.

5.5 Electrical Noise

Following installation of the pulse counting system at the field station, considerable difficulty was experienced in overcoming noise interference. This noise, generated mainly by the relays and contactors in the main power supply, was picked up by the photomultiplier circuitry and passed to the counting system. The problem was finally

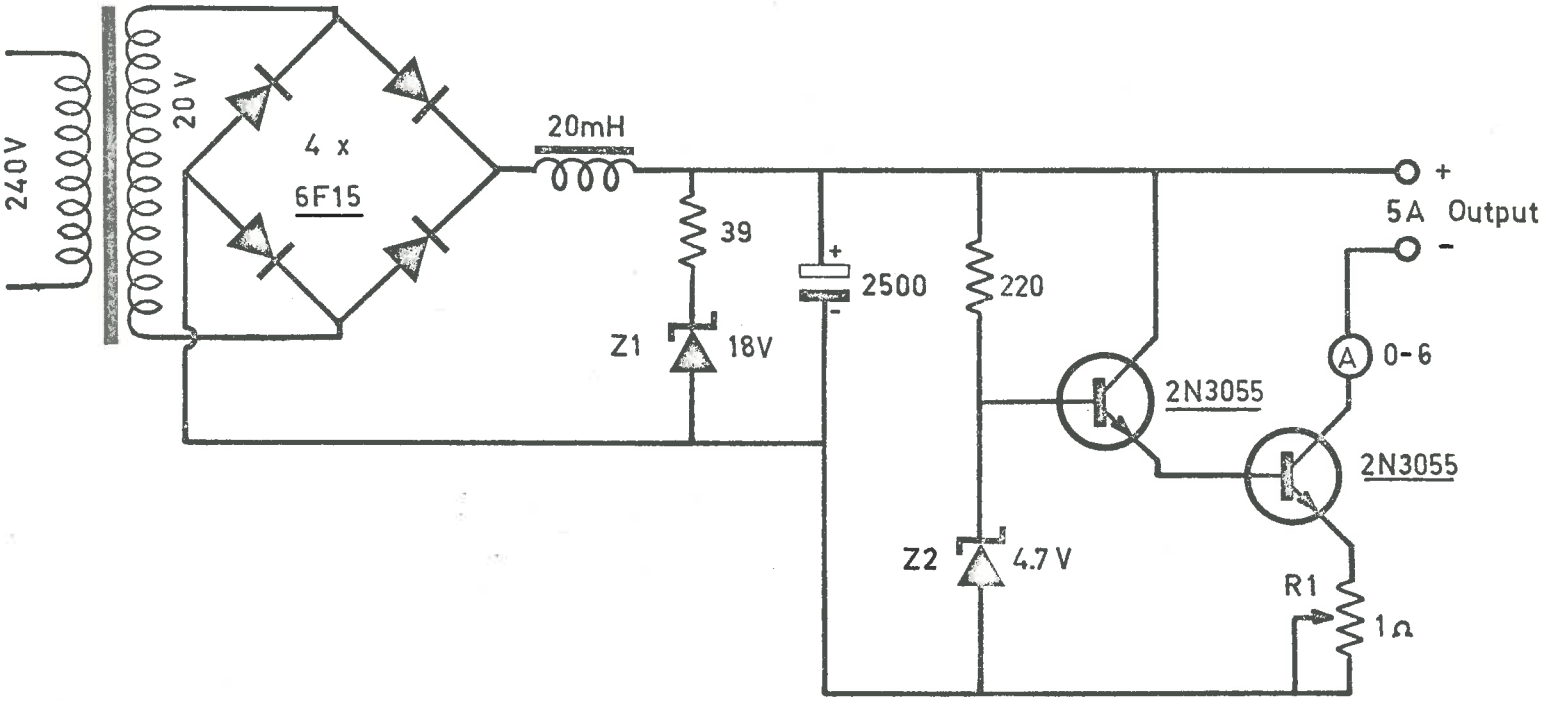

Figure 5.5 Circuit diagram of Peltier battery power supply.

overcome by electrostatic shielding of all leads to and from the main power supply, and by magnetic shielding of the photomultiplier and preamplifier units. It was also found necessary to decouple separately all power supplies to the preamplifier housing.

CHAPTER 6

SIGNAL RECORDING AND ANALYSIS

6.1 Introduction

Regular observations of the atmosphere using the laser radar equipment described in Chapters 4 and 5 commenced in early April, 1969. The equipment was initially located at the Mawson Institute for Antarctic Research field station at Mt. Torrens, South Australia, approximately 30 miles from the city of Adelaide. The elevation of Mt. Torrens (1913 ft.) helped to reduce the loss of signal due to the dust in the lower troposphere, and the site was sufficiently far from the city lights that these were not a significant source of interference. The main disadvantage of the site was found to be the frequent occurrence of mist which formed in the early evening following a warm day, as a result of the rapid temperature drop after sunset. This problem was particularly prevalent during the summer months, and severely restricted the number of occasions on which observations could be attempted. Consequently, it was decided to seek a more suitable operating site. During September and October, 1969, the equipment was transferred from the field station to a mobile instrumentation van, on loan from the Commonwealth Department of Supply. The modifications which were made to the van, and the equipment installation, have been described in Chapter 4.

The complete laser radar system is now easily transportable, and it had been intended to try a number of different operating sites.

However, tests carried out with the equipment inside the University grounds, almost in the centre of the city of Adelaide, showed that signal strengths received from heights above 10 km were only about 10% lower than those recorded at Mt. Torrens. Further, it was found that the sky background count rate, while greater by nearly a factor of two, was still smaller than the photomultiplier dark count rate. Thus there appeared little to be gained by seeking a better site, while there was the possibility that useful information on industrial pollution could be obtained if the lower altitude limit of the equipment could be reduced sufficiently. Since November 1969, therefore, soundings have been carried out from the site in the University grounds.

Although the upper altitude limit of soundings carried out with the laser radar system has remained constant at 60 km, the lower altitude limit has been steadily reduced. At the beginning of August 1969, the lower limit was reduced from 12 km to 9 km, and towards the end of the same month to 3 km.* Over the 3-60 km altitude range, signal recording is carried out in a number of stages, involving the use of both analogue and digital recording techniques, as explained in the previous chapter. Analysis of the data is carried out on the CDC 6400 computer at the University of Adelaide. The detailed recording procedure and analysis of the resulting records is described in the following sections.

---

*Recent work by D.J. Gambling has reduced the lower limit of observations to 0.3 km.

6.2 Pulse Counting, 12-60 km Region

From altitudes above 12 km, the signal is too weak to allow the analogue technique to be used, and signal recording is carried out by counting pulses corresponding to individual signal photons received from a number of height intervals (channels). Because of the limited number of channels available in the recording system, the 12-60 km height range is covered in three stages:

12-22 km in 10 steps of 1 km

20-30 km in 10 steps of 1 km

20-60 km in 10 steps of 4 km.

At the start of a recording sequence, both rotating shutters must be phased. The transmitter shutter is adjusted in the manner described in Section 4.6. The phase of the receiver shutter is adjusted so that the receiver aperture is completely opened by the time the scattered light has returned from the height at which observations are to begin. In the case of observations in the 12-22 km height range, the shutter delay is set at 50-60 μsec, while a delay of 100 μsec is used in the case of observations beginning at 20 km. Receiver shutter phasing is carried out with the aid of a small lamp that illuminates the receiver aperture. The photomultiplier output is connected to a storage oscilloscope, which is triggered when the laser is fired. The resultant waveform on the screen of the oscilloscope allows the shutter delay to be measured.

In the case of observations in the 12-22 km height range, some attenuation of the received signal is necessary in order to limit the

maximum count rate to a value which can be accepted by the recording system. Although corrections applied to the recorded count allow the maximum count rate to be increased beyond the point where the system departs from linearity, it is desirable to limit these corrections to less than 25%. Large values of correction require that the resolving time of the recording system should be accurately determined. It is estimated that the resolving time is known to an accuracy of 10%, and the resultant uncertainty in a 25% correction factor is not larger than 3%.

The attenuation is achieved by means of gelatin foil neutral density filters, inserted in a holder close to the aperture which defines the receiver's field of view. In the case of observations in the 12-22 km height range, an attenuation factor of four is used. No attenuation is necessary for observations beginning at 20 km altitude.

In practice, the laser is triggered repetitively, at a rate of one firing every two seconds, and the signal received from a given height range is accumulated by the 10-channel counter. Recording is continued until the smallest count accumulated in any channel is sufficiently large to provide the required statistical accuracy, usually set at 5%. This requires a count of at least 400 pulses to be accumulated in any channel. Under clear atmospheric conditions, this accuracy is achieved after approximately 200 laser firings for the 12-22 km region, and 300 firings in the 20-30 km region. In the case of observations in the 20-60 km height range, about 10,000 firings would be required in order

to accumulate 400 counts in the last channel (56-60 km). In the interests of laser life, observations in this upper region are therefore usually terminated after 500 firings, and the results of several nights' recordings are combined in order to improve accuracy at high altitudes.

The background count rate is measured before and after each recording sequence, by opening one of the counter channels for a given time, usually 10 secs. The resultant count represents the combined contributions due to sky radiation and photomultiplier dark current. It has been found that the background count rate is generally in the range 200 to 250 counts per sec, and approximately 60% of this is due to photomultiplier dark current. The photomultiplier contribution could be reduced by selection of a better tube, and by cooling the tube to a lower temperature. However, in the present system, the combined background contribution to the total signal received from an altitude of 60 km is less than 20%, and the maximum height to which observations could be carried out would thus not be increased significantly by a decrease in the background count rate. The height limitation of the present equipment is clearly set by the statistical uncertainty in the recorded count, and could only be increased by greatly increased recording times.

The results of an observation carried out on the night of 29th November 1969 are summarised in Table 6.1. The table lists the total count recorded in each channel for each of the three height ranges, and the number of firings carried out for each height range. It is of

interest to compare the observed count rates with those predicted from theory in Section 2.4, and the results from a number of heights are shown in Table 6.2. The predicted count rates have been evaluated for a laser output energy of 0.2 joules. The observed count rates have been corrected for the resolving time of the recording system, the background count rate, and any attenuation deliberately introduced to limit the maximum count rate.

TABLE 6.1

Channel Number	12-22 km 200 firings	20-30 km 300 firings	20-60 km 500 firings
1	3630	3875	17583
2	3069	2897	6320
3	2504	2161	2374
4	2113	1645	980
5	1721	1239	412
6	1432	1049	212
7	1173	779	109
8	757	602	60
9	584	479	28
10	403	422	20
Filter Factor	4x	-	-
Channel Width	1 km	1 km	4 km

TABLE 6.2

Height (km)	Predicted Rate (sec^{-1})	Observed Rate (sec^{-1})	Ratio Observed/Predicted
10	6.2×10^{7}	-	-
20	3.2×10^{6}	1.9×10^{6}	0.59
30	3.0×10^{5}	1.8×10^{5}	$0.60 \pm .01$
40	3.8×10^{4}	2.2×10^{4}	$0.58 \pm .03$
50	5.9×10^{3}	4.2×10^{3}	$0.71 \pm .09$
60	1.2×10^{3}	1.0×10^{3}	0.87 ± 0.20

It can be seen that, at heights up to 40 km, the observed count rate is 60% of the predicted count rate. This discrepancy indicates that one or more of the values of atmospheric transmission, receiver efficiency, or detector quantum efficiency have been overestimated for purposes of calculation. The observed ratio could, for example, be accounted for by a value of atmospheric transmission T equal to 0.62, instead of the value used of 0.8. The increasing value of the ratio for heights above 40 km is not significant as it is due to the increasing statistical uncertainty in the observed count rate.

6.3 Analogue Signal Recording Below 12 km

The analogue recording technique used for altitudes below 12 km has been described in Section 5.3. The receiver and transmitter rotating shutters are not used, and both are locked in the open

position. A filter is inserted in the receiver in order to prevent overloading of the detector photocathode, and the gain of the photomultiplier is controlled by adjustment of the E.H.T. voltage in order to limit the maximum output current to the linear operating range of the tube. The photomultiplier output is connected through low-capacitance coaxial cable to a Tektronix 564 storage oscilloscope.

The receiver's normal field of view of 2 mrad allows complete overlap between the transmitter and receiver beams at an altitude of 1 km, and observations from this altitude upwards are possible. However, because of the large amount of manual data reduction involved in analysis of the analogue records, observations carried out to date have almost always been limited to the altitude region above 3 km.

6.4 Interpretation and Presentation of Results

It was shown in Chapter 2 that the scattered intensity $S'(h)$ received from a height h can be expressed by a relation of the form

$$S(h) = KT^2(h)B(h,\Pi)/h^2 \qquad \ldots 6.4$$

where K is a constant for the equipment, $T(h)$ is the optical transmission between the equipment and the height h, and $B(h,\Pi)$ is the backscattering coefficient of the atmosphere at height h. In the case of an atmosphere containing both molecular and aerosol components,

$$B(h,\Pi) = B_r(h,\Pi) + B_a(h,\Pi)$$

where $\beta_r(h,\pi)$ and $\beta_a(h,\pi)$ represent the molecular and aerosol components respectively.

It is shown in Section 6.5 that it is possible to calculate a continuous profile of the quantity S(h) from the laser radar records. However, it is not possible to calculate $\beta(h,\pi)$ without a knowledge of both the quantities K and T(h) in equation 6.1. The constant K depends on such parameters as receiver efficiency, transmitter output energy, and photomultiplier quantum efficiency, all of which are difficult to measure accurately and, with the exception of the last quantity, may change appreciably with time. The value of T(h), the atmospheric transmission, is also in general an unknown quantity. Sandford (1967) has described a method whereby the transmission to a given height h may be measured with the laser radar itself, but the method is not applicable to the present system since it requires measurements at a variety of zenith angles. The method further requires that the atmosphere up to the height h should be horizontally homogeneous, and observations carried out by Sandford have shown that this is not always the case.

Absolute calibration using the known emission intensities of certain stars has also been proposed. This method however requires that the laser system should be steerable, and further suffers from the fact that the calibration is not carried out at the laser emission wavelength. Long (1963) has pointed out that the atmospheric transmission can change significantly for very small changes in operating

wavelength, due to absorption by water vapour in the atmosphere.

For these reasons, absolute calibration of the scattering profiles in terms of the backscattering coefficient has not been attempted. Instead, a quantity called the scattering index I(h) which is proportional to the total atmospheric backscattering coefficient at any height h is calculated, and the resultant profile is fitted to a curve of I(h) calculated for the case of scattering by a purely molecular atmosphere, in the following way. It is necessary to assume that a region of the atmosphere within reach of meterological sounding balloons is essentially free of aerosol scattering, at least within the limits of accuracy set by the equipment. This assumption is justified later. Then at a height h_o within this region,

$$S(h_o) = KT^2(h_o)\ B_r(h_o,\Pi)/h_o^2$$

The molecular density at the height h_o is known from balloon data, allowing $B_r(h_o,\Pi)$ to be calculated. Since $S(h_o)$ is known from the laser results, the quantity $KT^2(h_o)$ may be evaluated. Now, at any adjacent height $h = h_o + dh$,

$$S(h) = KT^2(h_o)T^2(dh)[B_r(h,\Pi)+B_a(h,\Pi)]/h^2 \qquad \ldots 6.2$$

where T(dh) represents the transmission between heights h_o and h. It is shown in the next section that the term T(dh) can be evaluated during analysis of the laser data, and hence it is possible to calculate the scattering index I(h) defined by

$$I(h) = S(h)h^2/KT^2(h_o)T^2(dh)$$

From equation 6.2, it can be seen that I(h) is proportional to the total backscattering coefficient at the height h. For the case of scattering by a purely molecular atmosphere, the scattering index is proportional to the Rayleight backscattering coefficient $\beta_r(h,\Pi)$, which can be calculated from the molecular densities derived from balloon measurements. The scattering index curve derived from the laser results is normalised to the $\beta_r(h,\Pi)$ curve at the height h_o.

The choice of the normalisation height h_o presents a problem, since it has been suggested by several workers (for example, Volz and Goody, 1962) that no region of the atmosphere is completely free of aerosol scattering. However, the aerosol sampling experiments carried out by Junge, Chagnon and Manson (1961) have revealed a very rapid decrease in aerosol concentration for heights above 20 km, and these results have been borne out by rocket measurements of the vertical distribution of diffuse sky light carried out by de Bary and Rossler (1966). Many workers (for example, Clemesha et al., 1967(b)) have therefore used the 30 km altitude region for normalisation of their results. However, in the present work, it was considered that the statistical errors inherent in individual points of a single experimental profile in the 30 km region were too great to allow satisfactory normalisation at this height by automatic computation. It was also found that not all of the meteorological balloons launched at Adelaide reached an altitude of 30 km.

For these reasons, a lower altitude than 30 km was sought for normalisation of the results. From the results of Junge et al. (1961)

it was noted that the concentration of aerosol particles in the 0.1 - 1.0μsize range reaches a local minimum near 12 km altitude. Although the value of the minimum concentration is considerably greater than the concentration at 30 km, the molecular density is also greater at 12 km, and calculations showed that the turbidity, defined by the ratio of aerosol to molecular scattering coefficients, should be approximately equal at the two heights. The concentration of Aitken nuclei in the size range 0.01 - 0.1 μ shows no such minimum near 12 km, their numerical concentration being two orders of magnitude greater than that of the larger particles. However, the nuclei are very much less effective as scatterers at optical wavelengths than the larger particles, and it was considered that their contribution to the total scattering would be negligible. This assumption is again borne out by the results of de Bary and Rossler (1966), who found a local minimum in aerosol scattering in the region of 12 - 16 km.

Initial normalisation of the profiles obtained in the present work is therefore carried out at a height near 10 km. The actual height used is chosen individually for each profile, so that the observed scattering at heights in the vicinity of the normalisation height is never smaller than the scattering predicted for a molecular atmosphere. This method of normalisation of the profiles has proved quite satisfactory for purposes of computation. It has been found that profiles normalised in this manner generally show good agreement with predicted values in the 30 km region, thus indicating that normalisation at either of these height regions leads to equivalent results, within the

accuracy of the present measurements.

For consistency with the results of other workers, the profiles presented in Chapter 7 have, where necessary, been individually renormalised so that the observed points agree with the theoretical profiles in the 30 km altitude region.

Molecular densities over the 0-30 km altitude range are available from the results of daily meteorological balloon flights from the Adelaide airport. For the altitude range above 30 km, no day to day direct measurements of atmospheric density are available, and it has been necessary to use the values tabulated in the U.S. Standard Atmosphere (1962). The values of molecular density obtained from these two sources generally overlap quite well in the 30 km height region, although differences of 5% have on occasion been observed, and these can introduce a discontinuity in the scattering index profile calculated for a molecular atmosphere.

It should be noted that the molecular densities obtained from the U.S. Standard Atmosphere represent average conditions only, and departures from the tabulated densities over the 30-60 km height range predicted by the U.S. Standard Atmosphere Supplements (1966) amount to -5% in the winter months, and +10% in the summer months. The uncertainty in atmospheric density above 30 km introduces a corresponding uncertainty in the scattering index profile. It will be shown in Chapter 7, however, that for altitudes above 30 km, the uncertainty in individual profiles due to statistical errors is generally greater than

that due to variations in atmospheric density.

6.5 Analysis of Digital Records

From the result of one observing sequence, three sets of 10 numbers are obtained, each number being the count read out of a particular counter channel, and representing the total pulse count received from a given height interval. It is necessary to apply a number of corrections to the recorded counts before the scattering index I(h) defined in the previous section can be calculated. These corrections are now considered in turn.

6.5.1 Resolving Time Correction

The recorded counts are first corrected for the finite resolving time of the pulse counting system. From the total count recorded in each channel, an average value of the count rate can be calculated, and, by substitution in equation 2.9, a correction factor is obtained which is applied to the recorded count to obtain the true signal count. Although the actual count rate decreases during the time that a channel is open, calculations have shown that in the worst case the error introduced by correcting the average count rate is less than 1%.

6.5.2 Background Count Correction

From the average of the background count rates measured before and after each stage of the recording sequence, the expected background count per channel is calculated and subtracted from the total count recorded in each channel. No correction is made for spurious

signals introduced by multiple scattering effects, since measurements carried out with the receiver and transmitter beams deliberately misaligned have shown that the effect is negligible for observations at all altitudes up to 60 km.

6.5.3 Count Rate Correction

The count recorded in a given channel represents the total signal count received from a particular height range. Since the count rate varies as a non-linear function of height throughout the time that a channel is open, it is not possible to calculate the count rate S(h) corresponding to a particular height h directly. Instead, the following method is used. It is assumed that the variation with height of the count rate over a region of height equivalent to three channel widths can be represented by a function of the form

$$S(h) = ah^2 + bh + c$$

The values of the constants a and b determine the slope of the curve, and are calculated for each channel in turn by substituting into the above equation the average count rate and mean height for that channel and each of two adjacent channels. The value of the constant c is chosen so that

$$\int_{h_1}^{h_2} S(h)dh = C$$

where h_2 and h_1 are the upper and lower limits of the centre channel, and C is the actual count recorded in that channel. The constants a, b and c thus determine the variation of count rate S(h) with height h

throughout a particular channel, and the actual count rate may thus be calculated for any height within that channel. The height used is the mean of the channel limits h_1 and h_2.

This method is modified for the case of observations over the 20-60 km height range, where the rapidly increasing statistical errors in individual data points do not allow the function S(h) to be evaluated sufficiently accurately by the technique described above. Instead, it is assumed that over this height range, S(h) is of the form $[\exp(-h/H)]/h^2$, where H is the scattering scale height. This variation in S(h) is that which would be expected for the case of scattering by a molecular, isothermal atmosphere, but fits the observed variation quite well for heights above 30 km. The value of the scale height H is obtained from the U.S. Standard Atmosphere (1962). Over the 20-30 km height range, the observed variation in S(h) is more rapid, corresponding to a smaller scattering scale height, because of the presence of aerosols in this region. The value of H in this region is therefore calculated from the results of the previous recording stage, which covers the 20-30 km height range in steps of 1 km.

6.5.4 Transmission Correction

It was shown in Section 6.4 that in order to obtain the scattering index profile I(h), it is necessary to correct the signal count rate profile S(h) for the effects of atmospheric attenuation. The main processes that attenuate laser radiation in the height range of interest are scattering by molecules and aerosols, and absorption by

ozone (Elterman, 1964). The extinction optical thickness of an atmospheric layer dh may therefore be written

$$\tau_{ext}(h) = (\beta_r(h) + \beta_o(h) + \beta_a(h))dh \qquad ...6.3$$

where $\beta_r(h)$ and $\beta_a(h)$ are the volume scattering coefficients for the molecular and aerosol components respectively, and $\beta_o(h)$ is the ozone absorption coefficient. The transmission T(dh) through the layer dh is given by

$$T(dh) = \exp(-\tau_{ext}(h))$$

The values of $\beta_r(h)$ are calculated from the known molecular densities, while values of $\beta_o(h)$ are taken from Elterman's (1964) tabulations. The values of $\beta_a(h)$ are estimated from the laser radar results in the following way. It has been shown previously that the signal count rate S(h) received from a height h is given by the expression

$$S(h) = KT^2(h)[B_r(h,\Pi)+B_a(h,\Pi)]/h^2 \qquad ...6.4$$

where K is a constant for the equipment. T(h) is the transmission between the equipment and the height h, and $B_r(h,\Pi)$ and $B_a(h,\Pi)$ are the molecular and aerosol backscattering coefficients of the atmosphere at height h respectively. It has also been shown that the quantity $KT^2(h_o)$ can be evaluated for the normalisation height h_o, where the aerosol backscattering coefficient is assumed to be negligible. Now, if the height h is sufficiently close to the normalisation height h_o, it is possible to substitute, as a first approximation, the value of $KT^2(h_o)$ into equation 6.4 above, instead of the true value $KT^2(h)$,

and hence to estimate the quantity $B_a(h,\Pi)$ since $S(h)$ is known, and $B_r(h,\Pi)$ can be calculated from the known molecular density at height h. Hence it is possible to evaluate the aerosol volume scattering coefficient $\beta_a(h)$ since

$$B_a(h,\Pi) = \beta_a(h)P_a(\Pi)$$

where $P_a(\Pi)$ is the aerosol phase function for backscattering. The value used is $1/16\,\Pi$ (Deirmendjian, 1965).

It is assumed that the aerosol scattering coefficient increases linearly with height between h_o and h, and one half of the calculated value of $\beta_a(h)$ is substituted in equation 6.3, in order to calculate $T(dh)$, the transmission between heights h_o and h. This value of $T(dh)$ is used to calculate the scattering index $I(h)$ at height h, as previously described. In principle, it would be possible to substitute a corrected value of $T(h)$, given by $T(h) = T(h_o)T(dh)$ into equation 6.4, in order to calculate a more accurate value of $B_a(h,\Pi)$ by an iterative process. However, this is not done in practice, since it has been found that the higher order corrections are negligible. The corrected value of the transmission is, however, used in the next stage of the calculation, for $h = h_o + 2dh$. In this way, transmission corrections are evaluated for the whole profile, to each side of the normalisation height h_o. In practice, the corrections are terminated for heights above 20 km, since statistical errors in the recorded signal make determination of $\beta_a(h)$ unreliable, and the corrections in any case become negligible.

The final stage in analysis of the digital records consists of combining the results of the three recording stages into one continuous profile. The recording stages have been chosen so that some overlap occurs in the height region covered by each stage, and this overlap is used to fit together the three sets of data.

6.6 Analysis of Analogue Records

The analogue recording technique described in Section 5.3 results in a series of photographs, each of which allows the signal strength over a particular height range to be measured. The trace on each photograph is digitised manually, by comparing the trace against a graticule.

The data points from each photograph are scaled in order to overlap with those from preceding photographs, and combined to form a continuous profile of signal strength $S(h)$ as a function of height. The data points are corrected for transmission effects in a manner similar to that used for the digital records, except that corrections begin near the high altitude limit of the profile, near 10 km, and are continued successively downwards. The corrected profile is joined to that obtained by the digital recording technique.

CHAPTER 7

RESULTS OF LASER RADAR MEASUREMENTS

7.1 General Features

The results of all observations carried out during 1969 are presented in composite form in Fig. 7.1, as a curve representing the mean of 40 individual profiles. The individual observations, from which the mean was calculated, were not evenly distributed throughout the year, and the mean profile is therefore not representative of average conditions during 1969. The distribution of observations carried out is shown in Table 7.1

TABLE 7.1

Month	No. of Profiles
April	12
May	7
June	7
July	1
August	7
November	3
December	3

The results have been plotted as values of the observed scattering index I(h) as a function of height. The value of the scattering index at a given height is proportional to the total backscattering coefficient B(h, Π) (cm^{-1} $sterad^{-1}$) at that height. For reasons discussed in Section 6.4, absolute calibration of the observed profile

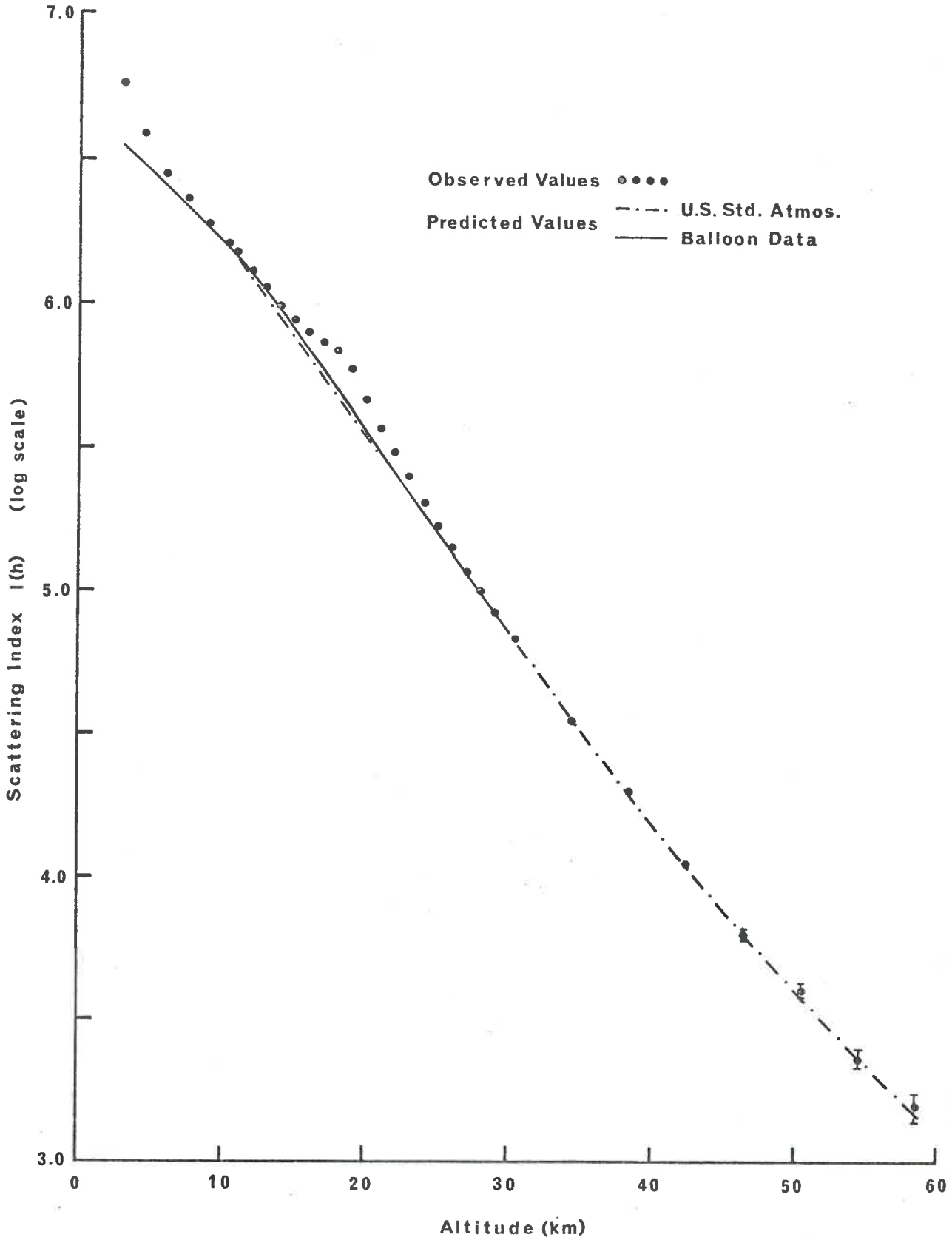

Figure 7.1 Observed variation of scattering index during 1969. The experimental points are compared with values predicted for a molecular atmosphere.

in terms of the backscattering coefficient has not been attempted, and the experimental profile is compared with one calculated for the case of scattering by a purely molecular atmosphere. The observed values of scattering index have been normalised to the calculated profile at an altitude of 30 km.

For the height range below 30 km, molecular densities were obtained from the results of meteorological balloon flights, and the mean of these measurements for those days on which laser observations were carried out has been used in Fig. 7.1. For heights above 30 km, molecular densities were obtained from the U.S. Standard Atmosphere, 1962. It can be seen from Fig. 7.1 that at 30 km altitude there is good overlap between the molecular density predicted by the U.S. Standard Atmosphere, and the mean of the measured densities.

The variation in scattering index follows that predicted for a molecular atmosphere quite well, with the exception of an altitude region between 15 and 25 km, and for all heights below 10 km. In these regions, enhanced scattering is evident. This may be seen more clearly from Fig. 7.2, in which the variation of the ratio of observed to predicted values of the scattering index has been plotted for the 3-60 km height range, again for the mean of all observations carried out during 1969. The scattering ratio profile has the advantage of bringing out more clearly the departures from the scattering expected for the case of a purely molecular atmosphere.

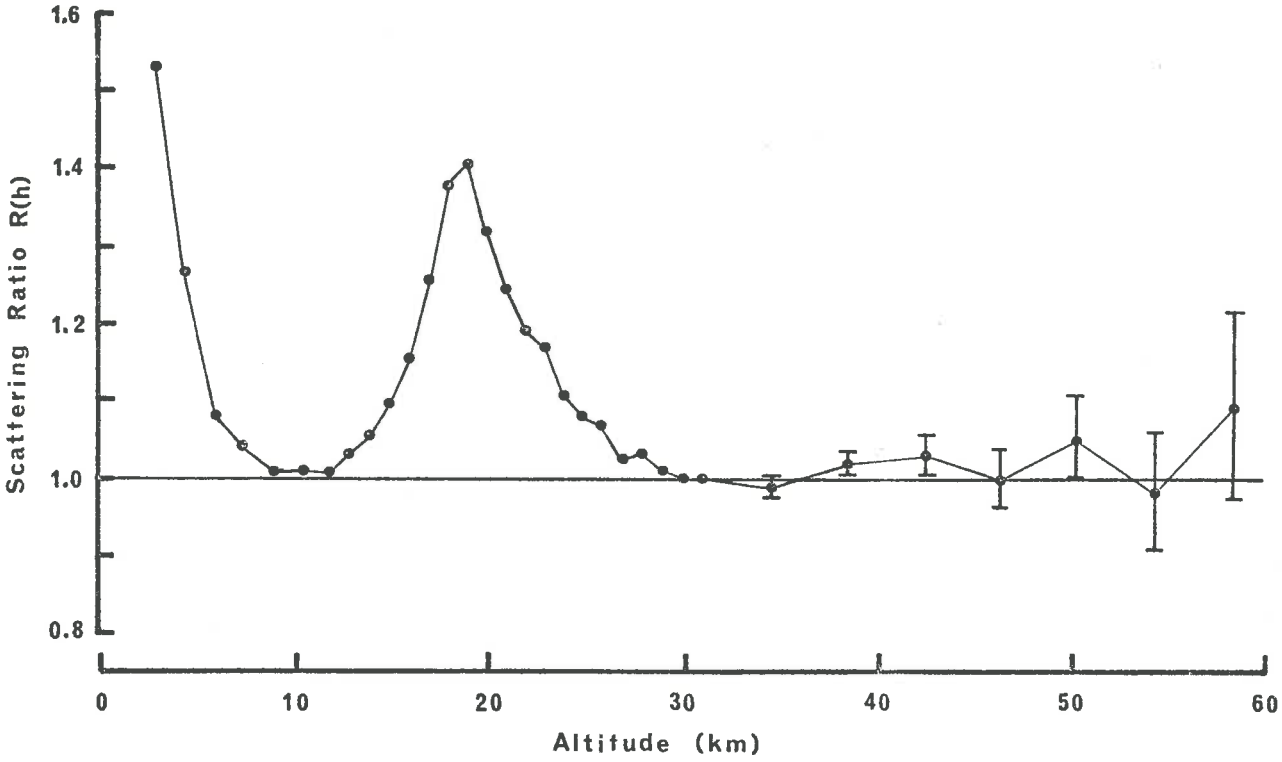

Figure 7.2 Values of the ratio R(h) between observed and predicted values of the scattering index for the mean of all observations carried out in 1969.

In the following sections, the features of the observed scattering profiles are discussed in greater detail.

7.2 The Altitude Region Above 30 km

Over the 30-60 km altitude range, the observed variation in scattering index throughout 1969 followed, within the accuracy of the measurements, that predicted by the U.S. Standard Atmosphere (1962). This may be seen not only in the mean profile of the scattering ratio R(h) for the whole of the year (Fig. 7.2), but also in the mean profiles for each month (Fig. 7.3). Although the fluctuations in the plotted values are greater in the case of the monthly profiles, these all appear to be statistical in nature, being generally within the expected error (one standard deviation). There appears to be no systematic trend away from R(h) = 1 at any height above 30 km.

The uncertainty in the monthly profiles of R(h) near 60 km altitude is 20 to 30%. The seasonal variation in atmospheric density at this altitude predicted by the U.S. Atmosphere Supplements (1966) for a latitude of 30^0 is approximately 10%. It is clear, therefore, that the present results are not capable of revealing the seasonal variation in atmospheric density.

The results of the present observations are in good agreement with the results of observations carried out in the northern hemisphere (for example; Kent, Clemesha and Wright, 1967; Bain and Sandford, 1966(a); and Collis and Ligda, 1966). The results of Kent et al, and Bain and Sandford, are reproduced in Fig. 7.4(a) and (b) respectively.

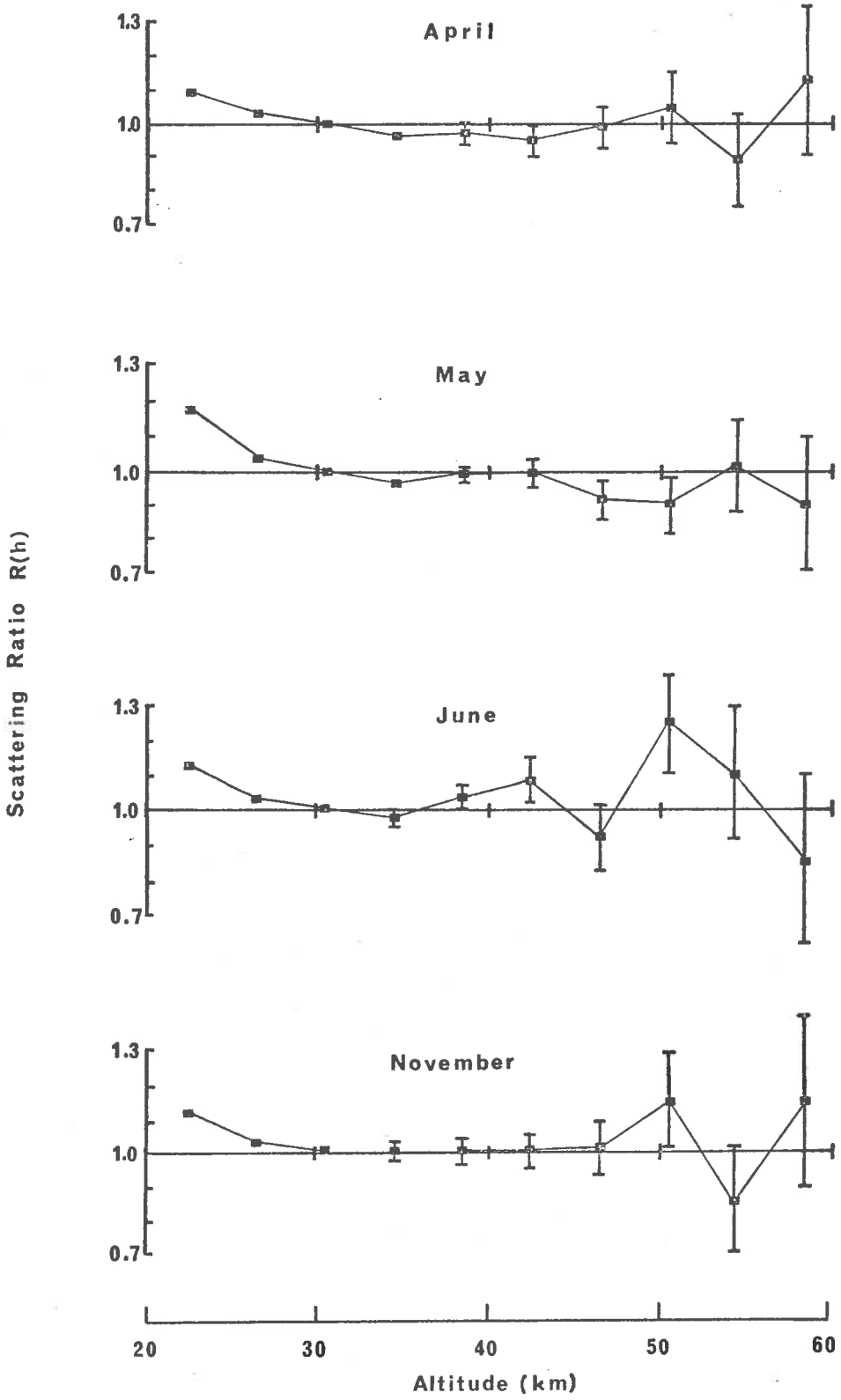

Figure 7.3 Values of the scattering ratio obtained for the mean of all observations during each of four months in 1969.

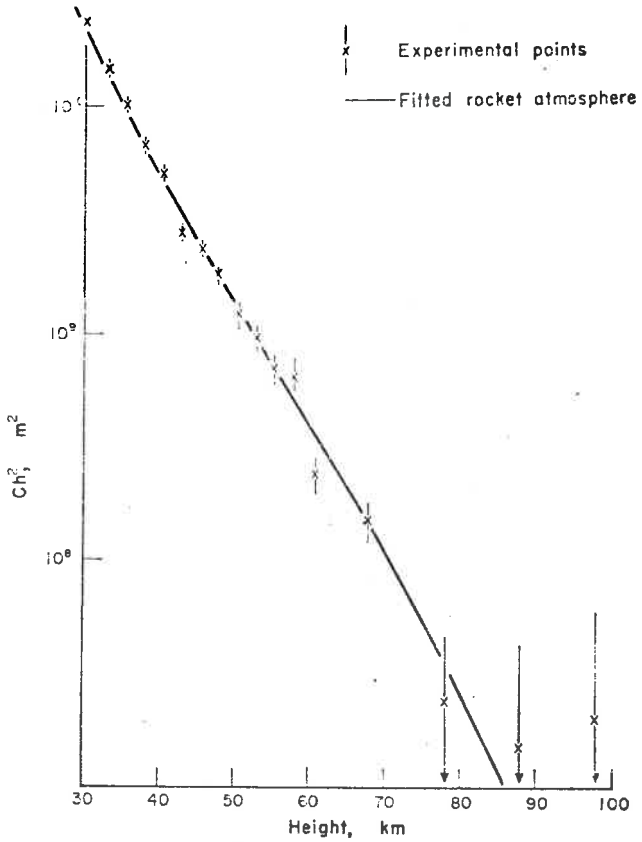

Figure 7.4(a) Variation of scattering index (Ch^2) with altitude measured by Kent, Clemesha and Wright (1967).

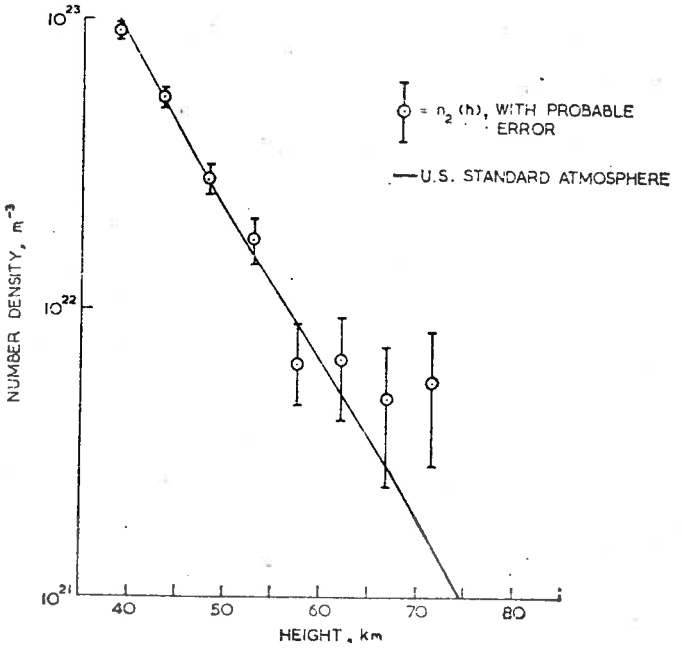

Figure 7.4(b) Laser radar return in terms of equivalent molecular density (Bain and Sandford, 1966(a))

The measurements of Kent et al, carried out at Kingston, Jamaica (Lat. 18°N) are presented in terms of the scattering index Ch^2, which is the same as the quantity I(h) used in the present work. Bain and Sandford, working at Slough, England (Lat. 51°N) present their results in terms of molecular number density (m^{-3}). In each case, the observed results were normalised to a profile representing the signal which would be received by scattering from a purely molecular atmosphere. It can be seen from Fig. 7.4 that in each case the experimentally observed points follow quite closely the predicted profile up to an altitude of 60 km.

At altitudes above 60 km, the results of many early laser radar measurements indicated significant enhancements of scattering at various heights up to 140 km (for example; Fiocco and Smullin, 1963; McCormick et al., 1966). The results of these early observations can almost certainly be attributed to the effects of unsuppressed laser fluorescence, and momentary photomultiplier overload (Bain and Sandford, 1966(b)). It is significant that later results published by workers who had previously detected large scattering enhancements at high altitudes showed these enhancements to have been largely eliminated after precautions had been taken to reduce spurious signals (for example, McCormick et al., 1967).

Recently, measurements have been carried out in Jamaica by Wright, Sandland, Kent and Clemesha (1969) using a greatly improved laser radar. The new laser system is the most sensitive so far reported, being able, even in incomplete form, to produce scattering profiles to

90 km. from a sequence of 10 laser firings, and would appear to be capable of detecting the fluctuations in atmospheric density due to both gravity waves and tidal oscillations. However, the observations generally confirm the fact that the mean variation of atmospheric scattering index follows that predicted for a molecular atmosphere, at least to an altitude of 90 km.

The results of all these measurements are generally interpreted to mean that the atmosphere above 30 km is free of significant amounts of aerosol. This interpretation has, in turn, been used by most authors to justify the use of the 30 km altitude region for the calibration of scattering profiles. However, the same variation of scattering index with height would be observed from an atmosphere containing aerosols, provided that the optical mixing ratio (turbidity) between the aerosol and molecular components were constant with height. The presence of dust at all levels of the atmosphere up to 65 km is indicated by the results of twilight measurements carried out by Vola and Goody (1962), who found a value for the average turbidity near 30 km altitude of about 0.2 (in the red region of the spectrum).

The turbidity $\tau(h)$ is defined by

$$\tau(h) = \beta_a(h)/\beta_r(h)$$

where $\beta_a(h)$ and $\beta_r(h)$ are the aerosol and molecular volume scattering coefficients respectively. If we assume a value of 6 for the ratio of the molecular to aerosol phase functions for backscattering (Deirmendjian, 1965), it is possible to calculate the value of the

scattering ratio R(h) which would be produced by an aerosol concentration of $\tau = 0.2$, since

$$R(h) = \frac{B_r(\Pi,h) + B_a(\Pi,h)}{B_r(\Pi,h)}$$

$$= 1 + P_a(\Pi)\beta_a(h)/P_r(\Pi)\beta_r(h)$$

where $B(\Pi,h)$ and $P(\Pi)$ are the backscattering coefficients and phase functions respectively, for the aerosol and molecular components. The value of R(h) obtained is approximately 1.05. The resultant error introduced into the scattering ratio profile would thus be 5%. This error is comparable with the other errors involved in the present measurements.

7.3 The 5 to 30 km Altitude Region

Examples of the observed variation in scattering ratio R(h) over the 5 to 30 km altitude region are shown in Figs. 7.5 and 7.6. The observed values of R(h) have been plotted as a function of altitude together with temperature measurements taken by meterological balloons on the corresponding days. The relationship between the variation in temperature and the R(h) profile is discussed later. All scattering ratio profiles have been normalized to R(h) = 1 near 30 km altitude.

It can be seen that considerably enhanced scattering is evident at all heights below 30 km, with the exception of a narrow region near 10 km altitude. In this region, the observed scattering is generally close to that predicted for a molecular atmosphere. Occasionally,

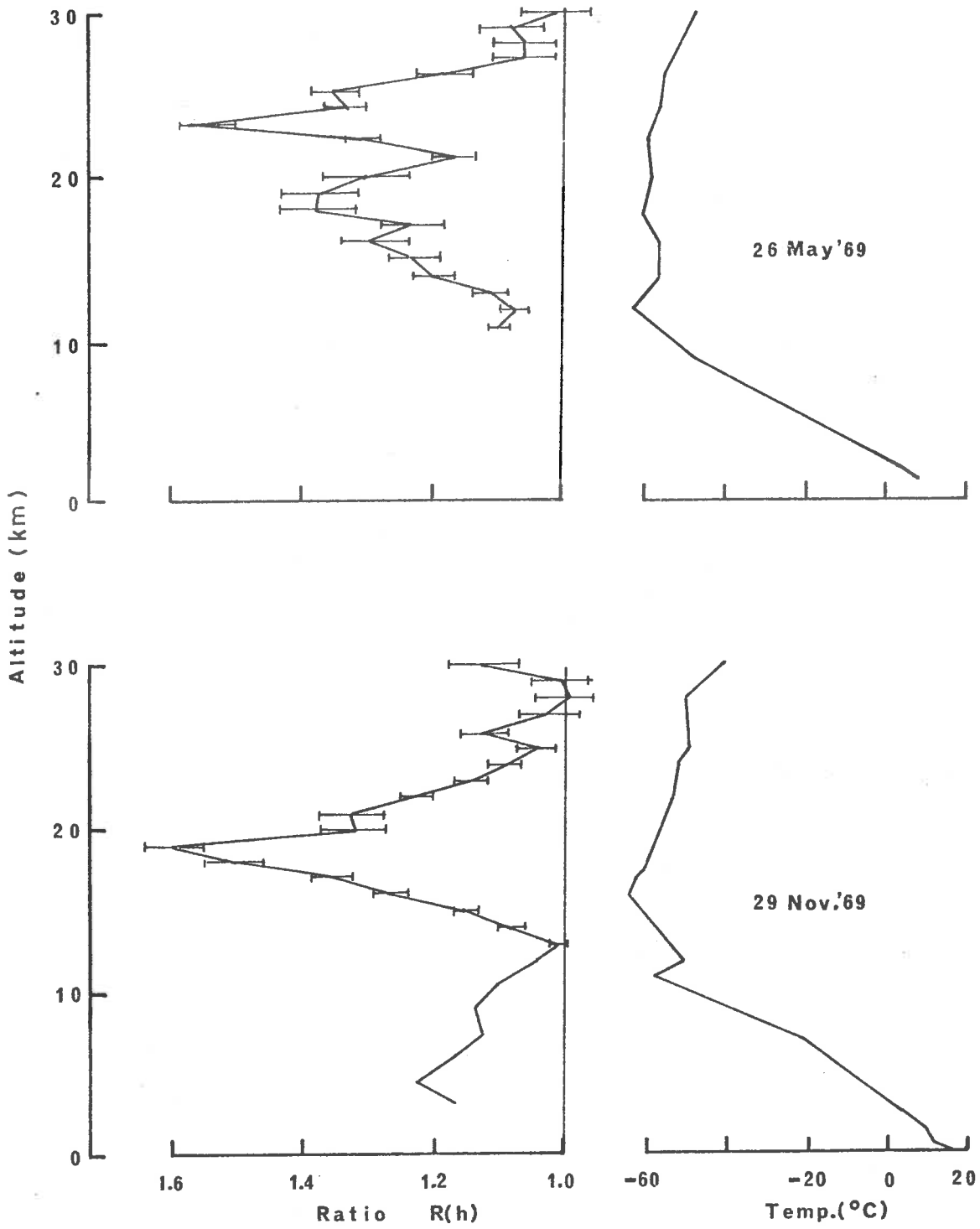

Figure 7.5 Scattering ratio measurements compared with corresponding temperature profiles.

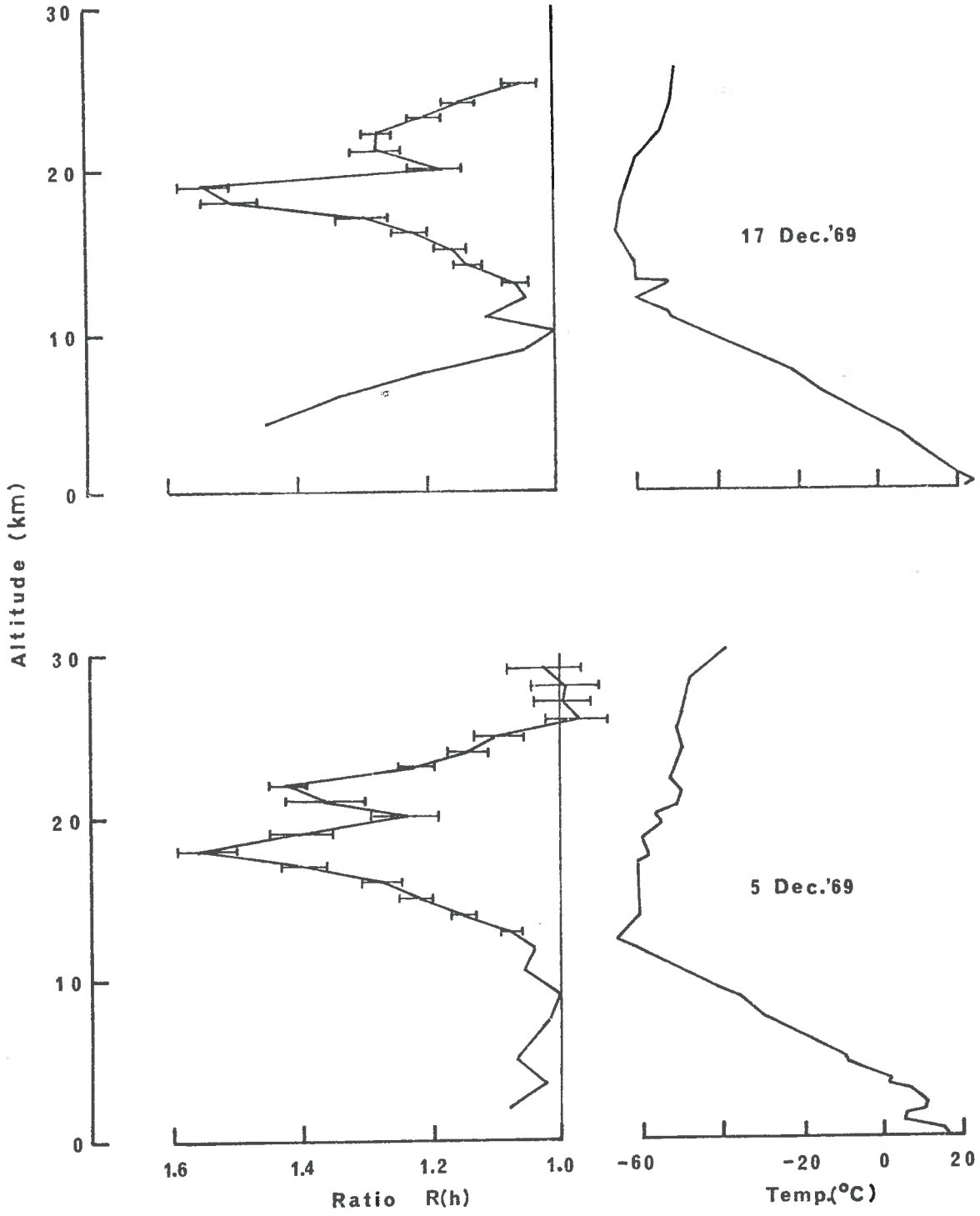

Figure 7.6 Scattering ratio measurements compared with corresponding temperature profiles.

values of R(h) less than unity have been observed near 10 km, indicating the existence of significant turbidity at the normalizing height (30 km) on those occasions. However, the long-term averaged values of turbidity near 10 and 30 km are very nearly the same, as may be seen from the average R(h) profile for 1969 shown in Fig. 7.2.

7.3.4 The 3 to 10 km Altitude Region

Below 10 km altitude, considerable variation has been observed in the shape of individual R(h) profiles. In general, the observed value of R(h) increases with decreasing height. The increase in turbidity is caused by the increasing aerosol concentration near the earth's surface. Blifford and Ringer (1969), in a series of measurements using aircraft borne impactors, found an average increase in particle concentration of 1.5 orders of magnitude between altitudes of 9 and 3 km. Over this height range, the air density changes by a factor of about 2, and if a roughly constant particle size distribution is assumed, then the turbidity would change by approximately one order of magnitude. The change in R(h) between 3 and 9 km altitude observed on 17th December 1969 is consistent with this change in turbidity (Fig. 7.6).

On some occasions, only a small increase in the value of R(h) with decreasing altitude below 10 km has been observed, indicating low values of turbidity in this region. These observations have generally (though not always) been associated with the existence of a temperature inversion low in the troposphere, which acts as a barrier to the upward convection of dust from the earth's surface. This effect is

well illustrated by the profile obtained on 5th December, 1969 (Fig. 7.6).

7.3.2 The 10 to 30 km Altitude Region

All profiles of R(h) obtained have shown evidence of enhanced scattering between altitudes of 10 and 30 km. The enhancement is attributed to the well-known stratospheric aerosol layer, which has been detected both by direct particle collection experiments (Junge et al. 1961), and by optical scattering measurements (Vols and Goody, 1962; Fiocco and Grams, 1964). Much earlier, Gruner had predicted the existence of a layer of particulate material in the lower stratosphere from observations of the purple light phenomenon during twilight (Gruner, 1958).

In the following sections, the features of the stratospheric aerosol layer observed in the present study are discussed, and compared with the results obtained by other workers.

7.4 The Stratospheric Aerosol Layer

7.4.1 General Features

The general features of the observed scattering ratio profiles may be seen in Figs. 7.5 and 7.6. Error bars have been used to indicate the statistical reliability in the plotted points, and represent one standard deviation. Corresponding temperature profiles obtained from meteorological balloon data have also been plotted. In good agreement with the findings of Elterman et al. (1969), the peak in the scattering

ratio profile was always observed to occur above the height at which the temperature minimum occurred. The average separation between the scattering ratio peak and the temperature minimum was found to be 2.1 km. This compares with an average separation of 1.5 km found by Elterman et al.

The profiles obtained during April and May, 1969 differed in character from the profiles observed later in the year. All profiles obtained after May have featured a well-defined peak in the scattering ratio at an altitude between 17 and 20 km, although a smaller amplitude peak has also occasionally been observed between 22 and 23 km (for example, December 5th and 17th, Fig. 7.6). Several profiles obtained in April and May, however, showed the higher altitude peak to have the greater amplitude, and to occur at a slightly higher altitude, between 23 and 25 km (for example, May 26th, Fig. 7.5). Unfortunately, the statistical errors associated with the early results were greater than those in later observations, and some of the irregularities in the observed profiles may be statistical in nature. However, taken collectively, the results indicate generally more disturbed conditions in the stratospheric aerosol layer in the autumn months. It will be necessary to repeat the observations during April-May 1970 in order to establish conclusively whether disturbed conditions are general during the southern autumn months.

Disturbed conditions during April-May would be consistent with the seasonal influx of dust to the mid-latitude southern stratosphere

from an equatorial "reservoir". Such a mechanism has been proposed by Dyer and Hicks (1965 and 1968) to explain the observed seasonal variation in attenuation of direct solar radiation at a number of observing stations over both hemispheres. Dyer (1969) suggested that material builds up near equatorial regions during summer, and is removed during autumn-winter by a poleward transport process. Using as a tracer the dust injected into the equatorial stratosphere by the volcanic eruption of Mt. Agung (Bali, 8°S) on March 17, 1963, Dyer and Hicks (1965) found that the poleward transfer process involves a time of the order of five months to middle latitudes, and eleven months to polar latitudes. Their observations during 1963-65 indicate quite clearly a recurrent winter maximum in the dust content of the atmosphere above Aspendale, Australia (38°S).

In the present study, consistently higher peak scattering ratios were observed during the winter months. This may be seen in Figs. 7.7 and 7.8, which depict the monthly mean profiles of R(h) obtained in the period April 1969 - January 1970. The number of individual profiles comprising each mean profile during 1969 is listed in Table 7.1. The January 1970 mean was obtained from 2 profiles. Error bars representing one standard deviation have been used to indicate the statistical reliability of the plotted points.

The smallest values of scattering ratio were observed in April, 1969. Values of R(h) thereafter increased, reaching a maximum value of R(h) = 1.9 in July. Values of R(h) then showed a decreasing trend,

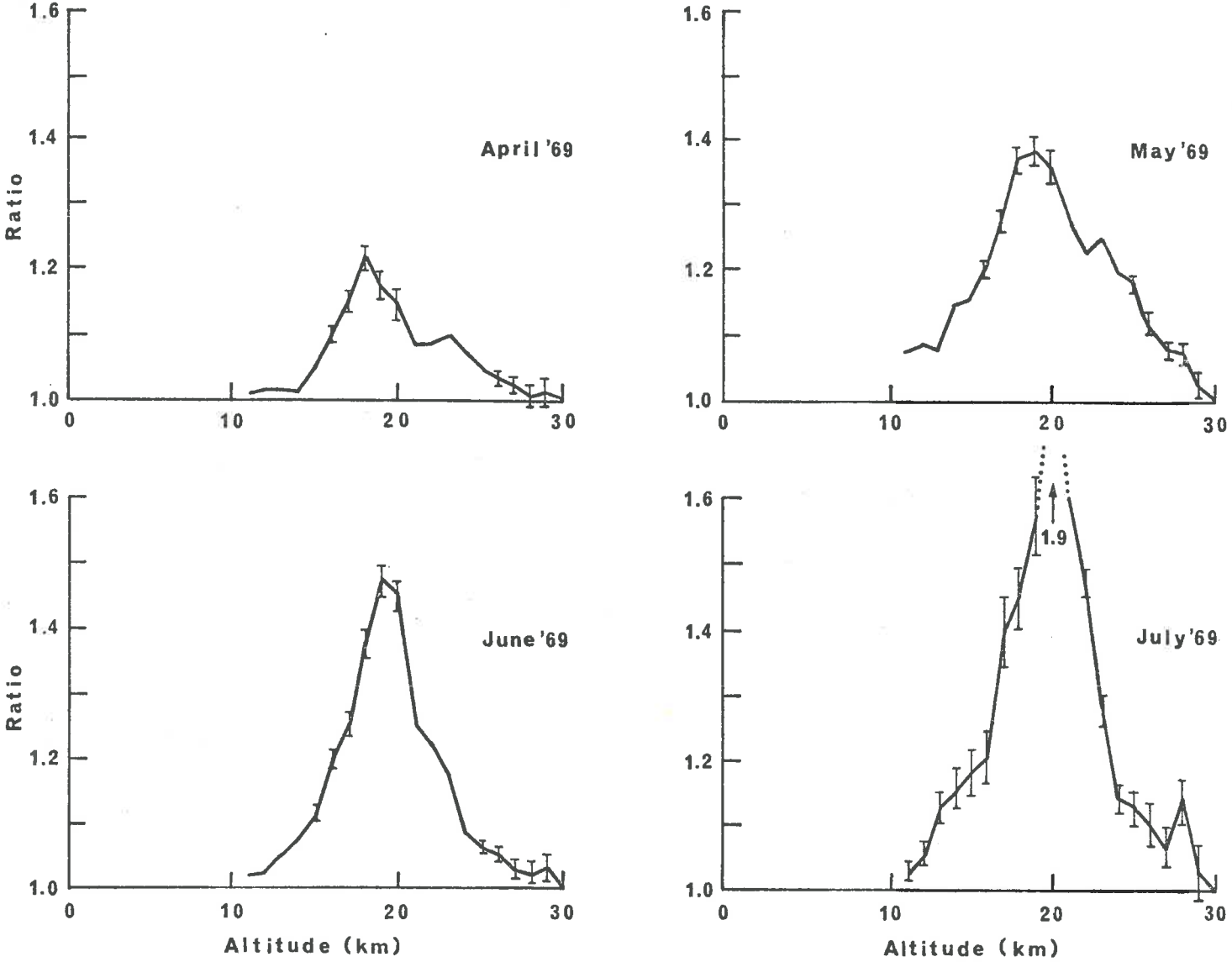

Figure 7.7 Monthly mean profiles of the scattering ratio R(h).

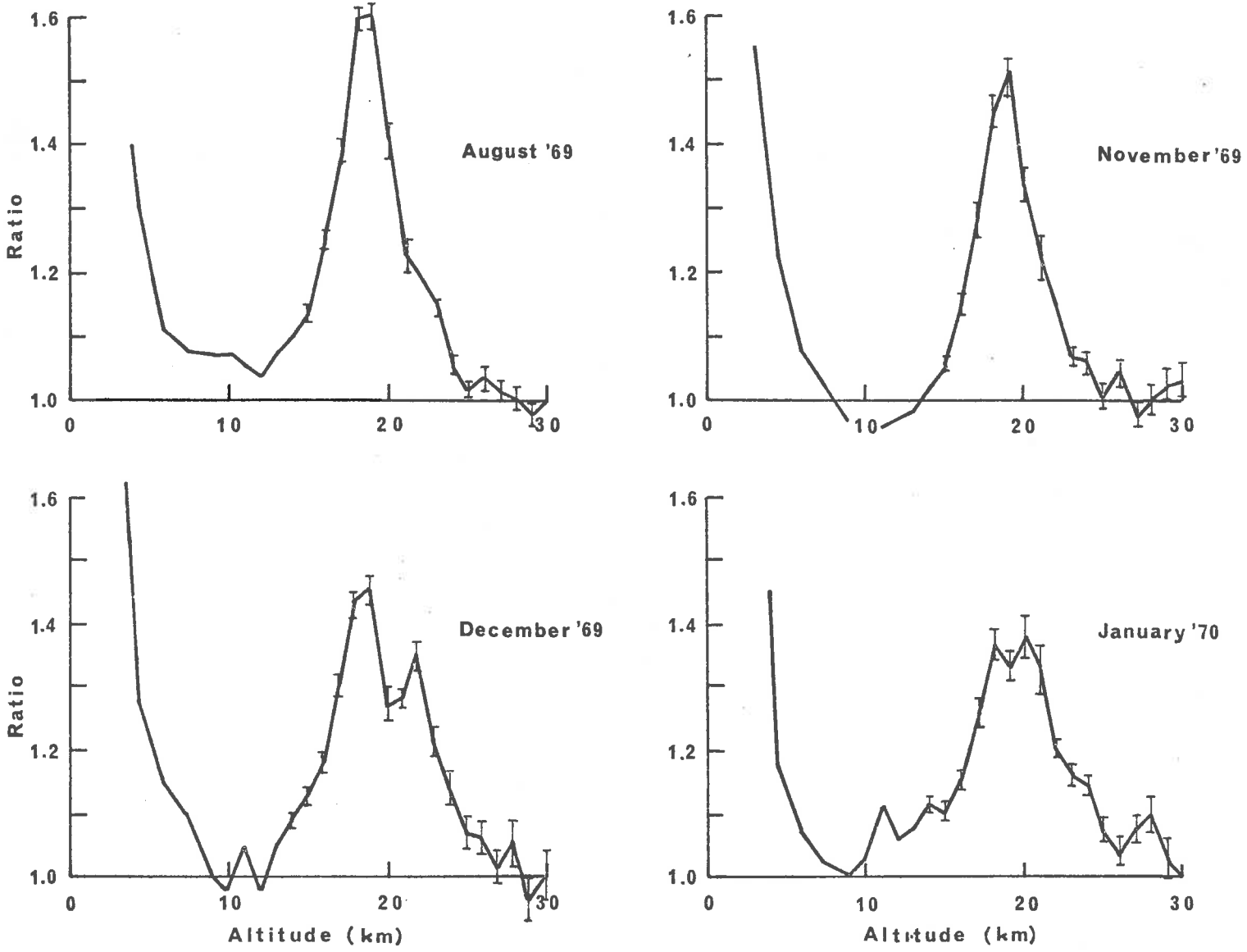

Figure 7.8 Monthly mean profiles of the scattering ratio R(h).

which was still evident in January, 1970. These results indicate that the concentration of dust over Adelaide (35°S) reached its highest value during the winter months. This result is in good agreement with the observations of Dyer and Hicks, obtained at nearly the same latitude. From the present observations, however, it is not possible to determine whether the variation observed over Adelaide is part of a regular cycle, and more extended measurements are clearly required.

No significant changes in the shape of the stratospheric scattering layer have been observed in soundings carried out during the course of one night, although significant changes have been observed over periods of several days. The rate at which changes took place was, however, highly variable, as may be seen from two sequences of observations shown in Fig. 7.9. In the sequence of observations carried out between 27th June and 2nd July, each profile is quite different from the preceding one, although only 5 days separate the first from the last. On the other hand, much slower change is evident in the sequence recorded between 1st and 18th August. During this month, a narrow peak with a very well defined upper boundary persisted for more than 12 days, and only showed signs of broadening after 18 days. During this time, the height at which the maximum value of R(h) occurred decreased from 20 to 18 km.

Interpretation of changes in the shape of observed scattering ratio profiles can only be conjectural. However, the changes observed in the period 1st to 18th August suggest a slow downward sedimentation of the dust in the layer, causing the decrease in altitude of the

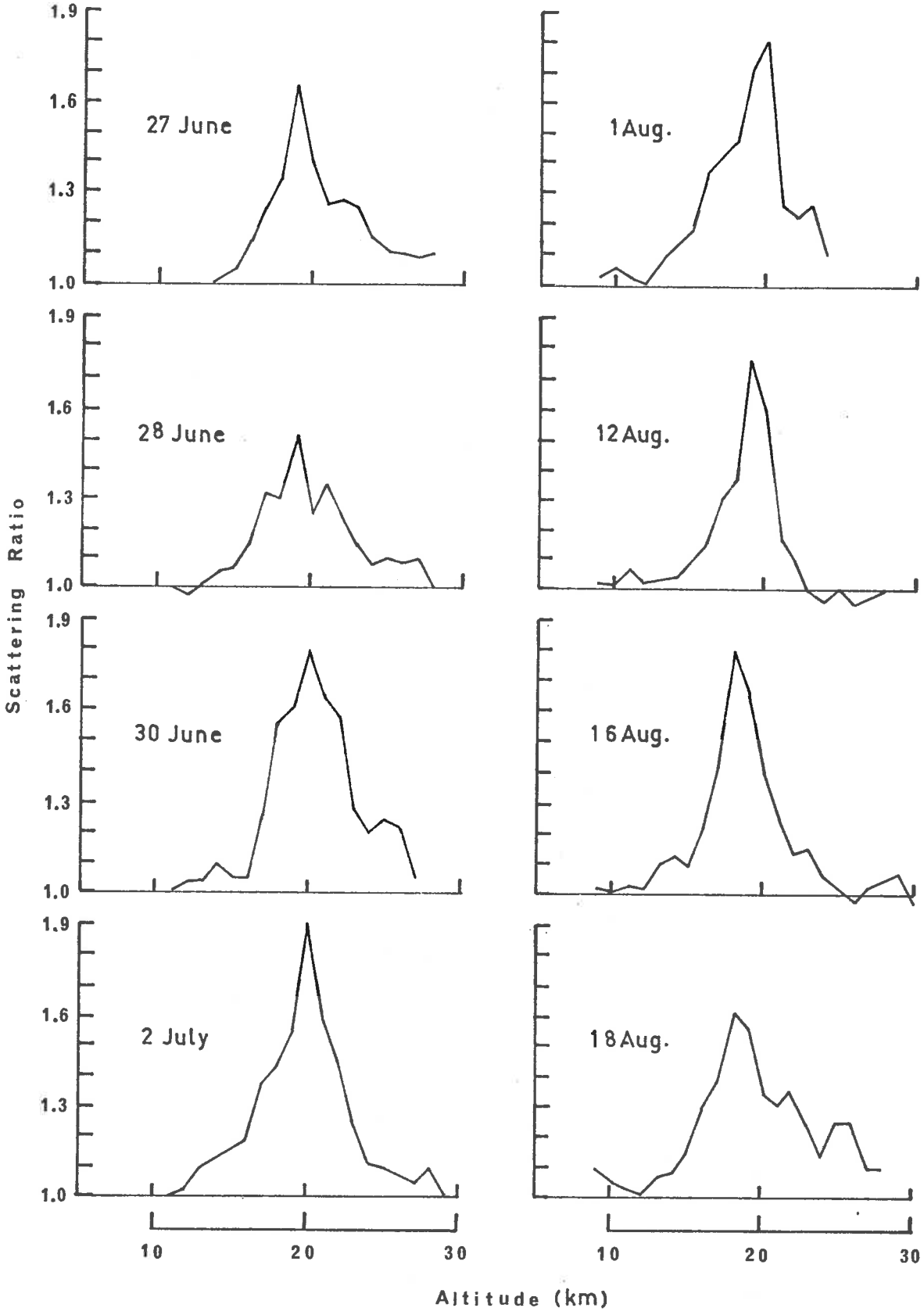

Figure 7.9 Changes in scattering ratio profiles during two sequences of observations in 1969.

scattering ratio peak. The step which is evident in the profile at 23 km altitude on the 16th August, and is better developed on the 18th, suggests the influx of new material, possibly by transport from the higher equatorial stratosphere. The observed rate of subsidence of the scattering ratio peak implies a particle fall rate of 1.5×10^{-1} cm/sec. This may be compared with the results of calculation carried out by Junge, Chagnon and Manson (1961) of the rate of fall of spherical particles of 2 g/cm^3 density near 20 km altitude. Their estimates ranged between 1.5×10^{-2} cm/sec for particles of 0.3 μ radius to 3.5×10^{-1} cm/sec for particles of 3.0 μ radius. In view of the uncertainty that exists regarding the density and size distribution of the stratospheric aerosol, the fall rate deduced from the laser radar results is not inconsistent with the values predicted by Junge et al.

The interpretation presented above is subject to much uncertainty, since changes in the observed scattering ratio profiles will be influenced by both zonal and meridional movement of the dust layer as a whole. These movements cannot be deduced from observations carried out at a single site. However, correlation of results from two or more laser soundings carried out simultaneously from sites separated by distances of the order of a few kilometers would allow bodily movements of the aerosol layer to be investigated. In this way, measurements of air movements in the stratosphere could also be obtained.

7.4.2 Stratospheric Aerosol Concentration and Composition

The backscattering function $\Sigma_a(\Pi,r)$ ($cm^2 sterad^{-1}$) of a single spherical particle may be calculated by means of the Mie theory of scattering, described in detail by Van de Hulst (1957). In the case of an ensemble of particles of different sizes, an average backscattering function per particle $\overline{\Sigma_a(\Pi)}$ may be found by integration of $\Sigma_a(\Pi,r)$ over the range of particle sizes. If $dN(r)$ is the number of particles having radii between r and r + dr, then

$$\overline{\Sigma_a(\Pi)} = \int_{r_1}^{r_2} \Sigma_a(\Pi,r)\, dN(r) \Big/ \int_{r_1}^{r_2} dN(r)$$

where r_1 and r_2 are the limits of particle sizes.

The value of $\overline{\Sigma_a(\Pi)}$ may be used to calculate the particle concentration $N_a(h)$ (cm^{-3}) at a given height from the measured value of the scattering ratio R(h), since

$$R(h) = \frac{B_r(\Pi) + B_a(\Pi)}{B_r(\Pi)} = 1 + \frac{B_a(\Pi)}{B_r(\Pi)}$$

where $B_a(\Pi)$ and $B_r(\Pi)$ are the aerosol and molecular backscattering coefficients ($cm^{-1} sterad^{-1}$) respectively, and

$$B_a(\Pi) = N_a(h)\, \overline{\Sigma_a(\Pi)}$$

In order to calculate $\overline{\Sigma_a(\Pi)}$ for the stratospheric aerosol, it is necessary to have an accurate description of the nature of the particles, and their size distribution. The results of some recent

investigations into the nature of the stratospheric aerosol have been reviewed in Chapter 1. It is clear that the results of these studies have not shown good agreement, and do not allow a consistent picture of the stratospheric aerosol to be drawn.

The particle collection experiments of Junge et al. (1961), Friend (1966), and Mossop (1965), indicate that aerosols in the stratosphere are predominantly ammonium sulphate, or persulphate particles, many of which appeared to be moist at the time of collection. The values of the refractive index of ammonium sulphate (1.50) and of water (1.33) have therefore both been used in calculations pertaining to the stratospheric aerosol by different authors. Dave and Mateer (1968) have used a mean value of 1.4.

The results of most collection experiments indicate a roughly spherical shape for the particles before collection, thus justifying the use of Mie theory in calculations of their scattering properties. However, considerable uncertainty exists regarding the size distribution of the particles. Junge et al. (1961) found that the size distribution in the range of particle radii between 0.1 and 1μ could be described by a power law of the form

$$\frac{dn(r)}{d \log r} \propto \frac{1}{r^{\alpha}}$$

where the value of the exponent was approximately 2. In a later study Mossop (1965) found a lower radius limit to the size distribution at about 0.4 μ, and deduced a value of about 4 for the exponent. Friend

(1966) claimed that the aerosol size distribution could be better described as log-normal, with geometric mean radius 0.305 μ, and geometric standard deviation of 1.30.

Values of $\overline{\Sigma_a(\pi)}$ for ensembles of particles having a power law size distribution have been calculated by McCormick et al. (1968), for different values of the exponent, and of the upper and lower radius limits r_2 and r_1. The particles were assumed to have a refractive index of 1.5. The values of $\overline{\Sigma_a(\pi)}$ corresponding to the laser wavelength (0.6943) and with radius limits r_1 = 0.08 μ and r_2 = 3.0μ have been reproduced in Table 7.2 for values of the exponent between 2.5 and 4 (Models 1-4). The value of the upper radius limit r_2 has little effect on the value of $\overline{\Sigma_a(\pi)}$ because of the rapidly decreasing particle concentration with increasing radius, especially for higher values of the exponent. This may be seen by comparing Model 3 with Model 5, in which the value of r_2 has been increased to 10 μ.

The value of $\overline{\Sigma_a(\pi)}$ is strongly dependent on the lower radius limit r_1, in spite of the decreasing scattering efficiency of the smaller particles (Bullrich, 1964), because of their high relative concentration. Junge et al. (1961) found that the power law size distribution was obeyed to a lower radius limit of 0.1 μ, below which the decreasing collection efficiency of their impactors caused a rapid cut-off. The lower radius limit of 0.08 μ used in Models 1-5 corresponds approximately to this value. In Model 6, the value of r_1

has been reduced to 0.04 μ, in order to allow for the possibility that the true lower radius limit to the power law size distribution lies below the cut-off size limit of the impactors used by Junge et al.

Model 7 has been included in order to take account of the findings of Mossop (1965) and Friend (1966), who found that the lower limit of particle radius occurred at a value close to 0.3 μ, and that the concentration decreased with increasing particle size according to a value for the exponent between 3 and 4. Model 7 therefore assumes a value of $r_1 = 0.3\ \mu$, and $a = 4.0$.

Model 8 describes a log-normal particle size distribution (Friend, 1966). The distribution used was the one obtained by Dave and Mateer (1968) from the averaged results of Mossop (1965) and Friend (1966) and is described by the function

$$dn(r)/d\log r \propto \exp\left[-(\log \frac{r}{r_o})^2/2s^2\right]$$

where the mean radius $r_o = 0.35\ \mu$ and the standard deviation $s = 0.3$ (natural log units). Although Dave and Mateer used a value of 1.4 for the aerosol refractive index, a value of 1.5 has been used in the present calculations, in order to allow comparison with the results of McCormick et al. Fortunately, the effect of this change on the value of $\overline{\Sigma_a(\Pi)}$ is relatively small, the value corresponding to a refractive index of 1.5 being approximately three times greater. The boundary values r_1 and r_2 used in Model 8 are the same as those used

in Models 1-4. In this case, a change in the values of r_1 and r_2 would have little effect on the value of $\overline{\Sigma_a(\pi)}$, due to the rapid decrease of particle number density away from r_o.

TABLE 7.2

Model	Type	Size Limits r_1	Size Limits r_2	$\overline{\Sigma_a(\pi)}$ ($cm^2 steread^{-1}$)
1	Power Law, a = 2.5	0.08	3.0	6.7×10^{-11}
2	" " a = 3.0	0.08	3.0	2.8×10^{-11}
3	" " a = 3.5	0.08	3.0	1.4×10^{-11}
4	" " a = 4.0	0.08	3.0	8.6×10^{-12}
5	" " a = 3.5	0.08	10.0	1.5×10^{-11}
6	" " a = 3.5	0.04	3.0	1.4×10^{-12}
7	" " a = 4.0	0.3	3.0	6.4×10^{-10}
8	Log-normal	0.03	3.0	4.2×10^{-10}

Fig. 7.10 shows the values of particle concentration corresponding to observed values of the scattering ratio R(h) for each of the models listed in Table 7.2 (with the exception of Model 5), at an altitude of 19 km. The peaks in the scattering ratio curve occurred most frequently at this altitude, and observed values have ranged between 1.3 and 2.0. Most of the peak scattering ratios observed by Grams and Fiocco (1967) working at Lexington, Massachusetts (42°N) also fell within this range.

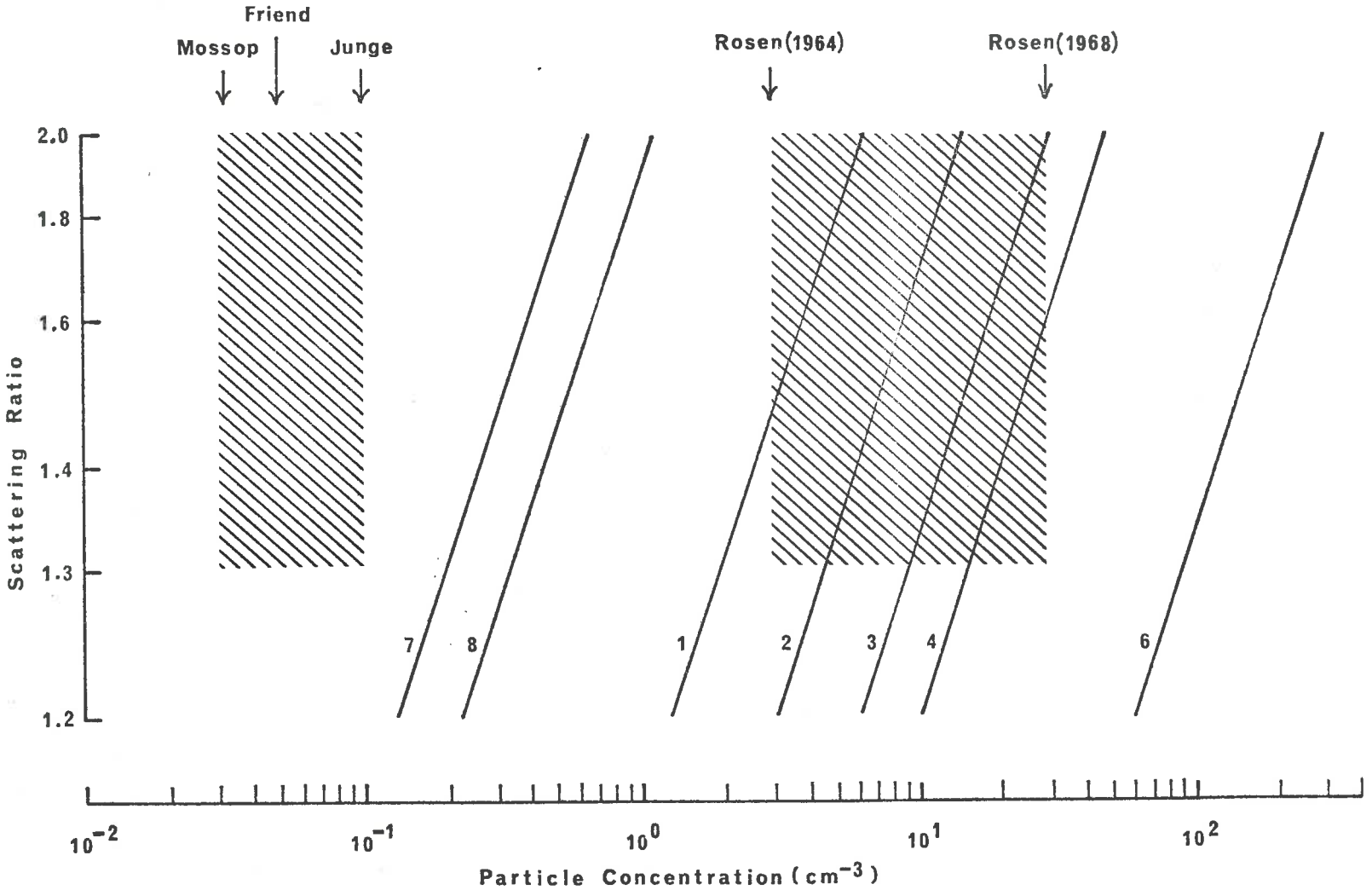

Figure 7.10 Particle concentrations at 19km. altitude corresponding to values of the scattering ratio between 1.2 and 2.0, for various size distribution models. The shaded areas indicate the results of particle sampling experiments.

It is apparent from Fig. 7.10 that the value of particle concentration deduced from a particular value of the scattering ratio depends markedly on the size distribution model which is used. For a given model, values of R(h) between 1.2 and 2.0 represent a 5:1 variation in aerosol concentration, while values of concentration corresponding to the extreme models used (Models 6 and 7) differ by almost three orders of magnitude. It is clear, therefore, that it will not be possible to deduce values of particle concentration from the results of laser radar experiments until a more accurate description of the aerosol size distribution is available.

The range of stratospheric particle concentrations obtained by "in situ" measurements has been indicated by the shaded areas in Fig. 7.10. The areas are bounded by the upper and lower limits of observed scattering ratios, and by the limits of aerosol concentration values obtained by the particle collection experiments of Junge (1961), Mossop (1965) and Friend (1966) on the one hand, and by the photoelectric counter measurements of Rosen (1964, 1968) on the other. It is apparent that values of the aerosol concentration deduced on the basis of Model 6, which features a lower radius limit r_1 of 0.04μ, are considerably higher than those found by any of the "in situ" measurements, and it is concluded therefore that this is not a realistic model for the stratospheric aerosol.

The aerosol concentrations deduced on the basis of Models 7 and 8 lie between those values obtained by particle collection experiments,

and those obtained by the photoelectric counting technique. This suggests that either of these models could provide a good description of the stratospheric particle size distribution, if it were assumed that the true particle concentration lies between the values indicated by the two different types of sampling technique.

It is significant, however, that the concentration values deduced on the basis of Models 1-4 are in good agreement with the values obtained by Rosen (1964 and 1968) using a photoelectric counter. The principal difference between this technique and the collector measurements is that the photoelectric counter includes any volatile component, such as condensed water vapour. The results obtained from the laser radar are also sensitive to the presence of droplets of volatile material in the scattering volume. The good agreement between the laser results and the concentrations found by Rosen would thus indicate the presence of a significant amount of condensation in the stratosphere. The condensation may occur on the Aitken nuclei, which were found by Junge (1961) to have concentrations of 1 to 10 cm^{-3} in the stratosphere.

Since the only difference between Models 7 and 4 lies in the value of the lower radius limit r_1, Model 4 having the smaller value at $r_1 = 0.08\ \mu$, it is reasonable to suppose that most of the condensed droplets would have sizes in the 0.08 to 0.3 μ range. The mean concentration suggested from Fig. 7.10 is 10 cm^{-3}, and an average radius of 0.2 μ would result in a water mixing ratio near 19 km

altitude of 10^{-9} gm/gm. This is well below the value of 2×10^{-6} gm/gm obtained in a series of balloon measurements up to 28 km altitude by Mastenbrook (1968). It would thus appear that only a small fraction of the water available in the stratosphere need exist in condensed form in order to account for the observed scattering.

7.4.3 Comparison with other Measurements

Values of the peak scattering ratio observed in the present study ranged between 1.2 and 2.0 and the mean of all observations during 1969 was 1.4. The mean R(h) profile has been compared with profiles obtained by other groups working in the northern hemisphere in Fig. 7.11. Grams and Fiocco (1967) worked at Lexington, Mass. (42°N), Goyer and Watson (1968) at Sacramento Peak, New Mexico (35°N) and Clemesha, Kent and Wright (1966) in Kingston, Jamaica (18°N).

All profiles show the existence of a peak in the scattering ratio near 20 km altitude. The highest altitude at which the peak occurred was observed by Clemesha et al. at Kingston, and probably corresponds to the higher tropical tropopause. The two profiles obtained in the mid-latitude northern hemisphere both show a peak scattering ratio near 18 km, in good agreement with the present work.

From Fig. 7.11, it would appear that the values of peak scattering ratio observed in the southern hemisphere are considerably lower than those found in the northern hemisphere. However, it should be noted that the low value of the average peak scattering ratio found in

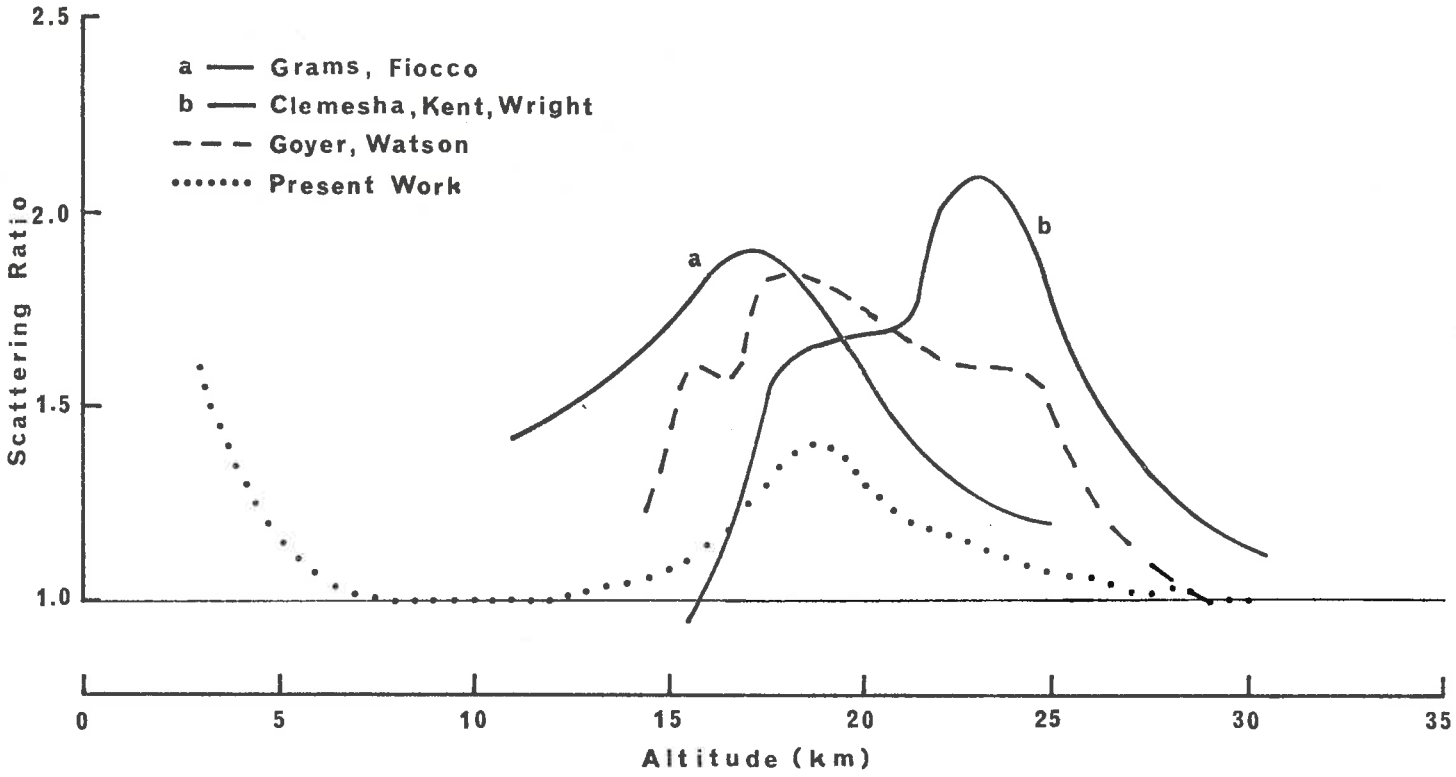

Figure 7.11 Values of scattering ratio observed in the present study compared with the results of other investigators.

the present work is due partly to the large number of profiles obtained during April and May, 1969, when low values of the peak scattering ratio were predominant. Values obtained in individual observations have ranged between 1.3 and 2.0. The higher values are in better agreement with the results obtained in the northern hemisphere.

It is not known whether the profiles of Gleneesha, Kent and Wright, and Goyer and Watson, are typical of average conditions, or represent higher than normal values. The profile of Grams and Fiocco is the average of 66 individual profiles recorded during 1964 and 1965. The good agreement between this and the results of the other two groups suggests that the results obtained at Kingston and Sacramento Peak are fairly typical. However, it is possible that the results obtained by Grams and Fiocco were affected by the increased dust content of the stratosphere following the volcanic eruption of Mt. Agung, in March 1963. It is significant that the peak scattering ratios observed by Grams and Fiocco in early 1964 were higher than those observed in the same period one year later. In agreement with the present work, the results of Grams and Fiocco also indicate the existence of higher peak scattering ratios during winter.

It is clear from the above discussion that meaningful comparison of results between northern and southern hemispheres will only be possible when records obtained over at least one full year from equipment operating at similar latitudes are available. This is at present not possible due to the lack of sufficient data.

A large number of stratospheric scattering profiles has been obtained by Elterman, Wexler and Chang (1969) using a modulated searchlight beam, at Sacramento Peak, New Mexico (35°N). These results have not been included in Fig. 7.11, because of the difficulty in converting the turbidity values at 0.55 μ wavelength measured by Elterman et al. to equivalent values of the scattering ratio at 0.7 μ. However, an approximate comparison can be attempted, in the following way.

The turbidity $\tau(h,\lambda)$ is defined by

$$\tau(h,\lambda) = \beta_a(h,\lambda)/\beta_r(h,\lambda)$$

where $\beta_a(h,\lambda)$ and $\beta_r(h,\lambda)$ are the scattering coefficients at wavelength λ for the aerosol and molecular components, respectively. It may be shown (Van de Hulst, 1957) that

$$\beta_a(h,\lambda) = \int_{r_1}^{r_2} \sigma(m,r,\lambda)\, dn(r)$$

where $\sigma(m,r,\lambda)$ is the scattering cross-section of each particle of refractive index m and radius r at the wavelength λ. $dn(r)$ is the concentration of particles with radius between r and r + dr, and r_1 and r_2 are the limits of particle radius. For reasons discussed in the previous section, the particle size distribution $dn(r)$ and the radius limits r_1 and r_2 cannot at present be specified with any certainty. However, it is of interest to consider the consequences of assuming certain particle size distributions.

If a power law size distribution, and in particular Model 2 (Table 7.2) is assumed for the stratospheric aerosol, it is found that $\beta_a(h,\lambda) \propto \lambda^{-1}$, and $\beta_a(h,0.7)/\beta_a(h,0.55) \simeq 0.8$. On the other hand, the lognormal size distribution (Model 7) yields the result $\beta_a(h,0.7)/\beta_a(h,0.55) \simeq 1$. The mean turbidity profile obtained by Elterman et al. had a peak value near 18 km of 2.1. The two models assumed above would thus yield values of 1.7 and 1.9 respectively for the peak backscattering ratio at 0.7 μ. These values are in remarkably good agreement with the value of 1.85 found by Coyer and Watson (1968) using laser radar at the same location. It must however be pointed out that the measurements of Elterman et al. were carried out two or three years earlier than those of Coyer and Watson.

CHAPTER 8

OBSERVATIONS USING THE TWILIGHT TECHNIQUE

8.1 Introduction

The variation in sky brightness during twilight has been measured by a number of workers in an attempt to study atmospheric structure (for example, Bigg, 1956; Volz and Goody, 1962). However, the interpretation of the resultant intensity profiles is subject to several uncertainties, which have been summarised in Chapter 1, and it has been evident for some time (Bigg, 1964) that it would be desirable to compare the results obtained by the twilight technique with those of an independent experiment, in order to determine the accuracy of the twilight measurements.

The opportunity for such a comparison presented itself following completion of the laser radar system, as twilight measurements had been carried out at Adelaide since October, 1965. The measurements had been started at the request of the Commonwealth Bureau of Meteorology, in an attempt to detect the arrival over southern Australia of the volcanic dust resulting from the eruption of Mt. Taal (14°N, 121°E) on 28th September, 1965. The laser radar system was at that time far from complete.

In view of the limited time which was available for setting up the experiment, the method described by Bigg (1956 and 1964) was adopted because of its simplicity. Although the details of Bigg's analysis had

been criticised by a number of workers (for example, Megrelishvili, 1958; Volz and Goody, 1962; Volz, private communication) there nevertheless seemed little doubt that the profiles obtained by Bigg were influenced by the presence of the stratospheric aerosol layer, and it was considered that the method should be capable of detecting a significant increase in stratospheric dust concentration.

One of the main experimental disadvantages of the twilight sounding method is the need for cloud-free conditions between the photometer and the sunset point throughout the duration of the measurement. This distance can extend to several hundred kilometres, depending on the maximum height which is to be observed. Unfortunately, the photometer used in the present study was located near the coast, and thus was in the path of cold fronts containing moist air, and this severely limited the number of occasions on which observations could be attempted. In spite of this limitation, 8 cloud-free profiles were obtained between the commencement of observations and the end of 1965, and 16 profiles were obtained during 1966. In 1967, weather conditions were significantly less favourable, and only 8 profiles were obtained. Observations were then terminated, except for 4 recordings which were carried out in conjunction with laser soundings during 1969.

8.2 Theory and Limitations of the Twilight Method

The theoretical aspects of the twilight scattering method have been described by Bigg (1956 and 1964). For a fixed elevation of the line of sight, the height of the earth's shadow boundary appears to increase

as the sun sets further below the horizon. It can be shown that for single scattering from a molecular atmosphere, dI/dh, the rate of change of brightness of the twilight sky with height of the shadow boundary, is related to the scale height H of the atmosphere by the following relation:

$$-\frac{1}{I}\frac{dI}{dh} = \frac{1}{H}$$

where 1/H is termed the "inverse scale height". Thus in the case of a purely molecular atmosphere, the graph of $-\frac{1}{I}\frac{dI}{dh}$ versus h, hereafter called the "twilight profile", would deviate little from a straight line. However, in the case of the real atmosphere containing aerosols, the twilight profile is modified. Bigg (1964) has shown that a thin aerosol layer would produce a positive peak in the twilight profile. The profile will also be smoothed and shifted in the direction of increasing h due to the screening effect of the dust and water vapour suspended in the lower atmosphere. Although this effect will decrease with increasing wavelength, Bigg's results have been criticised by Megrelishvili (1958) on the grounds that the screening effect of the earth's lower atmosphere extends to an altitude of 20 km, below which height observations cannot be carried out using the twilight method.

Megrelishvili's value of the screening height is considerably greater than that calculated by Volz and Goody (1962), who found a value of 10 km for the red region of the spectrum, and 6 - 7 km for the near infrared region, where most of Bigg's observations were

carried out. On the other hand, Vola has pointed out (private communication) that the presence of a stratospheric dust layer will affect not only the corresponding region of the twilight profile, but to a lesser extent, and in the opposite sense, all regions of the profile corresponding to lower heights. The method of integrating the twilight profile over a given height range used by Rigg in order to obtain a measure of the stratospheric dust content can therefore lead to a cancellation of the dust contribution, if integration is carried out over too great a height range.

A further complication in the analysis of twilight data is due to the uncertain contribution that multiple scattering makes to the total sky brightness. According to Hulburt (1953) multiple scattering becomes the main factor determining the brightness of the twilight sky near the zenith for solar depressions greater than about 7°. More extensive calculations (Divari and Plotnikova, 1964) have shown that at the elevation and azimuth angles used by Rigg, and in the present study, the ratio of secondary to primary scattered intensities varies from 0.26 at 6° solar depression to 2.5 at 10° solar depression. It is clear that the simple analysis adopted by Rigg will not be adequate for solar depressions exceeding 6°-7°, and may be in error for considerably smaller solar depression angles.

8.3 Experimental Procedure and Analysis

All observations were carried out at an angle of elevation of 19°,

and in the azimuth of the sun at the time of sunset. Light gathered from a 0.5° field of view by a 6 in. diameter Cassegrain-type telescope was passed through a Wratten No. 29 red filter to an EMI 9558B photomultiplier. The combined response of the filter and photocathode extended from 6200Å to about 8000Å. The output from the photomultiplier was amplified by a D.C. amplifier, the output of which was maintained within the range 3.0 to 3.1 volts by stepwise adjustment of the E.H.T. voltage, and hence the gain, of the photomultiplier. A pen recorder with 0.1 volt full scale sensitivity and 0.5 sec response time was placed between this varying output and a steady potential of 3.0 volts. Whenever the pen recorder reached the limit of its deflection, the gain of the photomultiplier was adjusted to bring the trace back to the other end of the scale.

Under these conditions we may write $AI = kV$, where I is the light intensity incident on the photomultiplier, A is the instantaneous amplification of the system, and V is the output voltage of the amplifier. Thus $A\frac{dI}{dt} = k\frac{dV}{dt}$, and we obtain

$$\frac{1}{I}\frac{dI}{dt} = \frac{1}{V}\frac{dV}{dt}$$

Thus,

$$-\frac{1}{I}\frac{dI}{dh} = -\frac{1}{V}\frac{dV}{dt}\frac{dt}{dh}$$

$$= -\frac{1}{V}\frac{dV}{dt}\frac{dt}{d\Theta}\frac{d\Theta}{dh}$$

where θ is the solar depression angle.

Since V is approximately constant, being maintained within the range 3.0 to 3.1 volts, then

$$-\frac{1}{I}\frac{dI}{dh} \propto \frac{dV}{dt}\frac{dt}{d\theta}\frac{d\theta}{dh}$$

In this equation, dV/dt is simply the slope of the pen recorder trace. The term dt/dθ is the differential of Central Standard Time with respect to solar depression. The quantity dθ/dh is the differential of solar depression with respect to the shadow height, and may be deduced by means of a ray tracing method in which a ray tangential to the earth's surface, or a parallel ray at some distance equal to the screening height above it, is corrected for refraction over small height intervals. Unfortunately, uncertainty exists in the actual height of the grazing ray, and hence in the allowance which should be made for refraction.

The effect on the twilight profile of different values of the screening height h_s is shown in Fig. 8.1, where a typical twilight profile (17th Feb. 1969) has been analysed assuming values of h_s = 0, 1, 3 and 6 km. The primary effect of an increasing value of h_s is to move the peak in the twilight profile to a greater altitude. The increase in height is greater than the increase in h_s, due to the decrease in refraction at higher altitudes. The change in total refraction has a small effect at small values of the solar depression

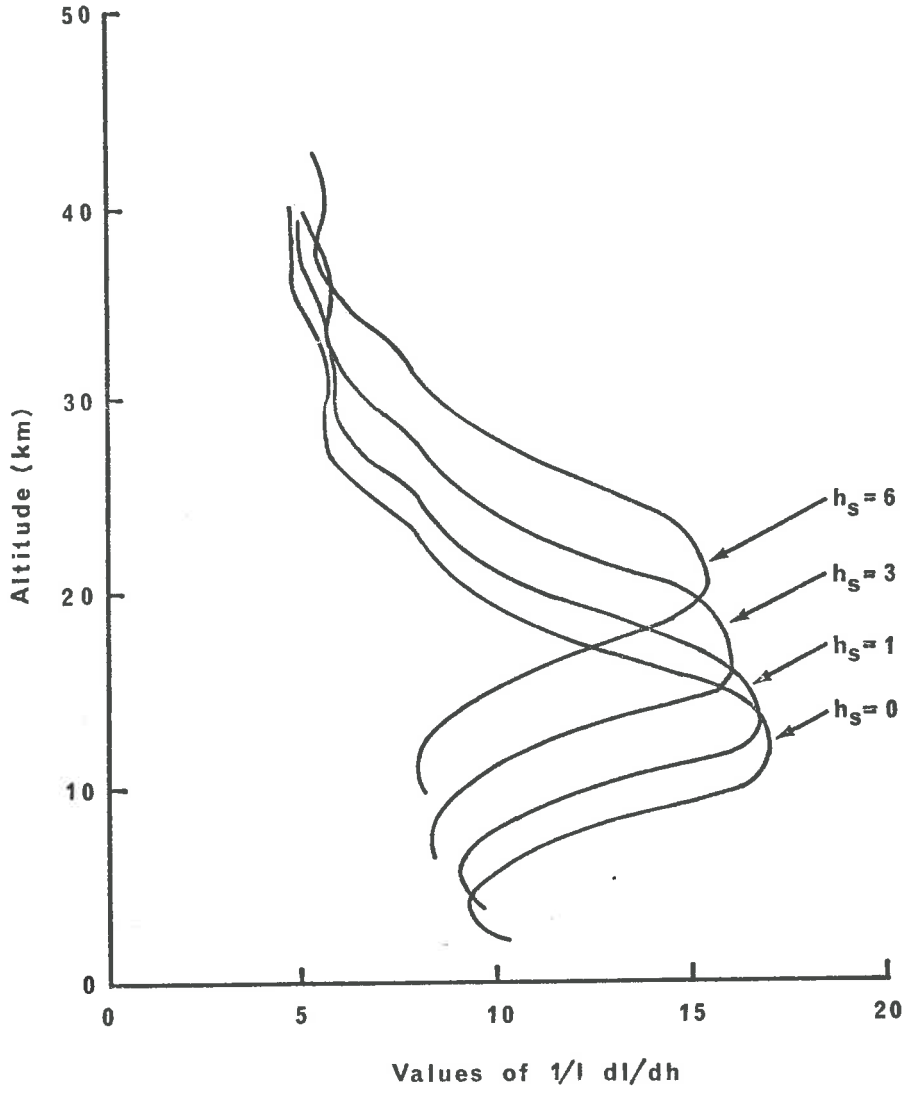

Figure 8.1 Twilight profile of 17th. Feb. 1969 analysed assuming different values of the screening height h_s.

angle, with the result that the peak in the profile is broadened for increasing values of h_s.

8.4 Comparison with Laser Results

It is not possible to deduce the appropriate value of the screening height h_s from the twilight profile itself (Rosenberg, 1966). In an attempt to deduce the true value of h_s, twilight profiles were compared with profiles of scattering ratio obtained using the laser radar. The measurements in each case were carried out within a few hours of each other.

It was found that the peak in the twilight profile could be made to occur at the same height as the peak in the scattering ratio curve if a value of about 6 km were assumed for the screening height. This value is in good agreement with the value deduced theoretically by Vols and Goody (1962) for the near infrared region of the spectrum. However, it was also found that the required value of screening height varied between individual profiles, by several kilometres. This may be seen in Fig. 8.2, where two twilight profiles of $\frac{1}{I}\frac{dI}{dh}$ have been compared with corresponding profiles of scattering ratio obtained with the laser radar. A screening height of 6 km was assumed in the analysis of both twilight profiles.

To some extent, the variation in the value of h_s can be attributed to the fact that the region of the stratosphere observed during the twilight measurements is several hundred kilometres to the west of the region observed by the laser radar. The apparent variation in h_s

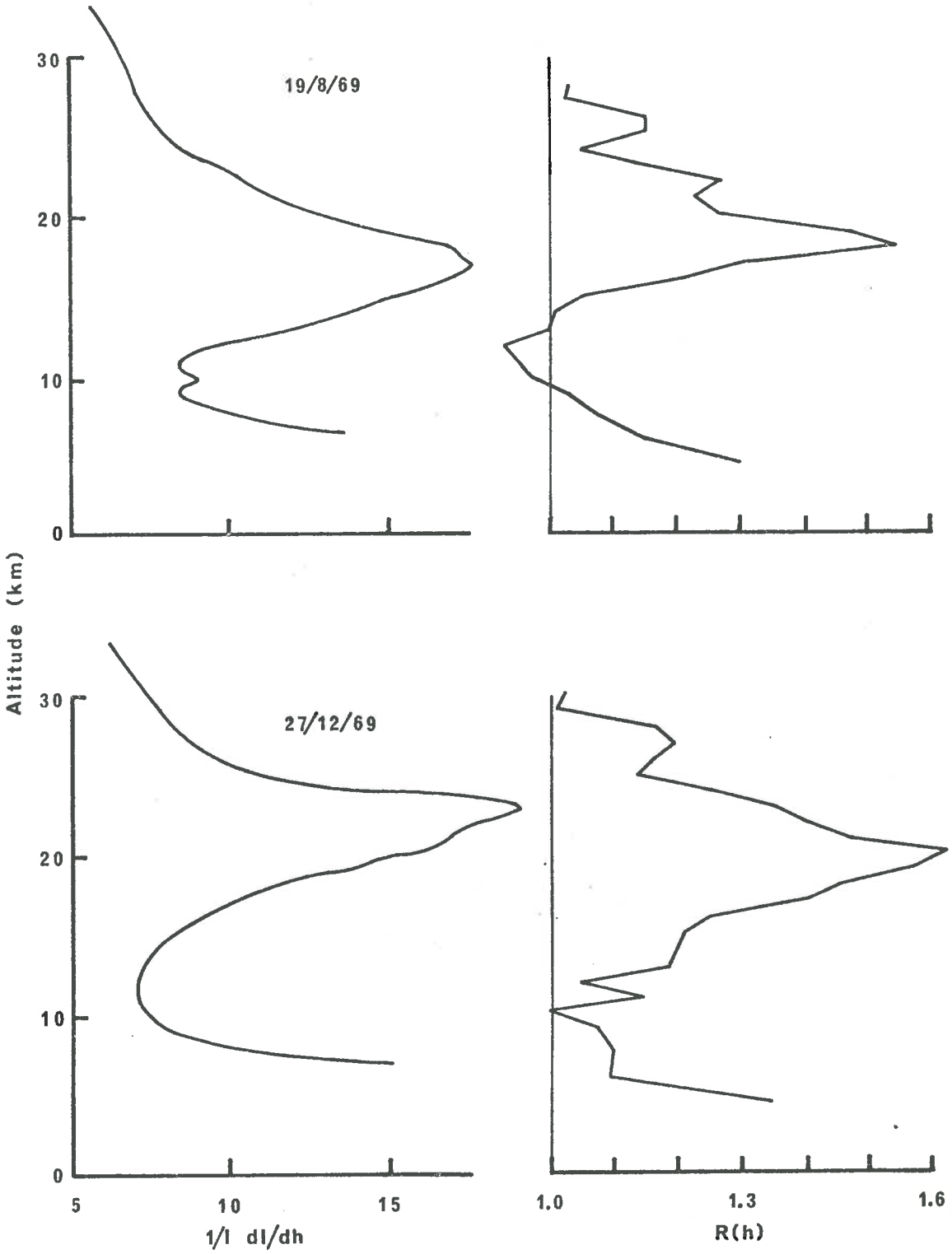

Figure 8.2 Two twilight profiles compared with corresponding laser soundings.

could therefore be caused by a real difference in the height of occurrence of peak turbidity of the stratospheric aerosol layer. However, it is equally likely that there is a real day to day variation in the value of h_s, caused by changes in the dust and moisture content of the lower atmosphere. In order to resolve this question, it would be necessary to ensure that the same region of the stratosphere were observed in each type of measurement. This could be achieved by locating the twilight photometer a sufficient distance to the east of the laser radar. However, this has not been attempted, in view of the small number of occasions when weather conditions are such as to allow both experiments to be carried out successfully.

From Fig. 8.2 it may be seen that although there is general agreement between the shapes of the profiles obtained by the two techniques, the small-scale features evident in the laser results have not been reproduced in the twilight profiles. It is significant that the twilight profiles were, in the absence of cloud disturbance, always much smoother than the laser profiles. Any small-scale structure in the twilight profiles was almost always accompanied by an increased noise level in the twilight record, and could generally be correlated with reports of scattered cloud towards the west during the time of sunset.

It would appear, therefore, that the vertical resolution of the twilight technique is considerably worse than the 1 km resolution of the laser radar, or the 0.5 km resolution suggested by considerations

based on the angular field of view of the photometer used in the present study. The poor vertical resolution could be accounted for by the lack of a sharp boundary to the earth's shadow, as suggested by Megrelishvili (1958).

Attempts to deduce the variation in the total dust content of the stratosphere from the twilight results have proved inconclusive. Using the method described by Bigg, the total area under the peak in the profile between heights of 11 and 30 km was taken to be a measure of the total dust content, and this quantity was plotted as a function of time. The result is shown in Fig. 8.3 Although the scatter in the plotted points is considerable, the values observed between late December, 1965 and February, 1966 appear to be higher than normal, and could indicate the presence of increased dust in the stratosphere from the eruption of Mt. Taal. It is significant, however, that the variation in total dust content during the remainder of 1966 is opposite to the seasonal variation found by Dyer and Hicks (1965), and in the present study (Section 7.4). The twilight results during 1967, on the other hand, indicated no significant seasonal variation at all.

It would appear, therefore, from the results of the twilight observations, and from the limited comparison with the laser results, that the twilight technique as described by Bigg is not capable of providing reliable information on the changes in stratospheric dust content and distribution. The lack of vertical resolution, and the variability in the screening height of the lower atmosphere, would

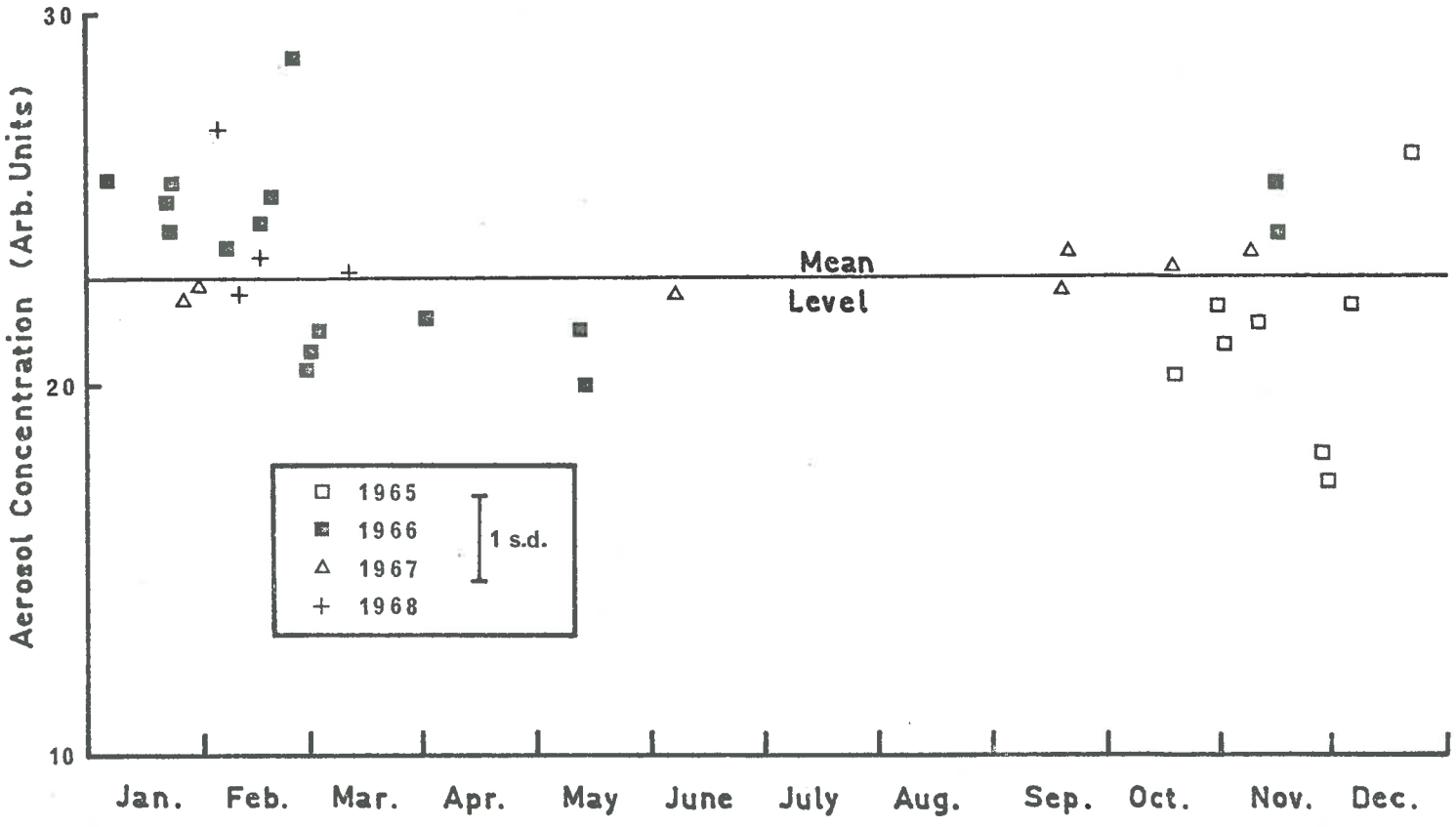

Figure 8.3 Variation in total stratospheric dust content deduced from the twilight measurements.

appear to be fundamental limitations to the usefulness of the method. The inconsistent seasonal variation in total dust content observed in the present study appears to justify Volz's contention that absolute intensity measurements are required before quantitative conclusions can be drawn.

CHAPTER 9

CONCLUSIONS and FUTURE WORK

9.1 The Laser Radar System

The laser radar system which has been constructed at Adelaide, South Australia (35°S, 139°E) allows a single operator to obtain in the space of approximately one hour, a complete scattering profile of the atmosphere over an altitude range of 3 to 30 km. The profile may be extended to an altitude of 60 km by combining the results of several nights of observations.

In the design of the present system, particular attention has been given to the elimination of all possible sources of spurious signals which could affect the accuracy of the observed scattering profiles, particularly from the higher altitudes. The good agreement between the observed profiles and those predicted by calculations based on a model molecular atmosphere up to the maximum observable height indicates that this aim has been achieved. It is estimated that the accuracy of the observed scattering profiles is of the order of 5% up to altitudes of approximately 40 km. Greater accuracies are achievable by means of extended recording periods.

The complete laser radar system is easily transportable. This feature was found useful when the first choice of operating site proved unsuitable, due to local weather conditions.

In spite of initial difficulties with the laser generator, the complete system has proved quite reliable, requiring a minimum amount of maintenance. In particular, the system appears to maintain its optical alignment indefinitely, following the initial setting-up procedure. It has thus been possible to establish a routine observational programme, subject only to weather conditions.

9.2 Results of Observations

The observations which have been carried out since May 1969 have allowed some preliminary conclusions to be reached regarding the behaviour of the stratospheric aerosol layer over southern Australia. It is believed that these are the first observations of this type carried out in the southern hemisphere.

The preliminary results indicate a marked seasonal variation in the stratospheric aerosol concentration, with the greatest values of concentration occurring during winter. A similar behaviour in the stratospheric aerosol layer over southern Australia had been inferred earlier by Dyer and Hicks (1965), from the results of observations of the attenuation of solar radiation. Dyer and Hicks proposed a seasonal influx of material into the mid-latitude stratosphere by transport from an equatorial "reservoir". The increased stratification of the aerosol layer observed with the laser radar during the autumn months has been taken as supporting the mechanism proposed by Dyer and Hicks.

The peak values of stratospheric turbidity observed in the present

study are generally lower than those reported from the northern hemisphere. However, in view of the strong seasonal dependence of the stratospheric aerosol concentration, it would be necessary to compare observations carried out over at least one full year at similar latitudes before one could conclude that there is any significant differences in turbidity between the two hemispheres. At present, there is insufficient data available from either hemisphere to allow such a comparison.

Comparison between the results of laser radar measurements and those of "in situ" particle sampling experiments is hampered by the lack of knowledge concerning the nature of the stratospheric aerosol. However, calculations carried out using a number of the models which have been proposed show that the laser radar results are in better agreement with the results of photoelectric particle sampling measurements than with those of direct particle collection experiments. This is interpreted as indicating a significant volatile component in the stratospheric aerosol. On current estimates of the water vapour content of the stratosphere, only a small fraction of the available water need exist in condensed form in order to account for the observed scattering coefficient.

Observations over the 30 to 60 km altitude range showed that the mean variation in scattering index with height throughout this region is similar to that predicted for a purely molecular atmosphere. This result is interpreted as indicating that this region is free of significant amounts of aerosol, and is used to justify normalisation

of the observed scattering profiles at a height near 30 km. The long-term averaged values of the turbidity at altitudes near 10 and 30 km are found to be very nearly the same, and advantage has been taken of this fact to allow normalisation of the observed scattering profiles at 10 km during automatic data reduction.

The scattering index profile for heights below 10 km is found to be highly variable, and appears to be influenced by the presence of temperature inversions low in the troposphere. These observations are consistent with the usual assumption that the earth's surface is the source of most of the tropospheric aerosol, the upward convection of which is influenced by the temperature variation throughout the troposphere. The observed height variation in turbidity is consistent with the variation in particle concentration found by Blifford and Ringer (1969) in a series of particle collection measurements using aircraft-borne impactors.

9.3 Comments

From the results of observations so far carried out, it is apparent that the laser radar technique offers a convenient method of studying the scattering properties of the atmosphere. Both short and long-term variations may be studied, over an altitude range extending from the low troposphere up into the middle stratosphere, with a relatively low powered system. Analysis and interpretation of the resulting data has been shown to be considerably more straightforward

than that of data obtained by the twilight technique.

At present, the main disadvantage of the laser radar technique is the lack of a method for achieving an absolute calibration of the observed scattering index profiles. Because of the experimental difficulties involved, no solution to this problem appears imminent. A secondary disadvantage of the technique is its relative technical complexity, and the resultant high initial cost of the required equipment. These disadvantages are, however, largely offset by the low operating costs of the complete equipment.

9.4 Future Work

In this section, the scope for further work using the laser radar technique is discussed. Consideration is given not only to those measurements which can be carried out with the present system, but also to techniques which should be considered in the design of new systems.

It was pointed out at various stages during the discussion in Chapter 7 that further observations of the stratospheric aerosol layer are required in order to allow more definite conclusions and comparisons to be made. The seasonal trend in aerosol concentration which is indicated by the results so far obtained should be investigated by observations carried out over at least one more year. At the same time, a body of data would be built up which would allow future comparison with data obtained by laser radar measurements in the northern hemisphere. It would obviously be desirable to coordinate stations in both hemispheres into a planned observational programme, in order to

ensure a meaningful comparison between results.

It would be of interest to compare laser radar results obtained over an extended period with the results of ozone concentration measurements being carried out over south-eastern Australia (Pittock, 1968). These measurements show that the maximum in ozone partial pressure occurs near an altitude of 24 km. A marked seasonal variation is found in the maximum ozone concentration, with peak values occurring during winter and spring of each year. Since it is likely that the same mechanism is responsible for the transport of both the aerosols and ozone, a real difference in the seasonal phases of the respective maxima would indicate a difference in the location of the source, or in the seasonal dependence of the rate of production, of each component.

Measurements described in Chapter 7 have shown that highly variable aerosol concentrations occur in the troposphere. The laser radar is ideally suited to an investigation of the effect of surface weather phenomena and vertical temperature structure on the tropospheric aerosol profile. Recent modifications to the Adelaide system by D. J. Gambling have reduced the lower limit of observations to an altitude of less than 1 km. It has also been found that observations can be carried out to an altitude of 5 km in daylight, allowing continuous observation of the tropospheric aerosol to this altitude.

It is shown in Chapter 2 that a significant increase in the maximum height which can be studied with the laser radar would call for a major increase in laser output energy, or in the receiver collecting surface

area. It is therefore unlikely that the height limitation of the present system will be increased beyond approximately 40 km. However, the results of observations so far carried out indicate the need for more accuracy in the final profiles. This could be achieved by an increased number of laser firings, but since the statistical accuracy increases as the square root of the number of integrations, considerably longer recording times would be called for. It would obviously be an advantage therefore if the repetition rate of the equipment could be increased. Calculations show that it should be possible to increase the repetition rate of the present system by a factor of approximately 6, to 3 sec^{-1}, without exceeding the capability of the laser generator, provided that the power supply were capable of recharging at this rate. It is planned that a suitable power supply should be constructed in the near future.

The use of more than one wavelength for atmospheric sounding has often been proposed. Near-simultaneous observations carried out using two or more wavelengths would allow the wavelength dependence of the aerosol scattering coefficient to be determined, and thus provide more information on the aerosol size distribution. Wavelengths which have been suggested are the 1.06 and 0.7μ radiation from the neodymium in glass, and ruby lasers, respectively, as well as 0.53 and 0.35μ obtained by frequency-doubling of the output from these lasers. Frequency doubling efficiencies of the order of 10% can be achieved by the use of suitable crystals (for example, potassium dihydrogen phosphate).

A number of practical difficulties would appear to have prevented this type of multiple wavelength experiment from being carried out. Although high-energy neodymium lasers are readily available, the quantum efficiency of presently available photomultipliers is extremely low at the long wavelength (typically 0.2% for the EMI type S-1 photocathode). At the other extreme, the high quantum efficiency of 20% available at 0.34 μ is offset to a large extent by the low atmospheric transmission at this wavelength (40% to an altitude of 10 km from Elterman's (1964) tabulations), and by the absorption due to the spectral cut-off of glass components in the radar optical system. However, a wavelength of 0.55μ, obtained by frequency doubling the output of a neodymium laser, and used in conjunction with a laser operating at 0.7μ, should allow additional useful information to be obtained. Although atmospheric transmission at 0.55μ is slightly lower than at 0.7μ, the three times greater quantum efficiency available at 0.55μ would more than offset these losses. It must however be pointed out that considerably smaller values of scattering ratio should be observed at 0.55μ, because the λ^{-4} wavelength dependence of Rayleigh scattering will cause this to predominate. It is shown in Chapter 7 that the expected wavelength dependence of scattering by the stratospheric aerosol lies in the range λ^{-1} to λ^{0}. The observed backscattering ratios at 0.55μ should therefore be smaller by a factor of approximately 2.5.

It has been suggested that the difficulty of distinguishing between the aerosol and molecular components of the total backscattered signal could be resolved by the observation of a frequency-shifted component

of the atmospheric backscatter. Cooney et al. (1969) have used a ruby laser with an output at 6943Å, and measured the backscatter at 8283Å due to the Raman vibrational-rotational band of nitrogen. They found that the signal return at 8283Å was unaffected by the presence of a thin cloud in the field of view of the laser radar, while the return at 6943Å showed a strong discontinuity. The aerosol attenuation coefficient may thus be deduced, following calibration at any height where the molecular density is known provided the relative 6943/8283 system response is determined. Unfortunately, because of the ratio of approximately 500 between the Rayleigh and Raman cross-sections, the method is at present limited to low altitudes. It is of interest that Inaba and Kobayasi (1969) have published a list of the frequency shifts of the Q-branch vibrational-rotational Raman spectra of various gases involved in air pollution, or present in the normal atmosphere.

A more useful technique for the detection of specific atoms or molecules higher in the atmosphere would appear to be the use of a laser emission wavelength tuned to an appropriate resonance of the particular component. The cross-section for the resulting resonance scattering is many orders of magnitude greater than the Rayleigh cross-section. Bowman, Gibson and Sandford (1969, 1970) have demonstrated the usefulness of this technique by measuring the height profile of the small quantities of sodium which occur in a narrow layer at about 90 km altitude. The requirement for a tunable pulsed source can be met most conveniently by the flashlamp-pumped organic dye laser (Sorokin et al., 1968).

A somewhat different method whereby vertical concentration profiles of several of the atmospheric gas constituents can be determined has been developed theoretically by Dobbins and La Grone (1969). The method makes use of two laser signals of different wavelengths, one occurring in an absorption region of the particular gas, and the other in a nearby spectral region where no appreciable absorption takes place. However, because of the difficulty of generating the required wavelengths at the high powers necessary, only one measurement of this type appears to have been carried out. Schotland et al. (1965) utilised the small shift in operating wavelength achievable by thermal tuning of a ruby laser to measure the vertical distribution of water vapour in the atmosphere to an altitude of approximately 4 km, by observations on the 6942.15Å water vapour absorption line (Long, 1963).

BIBLIOGRAPHY

Abella, I.D., and Cummins, W.Z., 1961, J. App. Phys., 32, 1177.

Bain, W.C., and Sandford, M.C.W., 1966(a), J. Atmos. Terr. Phys., 28 543.

Bain, W.C., and Sandford, M.C.W., 1966(b), Nature, 210, 826.

de Bary, E., and Rossler, F., 1966, J. Geophys. Res., 71, 1011.

Bigg, E.K., 1956, J. Met., 13, 262.

Bigg, E.K., 1964, Tellus, 16, 76.

Blifford, I.H., and Ringer, L.D., 1969, J. Atmos. Sci., 26, 716.

Bowman, M.R., Gibson, A.J., and Sandford, M.C.W., 1969, Nature, 221, 456.

Bowman, M.R., Gibson, A.J., and Sandford, M.C.W., 1970, The Radio and Electronic Engr., 39, 29.

Broadfoot, A.L., and Kendall, K.R., 1968, J. Geophys. Res., 73, 426.

Bullrich, K., 1964, Advances in Geophys., 10, 99.

Chagnon, C.W., and Junge, C.E., 1961, J. Met., 18, 746.

Chamberlain, J.W., 1961, "Phys. of the Aurora and Airglow" Intl. Geophys. Ser., Vol. 2 (Acad. Press, N.Y.).

Clemesha, B.R., Kent, G.S., and Wright, R.W., 1966, Nature, 209, 184.

Clemesha, B.R., Kent, G.S., and Wright, R.W., 1967(a), Nature, 214, 261.

Clemesha, B.R., Kent, G.S., and Wright, R.W., 1967(b), J. App. Met., 6, 386.

Collis, R.T.H., and Ligda, M.G.H., 1966, J. Atmos. Sci., 23, 255.

Cooney, J., Orr, J., and Tomasetti, C., 1969, Nature, 224, 1098.

Dave, J.V., and Mateer, C.L., 1968, J. Geophys. Res., 73, 6897.

Deirmendjian, D., 1965, J. Geophys. Res., 70, 743.

Divari, N.B., and Plotnikova, L.I., 1966, Soviet Astronomy, 9, 840.

Dobbins, D.E., and La Grone, A.H., 1969, Radio Sci., 4, 407.

Dyer, A.J., 1969, Report presented to Aust. Inst. of Physics Summer School, La Trobe Uni.

Dyer, A.J., and Hicks, B.B., 1965, Nature, 208, 131.

Dyer, A.J., and Hicks, B.B., 1968, Quart. J. Roy. Met. Soc. 94, 545.

Elterman, L., 1951, J. Geophys. Res., 56, 509.

Elterman, L., 1954, Geophys. Res. Paper No. 29, Air Force Cambridge Res. Center, Cambridge, Mass.

Elterman, L., 1964, Environmental Res. Paper No. 46, Air Force Cambridge Res. Labs., L.G. Hanscom Field, Mass.

Elterman, L., 1966, Environmental Res. Paper No. 241, Air Force Cambridge Res. Labs., Bedford, Mass.

Elterman, L., 1967, Environmental Res. Paper No. 253, Air Force Cambridge Res. Labs., Bedford, Mass.

Elterman, L., Wexler, R., and Chang, D.T., 1969, App. Opt. 8, 893.

Fesenkov, V.G., 1923, Trudy. Glav. Ross. Astrofiz. Obs., 2, 7.

Fesenkov, V.G., 1934, Bull. Acad. Sci. USSR, Div. of Mathem. and Natural Sci., p1503.

Fiocco, G., and Grams, G., 1964, J. Atmos. Sci., 21, 323.

Fiocco, G., and Smullin, L.D., 1963, Nature, 199, 1275.

Friedland, S.S., Katzenstein, J., and Katzick, M.R., 1956, J. Geophys. Res., 61, 415.

Friend, J.P., 1966, Tellus, 18, 465.

Friend, J.P., Feely, H.W., Krey, P.W., Spar, J., and Walton, A., 1961, Report D.A.S.A. - 1300, U.S. Dept. of Defense.

Gadsden, M., 1965, App. Opt. 4, 1446.

Gonez, J.M., and Newell, P.B., 1966, J. Opt. Soc. Am., 56, 87.

Goyer, G.G., 1968, Bull. Am. Met. Soc., 49, 936.

Goyer, G.G., and Watson, R.D., 1968, Bull. Am. Met Soc., 49, 890.

Grams, G., and Fiocco, G., 1967, J. Geophys. Res., 72, 3523.

Graydon, A., 1956, Proc. Natl. Electronics Conf., 12, 1071.

Gruner, P., 1958, Handbuch Geophysik (Borntraeger, Berlin) 8, 432.

Hindle, J.H., 1957, "Amateur Telescope Making", Book I (Scientific American Inc., N.Y.)

Hulburt, E.O., 1937, J. Opt. Soc. Am., 27, 377.

Hulburt, E.O., 1953, J. Opt. Soc. Am., 43, 113.

Inaba, H., and Kobayasi, T., 1969, Nature, 224, 170.

Jackson, M.G., 1965, Nuclear Instr. and Methods, 33, 161.

Jenkins, F.A., and White, H.E., 1957, "Fundamentals of Optics", (McGraw-Hill, N.Y.)

Johnson, F.A., Meyer, R.C., Hopkins, R.E., and Mook, W.H., 1939, J. Opt. Soc. Am., 29, 512.

Junge, C.E., 1961, J. Met., 18, 501.

Junge, C.E., and Manson, J.E., 1961, J. Geophys. Res., 66, 2163.

Junge, C.E., Chagnon, C.W., and Manson, J.E., 1961, J. Met., 18, 81.

Kent, G.S., Clemesha, B.R., and Wright, R.W., 1967, J. Atmos. Terr. Phys., 29, 169.

Koerber, D., and Crosby, P., 1960, Tech. Note OID 15 (Weapons Res. Establishment, Salisbury, Sth. Aust.).

Long, R.K., 1963, Proc. I.E.E.E., 51, 859.

Maiman, T.H., 1960, Nature, 187, 493.

Maastenbrook, H.J., 1968, J. Atmos. Sci., 25, 299.

McClung, F.J., and Hellwarth, R.W., 1963, Proc. I.E.E.E., 51, 46.

McCormick, M.P., Lawrence, J.D., and Crownfield, F.R., 1968, App. Opt., 7, 2424.

McCormick, P.D., Poultney, S.K., Van Wijk, U., Alley, C.O., and Bettinger, R.T., 1966, Nature, 209, 798.

McCormick, P.D., Silverberg, F.C., Poultney, S.K., Van Wijk, U., Alley, C.O., and Bettinger, R.T., 1967, Nature, 215, 1262.

Megrelishvili, T.G., 1958, Bull. Acad. Sci. USSR, Geophys. Ser., p315.

Morton, G.A., 1968, App. Opt., 7, 1.

Monsop, S.C., 1965, Geochim. et Cosmochim. Acta, 29, 201.

Penndorf, R., 1957, J. Opt. Soc. Am., 47, 176.

Pittock, A.B., 1968, Quart. J. Roy. Met. Soc., 94, 563.

Rayleigh (Lord), 1871, Phil. Mag. 41, 107, 274, 447.

Rosen, J.M., 1964, J. Geophys. Res., 69, 4673.

Rosen, J.M., 1968, J. Geophys. Res., 73, 479.

Rosenberg, G.V., 1966, "Twilight" (Plenum Press, N.Y.).

Sandford, M.C.W., 1967, J. Atmos. Terr. Phys., 29, 1657.

Schotland, R.M. et al., 1965, Optical Sounding II, N.Y. Uni. School of Eng. and Sci., July 15, 1965.

Smullin, L.D., and Fiocco, G., 1962, Proc. I.R.E.E., 50, 1703.

Sorokin, P.P., Lankard, J.R., Moruzzi, V.L., and Hammond, E.C., 1968, J. Chem. Phys., 48, 4726.

Synge, E.H., 1930, Phil. Mag., 9, 1014.

U.S. Standard Atmosphere, 1962, U.S. Govt. Printing Office, Washington.

U.S. Standard Atmosphere Supplements, 1966, U.S. Govt. Printing Office, Washington.

Van de Hulst, H.C., 1957, "Light Scattering by Small Particles", (Wiley, N.Y.).

Vols, F.E., and Goody, R.M., 1962, J. Atmos. Sci., 19, 385.

Wright, H.W.H., Sandland, D., Kent, G.S., and Clemesha, B.R., 1969, Aeronomy Report, 32, 72.

APPENDIX I

Copy of Report:

"A 10-Channel High Speed Pulse Counter"
by K. Bartusek. University of Adelaide Report
ADP74 (June, 1969).

A 10-CHANNEL HIGH SPEED PULSE COUNTER

K. Bartusek

Department of Physics

University of Adelaide

June, 1969.

ADP 74.

THE UNIVERSITY OF ADELAIDE

DEPARTMENT OF PHYSICS

C O N T E N T S

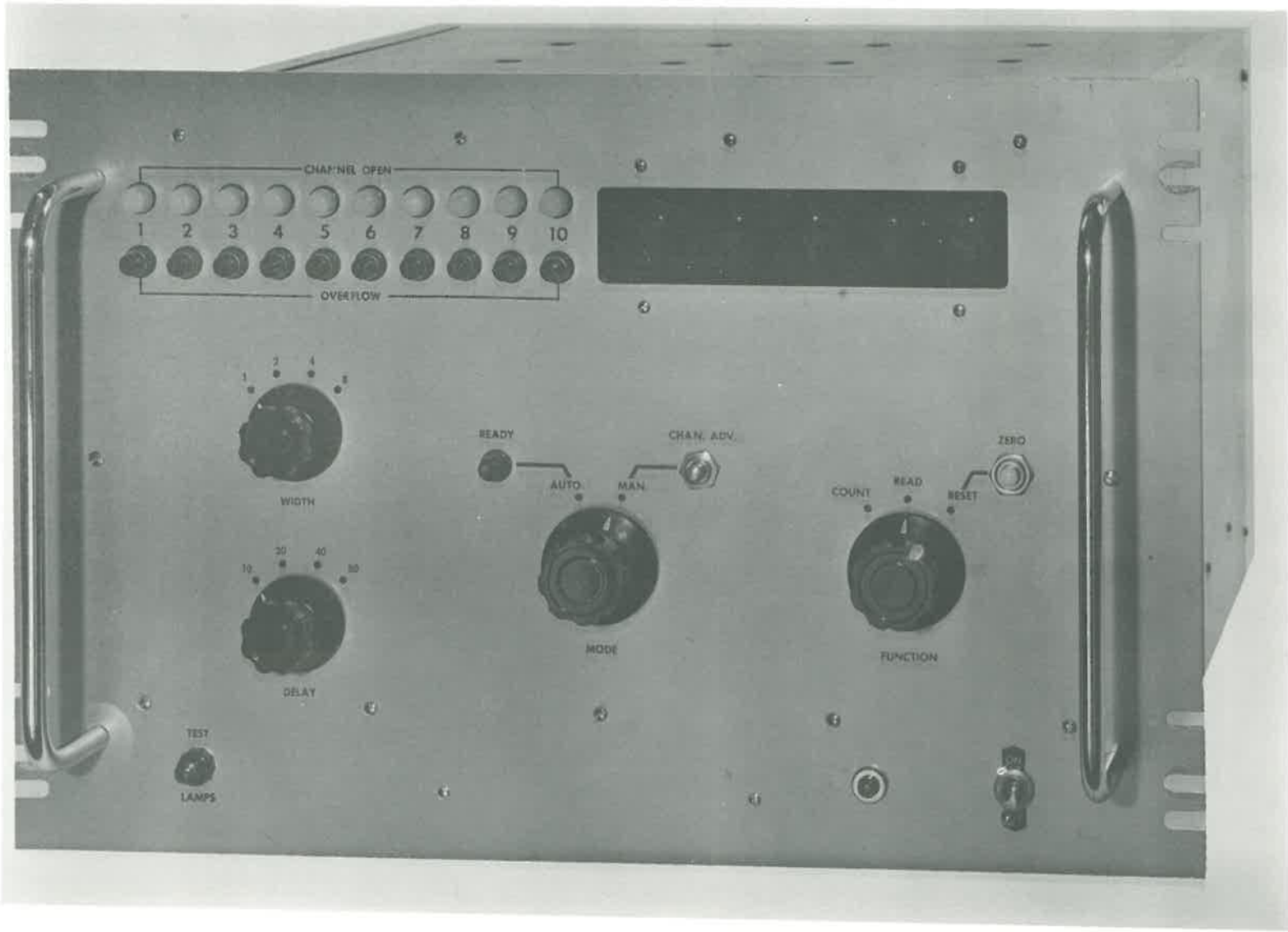

Frontispiece: 10-Channel Pulse Counter.

I. Introduction

This manual describes the operation and circuitry of a 10-channel high speed pulse counter. The counter has been developed specifically as the recording system for a laser radar, and is used to count single-photon pulses from a photomultiplier detector. The pulse resolving time is 50 nsec., allowing average count rates for random pulses of 2 MHz to be achieved. Higher count rates can be achieved if corrections are made for the finite resolving time.

The 10 channels form the 10 sequential range recording intervals. These range intervals (channel widths) may be set at 1, 2, 4 or 8 km by means of a front panel control. The delay between arrival of a trigger pulse and opening of the first channel may also be set by a front panel control to 10, 20, 40 or 80 km. The dead time between the closing of one channel and opening of the next is less than 100 nsec.

Readout of the counts accumulated in each channel is achieved by manually opening each channel, by means of a push-button control. The count is displayed on an in-line readout of 5 numerical indicator tubes. A light indicates which of the 10 channels is being read. Overflow indication for each channel is provided.

The total number of times that the counter has been triggered and has run through the recording cycle is counted automatically, and continuously displayed.

II. Specifications and Controls

Front Panel Controls

(1) Mode Switch, Ready Light, and Chan. Adv. Button.

(a) Auto - "Ready" light is on. Counter is ready to receive a trigger pulse, and will run through all channels once. "Channel Advance" button is inoperative, and readout indicates total number of times that recording sequence has been repeated ("Cycles" count).

(b) Manual - "Ready" light goes out. Pushing "Channel Advance" button opens first, and subsequent, channels in turn. Readout indicates total count in open channel. Counter ignores trigger pulses.

(2) Function Switch.

(a) Reset - Resets internal circuitry to standby state; allows an open channel to be closed without opening subsequent channels in "Manual" operation. Activates "zero" button.

(b) Read - Allows contents of a channel to be read, while inhibiting further counting. Counter responds to

trigger pulses (if "Mode" switch is in "Auto") but "Cycles" counter is inhibited.

(c) Count - Allows counting of signal pulses to proceed.

(3) Zero Button.

Sets contents of all counters to zero provided "Function" switch is in "reset" position. Disconnected otherwise. Counter must be zeroed each time at switch-on.

(4) Delay Control.

Sets delay between receipt of trigger pulse and opening of first channel to 10, 20, 40 or 80 km., i.e. determines range at which observations start.

(5) Width Control.

Sets channel width to 1, 2, 4 or 8 km.

(6) Lamp Test Button.

Lights all front panel lamps when power is applied. Used for testing lamps and lamp driver circuits.

(7) Channel Open Lamps.

10 lamps indicating the instantaneous state of each channel.

(8) Overflow Lamps.

10 lamps indicating a channel has received counts beyond its capacity. Further counting in that channel only is inhibited (readout for an overflowed channel will be 00000).

Rear Panel

(1) Count Input.

Terminates 50Ω . Requires + 4 volt pulses, minimum width 25 nsec. Rise and fall times less than 10 nsec.

(2) Trigger Input.

Sensitivity + 5V or + 50V as selected by rear panel switch. Rise time less than 1 usec., minimum pulse width 100 nsec.

Specifications

(1) Internal clock frequency: 150 KHz $\pm$.01% (corresponds to 1 km range interval).

(2) Input count rate: Resolving time 50 nsec.

(3) Channel count capacity:

(a) first 6 count channels: 10^5-1

(b) next 4 count channels: 10^4-1

(c) "Cycles" channel: 10^3-1

Construction

With the exception of the power supplies, the circuitry is based almost entirely on integrated circuits. The control sections of the instrument make use of Fairchild medium speed RTL micrologic. The counting and decoding sections use Texas Instruments series 74N high speed TTL semiconductor networks.

Construction of the instrument is on 24 double-sided fibreglass printed wiring cards, plugged into edge connectors for easy removal. Cards may be removed and replaced while power is applied to the instrument.

All the low voltage power supplies are electrically filtered and regulated, but are not short-circuit proof. However, over-voltage protection has been provided for the integrated circuits, in case of power supply failure.

III Circuit Logic and Operation

Refer to the simplified block diagram of Fig. 1. Consider first of all the "Auto" mode of operation. The clock oscillator runs continuously, but in the standby condition, between trigger pulses, the CONTROL circuit prevents clock pulses from passing to the following circuits.

On receipt of a start trigger pulse, the CONTROL circuit allows clock pulses to pass to the DELAY circuit. The

DELAY circuit counts the clock pulses, but blocks them until a predetermined number (determined by the "Delay" control setting) has been received. The DELAY circuit then passes subsequent clock pulses to the WIDTH circuit, which counts them down by a factor of 1, 2, 4 or 8 (determined by the "Width" control setting) before passing them to the SHIFT REGISTER as Shift pulses. The SHIFT REGISTER, on 11-stage twisted-ring counter, propagates a logical "0" from one stage to the next on the arrival of each Shift pulse. The logical "0" opens the count and read gates of the particular counter channel connected to that stage, and counting of signal pulses proceeds in that channel, until arrival of the next shift pulse.

When the logical "0" passes from the 11th stage (channel 10) of the SHIFT REGISTER back to the first stage (channel 0), a stop pulse is generated which resets the CONTROL circuit, thus stopping any further clock pulses from passing through. Simultaneously, the Preset level is activated, which returns the DELAY circuit to its initial state, and holds the WIDTH, SHIFT REGISTER, and CONTROL circuits in the "standby" state. The Preset level is de-activated again on receipt of the next Start pulse. The Stop pulses are also counted by the "Cycles" counter, thus indicating the number of times that the recording sequence has been completed.

In the "Manual" mode of operation, the Preset level is de-activated, and the WIDTH and DELAY circuits by-passed by the CONTROL circuit, which routes Manual pulses directly to the SHIFT REGISTER as shift pulses. Stop pulses are still generated by the SHIFT REGISTER, but ignored by both the CONTROL circuit and Cycles counter.

The readout gate in each channel holds the output of that channel at logical "0" when the channel is closed. When the channel opens (for either "Count" or "Read"), the readout gate passes the accumulated count (in BCD code) in that channel through the 11-input readout gating to the DECODER. The decoded count is displayed on a 5-digit numerical readout.

The following sections, with Figs. 2-9, provide a detailed description of the logic involved in the operation of each stage of the instrument. Figs. 10-17 are actual wiring diagrams for each of the printed circuit cards. The edge connector pins used for the various inputs, outputs, and supply voltages are indicated by circled numbers.

1. CONTROL Circuit

Refer to Fig. 2, and assume that the CONTROL circuit has been reset by taking the Reset level high and back to low. Consider the "Auto" mode of operation, which requires that the Activate level remains low. Under these conditions, S-R flip flop FF1 is reset such that its output Q is high ($\bar{Q}$ low). These outputs applied to the J and K inputs of J-K flip flop FF2, hold FF2 in the reset state, such that its Q output is high. Gate G4 is thus closed, and clock pulses are prevented from passing to the SHIFT REGISTER.

A Start pulse applied to FF1 causes FF1 to be set and to reverse the input to FF2, which then changes state on receipt of the next clock pulse and opens gate G4, allowing clock pulses to pass to the DELAY and WIDTH circuits, and then, as Shift pulses, to reach the SHIFT REGISTER. FF2 and G4 in combination form a synchronous gate, and obviate the possibility of initial clock pulses being shortened due to the random relation between start pulses and the clock oscillator.

Shift pulses continue to reach the SHIFT REGISTER until a Stop pulse arrives at G1, causing FF1 to be reset, and via FF2 to close G4. The Q output of FF1 activates gate G3, causing the Preset level to be activated, and to preset the DELAY and WIDTH circuits and the SHIFT REGISTER.

To prevent the possibility of both S and R inputs of FF1 being taken high simultaneously, both the Stop and Start inputs are A.C. coupled.

In the "Manual" mode of operation, the Activate level is taken high, setting FF1 and causing the Preset level to be removed from the SHIFT REGISTER (and DELAY and WIDTH circuits). Clock pulses are however prevented from reaching the SHIFT REGISTER because gate G5 is closed by the Activate level. Gate G7 is opened, allowing pulses generated by a pushbutton switch associated with FF3 to reach the SHIFT REGISTER as shift pulses. Thus the channel associated with any stage of the SHIFT REGISTER may be opened in turn, for either "Read" or "Count" functions. The SHIFT REGISTER may be reset at any stage by activating the Reset level.

2. Delay Circuit

Refer to Fig. 3. During Standby periods, the Preset level causes FF1 to be preset, and its output Q and $\overline{Q}$ to hold gate G6 open and G5 closed respectively. The 1,2,4,8 outputs of decades CD1 and CD2 are high. The desired delay is preselected by taking one of the 10,20,40,80 inputs, to gates G1-4 respectively, low. All other inputs are high.

On receipt of a Start pulse by the CONTROL circuit, the Preset level is removed, and Shift pulses are passed

to CD1 via G6. The pulses are counted down by a factor of 10 by CD1, each tenth pulse being passed to CD2. Each of the 1,2, 4,8 outputs of CD2 changes from high to low after 1,2,4,8 pulses respectively have been counted by CD2. The appropriate transition is passed by one of the gates G1-4 via G7 to FF1. The resulting change of state of FF1 causes gate G6 to close, and gate G5 to open, allowing Shift pulses to pass to the WIDTH circuits.

On completion of the recording cycle, the Preset level is again activated, causing all circuits to be reset.

3. Width Circuit

The WIDTH circuit (Fig. 4) consists essentially of three flip flops FF1-3, which count down the incoming Shift pulses by a factor of 2,4 or 8 respectively. Either the unmodified pulses, or the output of one of the flip flops, is selected by one of the gates G1-4, depending on which of the inputs 1,2,4, 8 is taken low by the "Width" selector switch. The pulses are passed to the SHIFT REGISTER via G5.

4. Shift Register

The SHIFT REGISTER (Fig. 5) consists of a ring counter having a logical inversion between both the input and output of the first flip flop (FF0) and the rest of the ring. During the Standby phase, the Preset level presets all flip flops

such that the Q terminal is low (logical "1"). On receipt of the first Shift pulse, the logical "1" in $F\overline{\emptyset}0$ shifts into FF1 as logical "0". The following Shift pulse shifts the "0" into FF2, resetting FF1 to "1". Succeeding Shift pulses cause the logical "0" to propagate around the ring until it arrives back at $F\overline{\emptyset}0$ (as logical "1" due to inversion at the input terminals of FF0) the change of state of FF0 causes a Stop pulse to be generated, which prevents the arrival of further Shift pulses.

Each of the flip flops FF1-FF10 is connected via a buffer to one of the 10 count channels. A channel is open when a logical "0" is present in the corresponding flip flop.

5. Counters

Each COUNTER (Fig. 6) consists of 5 cascaded decade counters CD1-5. The INPUT pulses to be counted are passed to CD1 via the count gate G2, while the BCD output levels go to the decoders via readout gates RG1-20. These gates are controlled by the control level, which is determined by the state of the corresponding flip flop in the SHIFT REGISTER.

Overflow indication is provided by the overflow flip flop FF0. Receipt of a count in excess of 10^5-1 will cause FF0 to change state, closing count gate G2 via the overflow

gate G1, and indicating an overflow condition on a front panel indicator light via the overflow output level.

The inhibit level is used to close count gate G2 during the "Read" mode of operation.

6. Decoders

Five binary to decimal decoders are used, one for each decade to be displayed. Since there are 11 counter channels, each of the A,B,C,D (binary 1,2,4,8) inputs to each decoder is a combination of 11 inputs, one from each channel, as shown in Fig. 7.

If we designate the A output of the first decade in channel 1 as 1A1, the same output in channel 2 as 2A1, etc., then, remembering that these outputs are inverted by the read gates RG, we have (referring to Fig. 7)

$$
\begin{aligned}
A &= \overline{M + Q} \\
&= \overline{M} \cdot \overline{Q} \\
&= L \cdot Q \\
&= \overline{\overline{1A1} + \overline{2A1} + \ldots + \overline{8A1}} \cdot \overline{\overline{9A1} + \ldots + \overline{11A1}} \\
&= \overline{\overline{1A1} + \overline{2A1} + \ldots + \overline{11A1}} \\
&= 1A1 \cdot 2A1 \cdot \ldots \cdot 11A1 \ .
\end{aligned}
$$

Since the gates RG hold at logical "1" all outputs

except those of the channel being read, say channel n,

then A = nA1

Similarly, each of the remaining inputs of each of the decoders will see only the output of channel n. The decoded 0 - 9 count is displayed on each of 5 "Nixie" tubes on the front panel.

7. Lamp Drivers

Each lamp driver (Fig. 8) consists of a single transistor arranged on a 2-input OR gate. A high level on either input causes the lamp in the collector circuit to light. One input is the Lamp Test level, the other input is either the Control or Overflow level from the appropriate count channel.

8. Count Input Driver

The incoming signal pulses are required to drive the inputs of all 10 count channels simultaneously. The necessary low output impedance drive is provided by an emitter follower input buffer (Fig. 9). The output of this stage is coupled to the channel inputs through 5 equal lengths of coaxial cable, each of which supplies 2 channels. Each channel input is parallel by 220 Ω, which is the maximum value allowable to maintain the counter input at logical "0"

in the absence of input pulses.

9. Clock Oscillator

The clock oscillator (Fig. 10) consists of a 2-transistor crystal controlled oscillator. The oscillator output waveform is squared by a Schmitt trigger formed from the two sections of a microcircuit dual gate. The output of this is then amplified and inverted. Two outputs are provided; the clock pulses and their complement.

IV Power Supplies

The regulated voltages required by the microcircuits used in the instrument are supplied by 3 identical rectifier-regulator circuits working from a common transformer T1 (Fig. 18). The output voltage of each filter-regulator section is compared with a preset voltage derived from a two-stage zener diode voltage reference. The difference, or error, voltage is amplified and used to control a series regulator transistor. The output voltage of each section is independently adjustable, and the maximum current capability is 1A.

Two of the regulator sections are adjusted to 5v. output, and supply the TTL microcircuits used in the instrument. The remaining section supplies 3.6v to the RTL microcircuits. The supply rails are supplied in each case through a 1 Amp

fuse, the output side of which is bypassed by a zener diode with breakdown voltage just higher than the output voltage of the power supply. The purpose of the fuses is to protect the microcircuits from over-voltage should a series regulator transistor short-circuit.

A second transformer T2 (Fig. 19) supplies the unregulated high voltages required by the Nixie tubes and decoder circuits, as well as a 6 volt regulated rail for the lamp drivers and clock oscillator.

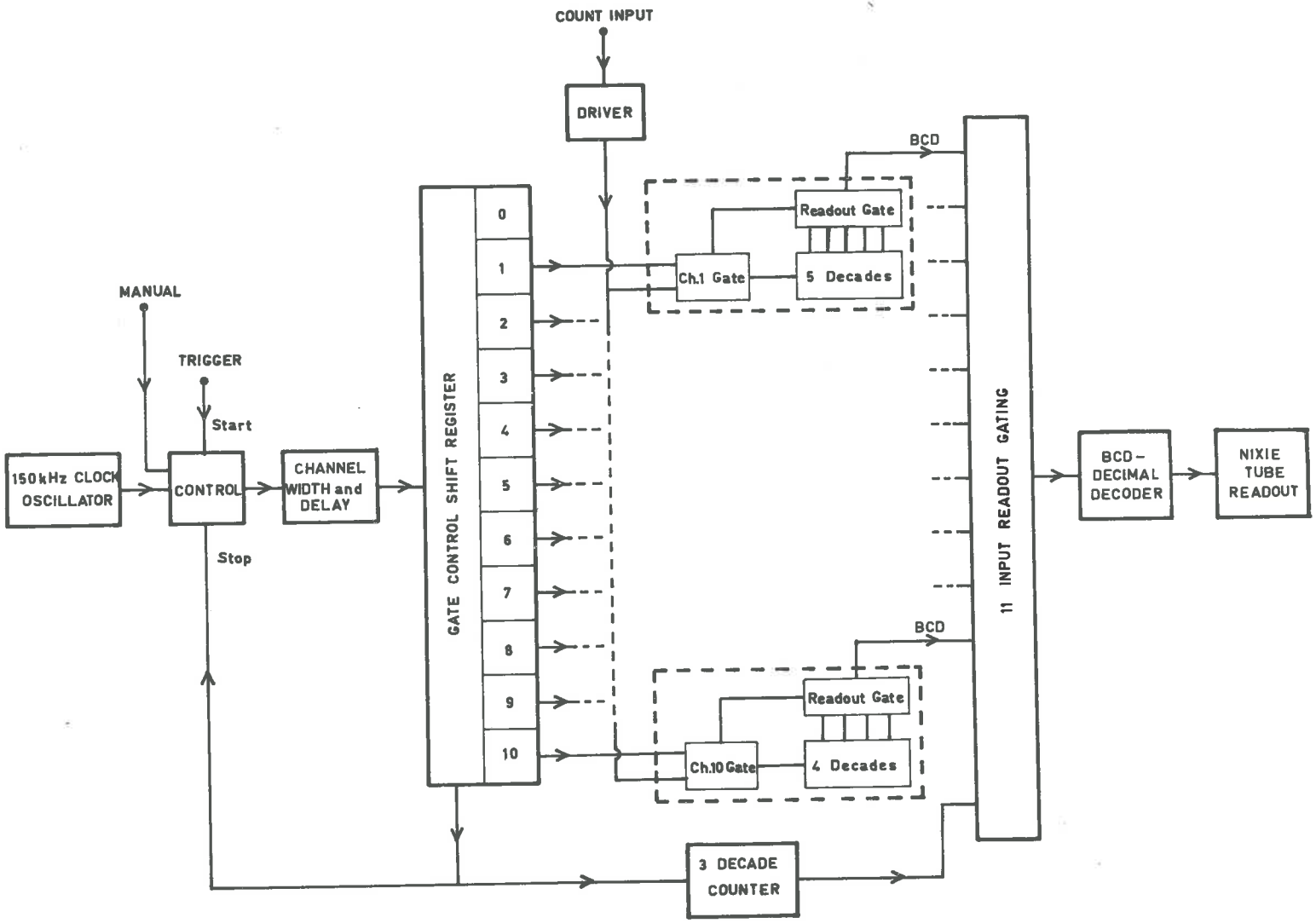

Fig. 1: Simplified Block Diagram of Complete Instrument.

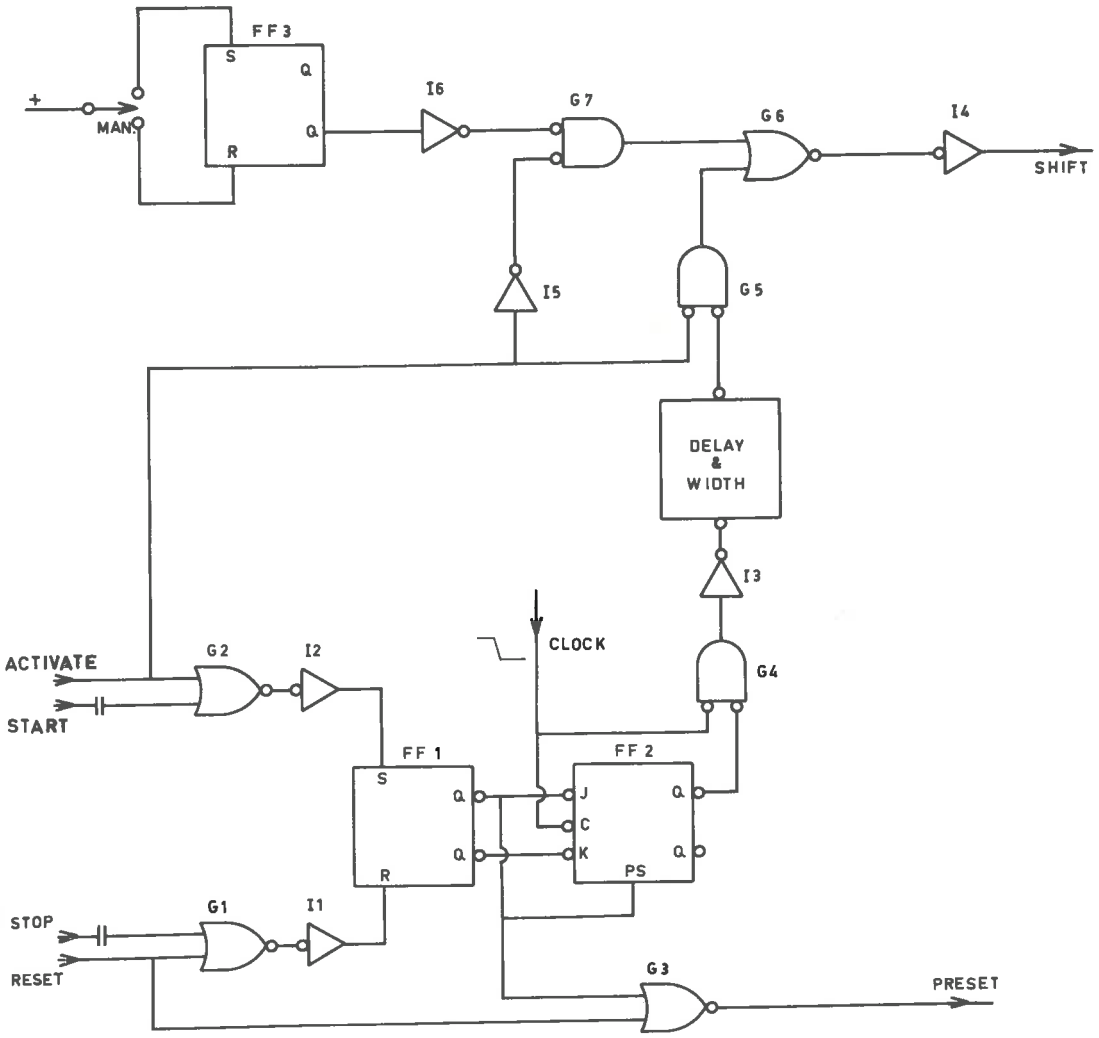

Fig. 2: Control Circuit Logic.

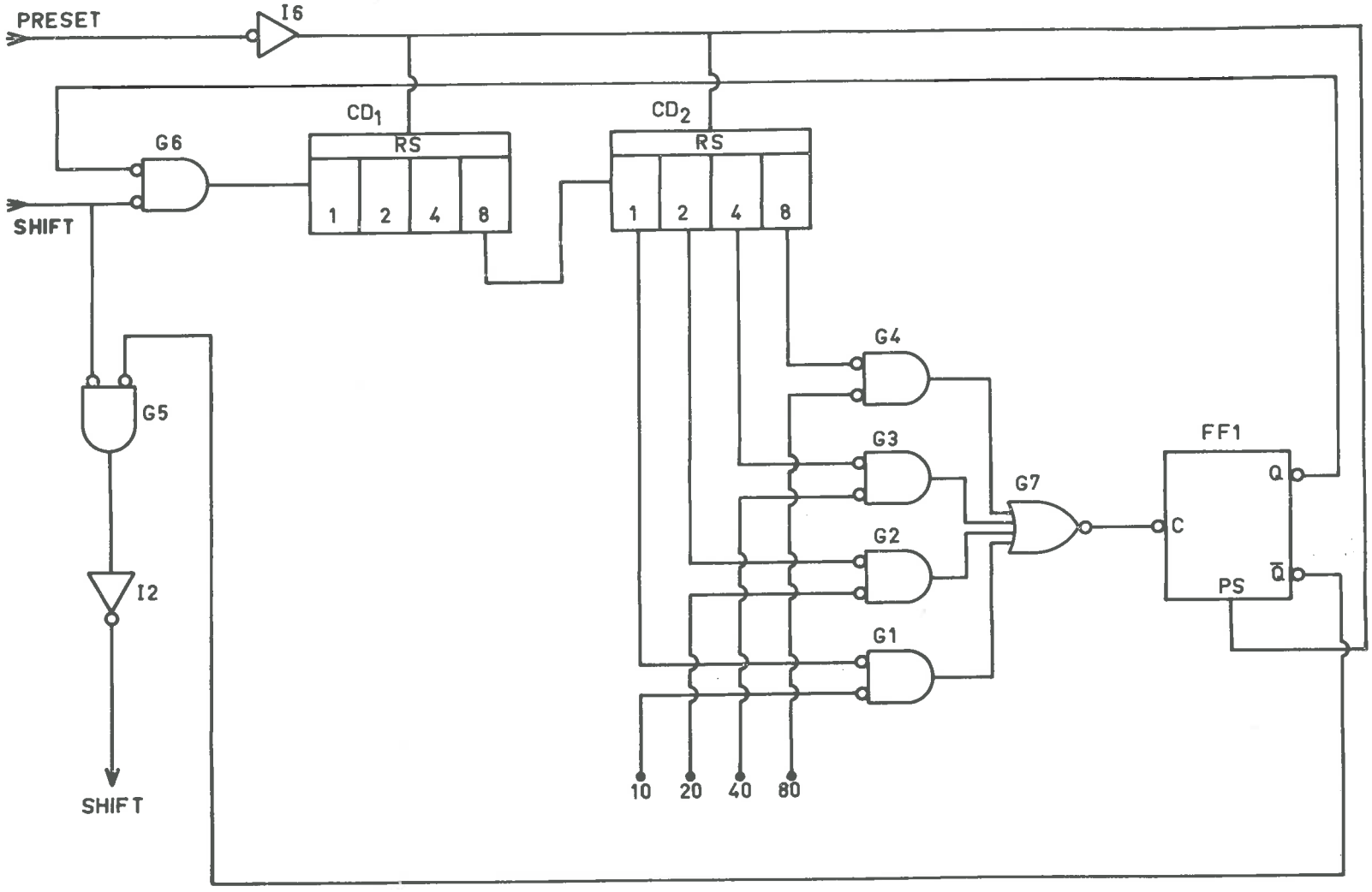

Fig. 3: Delay Circuit Logic.

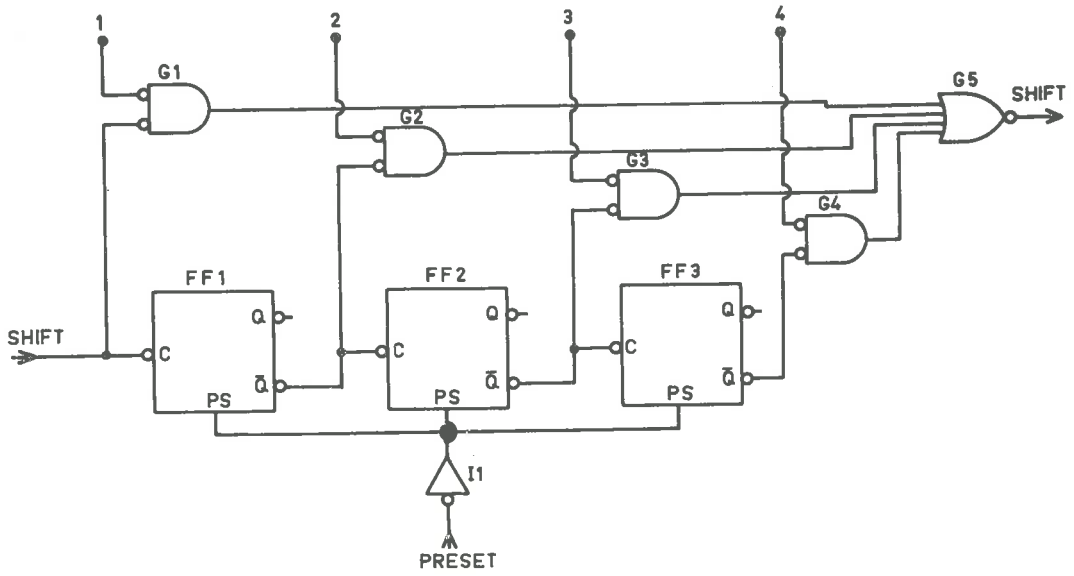

Fig. 4: Width Circuit Logic.

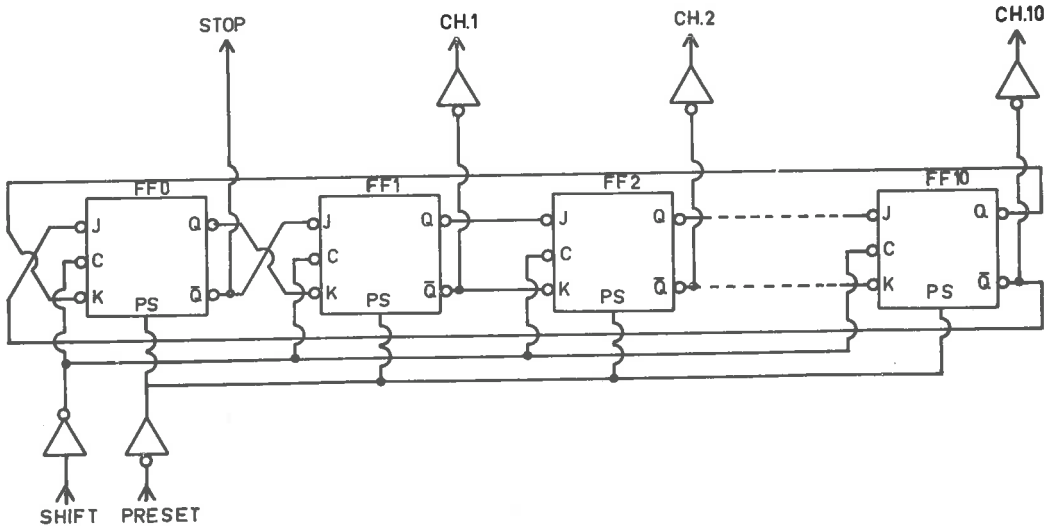

Fig. 5: Shift Register Logic.

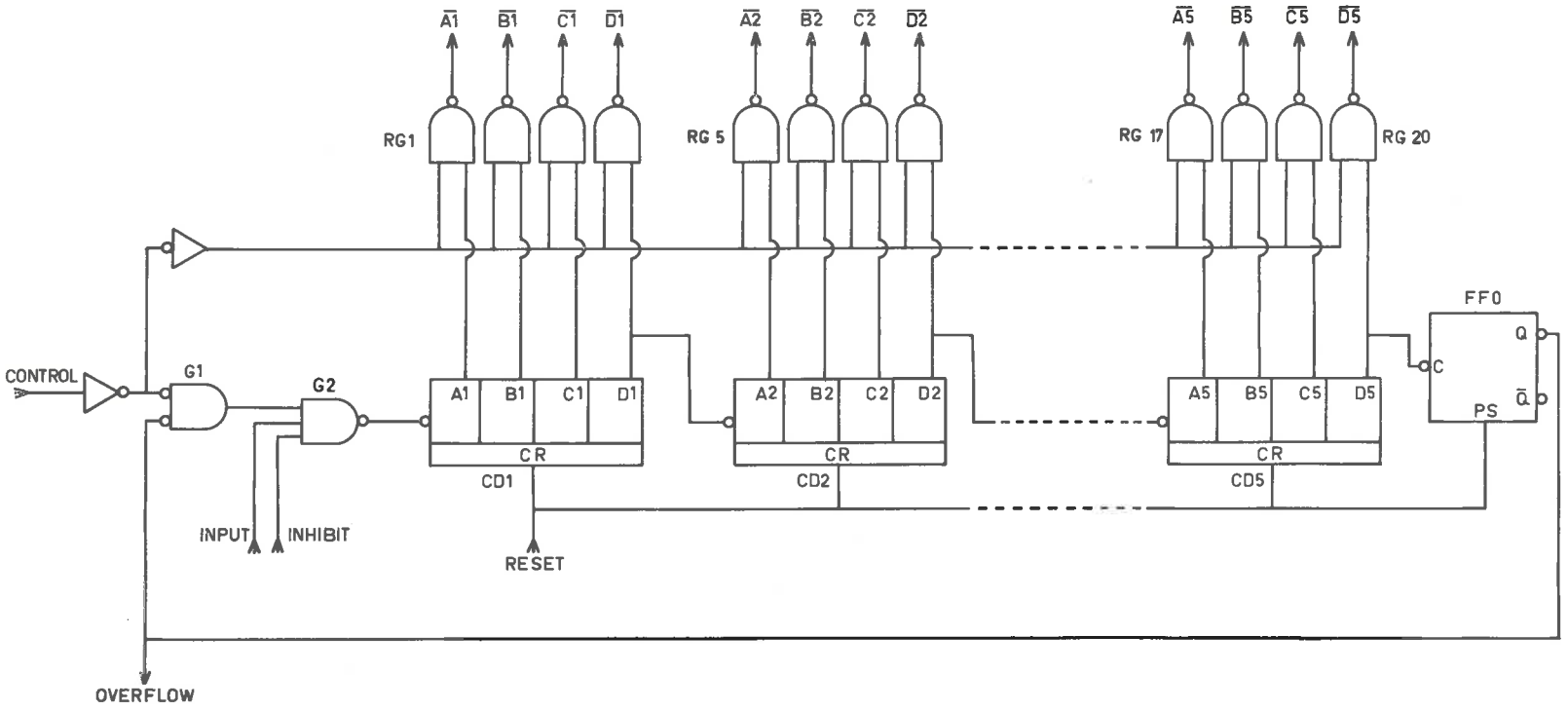

Fig. 6: Counter Logic.

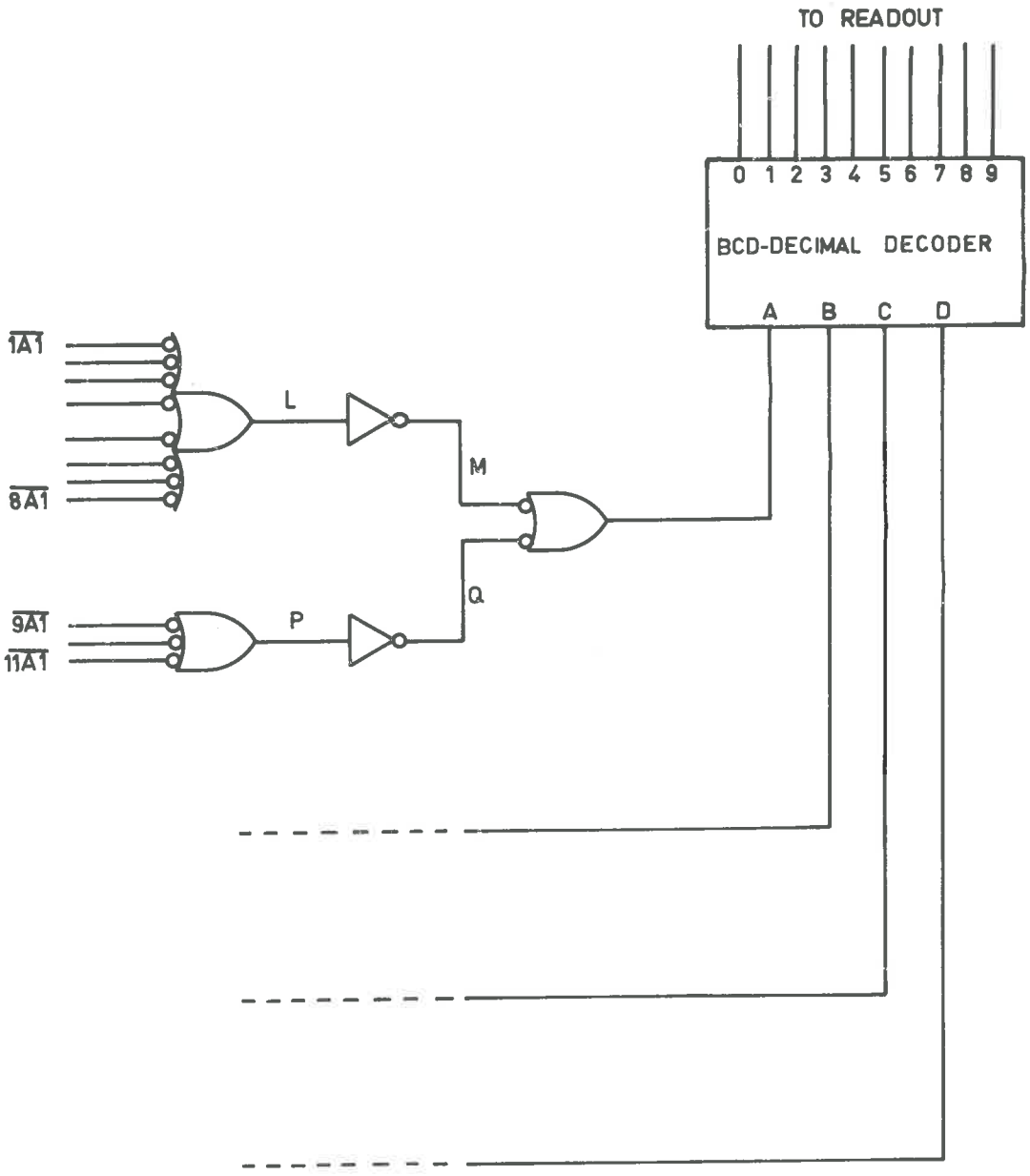

Fig. 7: Decoder Logic.

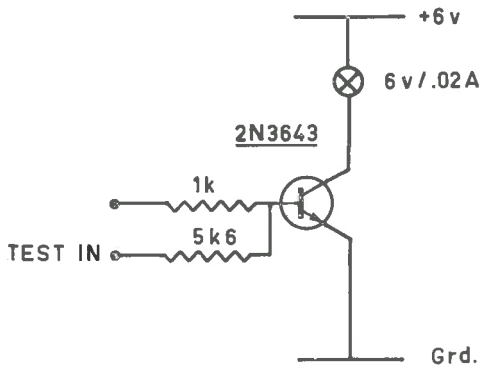

Fig. 8: Lamp Driver Circuit.

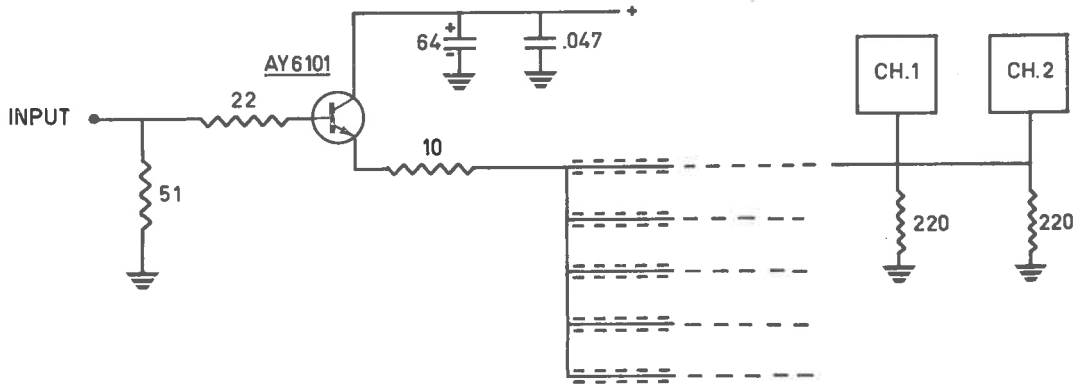

Fig. 9: Count Input Driver Circuit. Card KB.10a.

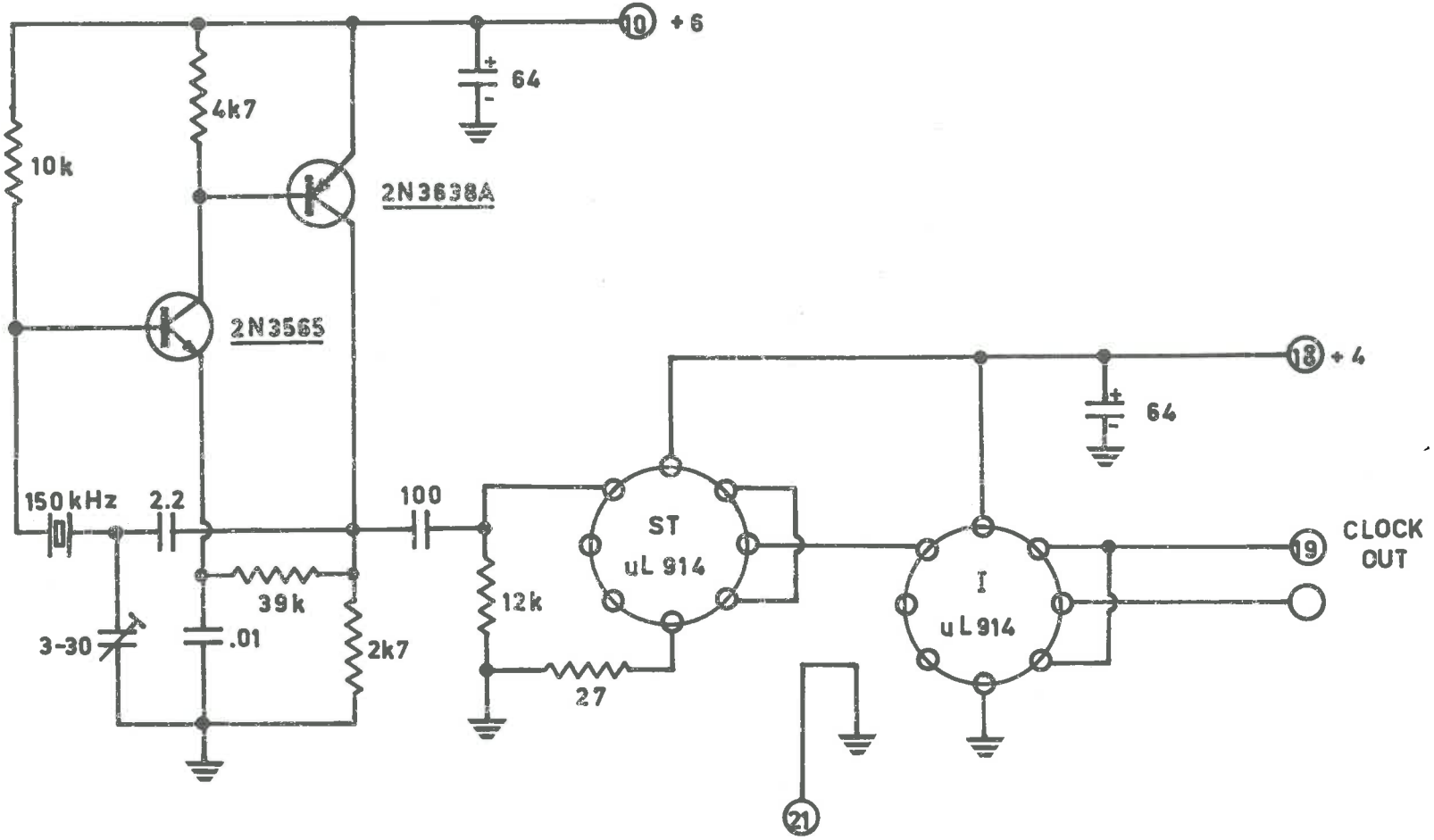

Fig. 10: Clock Oscillator Circuit. Card KB.04.

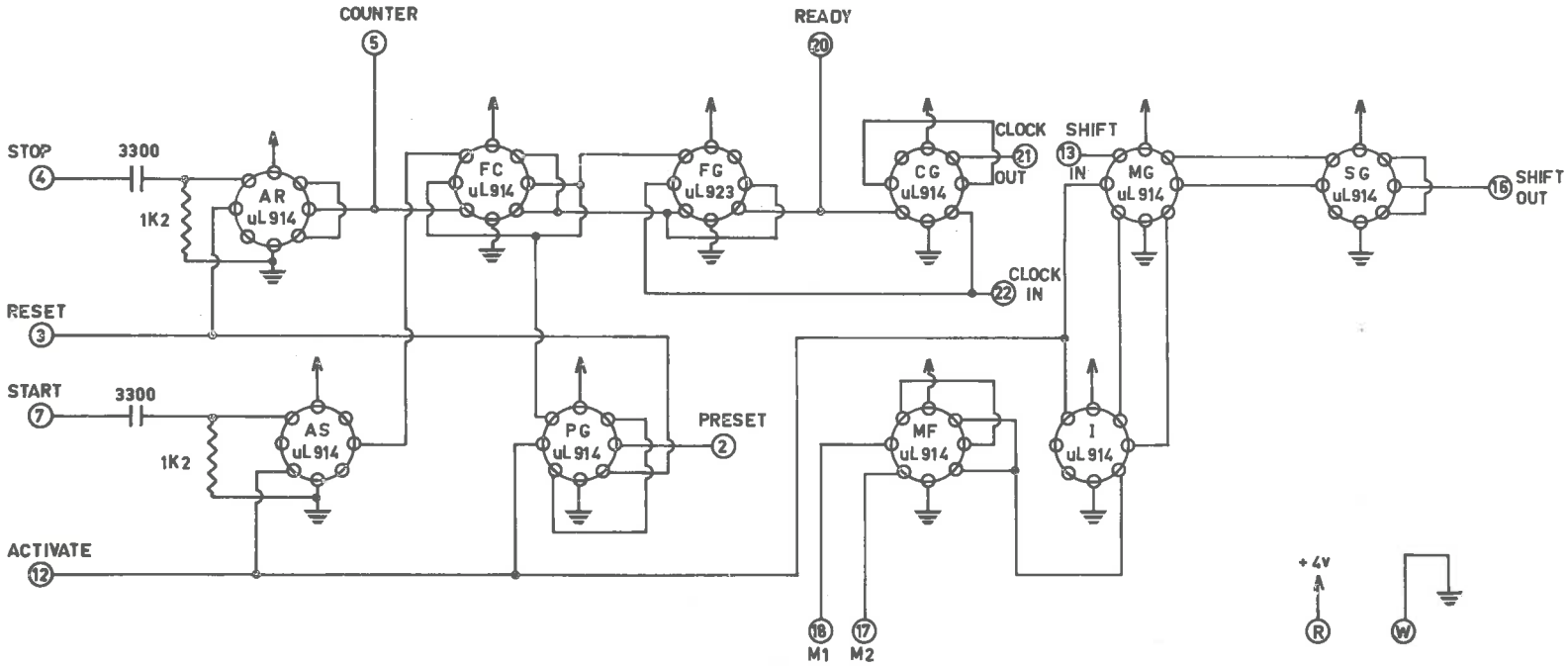

Fig. 11: Control Circuit. Card KB.06c.

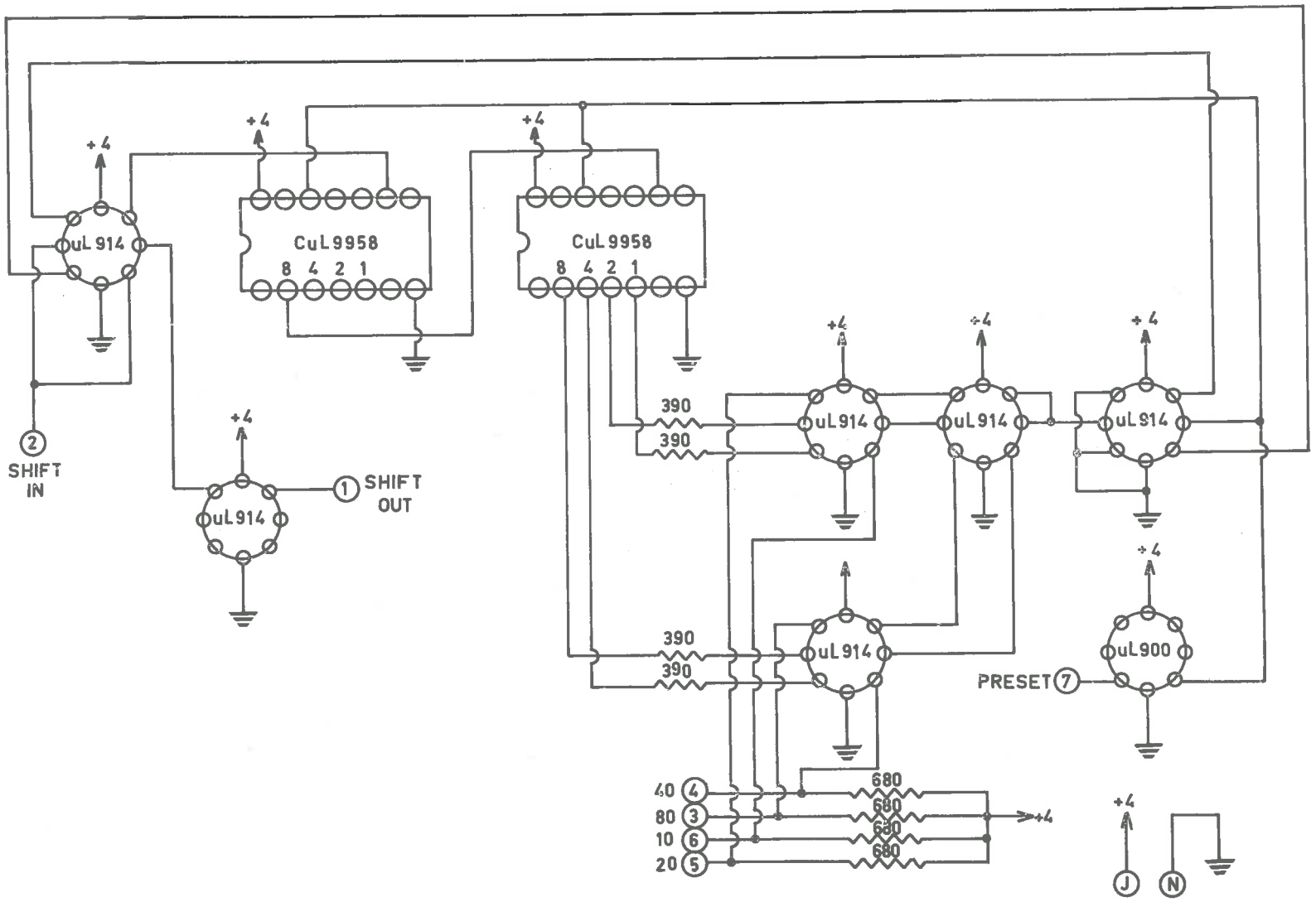

Fig. 12: Delay Circuit. Card KB.08a.

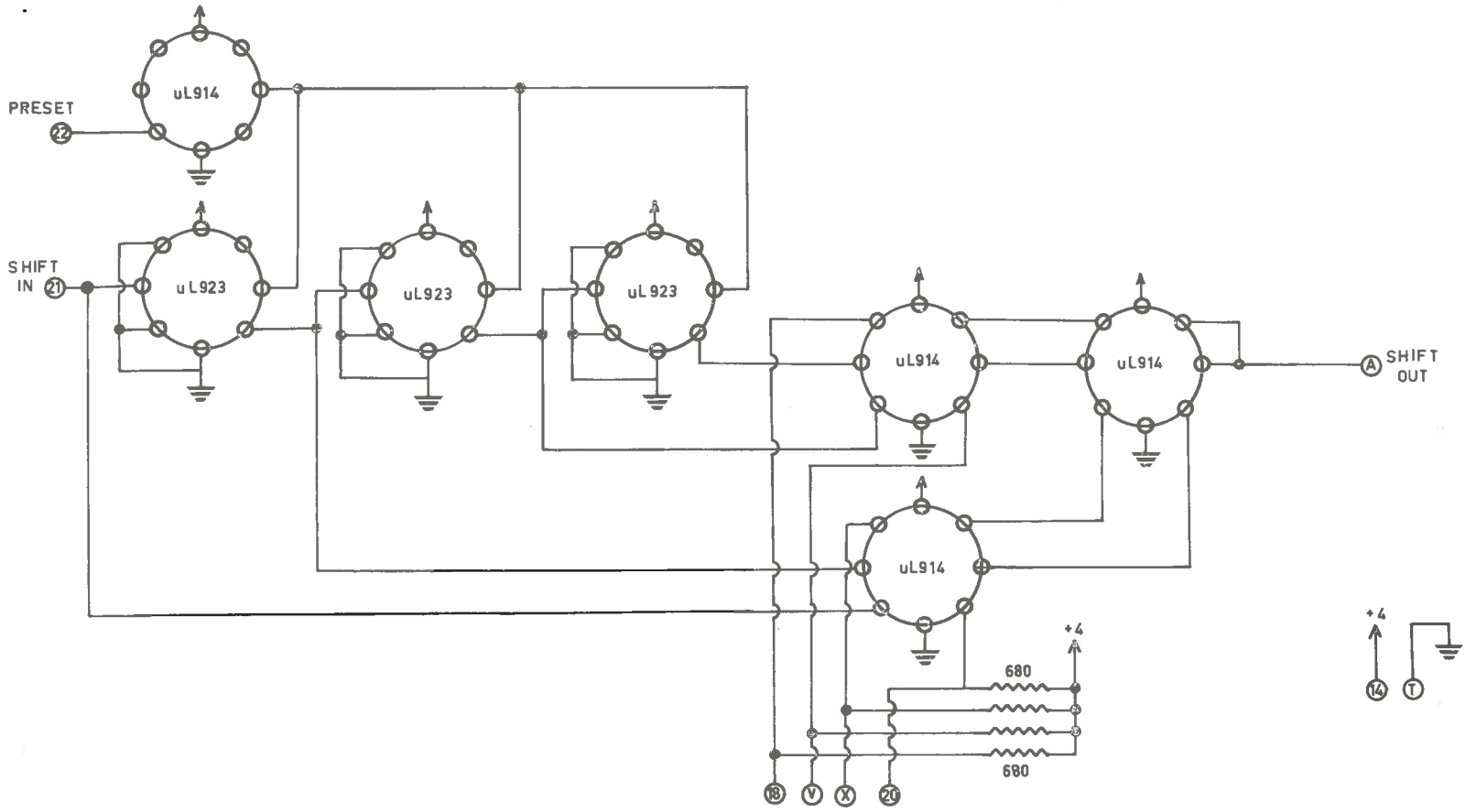

Fig. 13: Width Circuit, Card KB.07.

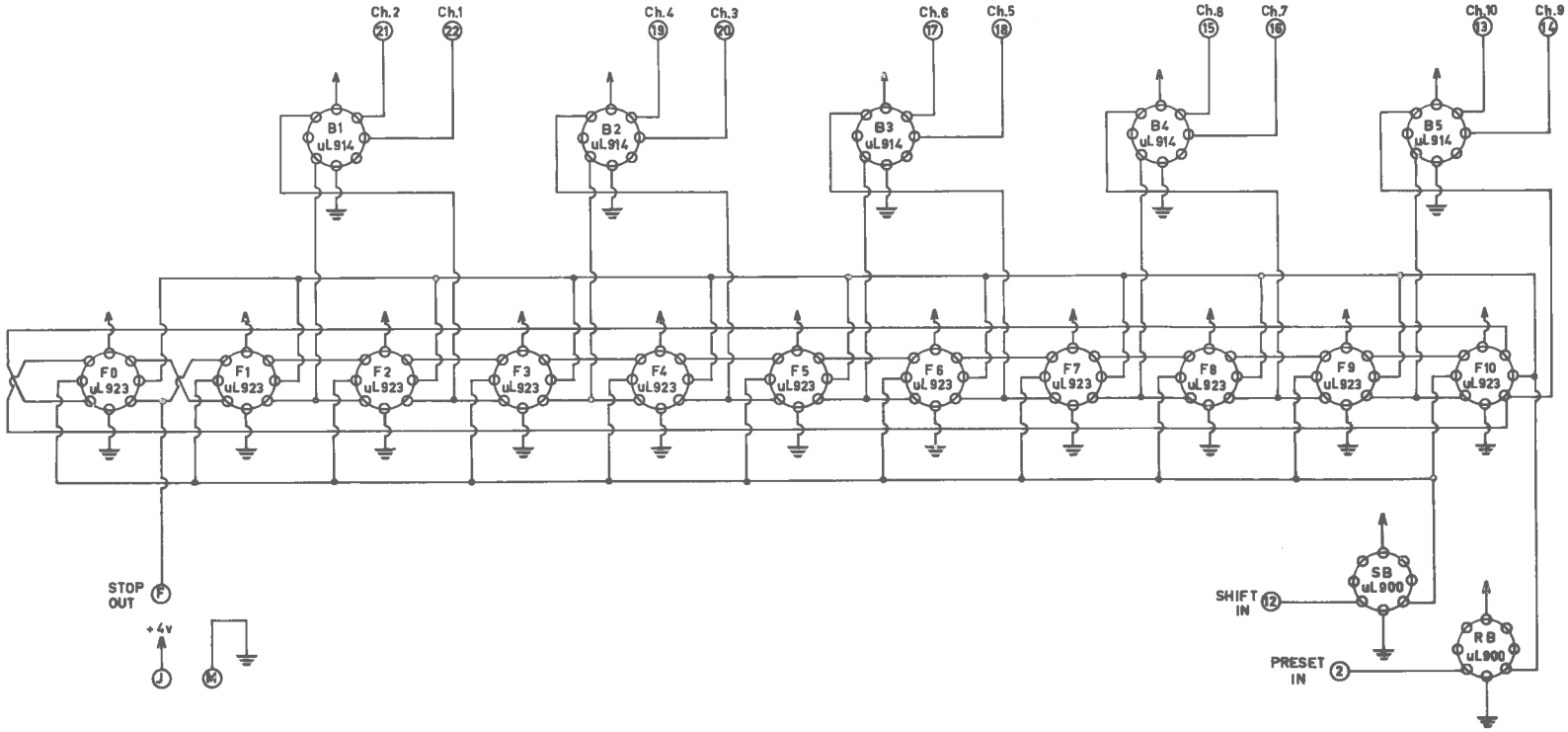

Fig. 14: Shift Register Circuit, Card KB.05.

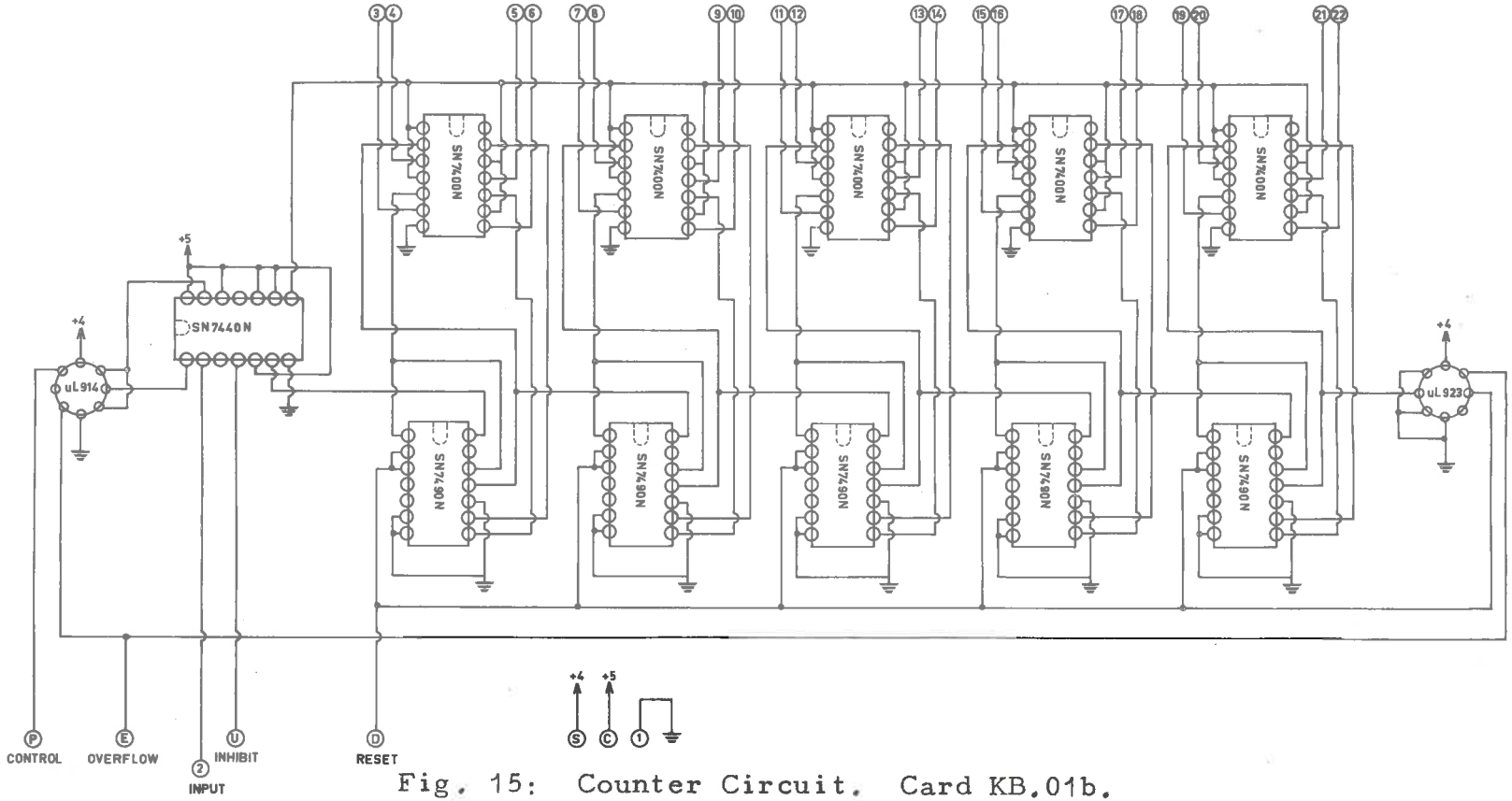

Fig. 15: Counter Circuit. Card KB.01b.

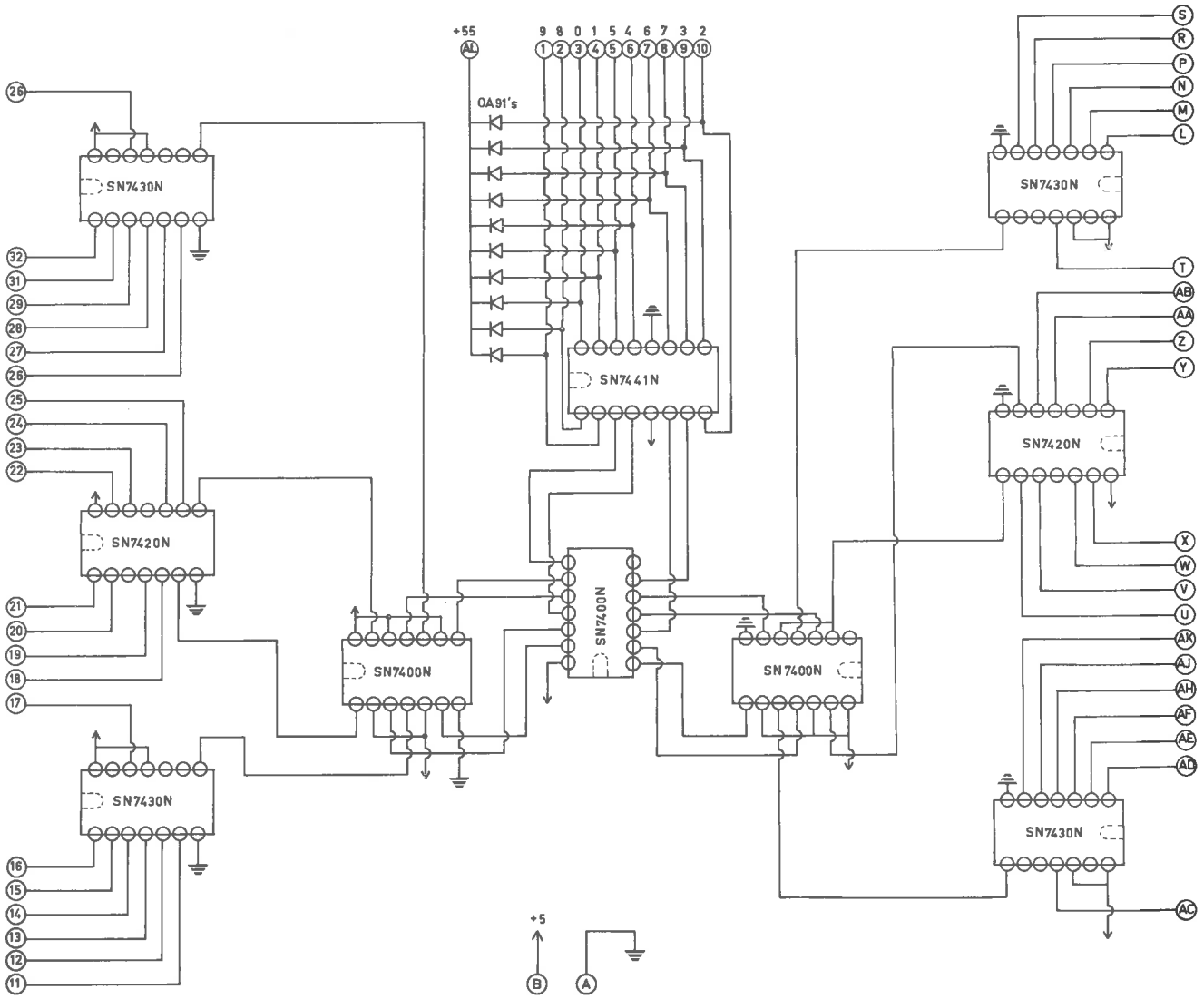

Fig. 16: Decoder Circuit. Card KB.02.

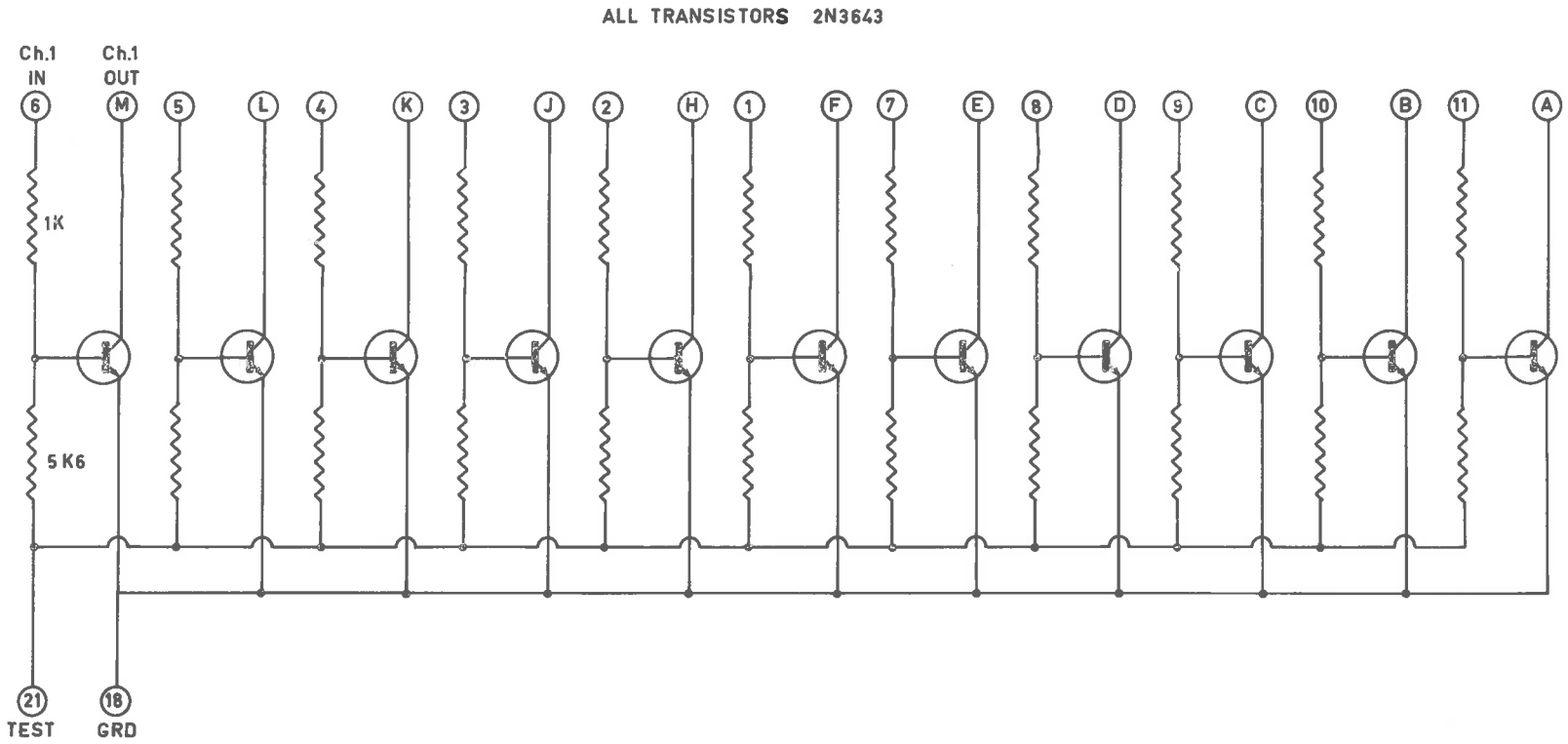

Fig. 17: Lamp Driver Circuit. Card KB.03.

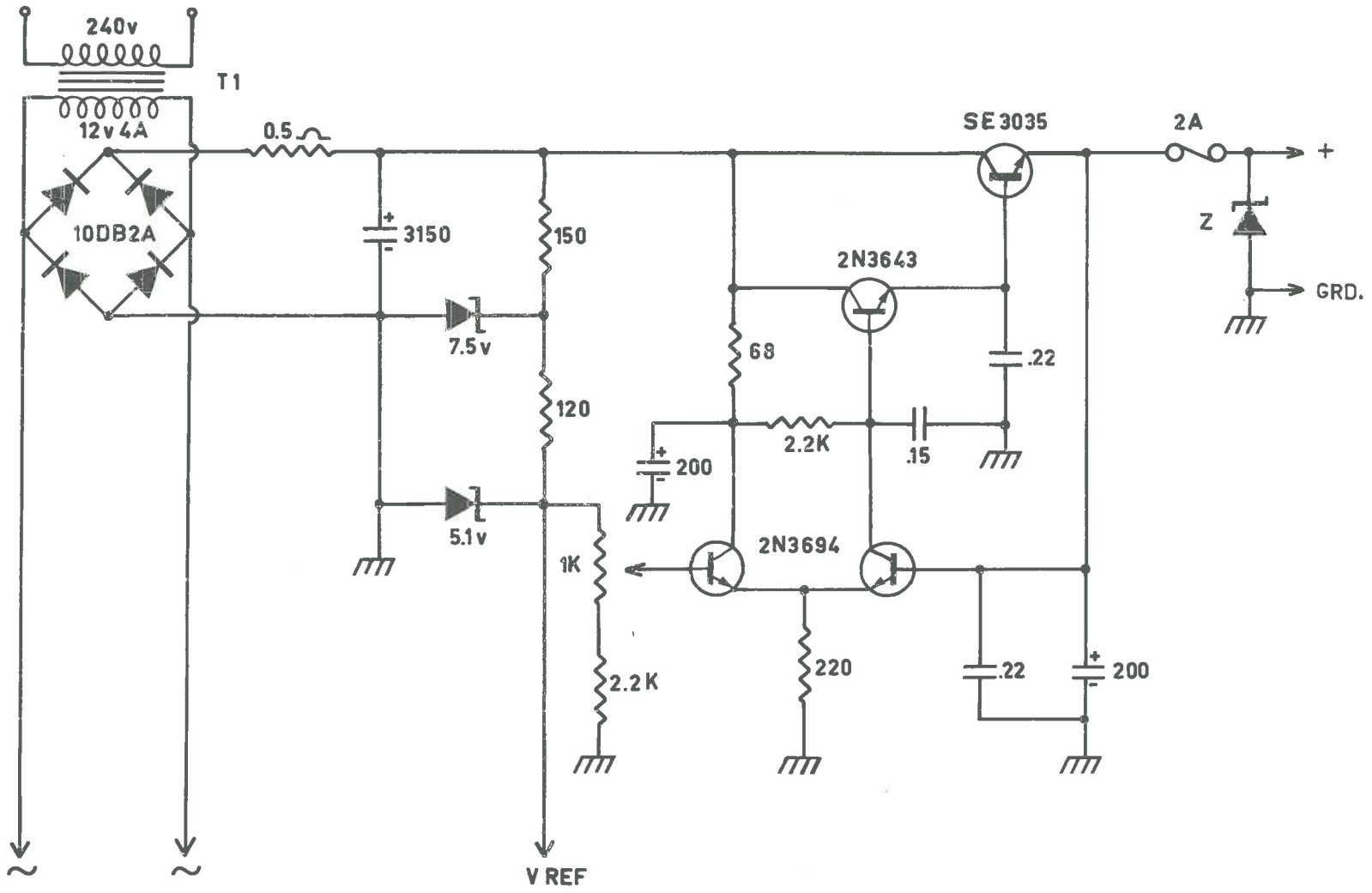

Fig. 18: Regulated Power Supply (one section).

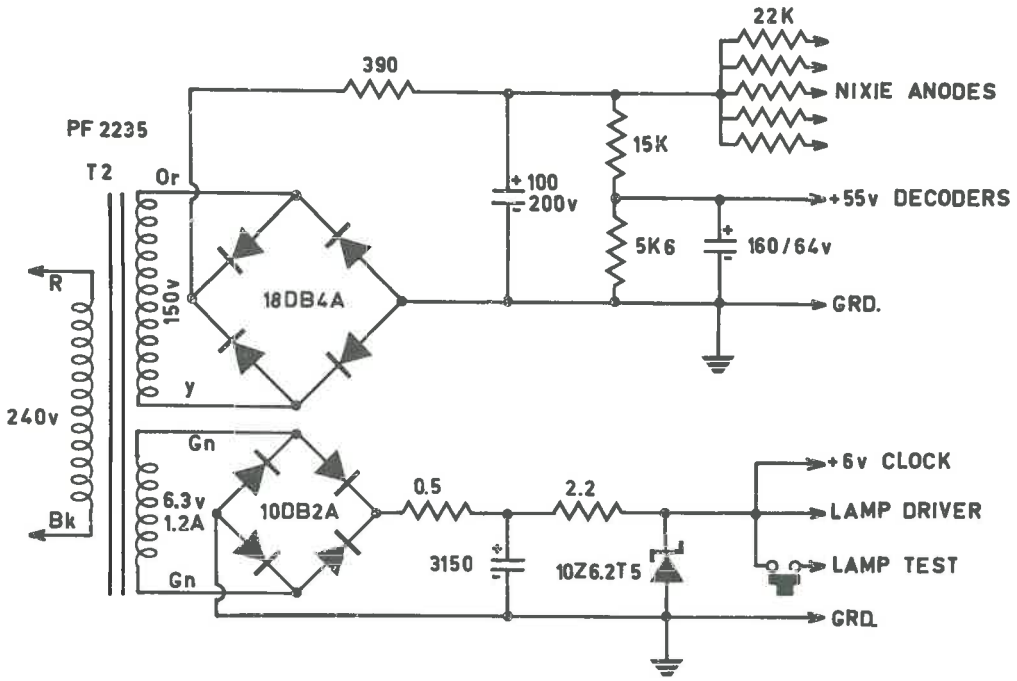

Fig. 19: High Voltage Power Supply.

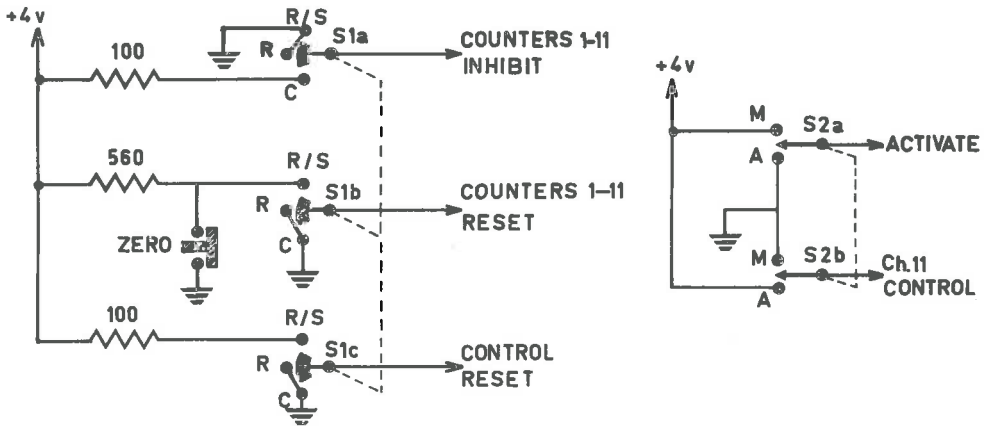

Fig. 20: Front Panel Control Wiring.

S1 FUNCTION SWITCH

S2 MODE SWITCH

APPENDIX II

Reprint of Paper:

"Stratospheric Aerosol Measurements by Optical Radar"

by K. Bartusek, D. J. Gambling, and W. O. Elford.

J. Atmos. Terr. Phys., 1970 (in the press).

GALLEY No. W.A.A 153
J.A.T.P. 2494 Pergamon Press, Oxford
1st Proof MS pages 1–15 Galleys 1–5
The Universities Press, Belfast 21.4.70

Journal of Atmospheric and Terrestrial Physics, 1970, Vol. [illegible], pp. [illegible]. Pergamon Press. Printed in Northern Ireland

Stratospheric aerosol measurements by optical radar

K. Bartusek, D. J. Gambling and W. G. Elford
Department of Physics, University of Adelaide, Adelaide, Australia

(*Received 5 November* 1969; *in revised form* 15 *February* 1970)

Abstract—A laser radar is being used at Adelaide, South Australia (35°S) for routine studies of upper atmosphere densities and aerosol concentrations to an altitude of 60 km. The transmitter operates at a wavelength of 0·694 μ and generates pulses of 0·2 J energy and 0·5 μsec pulse length at a rate of 20 per min. The receiver is a 12 in. Newtonian telescope equipped with an interference filter of bandwidth 8 Å. The light is detected by a cooled photomultiplier, and the recording is carried out by integrating photon counts from selected height intervals.

Results for the period February–June, 1969 show that, over the height range 10–60 km, the scattering can be considered as molecular with the exception of the region 13–24 km where enhanced scattering is attributed to aerosols. The maximum aerosol number density, averaged over the five months, is estimated as $7{\cdot}9 \times 10^5$ m^{-3} and occurs at a height of 18·5 km.

1. Introduction

Several research groups (e.g. Kent *et al.*, 1966; Bain and Sandford, 1966) are using the laser radar technique for routine studies of upper atmosphere densities and aerosol concentrations. Although generally limited to night-time laser method has the advantage, as compared with in situ sampling techniques, that data are continuously available, subject only to weather conditions. The altitude limit of existing systems ranges between 40 and 90 km. All observations reported to date have been carried out from locations north of the equator (Goyer, 1968), and thus there has been a lack of complementary data from the southern hemisphere.

In this paper a laser radar now in operation at Adelaide, South Australia (lat. 35°S) is described, and some preliminary results are presented. The equipment is capable of producing scattering profiles to an altitude of about 60 km with a height resolution of approximately 1 km.

The theory involved in this type of experiment has been adequately described in a number of papers (Kent *et al.*, 1966; Palmer and Zdunkowski, 1964), and will not be repeated here.

2. Equipment

(a) *Transmitter*

The basic element is a $6 \times \frac{5}{16}$ in. ruby rod having a Brewster face at one end, and a totally-internally reflecting wedge cut at the other. The optical cavity is completed by a sapphire flat having 16 per cent reflectivity. 'Q' switching and a 90° change in direction are achieved by a prism rotating at 12,000 rev/min within the optical cavity. The ruby rod is at one focus of an elliptical cavity and is optically pumped by an FX55 Xenon flash tube at the other focus. Both the ruby and flash tube are water cooled.

The laser generator was designed to produce pulses of 1 J energy at a repetition rate of one pulse per second. Unfortunately, in actual operation it was found that near 1 J output, the Q-switch prism had a very limited life and suffered severe pitting after 50–60 shots. In order to obtain a reasonable life it has been found

necessary to operate the laser at well below its rated energy output. During normal operation the energy per pulse is 0·2–0·3 J distributed between 3 spikes in 0·5 μsec. Under these conditions a prism life in excess of 10,000 shots has been obtained. The firing rate at present is approximately 20 shots/min.

A simplified diagram of the transmitting system is shown in Fig. 1(a). The laser output beam divergence of 10 mrad. is reduced by a factor of twelve in the collimator. A rotating shutter positioned at the focus of the first lens of the collimator is used to cut off the long duration fluorescent emission from the ruby following the main laser pulse. The shutter rotates at the same speed as the laser Q-switch, and is phased in such a way that it is completely closed less than 50 μsec after emission of the laser pulse.

A thin wire stretched across the exit aperture of the collimator scatters a small fraction of the beam to a high speed photo diode. The photodiode output waveform is displayed on an oscilloscope, allowing a constant visual check to be kept on the laser pulse shape during operation. The leading edge of the oscilloscope's time-base gating voltage is used to trigger the recording system.

(b) *Receiver*

A simplified diagram of the optical receiver is shown in Fig. 1(b). The scattered light is gathered by a 12-in. dia., 6-ft. focal length parabolic mirror, and directed by a diagonal flat to an aperture which defines the receiver's field of view. The position of the aperture can be adjusted by means of micrometer screws to allow the receiver's field of view to be aligned with the transmitted beam.

Immediately behind the aperature is a rotating shutter, whose function is to block the receiver for a short period following each laser firing. If this were not done, the intense scattering from the first few kilometers of the atmosphere would lead to overloading of the photomultiplier, and a consequent increase in the noise count. This shutter is also synchronised with the laser Q-switch, and phased so that the receiver aperture is completely uncovered by the time the scattered light has returned from the lowest level of the height range being studied. The shutter rotates at 24,000 rev/min, and its opening time is approximately 30 μsec.

The light passing through the aperture is collimated by a lens of 5-in. focal length and then passed through an interference filter to the detector. The interference filter has a bandwidth of 8 Å, and is mounted so that it may be tilted with respect to the beam axis, allowing it to be accurately tuned to the wavelength of the laser emission.

The detector is an E.M.I. type 9558 B photomultiplier. In order to minimize thermoelectric emission from the photocathode, a Peltier battery is used to cool the tube to approximately −15°C. At this temperature, the noise contribution due to the tube is of the order of 120 counts/sec.

(c) *Recording system*

A block diagram of the recording system is shown in Fig. 2. Single photon pulses from the photomultiplier are amplified by a preamplifier mounted on the photomultiplier housing, and passed through 50 Ω cable to the electronics rack. Following further amplification, the pulses pass to a high speed discriminator whose

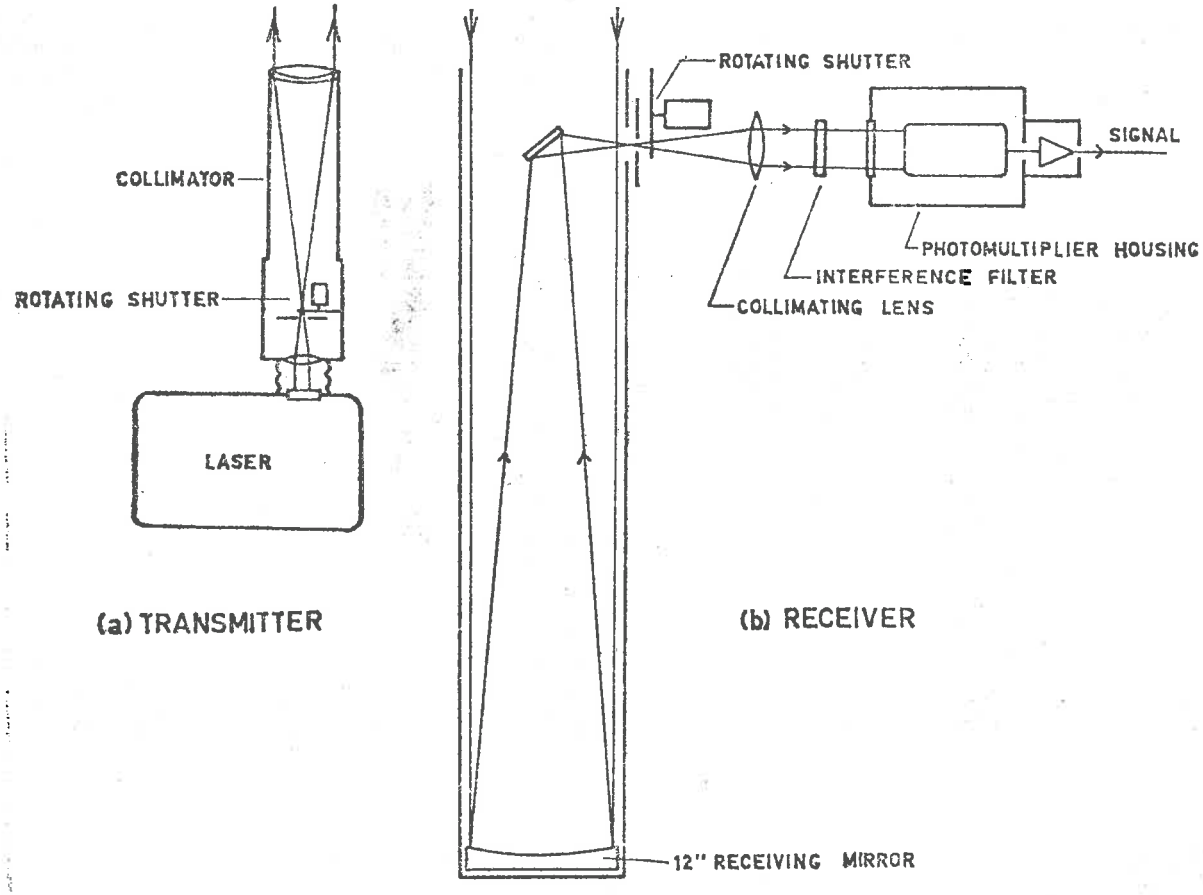

Fig. 1. Schematic diagram of the, (a) transmitting and, (b) receiving systems.

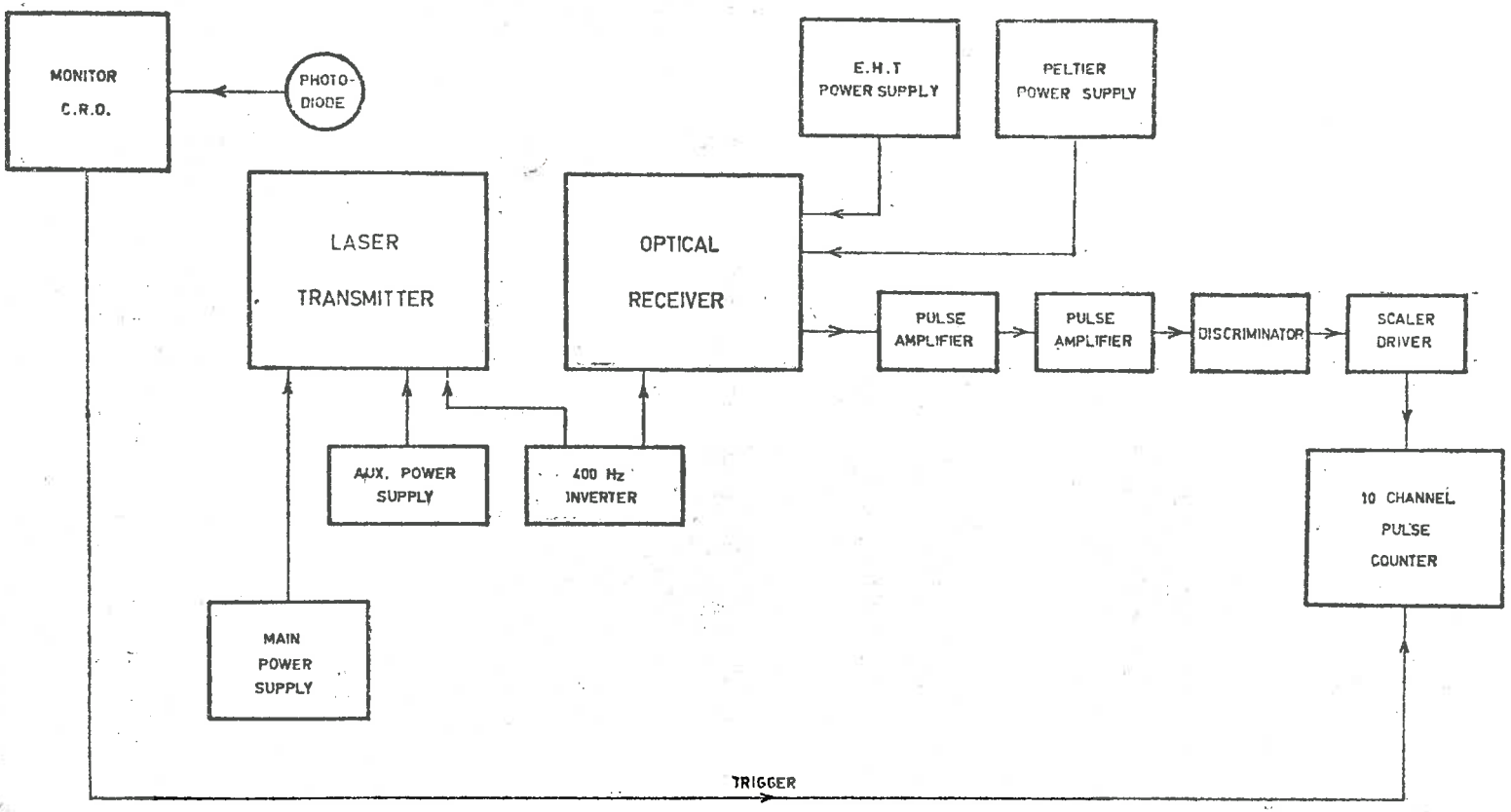

Fig. 2. Block diagram of the main electronic units of the laser radar.

threshold is adjusted to eliminate noise pulses due to the main power supply and triggering circuits.

The standarized output pulses from the discriminator are amplified and further shaped by the scaler driver, and passed to a 10-channel counter which has been specifically developed for the laser system. The channels form 10 successive recording intervals, which in the present equipment may be set at 1, 2, 4 or 8 km. The delay between the arrival of a trigger pulse and the opening of the first channel is adjustable, and may be set to 10, 20, 40 or 80 km.

The resolving time of the whole recording system is 50 nsec, and corrections for non-linearity are applied for average random pulse count rates over 0·2 MHz. In practice, the laser is triggered repetitively, and the signal return from a given height interval is accumulated by the counter. The signal count in each channel is read out manually at the end of a recording sequence, which is usually 200–300 shots. At altitudes up to approximately 20 km a neutral density filter is inserted in the receiver to reduce the count rate to a level which can be accepted by the recording system.

3. Results

The atmosphere contains, in general, a suspended particulate (or aerosol) component, whose concentration varies with height. The photon count $C(h)$ received from a small height interval Δh at height h is therefore a function of the Rayleigh backscattering coefficient $B_R(\pi, h)$ (m^{-1} sterad.$^{-1}$) for the molecular component, and the backscattering coefficient $B_A(\pi, h)$ for the aerosol component. For the case of vertical soundings, it can be shown that $C(h)$ is given by

$$C(h) = k \frac{B_R(\pi, h) + B_A(\pi, h)}{h^2} \Delta h, \tag{1}$$

where k is a constant for the particular laser radar equipment. For the case of observations over a range of equal height intervals, Δh can be absorbed in the constant, and

$$C(h) = K \frac{B_R(\pi, h) + B_A(\pi, h)}{h^2}. \tag{2}$$

The quantity $h^2C(h)$ is thus a measure of the total backscattering coefficient, or scattering index, of the atmosphere at height h.

In Fig. 3, experimentally derived values of $h^2C(h)$ are plotted as a function of height over the range 10–60 km: the graph is the mean of some 35 individual profiles taken over the period February–June, 1969. Included for comparison in Fig. 3 is a curve representing values of $h^2C(h)$ calculated for the case of pure molecular scattering. Molecular densities were obtained from the U.S. Standard Atmosphere 1962, and the laser results were normalized to the calculated curve at a height of 10 km. This choice of the level of normalization differs from that of previous workers who have usually chosen a height between 30 and 40 km where it is generally accepted that the scattering by aerosols is negligible compared to the Rayleigh scattering by the molecular atmosphere (Grams and Fiocco, 1967). In the present investigations the statistical error in the observed scattering index at 30–40 km for an individual profile was considered to be too large for this region to be suitable for normalization of the laser results. Hence a much lower height for

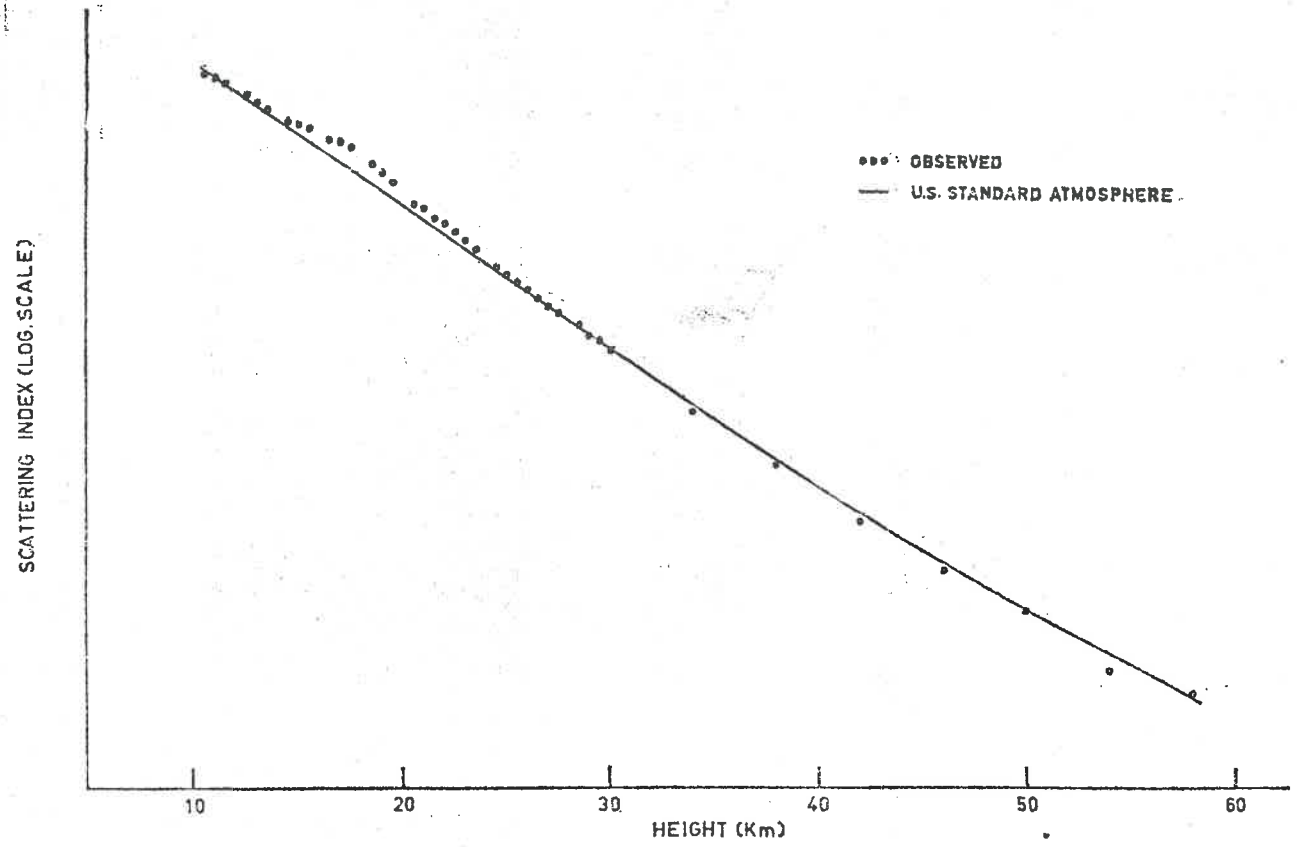

Fig. 3. Observed and calculated scattering profiles. The points representing the observations are the mean of 35 individual profiles for the period February–June, 1969.

normalization was sought and advantage was taken of the fact that particle sampling experiments (JUNGE *et al.*, 1961) have revealed a minimal aerosol number density at about 10 km. A simple analysis shows that within the accuracy of the laser experiment, the scattering at this height can be considered as molecular. A further advantage of the choice of the height of 10 km as the normalization level is that the lower portion of individual profiles can be compared with curves deduced from local radiosonde observations carried out on the same day. It is of interest to note that, at heights above 30 km, the experimental values of $h^2C(h)$ averaged over 35 individual profiles equal, within the limit of the experimental errors, the values calculated from the U.S. Standard Atmosphere, 1962, thus confirming the absence of significant numbers of aerosols above this level.

The mean experimental profile of $h^2C(h)$ vs. h shown in Fig. 3, is very similar in character to those obtained by workers in the Northern hemisphere (CLEMESHA *et al.*, 1966, GRAMS and FIOCCO, 1967). The departure of the observed points in the 13–24 km region from the curve calculated for pure molecular scattering is interpreted as indicating the existance of a broad aerosol layer in this region.

Figure 4 shows the ratio of experimentally observed to calculated scattering for the 10–30 km height range for four individual nights. In this region, the calculated values were derived from air densities obtained from the Bureau of Meteorology radiosonde observations at the nearby Adelaide Airport on the corresponding days, as it has been found that over this height range the radiosonde data often depart significantly from the Standard Atmosphere. The general character of the ratio profile is stable for periods of a day or so, but significant changes are observed over periods of about a week. Over the 5 month period of observation (February–June 1969), the peak ratio, occurring at approximately 19 km, increased steadily from 1·25 to 1·75. These ratios are smaller than corresponding values published by workers in the Northern Hemisphere. Observations are continuing in order to determine if the increasing trend is part of a seasonal variation.

The maximum height from which returns can be satisfactorily measured with the present equipment is limited both by the statistics of the received count, and by the background count rate. The background count is caused by photomultiplier noise, and to a lesser extent by night sky emission, and becomes equal to the signal count rate at about 65 km. At this altitude, the count rate due to backscattered laser photons is approximately 0·15 per km channel width per 100 laser firings. It is thus necessary to accumulate the count from a large number of laser firings to obtain statistically meaningful results from the 60 km region.

4. Estimation of Aerosol Number Density

It is possible to estimate the number density of the aerosol particles if certain assumptions are made regarding their properties. The particle sampling experiments carried out by JUNGE *et al.* (1961), FRIEND (1966) and MOSSOP (1965), indicate that aerosols in the stratosphere are predominantly ammonium sulphate (or persulphate) particles many of which are coated with a volatile substance which is most likely to be water. Many workers choose the refractive index of ammonium sulphate (1·50) in calculations pertaining to the stratospheric aerosol. However, it

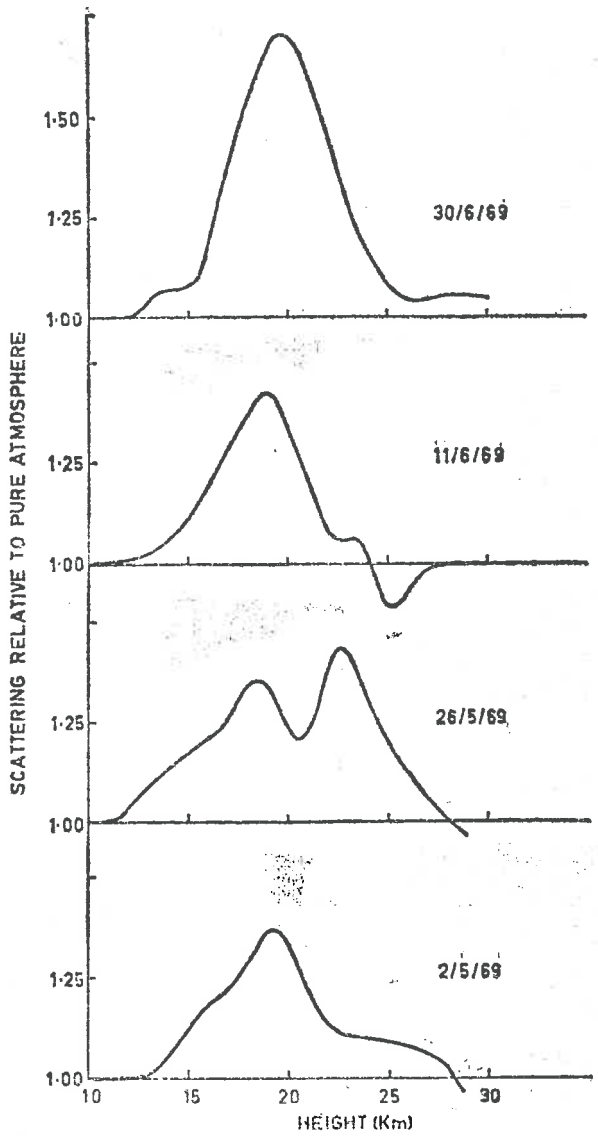

Fig. 4. Graphs of the ratios of observed to predicted scattering in the height range 10–30 km, showing the increase in the peak ratios during May and June, 1969.

is also reasonable to assume the refractive index to be that of water (1·33). Fortunately, the effect of this difference on the final number density answers is relatively small, and in the present calculations a value of 1·40 is chosen to conform with the work of Dave and Mateer (1963).

If it is assumed that the particles are spherical, the Mie theory of scattering can be applied to yield backscattering functions $\Sigma_a(\pi, r)$ (m^2 sterad.$^{-1}$) as functions of the particle radius r. Calculations based on a spherical shape for the atmospheric aerosol can be justified by the results of Powell *et al.* (1967). Their experiments showed that optical scattering properties of an ensemble of non-spherical, randomly

aligned particles differ from those of geometrically equivalent spherical particles only when the particles are highly elongated. The aerosol collection experiments of Mossop (1965) indicate that few of the atmospheric particles would fall into this category.

The averaged aerosol backscattering function $\overline{\Sigma_A(\pi)}$ is found by integration of $\Sigma_A(\pi, r)$ over the range of particle sizes. If $dN(r)$ is the number of particles having radii between r and $r + dr$, then

$$\overline{\Sigma_A(\pi)} = \int_{r_1}^{r_2} \Sigma_A(\pi, r)\, dN(r) \Big/ \int_{r_1}^{r_2} dN(r)$$

where r_1 and r_2 are the limits of particle sizes.

Junge's power law model has been used by many authors to describe the size distribution of stratospheric aerosols. However, this model has been shown by Friend (1966) to be suspect in the small size range. The lognormal size distribution used by Dave and Mateer (1963) has therefore been utilized in the present calculations. This distribution is specified by

$$\frac{dN(r)}{d(\log r)} \propto \exp\left[-\left(\log \frac{r}{r_0}\right)^2 \Big/ 2s^2\right]$$

where r_0 is the mean radius, and s is the standard deviation.

From the averaged results of Friend (1966) and Mossop (1965) we obtain $r_0 = 0{\cdot}35\ \mu$, and $s = 0{\cdot}30$ (using natural logarithms). The boundary values r_1 and r_2 in the integration are chosen to be $0{\cdot}04$ and $3{\cdot}0\ \mu$ respectively, and, for a wavelength of $0{\cdot}694\ \mu$,

$$\overline{\Sigma_A(\pi)} = 2{\cdot}93 \times 10^{-14}\ \text{m}^2\ \text{sterad.}^{-1}$$

An increase in the integration range would have little effect on the value of $\overline{\Sigma_A(\pi)}$, due to the rapid decrease of particle number density away from r_0. For example, an extension of the integration range to limits of $0{\cdot}01$ and $8{\cdot}0\ \mu$ only increases $\overline{\Sigma_A(\pi)}$ by approximately $0{\cdot}03$ per cent.

The ratio of observed to calculated scattering R, may be expressed by

$$R = \frac{B_r(\pi) + B_A(\pi)}{B_R(\pi)} = 1 + \frac{B_A(\pi)}{B_R(\pi)}$$

and its mean value at the height corresponding to the peak aerosol contribution in the stratosphere (18·5 km) is 1·5. Since $B_R(\pi)$ is known, and

$$B_A(\pi) = N_A\, \overline{\Sigma_A(\pi)}$$

N_A, the aerosol number density, may be calculated. The value obtained is

$$N_A = 7{\cdot}9 \times 10^5\ \text{m}^{-3}.$$

Direct sampling experiments carried out by Chagnon and Junge (1961) yielded a maximum particle density near 20 km altitude of $10^5\ \text{m}^{-3}$ for particles having radii between $0{\cdot}1$ and $1{\cdot}0\ \mu$. Rosen (1964) has found a maximum concentration of $3 \times 10^6\ \text{m}^{-3}$ for particles having radii greater than $0{\cdot}27\ \mu$. The

estimate obtained from the laser radar results presented here thus lies between these limits, and supports the assumption of a lognormal size distribution for particles in the stratosphere. For comparison, the above calculation has been repeated using the Junge size distribution $dN(r) \propto r^{-3}\,dr$ and yielded a value for N_A of $9{\cdot}8 \times 10^6\ m^{-2}$, an order larger than the number density derived using a lognormal distribution.

5. Conclusions

The laser radar equipment described in this paper is cabable of producing scattering profiles to an altitude of 60 km. Comparison of these profiles with curves calculated for purely molecular scattering shows the well-known stratospheric aerosol layer having a maximum concentration at 18·5 km. Assuming a lognormal size distribution for the stratospheric aerosol, the maximum number density is $7{\cdot}9 \times 10^5\ m^{-3}$, which lies between the estimates obtained from direct sampling experiments by Junge *et al.*, (1961) and Rosen (1964).

The authors believe that these are the first laser soundings of the atmosphere in the Southern hemisphere. The general form of the stratospheric aerosol layer appears very similar to that deduced from laser observations in the Northern hemisphere. However, the maximum concentration appears to be less in the Southern hemisphere.

Acknowledgements—This work was supported by grants from the Department of Supply and the University of Adelaide. The authors wish to thank Professor J. H. Carver and Mr. B. Roff for their continued encouragement. The observations were carried out at the field station of the Mawson Institute for Antarctic Research, at Mt. Torrens. Much of the mechanical design of the equipment was carried out by Mr. C. F. Vaskess.

References

Bain W. C. and Sandford M. C. W.	1966	*J. Atmosph. Terr. Phys.* **28**, 543.
Chagnon C. W. and Junge C. E.	1961	*J. Met.* **18**, 746.
Clemesha B. R., Kent G. S. and Wright R. W. H.	1966	*Nature, Lond.* **209**, 184.
Dave J. V. and Mateer C. L.	1968	*J. geophys. Res.* **73**, 6897.
Friend J. P.	1966	*Tellus* **18**, 465.
Goyer G. G.	1968	*Bull. Am. met. Soc.* **49**, 936.
Grams G. and Fiocco G.	1967	*J. geophys. Res.* **72**, 3523..
Junge C. E., Chagnon C. W. and Manson J. E.	1961	*J. Met.* **18**, 81.
Kent G. S., Clemesha B. R. and Wright R. W.	1966	*J. Atmosph. Terr. Phys.* **29**, 169.
Mossop S. C.	1965	*Geochim. Cosmochim. Acta* **29**, 201.
Palmer E. P. and Zdunkowski W. G.	1964	*J. geophys. Res.* **69**, 2369.
Powell R. S., Circle R. R., Vogel D. C., Woodson P. D. and Donn B.	1967	*Planet. Space Sci.* **15**, 1641.
Rosen J. M.	1964	*J. geophys. Res.* **69**, 4673.